การสังเคราะห์และสมบัติการยึดเหนี่ยวกับดีเอ็นเอของพิร์โรลิดินิลเพปไทด์นิวคลีอิกแอซิดที่มี (2*S*,3*S*)-3-แอมิโนเททระไฮโดรฟิวแรน-2-คาร์บอกซิลิกแอซิดเป็นตัวเชื่อม

นางสาวพิชชานันท์ ศรีวะรมย์

วิทยานิพนธ์นี้เป็นส่วนหนึ่งของการศึกษาตามหลักสูตรปริญญาวิทยาศาสตรมหาบัณฑิต
สาขาวิชาเคมี ภาควิชาเคมี
คณะวิทยาศาสตร์ จุฬาลงกรณ์มหาวิทยาลัย
ปีการศึกษา 2556
ลิขสิทธิ์ของจุฬาลงกรณ์มหาวิทยาลัย

SYNTHESIS AND DNA BINDING PROPERTIES OF PYRROLIDINYL PEPTIDE NUCLEIC ACID CONTAINING (2*S*,3*S*)-3-AMINOTETRAHYDROFURAN-2-CARBOXYLIC ACID SPACER

Miss Pitchanun Sriwarom

A Thesis Submitted in Partial Fulfillment of the Requirements
for the Degree of Master of Science Program in Chemistry
Department of Chemistry
Faculty of Science
Chulalongkorn University
Academic Year 2013

Thesis Title	SYNTHESIS AND DNA BINDING PROPERTIES OF PYRROLIDINYL PEPTIDE NUCLEIC ACID CONTAINING (2*S*,3*S*)-3-AMINOTETRAHYDROFURAN-2-CARBOXYLIC ACID SPACER
By	Miss Pitchanun Sriwarom
Field of Study	Chemistry
Thesis Advisor	ProfessorTirayut Vilaivan, D.Phil.
Thesis Co-Advisor	Panuwat Padungros, Ph.D.

Accepted by the Faculty of Science, Chulalongkorn University in Partial Fulfillment of the Requirements for the Master's Degree

.....Dean of the Faculty of Science

(ProfessorSupot Hannongbua, Ph.D.)

THESIS COMMITTEE

.....Chairman

(Assistant ProfessorWarinthorn Chavasiri, Ph.D.)

.....Thesis Advisor

(ProfessorTirayut Vilaivan, D.Phil.)

.....Thesis Co-Advisor

(Panuwat Padungros, Ph.D.)

.....Examiner

(Associate ProfessorNongnuj Muangsin, Ph.D.)

.....Examiner

(Assistant ProfessorWorawan Bhanthumnavin, Ph.D.)

.....External Examiner

(Chaturong Suparpprom, Ph.D.)

พิชชานันท์ ศรีวะรมย์ : การสังเคราะห์และสมบัติการยึดเหนี่ยวกับดีเอ็นเอของพิร์โรลิดินิลเพปไทด์นิวคลีอิกแอซิดที่มี (2*S*,3*S*)-3-แอมิโนเททระไฮโดรฟิวแรน-2-คาร์บอกซิลิกแอซิดเป็นตัวเชื่อม. (SYNTHESIS AND DNA BINDING PROPERTIES OF PYRROLIDINYL PEPTIDE NUCLEIC ACID CONTAINING (2*S*,3*S*)-3-AMINOTETRAHYDROFURAN-2-CARBOXYLIC ACID SPACER) อ.ที่ปรึกษาวิทยานิพนธ์หลัก: ศ. ดร.ธีรยุทธ วิไลวัลย์, อ.ที่ปรึกษาวิทยานิพนธ์ร่วม: อ. ดร.ภาณุวัฒน์ ผดุงรส, 149 หน้า.

เพปไทด์นิวคลีอิกแอซิด (Peptide nucleic acid) หรือพีเอ็นเอ (PNA) เป็นสารเลียนแบบดีเอ็นเอที่มีการเปลี่ยนโครงสร้างหลักของดีออกซีไรโบสฟอตเฟตซึ่งมีประจุลบด้วยโครงสร้างที่คล้ายคลึงเพปไทด์ พีเอ็นเอยังคงความสามารถในการเข้าคู่กับดีเอ็นเอและอาร์เอ็นเออย่างแข็งแรงและจำเพาะต่อลำดับเบสเหมือนกับดีเอ็นเอในธรรมชาติ แต่แสดงความแตกต่างที่สำคัญหลายประการ เช่น ความเสถียรทางเคมีและชีวภาพ มีประจุไฟฟ้าเป็นกลาง และความสามารถในการแทรกเข้าไปในสายคู่ของดีเอ็นเอ เมื่อไม่นานมานี้ ได้มีการรายงานถึงพิร์โรลิดินิลพีเอ็นเอ (acpcPNA) โดยมีโครงสร้างหลักเป็น โพรลิล-2-แอมิโนไซโคลเพนเทนคาร์บอกซิลิกแอซิด (ACPC) พีเอ็นเอที่ถูกจำกัดคอนฟอร์เมชันนี้แสดงสมบัติที่เป็นที่ต้องการหลายประการ รวมถึงการเข้าคู่ดีเอ็นเออย่างแข็งแรงและจำเพาะเจาะจง การเลือกเข้าคู่กับดีเอ็นเอได้ดีกว่าอาร์เอ็นเอ การเข้าคู่เฉพาะในทิศทางแอนติพาราเรล และการไม่สามารถเข้าคู่ระหว่างพีเอ็นเอด้วยกันเอง แต่ทว่าโครงสร้างหลักที่ไม่ชอบน้ำของ acpcPNA ทำให้เกิดแรงกระทำแบบไม่จำเพาะเจาะจงกับวัสดุที่ไม่ชอบน้ำหลายชนิด รวมไปถึงหลอดพลาสติกโพลีโพรพิลีนที่ใช้ทั่วไปในงานวิจัย ด้วยเหตุนี้จึงเป็นมูลเหตุจูงใจการพัฒนาพิร์โรลิดินิลพีเอ็นเอระบบใหม่ที่มีโครงสร้างหลักที่ชอบน้ำมากขึ้น โดยการแทนที่ ACPC ด้วยบีต้าแอมิโนแอซิดที่มีวงแหวนเททระไฮโดรฟิวแรนที่ชอบน้ำ ซึ่งจำเป็นต้องอาศัยโครงสร้างย่อยคือ เอ็น-เอฟมอค- (2*S*,3*S*)-3-แอมิโนเททระไฮโดรฟิวแรน-2-คาร์บอกซิลิกแอซิด (*SS*-ATFC) เพนตะฟลูออโรฟีนิลเอสเทอร์ ที่สามารถสังเคราะห์ได้จาก 2-ดีออกซี-ดี-ไรโบสรวมทั้งหมด 12 ขั้นตอน โดยมีปริมาณผลผลิตรวมร้อยละ 3 และนำหน่วยโครงสร้าง ATFC นี้ไปใช้ร่วมกับดี-โพรลีนมอนอเมอร์ที่ถูกดัดแปลงด้วยนิวคลีโอเบสเพื่อสังเคราะห์เป็นพีเอ็นเอใหม่ที่เรียกว่า atfcPNA ที่ซึ่งยังคงสามารถเข้าคู่กับดีเอ็นเอและอาร์เอ็นเอ แต่มีความแข็งแรงและความจำเพาะเจาะจงลดลงเล็กน้อยถึงปานกลาง (ขึ้นกับลำดับเบส) เมื่อเทียบกับ acpcPNA มาตรฐานจากการศึกษาโดย UV-T_m และ ซีดี สเปกโทรสโกปี สภาพขั้วที่สูงกว่าของ atfcPNA เมื่อเทียบกับ acpcPNA ได้รับการยืนยันด้วยวิธีรีเวิร์สเฟสเอชพีแอลซี การทดลองวัดการวาวแสงของ acpcPNA และ atfcPNA ที่ติดฉลากด้วยฟลูออเรสซีนแสดงให้เห็นอย่างชัดเจนถึงการจับแบบไม่จำเพาะเจาะจงที่ลดลงของ atfcPNA กับหลอดพลาสติก จากผลที่ได้ทั้งหมดแสดงว่าการแทนที่วงแหวนไซโคลเพนเทนใน acpcPNA ด้วยวงเททระไฮโดรฟิวแรนสามารถช่วยลดแรงกระทำแบบไม่จำเพาะเจาะจงที่ไม่ต้องการ โดยไม่รบกวนสมบัติการเข้าคู่กับดีเอ็นเอมากนัก ซึ่งเป็นผลที่มีความหมายสำคัญในนำพิร์โรลิดินิลพีเอ็นเอไปประยุกต์ใช้ในสถานการณ์ที่หลากหลาย

ภาควิชา เคมี	ลายมือชื่อนิสิต .....
สาขาวิชา เคมี	ลายมือชื่อ อ.ที่ปรึกษาวิทยานิพนธ์หลัก .....
ปีการศึกษา 2556	ลายมือชื่อ อ.ที่ปรึกษาวิทยานิพนธ์ร่วม .....

5472051623 : MAJOR CHEMISTRY
KEYWORDS: PEPTIDE NUCLEIC ACID (PNA) / CYCLIC AMINO ACID / SUGAR AMINO ACID / TETRAHYDROFURAN / ALPHA/BETA-PEPTIDE / FOLDAMER

PITCHANUN SRIWAROM: SYNTHESIS AND DNA BINDING PROPERTIES OF PYRROLIDINYL PEPTIDE NUCLEIC ACID CONTAINING (2*S*,3*S*)-3-AMINOTETRAHYDROFURAN-2-CARBOXYLIC ACID SPACER. ADVISOR: PROF.TIRAYUT VILAIVAN, D.Phil., CO-ADVISOR: PANUWAT PADUNGROS, Ph.D., 149 pp.

Peptide nucleic acid (PNA) is an analogue of DNA with the negatively charged deoxyribose phosphate backbone is replaced with a peptide-like structure. PNA retains the ability to bind strongly and sequence specifically to DNA and RNA similar to natural DNA, but exhibit several remarkable differences such as the high chemical and biological stability, the electrostatic neutrality and the ability to invade into double stranded DNA. Recently, pyrrolidinyl PNA with a prolyl-2-aminocyclopentanecarboxylic acid (ACPC) backbone (acpcPNA) was introduced as a new conformationally constrained PNA analogue that exhibit several desirable properties including the high affinity and specificity in binding to DNA, the high preference for binding to DNA over RNA, the exclusive binding in antiparallel orientation and the inability to form self-hybrids. Nevertheless, the hydrophobic prolyl-ACPC backbone of acpcPNA showed non-specific interactions with many hydrophobic materials, including the commonly used polypropylene plastic tubes. This motivated a development of a new pyrrolidinyl PNA with a more hydrophilic backbone by replacement of the ACPC with a beta-amino acid containing a hydrophilic tetrahydrofuran ring. This requires a building block named N-Fmoc-(2*S*,3*S*)-3-aminotetrahydrofuran-2-carboxylic acid (*SS*-ATFC) pentafluorophenyl ester, which was successfully synthesized from 2-deoxy-d-ribose overall 12 steps in 3% yield. The ATFC building blocks were oligomerized with nucleobase-modified-D-proline monomers, represented as atfcPNA. The ATFC was incorporated in to the PNA structure to give a new atfcPNA, which could still bind to DNA and RNA, but with slightly to moderately lowered affinity and specificity (depending on the base sequence) when compared to the benchmark acpcPNA according to UV-T_m and CD spectroscopy. The higher polarity of the atfcPNA than acpcPNA was confirmed by reverse phase HPLC. Fluorescence experiments preformed on fluorescein labeled acpcPNA and atfcPNA clearly demonstrated the reduced non-specific binding of atfcPNA to plastic tubes. These results suggest that the replacement of the cyclopentane ring in acpcPNA with the tetrahydrofuran ring can reduce undesirable non-specific interactions without much affect on the DNA binding properties, which may have important implications in many practical applications of pyrrolidinyl PNA.

Department:	Chemistry	Student's Signature	.....
Field of Study:	Chemistry	Advisor's Signature	.....
Academic Year:	2013	Co-Advisor's Signature	.....

ACKNOWLEDGEMENTS

I wish to sincerely thank and express my deepest gratitude to Professor Dr. Tirayut Vilaivan, and Dr. Panuwat Padungros for their advices and suggestions for research. I am also grateful to thesis examiners: Assistant Professor Dr. Warinthorn Chavasiri, Associate Professor Dr. Nongnuj Muangsin, Assistant Professor Dr. Worawan Bhanthumnavin and Dr. Chaturong Suparpprom for their valuable comments and suggestions. I would like to thank the Depatment of Chemistry, Chulalongkorn university for the Teaching Assistant schorlarship and the use of facilities, equipment, glassware, and chemicals; Dr. Woraluk Mansawat and members of TV group for their friendship, advices and their helpful. Finally, I would like to thank my mother for her moral support throughout the research and my best friends for their encouragement and social support throughout my study period.

CONTENTS

Page

Page

Page

Page

Page

LIST OF FIGURES

LIST OF TABLES

LIST OF ABBREVIATIONS AND SYMBOLS

%	percent
A	Adenine
A^{Bz}	N^6-benzoyladenine
Ac	acetyl
Ac_2O	acetic anhydride
ACN	acetonitrile
Å	angstrom
$[\alpha]_D$	specific rotation
BAIB	[bis(acetoxy)iodo]benzene
Boc	*tert*-butoxycarbonyl
br	broad
Bz	benzoyl
c	concentration
C	cytosine
calcd	calculated
C^{Bz}	N^4-benzoylcytosine
CCA	α-cyano-4-hydroxy cinnamic acid
CD	circular dichroism
$CDCl_3$	deuterated chloroform
cm^{-1}	unit of wave number
°C	degree celcius
d	doublet
dd	doublet of doublet
ddd	doublet of doublet of doublet
dddd	doublet of doublet of doublet of doublet
dt	doublet of triplet
D_2O	deuterium oxide
DBU	1,8-diazabicyclo[5.4.0]undec-7-ene
DIAD	diisopropylazodicarboxylate
DIEA	diisopropylethylamine
DMAP	4-dimethylaminopyridine
DMF	*N,N'*-dimethylformamide
DMSO	dimethylsulfoxide

DMSO-d_6	deuterated dimethylsulfoxide
DNA	deoxyribonucleic acid
[DNA]	concentration of DNA
δ	chemical shift
EtOAc	ethyl acetate
equiv	equivalent (s)
Fmoc	9-fluorenylmethoxycarbonyl
FmocOSu	9-fluorenylsuccinimidyl carbonate
g	gram
G	guanine
G^{Ibu}	N^2-isobutyrylguanine
HATU	*O*-(7-azabenzotriazol-1-yl)-*N,N,N',N'*- tetramethyluronium hexafluorophosphate
HOAt	1-hydroxy-7-azabenzotriazole
HPLC	High Performance Liquid Chromatography
HRMS	High Resolution Mass Spectrometry
h	hour
Ibu	isobutyryl
IR	infrared
J	coupling constant
Lys	lysine
m	multiplet
MALDI-TOF	Matrix-Assisted Laser Desorption/Ionization-Time of Flight
MeOH	methanol
MeOTs	methyl tosylate
mg	milligram
MHz	megahertz
min	minute(s)
mL	milliliter
mM	millimolar
MS	Mass Spectrometry
Ms	methanesufonyl (mesyl)
MsCl	methanesufonyl chloride
MSA	methanesulfonic acid
mmol	millimole
m.p.	melting point

m/z	mass to charge ratio
µL	microliter
µM	micromolar
nm	nanometer
NMR	Nuclear Magnetic Resonance
N_2	nitrogen (gas)
OD_{xxx}	optical density at xxx nm (= A_{xxx})
Pfp	pentafluorophenyl
PfpOTfa	pentafluorophenyl trifluoroacetic acid
PG	an unspecified protecting group
PNA	Peptide Nucleic Acid or polyamide nucleic acid
ppm	part per million
p-Tol	*p*-toluoyl
p-TolCl	*p*-toluoyl chloride
p-TsCl	*p*-toluenesulfonyl chloride (tosyl chloride)
[PNA]	concentration of PNA
RNA	ribonucleic acid
rt	room temperature
R_f	retention factor
s	singlet
t	triplet
td	triplet of doublet
T	Thymine
TEMPO	2,2,6,6-tetramethyl-1-piperinyloxyl
TFA	trifluoroacetic acid
THF	tetrahydrofuran
TLC	thin layer chromatography
T_m	melting temperature
t_R	retention time
Ts	*p*-toluenesulfonyl (tosyl)
UV	ultraviolet
X	an unspecified leaving group

CHAPTER I

INTRODUCTION

1.1 Peptide nucleic acid (PNA)

In 1991, Nielsen et al.[1] proposed a new DNA analogue by replacing the sugar phosphate backbone of natural DNA with a pseudopeptide (**Figure 1.1**) called aminoethylglycine (AEG). The resulting new DNA analogue was named Peptide Nucleic Acid (PNA, also known as aegPNA). PNA binds to DNA and RNA, *via* Watson-Crick base pairing, with higher affinity than DNA or RNA due to the absence of charge repulsion in the electrostatically neutral PNA backbone. As a result, PNA:DNA duplexes are more stable than DNA:DNA duplexes and the stability is independent of ionic strength. PNA is resistant to biochemical degradation processes by nucleases and proteases due to its unnatural peptide backbone. PNA is also capable of binding to DNA duplexes by strand invasion or triplex formation (**Figure 1.2**). These appealing properties of PNA make it a potential candidate as an agent for genetic manipulation and other therapeutics development, as biochemical research tools and as a probe for diagnostic purposes.[2-4]

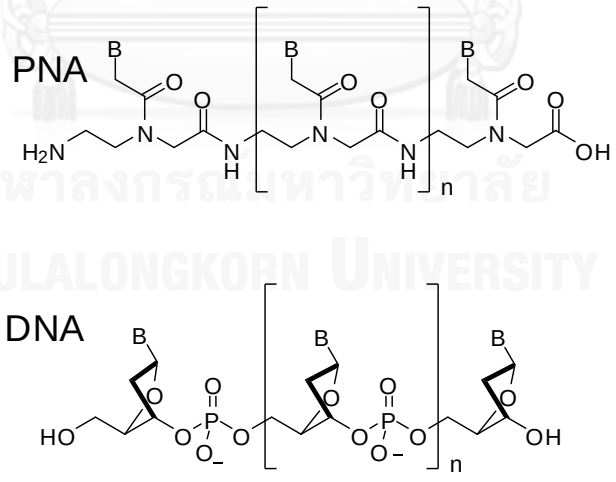

Figure 1.1 Chemical structures of PNA and DNA

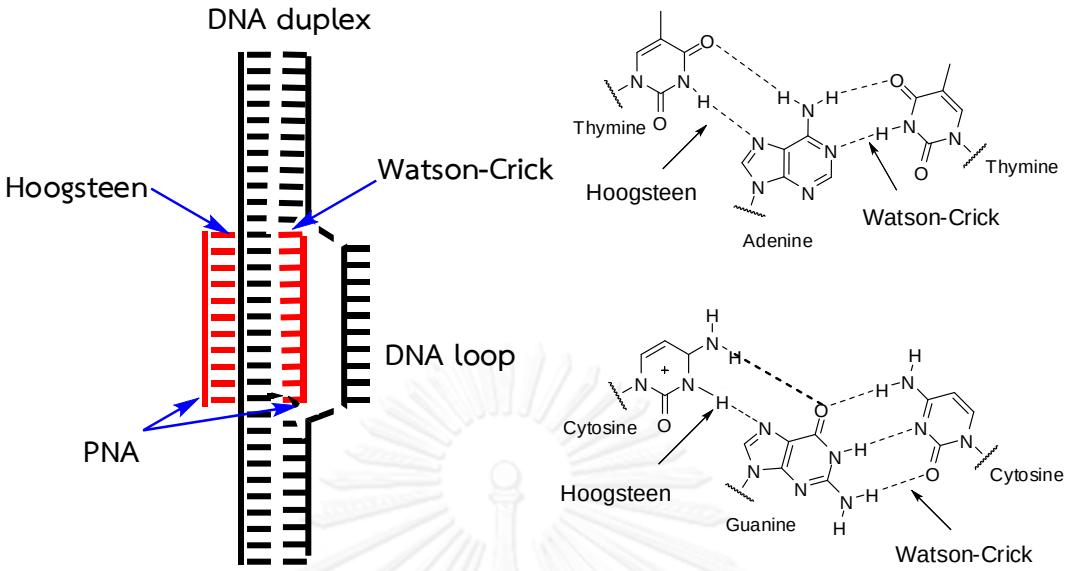

Figure 1.2 DNA duplex invasion by triplex-forming PNA (left) and base pairing schemes in the T:A:T (top, right) and C^+:G:C (bottom, right) triplex formation[4]

1.2 Pyrrolidinyl PNA

Pyrrolidinyl PNA was introduced as a new conformationally constrained analogue of PNA. It was proposed that the presence of the pyrrolidine ring should lock the PNA into a rigid conformation that is suitable for binding to its DNA or RNA target. This should result in an improved binding properties compared to the more flexible PNA developed by Nielsen. The chemical structure of pyrrolodinyl PNA consists of a proline that is modified with the nucleobase at the 4-position (equivlent to a nucleoside) and a spacer amino acid (equivalent to a phosphate group) (**Figure 1.3**). Originally, the configuration of the pyrrolidine ring was chosen to mimic that of natural nucleoside, but was also subsequently confirmed by comparing the DNA binding properties of all possible stereoisomers.[5-8] Many spacers have been studied systematically, and it was found that the spacer deriving cyclic β-amino acids is the most promising.[9-12]

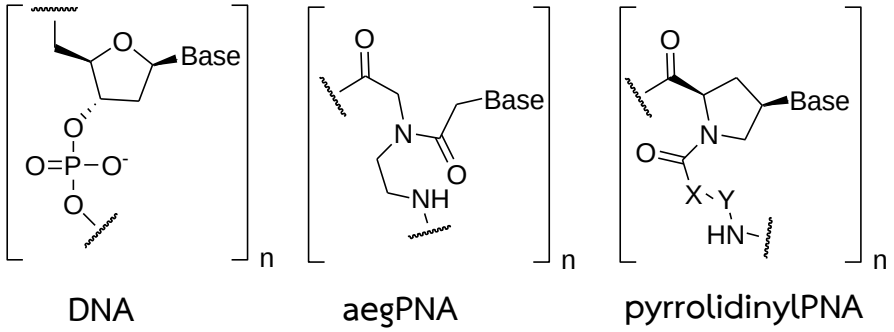

Figure 1.3 The generic structure of pyrrolidinyl PNA (right) compared to DNA (left) and Nielsen's aegPNA (middle)

1.2.1 Effects of stereochemistry on pyrrolidine ring and spacer

Starting from 2001, Vilaivan *et al.*[9, 10] had studied pyrrolidinyl PNA systems deriving from several combinations of pyrrolidinyl nucleoside and various β-amino acids. The first pyrrolidinyl PNA that exhibits strong DNA binding properties carried the five-membered ring cyclic β-amino acid; 1-aminopyrrolidine-2*R*-carboxylic acid (D-APC); in the structure.[10] The dapcPNA also exhibited selectivity in binding to DNA in preference over RNA. The ring nitrogen atom of the D-APC moiety can be protonated under physiological conditions and might be responsible for the electrostatic attraction to the negatively charged DNA strand.[11] Nevertheless, the synthesis of the D-APC spacer and its incorporation into PNA were inefficient. In 2005, new pyrrolidinyl PNA systems with pyrrolidinyl nucleoside and all four possible stereoisomers of 2-aminocyclopentanecarboxylic acid spacer were studied, and the (1*S*,2*S*)-isomer was identified to be the most suitable.[12] (**Figure 1.4**)

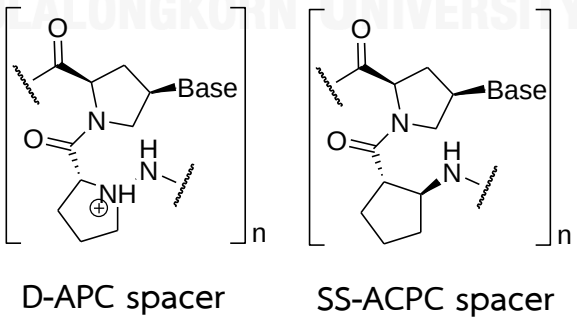

Figure 1.4 Pyrrolidinyl PNA containing five-membered ring cyclic β-amino acid[10, 12]

In 2006, a more detailed study on pyrrolidinyl PNA with *SS*-ACPC spacer (acpcPNA) was reported and the study was extended to mix-base sequences.[13] The acpcPNA recognize DNA with high affinity and sequence specificity. It also shows many unique properties not observed in aegPNA, for example, the preference for binding to DNA over RNA, a very strong preference for antiparallel over parallel binding mode, the inability to form self-hybrid between two complementary strands of acpcPNA. The high specificity of acpcPNA is especially useful for DNA sequence determinaion.[14, 15] So far the configuration of the pyrrolidine nucleoside was fixed as (2*R*,4*R*) to mimic the natural nucleosides. During 2010-2011, a systematic study on the effect of the configuration of the pyrrolidine ring revealed that the (2*R*,4*S*)-isomer of acpcPNA (also called *epi*-acpcPNA) (**Figure 1.5**) also showed similar DNA/RNA binding properties to the (2*R*,4*R*)-isomer.[16, 17] However, one striking difference between the two acpcPNA epimers is the ability of the *epi*-acpcPNA to form self hybrids with moderate stability whereas the acpcPNA cannot do so.

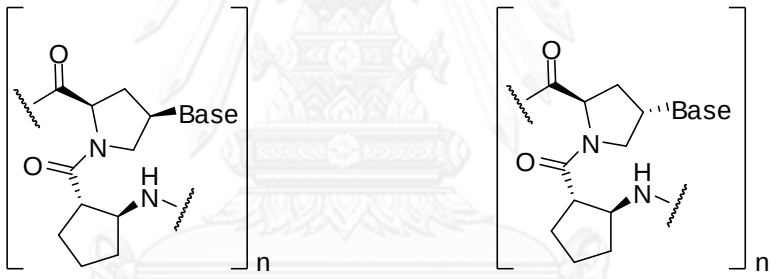

***(2'R,4'R)-SS*-ACPC PNA**
acpcPNA

***(2'R,4'S)-SS*-ACPC PNA**
***epi*-acpcPNA**

Figure 1.5 Two epimers of acpcPNA (left: acpcPNA, right: *epi*-acpcPNA) that show strong DNA binding properties[13, 16]

1.2.2 Effects of amino acid spacer (substituent, ring size)

In 2011, Reenabthue *et al.* showed that a CH_2 group in the cyclopentane ring of acpcPNA could be replaced by a nitrogen atom to produce a new apcPNA with similar binding affinity to DNA.[18] The nitrogen atom provides a convenient handle for backbone modification of the PNA. In 2012, Mansawat et al. studied the spacer ring size effects on the stability of pyrrolidinyl PNA:DNA hybrids and reported that the pyrrolidinyl PNA with four-membered ring spacer (acbcPNA) provided an improved

DNA binding affinity but the six-membered ring spacer showed no DNA binding at all (**Figure 1.6**).[19] The results were explained in terms of different torsional angles of the NH-C-C-CO part of the spacer. The four-membered ring appeared to have a native torsional angle that is most compatible with the DNA-bound conformation of dapcPNA and acpcPNA.

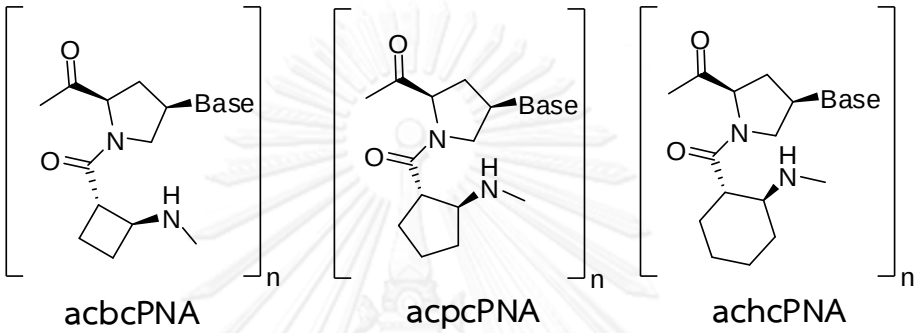

Figure 1.6 Pyrrolidinyl PNA containing different ring size of cyclic β-amino acid[19]

1.3 Limitation of PNA and how to solve the problem

Although PNA offers many advantages, the achiral and uncharged backbone of aegPNA resulted in unwanted consequences such as parallel/antiparallel binding selectivity, solubility in aqueous system, self-aggregation and nonspecific binding with hydrophobic molecules. In addition to pyrrolidinyl PNA described above, several other PNA analogues have been developed by other research groups over the past two decades. Some examples of which are shown in **Figure 1.7**. In this chapter, only modification with the aim to improve aqueous solubility and reduce non-specific aggregation will be discussed.

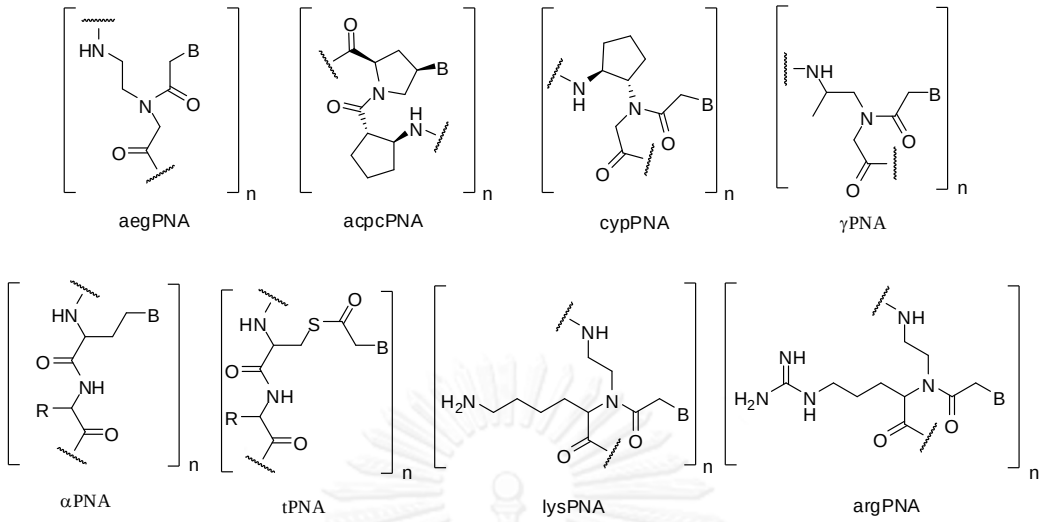

Figure 1.7 Chemical structure of DNA and PNA derivatives, and analogues[4]

Efforts to improve aqueous solubility have been made shortly after the introduction of aegPNA, for example, by incorporation of a hydrophilic group either to the end of the PNA molecule,[20, 21] to the PNA monomer,[22] or to the nucleobase.[23]

Recently, it was reported that introduction of a small substituent at the γ-position of aegPNA resulted in a γ-PNA that displays superior DNA binding properties over aegPNA, which was explained by the conformation pre-organization. To increase solubility in water and decrease non-specific aggregation of γ-PNA, incorporation of an (*R*)-diethylene glycol (DEG) substituent was made at the γ-position (**Figure 1.8**). The DEG-modified γ-PNA exhibited improved water solubility. The reduced non-specific binding was clearly demonstrated by electrophoresis and FRET experiments.[24]

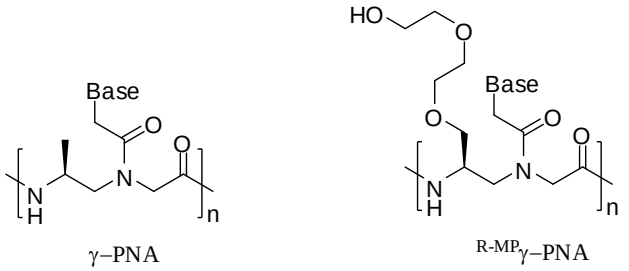

Figure 1.8 Chemical structure of γ-PNA and more water soluble (*R*)- diethylene glycol γ-PNA[24]

1.4 Sugar-derived cyclic β-amino acids and foldamers

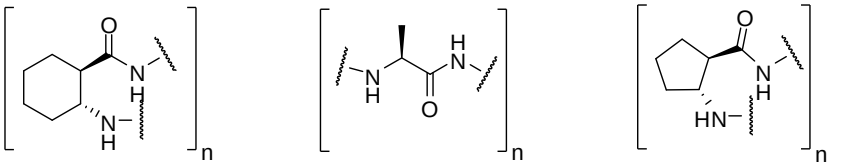

trans-(*RR*)-ACHC
14-helix

L-alanine
α-helix

trans-(*RR*)-ACPC
12-helix

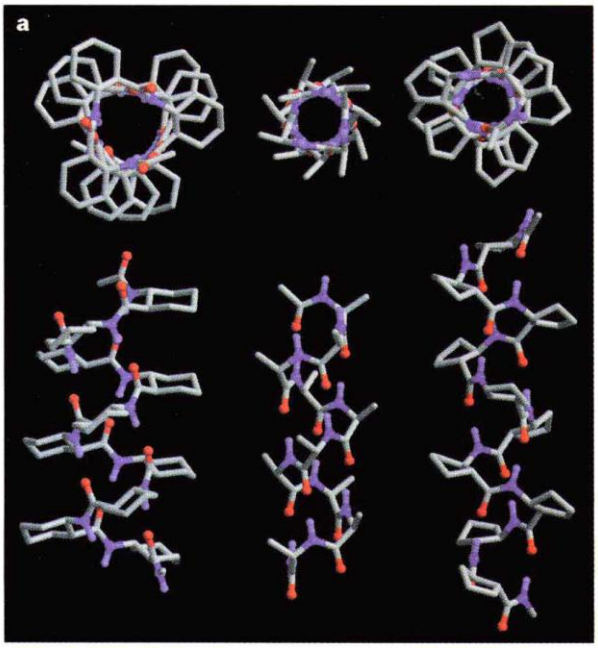

Figure 1.9 Regular structures of foldamers deriving from oligomers of (left to right) [*trans*-(*RR*)-ACHC, L-alanine, *trans*-(*RR*)-ACPC]. The structures were presented along and perpendicular to the helix axis (from N termini in the first case) (the figure was taken from reference[25])

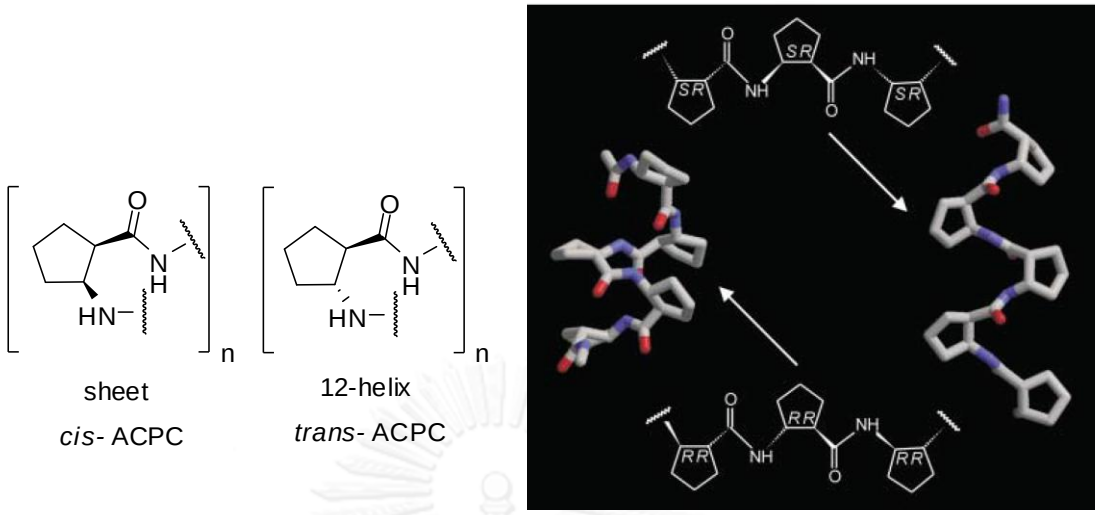

Figure 1.10 The closely similar *cis*- and *trans*-ACPC oligomers gave totally different folding patterns.[26]

Foldamers are synthetic oligomers that are designed to fold into a well-defined and predictable secondary structure through non-covalent interactions such as hydrogen bonding, hydrophobic interaction and π-π stacking.[25-28] One of the most widely studied types of foldamers are β-peptides deriving from cyclic β-amino acids (**Figure 1.9-1.10**).[25, 26, 28-33] Due to their structural rigidity, the ability to fine tune by changing the ring size, functional group and stereochemistry, and hydrophilic nature, sugar-derived amino acids (**Figure 1.11**) [34-38] are important building blocks for the synthesis of new foldamers.

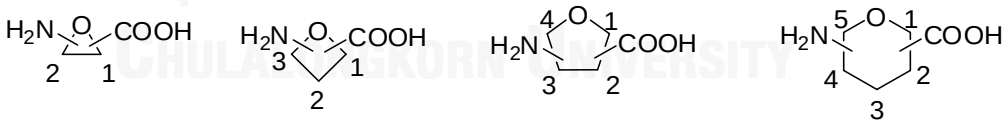

Figure 1.11 Various types of sugar-derived amino acids[37, 38]

L-Rhamnose-derived oxetane β-amino acids oligomers were synthesized and their solution structures (**Figure 1.12**) were investigated by NMR to show left-handed helical structures that were stabilized by a 10-membered hydrogen bonding (10-helix).[39, 40]

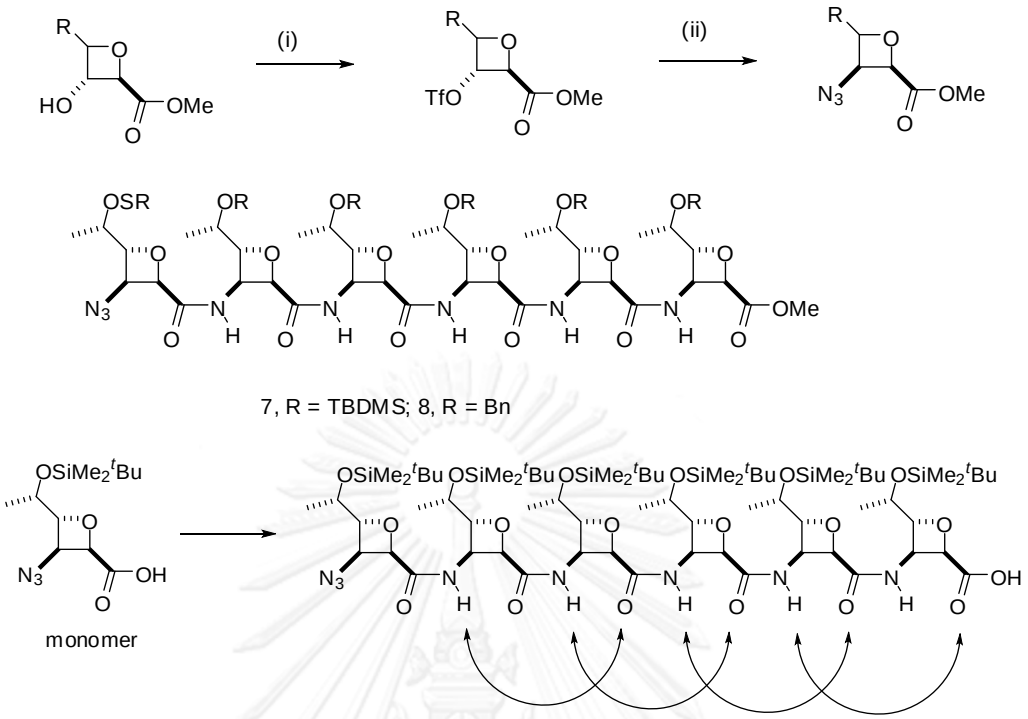

Figure 1.12 The 10-helix structure of oligomers of L-rhamnose-derived oxetane β-amino acids.[39, 40]

A number of foldamers derived from five-membered ring sugar-derived β-amino acids have been recently reported in the literature. For examples, an oligomer of xylofuranose-derived β-amino acid with a *cis*- arrangement between the amine and the carboxyl groups adopts a 14-helix conformation.[41]

The stereochemistry of the building block had significant impact on the folding pattern of the foldamers deriving from simple sugar-derived five-membered β-amino acids (FAA). Moreover, there are subtle differences between the carbocyclic and heterocyclic analogues (**Figure 1.13**). The homo-oligomers of *trans*-ACPC and *trans*-FAA adopts a similar 14-helix structure. However, the *cis*-ACPC oligomer adopts a non-helical sheet-like structure while the corresponding *cis*-FAA oligomer adopts a 14-helix (see **Figure 1.10**). It was suggested that replacement of the CH_2 in the cyclopentane ring with the oxygen may change the foldamer conformation due to loss of van der Waals contact within the backbone.[33, 42] Substitution of the THF ring with a methoxy group doesn't change the preference of the helix formation for both *cis*- and *trans*-FAA oligomers.[45]

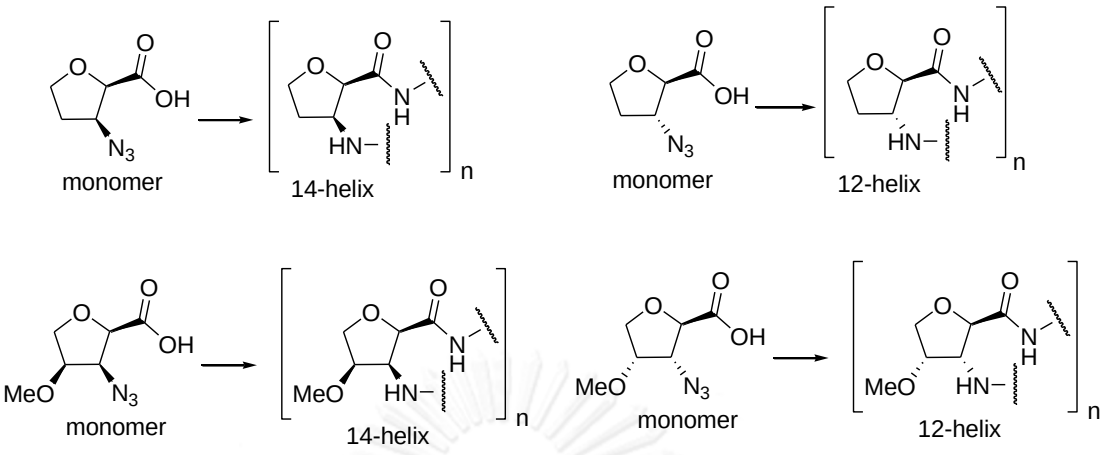

Figure 1.13 Foldamers derived from 2-aminotetrahydrofurancarboxylic acids (FAA)[33, 42]

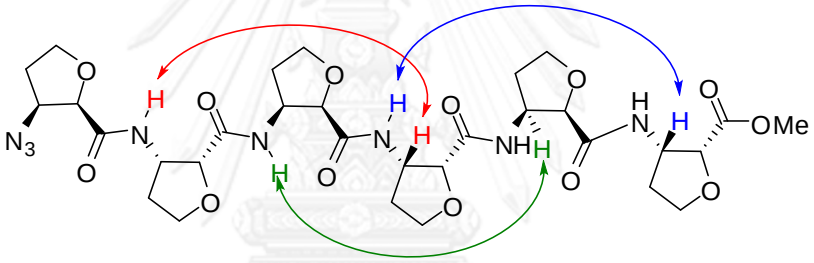

Figure 1.14 NOESY correlation in oligomers of *cis*-FAA revealing the 14-helical H-boding pattern[33]

Oligomers of a zidovudine (AZT)-derived *trans*-cyclic β-amino acid were synthezied and their structures were reported in 2008. An NMR study of the short oligomers suggested a right-handed 12-helix structure similar to *trans*-ACPC oligomers (**Figure 1.15**).[43] On the other hand, a different study on the same oligomer proposed a 8-helix.[44] The same (AZT)-derived cyclic β-amino acid had been used as a component of a new PNA with α/β-peptide backbone.[45]

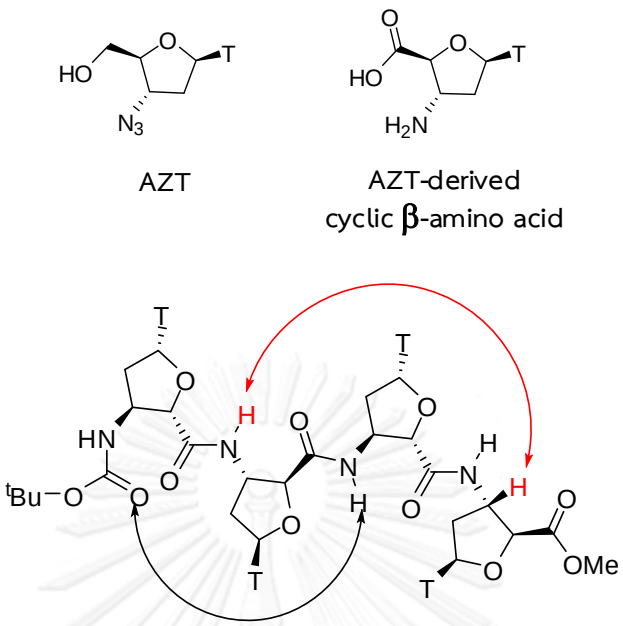

Figure 1.15 NOESY correlation in oligomers of AZT-derived *trans*-cyclic β-amino acid revealing the 14-helical H-bonding pattern.[43]

A water-soluble glycopeptide foldamer was synthesized from sugar-derived tetrahydrofuran δ-amino acids.[46] The formation of a well-defined helical structure was observed regardless of the substituent on the THF ring (OBn, azide). The azide-containing foldamers allow further functionalization with other biologically active groups via Click chemistry (**Figure 1.16**).

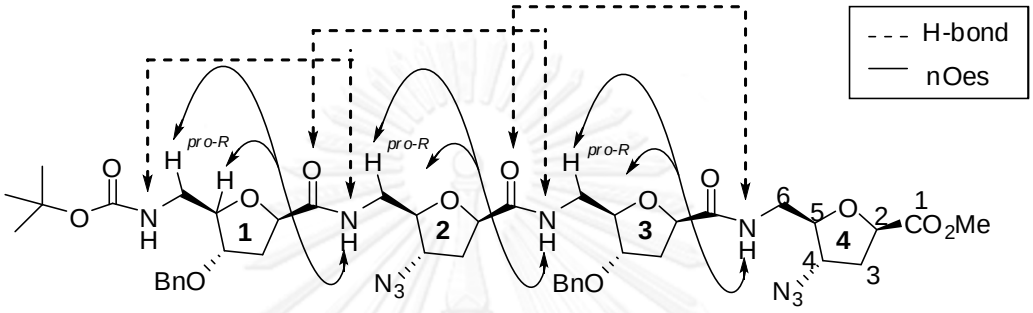

Figure 1.16 Chemical structure of water-soluble a foldamer deriving from sugar-derived tetrahydrofuran δ-amino acids.[46]

An example of foldamer derived from six-membered ring β-amino acids with a tetrahydropyran core was recently reported (**Figure 1.18**).[47] The mixed oligomers with alternating tetrahydropyran β-amino acids and β-alanine or L,D-alanines gave foldamers with 12/10 and 9/11 mixed helices, respectively. Interestingly, helices with opposite handedness can be accommodated within the same peptide chain.

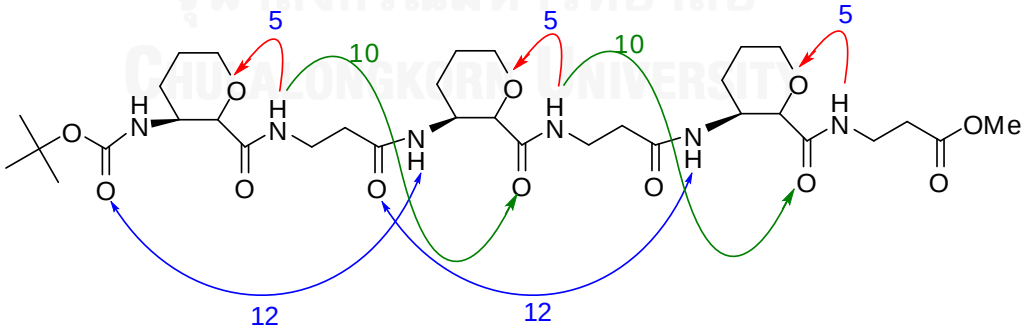

Figure 1.17 Chemical structure of a foldamer deriving from six-membered ring β-amino acids[47]

1.5 Rationale and objectives of this work

AcpcPNA carry the hydrophobic cyclopentane rings in the backbone which might be at least partially contribute to its hydrophobicity - which in turn results in undesirable non-specific interactions with hydrophobic molecules. This behavior limits the practical use of acpcPNA. We propose to synthesize a new pyrrolidinyl PNA with a replacement of the ACPC spacer with a more hydrophilic tetrahydrofuran β-amino acid with the aim to decrease the hydrophobicity of the PNA without affecting the DNA binding properties. This requires synthesis and characterization of the (2*S*,3*S*)-3-aminotetrahydrofuran-2-carboxylic acid (*SS*-ATFC) building block in a suitably protected form. The *SS*-ATFC will be incorporated into the new atfcPNA in a similar manner to the ACPC spacer. The atfcPNA will be studied for its DNA/RNA binding properties and non-specific interactions with hydrophobic materials and compared to acpcPNA under identical conditions.

SS-ATFC
(*2S*, *3S*)-3-aminotetrahydrofuran-2-carboxylic acid

atfcPNA

Figure 1.18 Chemical structure of *SS*-ATFC and atfcPNA

CHAPTER II

EXPERIMENTAL SECTION

2.1 General

All reactions were performed in clean and oven dried glassware. Melting points were recorded on an electrothermal melting point apparatus model 9100. Evaporation of solvents was carried out on a Büchi Rotavapor R 200 with Büchi Vacuum pump V 700 or a water aspirator. The reactions were monitored by thin layer chromatography (TLC) using Merck D.C. silica gel 60 F_{254} 0.2 mm pre-coated aluminium plates and visualized using either UV light (254 nm), *p*-anisaldehyde, ninhydrin, iodine, 2,4-DNP, aqueous potassium permanganate, or ceric molybdate reagent. Column chromatography was performed on silica gel 70-230 mesh (for general chromatography).

IR spectra were acquired as a neat film on NaCl plates on a Nicolet 6700 FTIR spectrometer. Optical rotations ($[\alpha]_D$) were measured on a Jasco P-1010 Polarimeter using sodium light (D line, 589.3 nm) and are reported in degrees; concentrations (c) are reported as g/100 mL. Proton (^{1}H) and carbon (^{13}C) nuclear magnetic resonance (NMR) spectra were recorded on a Varian Mercury-400 plus or a Bruker Advance 400, both are operating at 400 MHz (^{1}H) and 100 MHz (^{13}C). Chemical shifts (δ) are reported in parts per million (ppm) relative to tetramethylsilane (TMS) or referenced to the solvent used ($CDCl_3$ δ 7.27 ppm, DMSO-d_6 δ 2.50 ppm, D_2O δ 4.80 ppm). *J*-values correspond to two- or three-bond proton-proton coupling, unless otherwise noted and are reported in Hertz (Hz). High resolution mass spectrometry (HRMS) was performed on a MicroTOF (Bruker) spectrometer (Department of Chemistry, Faculty of Science, Mahidol University).

Reverse phase high performance column chromatography (reverse phase HPLC) experiments were performed on Water Delta 600 controller system equipped with a gradient pump and a Water 2996 photodiode array detector (D_2 lamp). Alternatively, Rheodyne 7725 manual sample loop (100 µL sample size), column: ACE 5 A71197, C18-AR, 150 x 4.6 mm, 5 µm particle size for separation and Vertisep UPS, 50 x 4.6 mm, 3 µm particle size for analytical purification. Peak monitoring and data processing were performed with the base Empower software. Fractions from

HPLC were collected manually and were assisted by real-time HPLC chromatogram monitoring. The combined fractions were freezed and lyophilized on a Freeze dryer (Labconco). MALDI-TOF mass spectra were obtained on a Microflex MALDI-TOF mass spectrometry (Bruker Daltonik GmbH, Bremen, Germany) in linear positive mode using α-cyano-4-hydroxy cinnamic acid (CCA) as matrix. A mixture of acetonitrile:water (1:1) containing 0.1% trifluoroacetic acid in was used as the diluent for preparation of MALDI-TOF samples. UV and T_m experiments were measured on a CARY 100 Bio UV-Visible spectrophotometer (Varian). Circular dichroism (CD) spectra were measured with a JASCO J-815 CD spectrometer. Fluorescence spectra were recorded with a Cary Eclipse fluorescence spectrometer (Agilent Technologies).

2.2 Materials and methods

All chemicals were purchased from Fluka, Merck or Sigma-Aldrich Chemical Co., Ltd., and were used as received without further purification. Solvents for reactions and crystallization were reagent grade and used without purification. Methanol was dried with 4Å molecular sieves (20% w/v). Dichloromethane was distilled from CaH_2 under nitrogen. Tetrehydrofuran and toluene for Mitsunobu reactions were dried over freshly cut sodium metal, using benzophenone as an indicator and then distilled under nitrogen. Commercial grade solvents were used for column chromatography. HPLC grade acetonitrile and methanol were purchased from BDH and passed through a membrane filter (13 mm ϕ, 0.45 μm Nylon Lida) prior to use. Anhydrous *N*,*N*-dimethylformamide (H_2O ≤ 0.01%) for the solid phase peptide synthesis was obtained from RCI Labscan and was further dried over activated 4Å molecular sieves. The solid support for peptide synthesis (TentaGel S-RAM Fmoc resin, 0.24 mmol/g) was obtained from Fluka. The protected amino acids (Fmoc-L-Lys(Boc)-OPfp) were purchased from Calbiochem Novabiochem Co., Ltd. 5(6)-Carboxyfluorescein *N*-hydroxysuccinimide ester was obtained from Sigma-Aldrich. Trifluoroacetic acid (98%) was obtained from Fluka. Nitrogen gas and hydrogen gas were obtained from Labgas (Thailand) Co., Ltd. with high purity up to 99.995%. MilliQ water was obtained from ultrapure water system with Millipak® 40 filter unit 0.22 μm, Millipore (USA). All oligonucleotides were purchased from Pacific Science (Bangkok, Thailand) or BioDesign Co., Ltd. (Bangkok, Thailand)

2.3 PNA monomers synthesis

The four Fmoc-protected, Pfp-activated pyrrolidinyl PNA monomers (Fmoc-A^{Bz}-OPfp, Fmoc-C^{Bz}-OPfp, Fmoc-G^{Ibu}-OH and Fmoc-T-OPfp), ACPC and APC spacer were synthesized by Ms. Boonsong Ditmangklo (T, ACPC), Ms. Duangrat Nim-Anussornkul (A^{Bz}, C^{Bz}) and Mr. Chayan Charoenpakdee (G^{Ibu}) using the previously reported methods.[13]

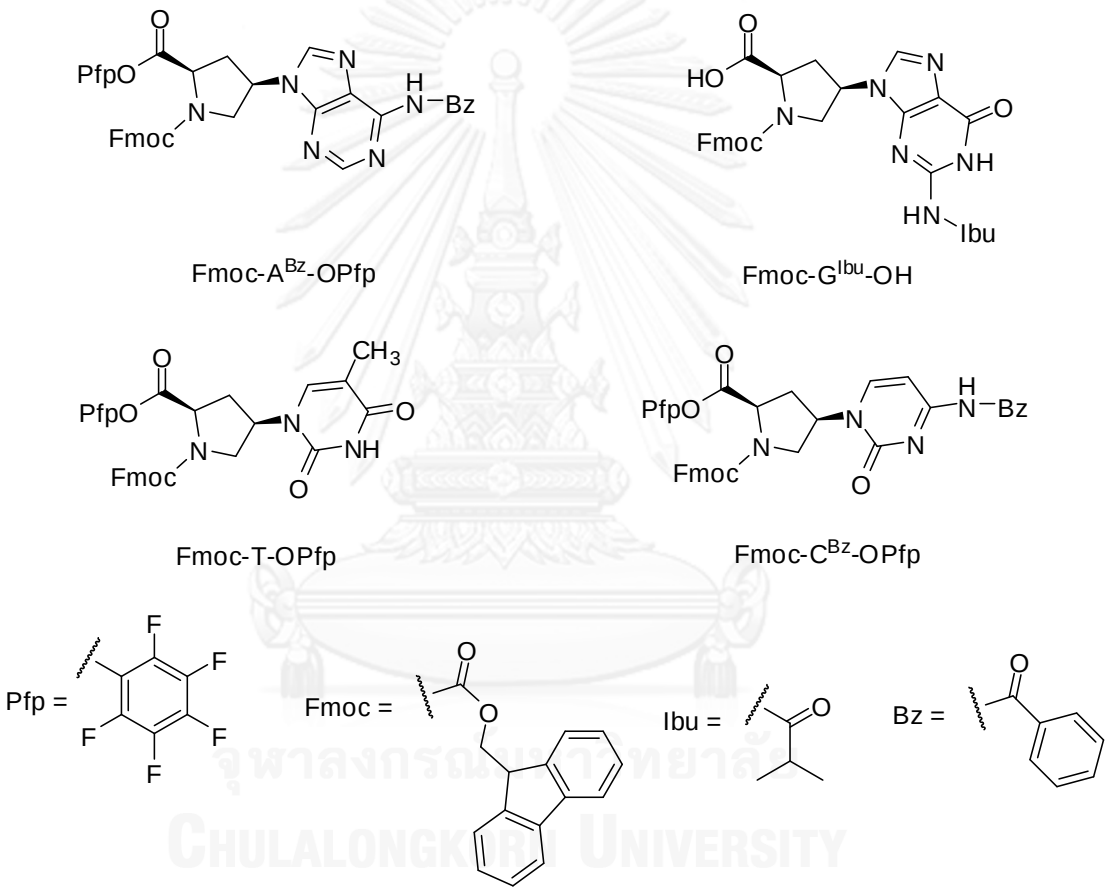

Figure 2.1 Structures of pyrrolidinyl PNA monomers used for the solid phase peptide synthesis.

2.4 ATFC spacer synthesis

2.4.1 The main pathway

2.4.1.1 2-Deoxy-D-ribose methyl glycoside (3) (mixture of α and β anomers)

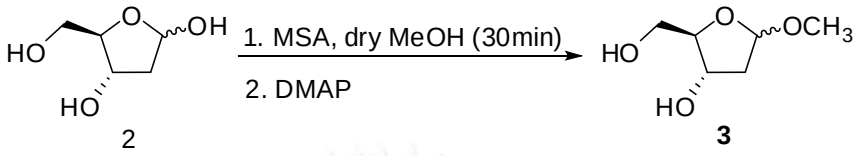

2-Deoxy-D-ribose (11.4 g, 84.9 mmol) was dissolved in anhydrous methanol (55 mL) under a nitrogen atmosphere and then methanesulfonic acid (0.27 mL, 4.16 mmol) was added at room temperature. The reaction reached completion after stirring for 30 minutes at room temperature as confirmed by TLC analysis (MeOH:CH_2Cl_2 1:9, *p*-anisaldehyde stain; R_f = 0.42). The reaction was then quenched by the portionwise addition of DMAP (1.02 g, 8.35 mmol). The reaction mixture was then concentrated under reduced pressure with azeotropic distillation with toluene to afford a brown syrup (14.15 g, >90% purity by TLC), which was used for the next steps without further purification.

2.4.1.2 5-O-p-Toluoyl-2-deoxy-D-ribose methyl glycoside (mixture of α and β anomers) (4a)

Conditions 1

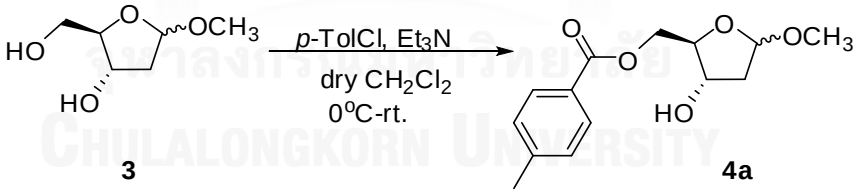

A solution of *p*-toluoyl chloride (5.5 mL, 41.6 mmol) in CH_2Cl_2 (35 mL) was added dropwise to a solution of compound **3** (6.638 g, 44.8 mmol) in anhydrous CH_2Cl_2 (20 mL) and Et_3N (11.2 mL, 80.3 mmol) at 0 °C under N_2 atmosphere. TLC analysis was used for monitoring the reaction (EtOAc:Hexanes 1:1; *p*-anisaldehyde stain; R_f = 0.33). The reaction mixture was quenched with satd NH_4Cl (50 mL x 2) and extracted with EtOAc (30 mL x 2). The combined organic extracts were washed with water (50 mL), and brine (50 mL), dried over Na_2SO_4, and concentrated under reduced pressure to

afford a brown syrup (9.34 g). The crude mixture was purified by column chromatography on silica gel (4.63 g, 48%). ^{1}H NMR (**Figure A2**)

Conditions 2

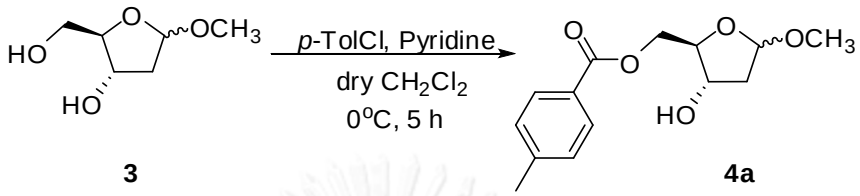

3 **4a**

p-Toluoyl chloride (13 mL, 98.3 mmol) dissolved in anhydrous CH_2Cl_2 (20 mL) was added dropwise to a solution of crude **3** (prepared from 84.9 mmol of **2**) in anhydrous 1:3 pyridine/CH_2Cl_2 (80 mL) at 0 ºC and stirred for 5 hours. The reaction mixture was then diluted with CH_2Cl_2 (20 mL) and washed with cold H_2O (50 mL x 2) and $CuSO_4$ solution (0.05 g/mL). The combined organic extracts were washed with satd $NaHCO_3$ (50 mL x 2), followed by 2 M HCl (50 mL x 2), then dried over Na_2SO_4, concentrated under reduced pressure to afford a brown syrup (21.64 g). The crude product was purified by column chromatography on silica gel to yield compound **4a** as a (colorless oil) in 67% (15.1 g, 56.8 mmol) from **2.** TLC analysis (EtOAc:Hexanes 2:3; *p*-anisaldehyde stain; R_f = 0.27). ^{1}H NMR (400 MHz, $CDCl_3$) (**Figure A2**) δ 2.06-2.23 [2H, m, C$\underline{H}_2$(2)], 2.43 (3H, s, toluoyl C$\underline{H}_3$),3.00-3.02 [1H, d *J* = 10.2 Hz, O$\underline{H}$], 3.42 [3H, s, OC$\underline{H}_3$], 4.26 [1H, t *J* = 7.7 Hz, C$\underline{H}$(4)], 4.31-4.47 [3H, m, C$\underline{H}$(3), C$\underline{H}_2$ (5)], 5.16 [1H, d *J* = 4.5 Hz, C$\underline{H}$(1)], 7.25 (4H, d *J* = 8.1 Hz, toluoyl Ar C$\underline{H}$), 7.92 (2H, d *J* = 8.2 Hz, toluoyl Ar C$\underline{H}$); ^{13}C NMR (100 MHz, $CDCl_3$) (**Figure A3**) δ 21.6 (toluoyl $\underline{C}H_3$), 40.9 [$\underline{C}H_2$(2)], 54.9 (O$\underline{C}H_3$), 64.4 [CH_2(5)], 73.1 [$\underline{C}$H(3)], 85.1 [$\underline{C}$H(4)], 105.5 [CH(1)], 127.0 (toluoyl Ar $\underline{C}$), 129.1 (toluoyl Ar $\underline{C}$H), 129.7 (toluoyl Ar $\underline{C}$), 143.9 (toluoyl Ar $\underline{C}$), 166.4(C=O); IR (thin film) (**Figure A4**) ν_{max} 3467.5, 2949.5, 2917.7, 2828.0, 1716.7 (C=O), 1609.7, 1447.6, 1268.2, 1181.4, 1077.2, 842.8, 758.8 cm^{-1}.

2.4.1.3 5-O-p-Toluoyl-3-O-tosyl-2-deoxy-D-ribose methyl glycoside (5a) (mixture of α and β anomers)

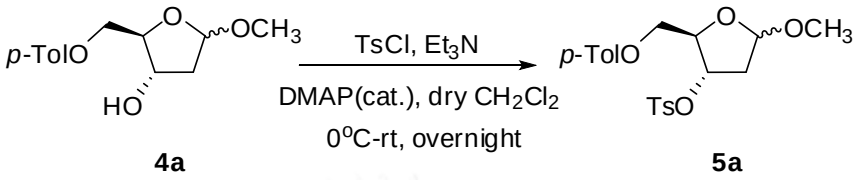

4a **5a**

A solution of **4a** (4.26 g, 16.0 mmol) and DMAP (183 mg, 1.5 mmol) in anhydrous CH_2Cl_2 (10 mL) was cooled to 0 °C under a N_2 atmosphere and treated with Et_3N (5.00 mL, 35.8 mmol), and a solution of TsCl (4.011 g, 21.0 mmol) in CH_2Cl_2 (5 mL). The reaction mixture was allowed to warm to room temperature and monitored by TLC (EtOAc:Hexanes 2:3; *p*-anisaldehyde stain; R_f = 0.42), and then diluted with EtOAc (30mL) and water (40 mL). The reaction mixture was then quenched at 0 °C with 2 M HCl (40 mL x 2) and neutralized with satd. $NaHCO_3$. The combined organic extracts were washed with water (40 mL), brine (40 mL), dried over Na_2SO_4 and evaporated. The crude product (6.40 g) was purified by column chromatography on silica gel to afford compound **5a** (5.59 g, 13.3 mmol, 83% from **4a**). ^{1}H NMR (400 MHz, $CDCl_3$) (**Figure A5**) δ 2.13 [1H, dd *J* = 1.3, 14.8 Hz, C$\underline{H}_a$H$_b$(2)], 2.34 [1H, m, CH$_a$$\underline{H}_b$(2)], 2.39 (3H, s, tosyl C$\underline{H}_3$), 2.42 (3H, s, toluoyl C$\underline{H}_3$), 3.36 [3H, s, OC$\underline{H}_3$], 4.20 [1H, dt *J* = 2.3, 5.6, Hz, C$\underline{H}_a$H$_b$(5)], 4.38-4.44 [2H, m, CH$_a$$\underline{H}_b$(5), C$\underline{H}$(4)], 4.93 [1H, ddd *J* = 2.4, 3.9, 8.3 Hz, C$\underline{H}$(3)], 5.06 [1H, d *J* = 5.1 Hz, C$\underline{H}$(1)]; ^{13}C NMR (100 MHz, $CDCl_3$) (**Figure A6**) δ 21.6 (tosyl $\underline{C}H_3$), 21.7 (toluoyl $\underline{C}H_3$), 39.2 [$\underline{C}H_2$(2)], 55.1 (O$\underline{C}H_3$), 63.0 [$\underline{C}H_3$(5)], 79.4 [$\underline{C}$H(3)], 80.1 [$\underline{C}$H(4)], 104.5 [$\underline{C}$H(1)], 126.9 (toluoyl Ar $\underline{C}$), 127.9 (toluoyl Ar $\underline{C}$H), 129.1 (toluoyl Ar $\underline{C}$H), 129.7 (tosyl Ar $\underline{C}$H), 129.9 (tosyl Ar $\underline{C}$H), 133.4 (tosyl Ar $\underline{C}$), 144.0 (toluoyl Ar $\underline{C}$H), 145.1 (tosyl Ar $\underline{C}$), 166.0 ($\underline{C}$=O); IR (thin flim) (**Figure A7**) ν_{max} 3027.6, 2949.5, 2929.3, 2836.7, 1922.2, 1716.7, 1606.8, 1450.5, 1363.7, 1276.8, 1172.7, 1106.1, 1056.9, 984.6, 920.9, 848.5, 810.9, 753.0, 666.2, 567.8, 550.5 cm^{-1}; HRMS (ESI+) (**Figure A8**) calcd for $C_{21}H_{24}O_7SNa$ (M+Na$^+$) 443.1135, found 443.1137.

2.4.1.4 5-O-p-Toluoyl-3-O-tosyl-1,2-dideoxy-D-ribose (6a)

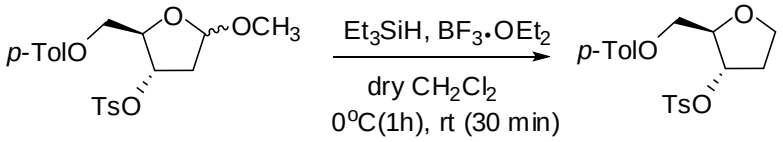

5a **6a**

A solution of compound **5a** (2.41 g, 5.74 mmol) in anhydrous CH_2Cl_2 (2 mL) was cooled to 0 °C and treated with Et_3SiH (2.90 mL, 18.2 mmol), followed by dropwise addition of $BF_3{\cdot}OEt_2$ (2.00 mL, 16.2 mmol). The progress of the reaction was monitored by TLC (EtOAc:Hexanes 1:1;negative *p*-anisaldehyde stain; R_f = 0.58). The reaction mixture was then neutralized with satd. $NaHCO_3$ (30 mL), and extracted with CH_2Cl_2 (3 x 10 mL). The combined organic extracts were dried over Na_2SO_4, and evaporated. The crude product (2.31 g) was purified by column chromatography to afford a colorless oil **6a** (1.92 g, 4.57 mmol, 86% from **5a**). ^{1}H NMR (400 MHz, $CDCl_3$) (**Figure A9**) δ 2.12 [2H, td *J* = 5.6, 7.8 Hz, C$\underline{H}_2$(2)], 2.40 (tosyl C$\underline{H}_3$), 2.42 (toluoyl C$\underline{H}_3$), 3.94 [1H, q *J* = 8.4 Hz, C$\underline{H}_a$H$_b$(1)], 4.05 [1H, m, CH$_a\underline{H}_b$(1)], 4.16-4.27 [3H, m, C$\underline{H}_2$(5), C$\underline{H}$(4)], 5.00 [1H, m, C$\underline{H}$(3)], 7.24 (2H, d *J* = 8.1 Hz, toluoyl Ar C$\underline{H}$), 7.28 (2H, d *J* = 8.2 Hz, tosyl Ar C$\underline{H}$), 7.77 (2H, d *J* = 8.1 Hz, tosyl Ar C$\underline{H}$), 7.87 (2H, d *J* = 8.3 Hz, toluoyl Ar C$\underline{H}$); ^{13}C NMR (100 MHz, $CDCl_3$) (**Figure A10**) δ 21.6 (toluoyl C$\underline{H}_3$), 21.7 (tosyl C$\underline{H}_3$), 33.1 [C$\underline{H}_2$(2)], 63.6 [C$\underline{H}_2$(5)], 67.4 [C$\underline{H}_2$(1)], 81.6 [C$\underline{H}$(3)], 82.2 [C$\underline{H}$(4)], 126.9 (toluoyl Ar C$\underline{}$), 127.8 (tosyl Ar C$\underline{H}$), 129.2 (toluoyl Ar C$\underline{H}$), 129.7 (toluoyl Ar C$\underline{H}$), 130.0 (tosyl Ar C$\underline{H}$), 133.6 (tosyl Ar C$\underline{}$), 144.0 (toluoyl Ar C$\underline{}$), 145.1 (tosyl Ar C$\underline{}$), 166.1 (C$\underline{}$=O); IR (thin film) (**Figure A11**) ν_{max} 2958.2, 2880.1, 1716.75 (C=O), 1606.8, 1447.6, 1363.7, 1268.2, 1172.7, 1091.6, 1016.4, 955.6, 906.4, 816.7, 753.0, 669.1, 553.4 cm^{-1}; $[\alpha]_D^{23}$ = +30.1° (*c* = 1.0 g/100 mL, CH_2Cl_2); HRMS (ESI+) (**Figure A12**) calcd for $C_{20}H_{22}O_6SNa$ (M+Na$^+$) 413.1029, found 413.1026.

2.4.1.5 ((2R,3R)-3-Hydroxytetrahydrofuran-2-yl)methyl-4-methylbenzoate (7a)

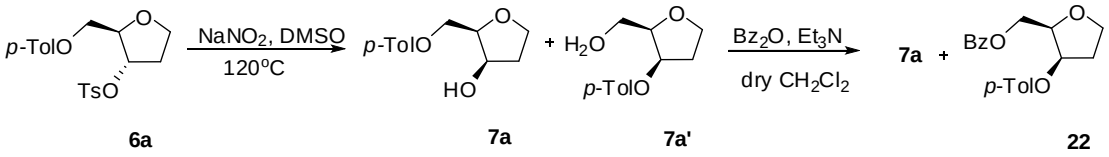

6a **7a** **7a'** **22**

A solution of compound **6a** (1.08 g, 2.77 mmol) in DMSO was treated with $NaNO_2$ (0.96 g, 13.9 mmol) and heated to 120 °C for 5 hours. The reaction was monitored by TLC analysis (EtOAc:Hexanes 1:1; R_f = 0.27), and then diluted with water. The aqueous layer was then extracted with CH_2Cl_2 (3 x 10 mL) and the combined organic extracts were washed with brine, dried over Na_2SO_4 and evaporated. The crude product was purified by column chromatography to afford a mixture of **7a** and the toluoyl migrate product **7a'** in a 1:1 ratio as determined by NMR analysis (0.41 g, 1.75 mmol, combined yield 63% from **5a**). The regioisomeric mixture was dissolved in anhydrous CH_2Cl_2 (3 mL), cooled to 0 °C and then treated with Et_3N (1.25 mL, 8.96 mmol) and Bz_2O (0.3370 g, 1.49 mmol). The reaction mixture was concentrated to dryness and purified by column chromatography on silica gel to yield **7a** in 28% yield from **6a** (0.18 g, 0.77 mmol). ^{1}H NMR (400 MHz, $CDCl_3$) (**Figure A13**) δ 2.05 [1H, dddd *J* = 1.5, 3.8, 7.1, 13.4 Hz, C$\underline{H}_a$H$_b$(4)], 2.18 [1H, m, CH$_a$$\underline{H}_b$(4)], 2.41 (3H, s, toluoyl C$\underline{H}_3$), 3.89 [1H, ddd *J* = 3.8, 8.6 Hz, C$\underline{H}_a$H$_b$(5)], 3.96 [1H, ddd *J* = 3.3, 5.4, 7.1 Hz, CH(2)], 4.11 [1H, dt *J* = 7.3, 8.5 Hz, CH$_a$$\underline{H}_b$(5)], 4.37 (1H, dd *J* = 5.4, 11.6 Hz, C$\underline{H}_a$H$_b$ methyl benzoate), 4.38 [1H, m, C$\underline{H}$(3)], 4.77 (1H, dd, *J* = 7.1, 11.6 Hz, CH$_a$$\underline{H}_b$ methyl benzoate), 7.24 (2H, d, *J* = 8.0 Hz, toluoyl C$\underline{H}$), 7.94 (2H, d, *J* = 8.2 Hz, toluoyl C$\underline{H}$); ^{13}C NMR (100 MHz, $CDCl_3$) (**Figure A14**) δ 21.7 (toluoyl $\underline{C}H_3$), 35.1 [$\underline{C}H_2$(4)], 62.6 ($\underline{C}H_2$ methylbenzoate), 66.5 [$\underline{C}H_2$(5)], 71.5 [$\underline{C}$H(3)], 80.6 [$\underline{C}$H(2)],126.9 (toluoyl Ar $\underline{C}$), 129.2 (toluoyl Ar $\underline{C}$H), 129.8 (Ar $\underline{C}$), 144.1 (toluoyl Ar $\underline{C}$), 167.2 ($\underline{C}$=O); IR (ATR) (**Figure A18**) ν_{max} 3420.7, 2986.2, 2950.6, 2923.3, 2896.0, 2868.7, 1704.4 (C=O), 1611.5, 1444.7, 1269.8, 1174.2, 1100.4, 1021.1, 969.2, 834.5, 750.6, 693.2 cm^{-1}; m.p. 65-67 °C; $[\alpha]_D^{23}$ = –4.3° (*c* = 1.0 g/100 mL, CH_2Cl_2).

2.4.1.6 ((2R,3R)-3-(Methylsulfonyloxy)tetrahydrofuran-2-yl)methyl 4-methylbenzoate (8a)

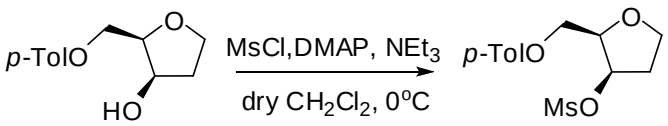

7a **8a**

A solution of **7a** (0.49 g, 2.05 mmol) in anhydrous CH_2Cl_2 (4 mL) was cooled to 0 °C and treated with DMAP (50 mg, 0.41 mmol), Et_3N (1.15 mL, 8.25 mmol) and MsCl (0.48 mL, 6.15 mmol). After 1 hour, the reaction reached completion as indicated by TLC (Acetone:CH_2Cl_2 1:4; R_f = 0.76), and it was then diluted with H_2O (10 mL) and EtOAc (10 mL). The aqueous layer was extracted with EtOAc (3 x 10 mL) and the combined organic extracts were washed with brine, dried over Na_2SO_4 and concentrated under reduced pressure. The crude product (0.62 g) was purified by column chromatography to afford **8a** as a white solid (0.58 g, 90% from **7a**). ^{1}H NMR (400 MHz, $CDCl_3$) (**Figure A19**) δ ppm 2.32-2.46 [2H, m, C$\underline{H}_2$(4)], 2.41 (3H, s, toluoyl C$\underline{H}_3$), 3.96 [1H, dt *J* = 2.7, 8.5 Hz, C$\underline{H}_a$H$_b$(5)], 4.15 [1H, q *J* = 8.2 Hz, CH$_a\underline{H}_b$(5)], 4.25 [1H, dt *J* = 4.0, 6.1 Hz, C$\underline{H}$(2)], 4.53 (2H, d *J* = 6.0 Hz, C$\underline{H}_2$ methylbenzoate), 5.38 [1H, br m, C$\underline{H}$(3)], 7.24 (2H, d *J* = 8.1 Hz, toluoyl Ar C$\underline{H}$), 7.94 (2H, d *J* = 7.8 Hz, toluoyl Ar C$\underline{H}$); ^{13}C NMR (100 MHz, $CDCl_3$) (**Figure A20**) δ 21.7 (toluoyl $\underline{C}H_3$), 34.0 [$\underline{C}H_2$(4)], 38.5 (mesyl $\underline{C}H_3$), 62.2 ($\underline{C}H_2$ methylbenzoate), 66.5[$\underline{C}H_2$(5)], 78.8 [$\underline{C}$H(3)], 79.9[$\underline{C}$H(2)], 127.0 (toluoyl Ar $\underline{C}$), 129.2 (toluoyl Ar $\underline{C}$H), 129.8 (toluoyl Ar $\underline{C}$H), 144.0 (toluoyl Ar $\underline{C}$), 166.2 ($\underline{C}$=O); IR (KBr) (**Figure A21**) ν_{max} 3424.1, 3024.8, 2964.0, 2940.8, 2891.6, 2862.7, 1722.5 (C=O), 1609.6, 1349.2, 1271.1, 1178.5, 1109.0, 1010.6, 967.2, 897.7, 750.2, 524.4 cm^{-1}; m.p. 102-104 °C; $[\alpha]_D^{23}$ = -44.1° (*c* = 1.0 g/100 mL, CH_2Cl_2); HRMS (ESI+) (**Figure A22**) calcd for $C_{14}H_{18}O_6SNa$ (M+Na$^+$) 337.0716, found 337.0716.

2.4.1.7 Alternate synthesis of ((2R,3R)-3-(methylsulfonyloxy)tetrahydrofuran-2-yl)methyl 4-methylbenzoate (8a)

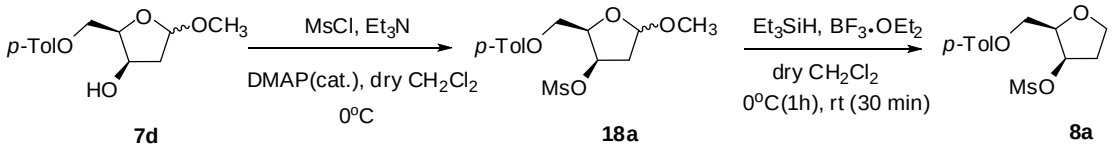

7d **18a** **8a**

A solution of **7d** (0.45 g, 1.7 mmol) in anhydrous CH_2Cl_2 (2 mL) was cooled to 0 °C and treated with DMAP (48.0 mg, 0.40 mmol), Et_3N (0.95 mL, 6.8 mmol) and MsCl (0.40 mL, 5.2 mmol). After the completion of the reaction as indicated by TLC analysis (Acetone:CH_2Cl_2 1:4; R_f = 0.76), it was then poured into cold water and extracted with EtOAc. The organic layer was extracted with saturated $NaHCO_3$, dried over anhydrous Na_2SO_4 and concentrated to dryness. After removal of the solvent, the crude **18a** (0.50 g) was dried over a water bath. It was next dissolved in anhydrous CH_2Cl_2 (2 mL), cooled to 0 °C and treated with Et_3SiH (0.70 mL, 4.4 mmol) under N_2 atmosphere, followed by dropwise addition of BF_3•OEt_2 (0.50 mL, 4.0 mmol). The reaction was stirred at 0 °C for 1 hour and then allowed to warm up to room temperature for 0.5 hours. The progress of the reaction was monitored by TLC (EtOAc:Hexanes 1:1; negative *p*-anisaldehyde stain; R_f = 0.58). The reaction mixture was neutralized with saturated $NaHCO_3$ and the aqueous phase was extracted with CH_2Cl_2. The combined organic phases were dried over anhydrous Na_2SO_4 and purified by a silica column chromatography to give compound **6a** as colorless oil (0.31 g, 60% from **7d**). Spectroscopic data are identical to **8a** obtained by the previous procedure.

2.4.1.8 ((2S,3S)-3-Azidotetrahydrofuran-2-yl)methyl-4-methylbenzoate (9a)

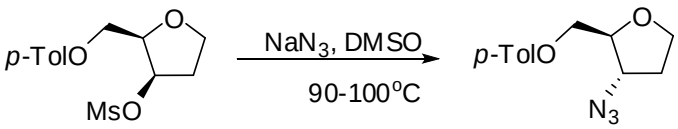

8a **9a**

A solution of **8a** (0.14 g, 0.46 mmol) in DMSO (2 mL) was treated with NaN_3 (0.21 g, 3.15 mmol) and then heated at 90 °C for 2 hours. The progress was monitored by TLC analysis (EtOAc:Hexanes 2:3; R_f = 0.62). After completion of the reaction, it was diluted with water (15 mL) and extracted with EtOAc (3 x 15 mL). The combined organic extracts were dried over Na_2SO_4, and concentrated to dryness to afford compound **9a** as colorless oil (113 mg, 94%), which was subjected to the next step without further purification. ^{1}H NMR (400 MHz, $CDCl_3$) (**Figure A23**) δ 2.04-2.11 [1H, m, C$\underline{H}_a$H$_b$(4)], 2.29 [1H, m, CH$_a$$\underline{H}_b$(4)], 2.42 (3H, s, toluoyl C$\underline{H}_3$), 3.95 [1H, dd *J* = 7.9, 15.9 Hz, C$\underline{H}_a$H$_b$(5)], 4.05-1.10 [3H, m, CH$_a$$\underline{H}_b$(5), C$\underline{H}$(2), C$\underline{H}$(3)], 4.38 (2H, d *J* = 5.0 Hz, C$\underline{H}_2$ methylbenzoate); ^{13}C NMR (100 MHz, $CDCl_3$) (**Figure A24**) δ 21.7 (toluoyl $\underline{C}H_3$), 32.2 [$\underline{C}H_2$(4)], 62.9 [$\underline{C}$H(3)], 64.4 ($\underline{C}H_2$ methylbenzoate), 67.4 [$\underline{C}H_2$(5)], 81.5 [$\underline{C}$H(2)], 127.0 (toluoyl Ar $\underline{C}$), 129.2 (toluoyl Ar $\underline{C}$H), 129.7(toluoyl Ar $\underline{C}$H), 144.0 (toluoyl Ar $\underline{C}$), 166.3 ($\underline{C}$=O); IR (thin flim) (**Figure A25**) ν_{max} 2952.4, 2872.4, 2098.7, 1716.7, 1606.7, 1271.1, 1172.7, 1103.2, 750.2 cm^{-1}; $[\alpha]_D^{23}$ = +63.6° (*c* = 1.6 g/100 mL, CH_2Cl_2); HRMS (ESI+) (**Figure A26**) calcd for $C_{13}H_{15}N_3O_3Na$ (M+Na$^+$) 284.1006, found 284.1003.

2.4.1.9 ((2S,3S)-3-(tert-Butoxycarbonylamino)tetrahydrofuran-2-yl)methyl 4-methylbenzoate (10)

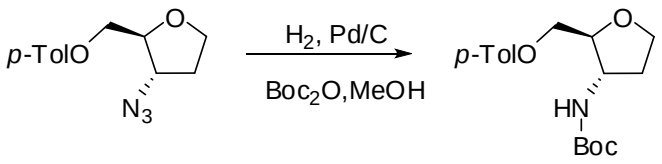

9a **10**

A solution of **9a** (0.47 g, 1.80 mmol) in MeOH (5 mL) was treated with Boc_2O (1.03 g, 4.73 mmol) and Pd/C (20% w/w, 74.2 mg). The reaction flask was flushed with H_2 gas and a H_2 balloon was attached through a rubber septum. The reaction was monitored by TLC analysis (EtOAc:Hexanes 2:3; ninhydrin stain; R_f = 0.46) until completion. It was then filtered through celite, concentrated to dryness and the residue was washed with hexanes to afford **10** as a white solid (0.43 g, 72% from **9a**). ^{1}H NMR (400 MHz, $CDCl_3$) (**Figure A27**) δ 1.44 [9H, s, Boc C$\underline{H}_3$], 1.83 [1H, dt, *J* = 5.7, 12.8 Hz C$\underline{H}_a$H$_b$(4)], 2.34 [1H, ddd, 5.6, 12.9, 14.8 Hz, CH$_a\underline{H}_b$(4)], 2.40 (3H, s, toluoyl C$\underline{H}_3$), 3.90-4.03 [3H, m, C$\underline{H}_2$(5), C$\underline{H}$(2)], 4.16 [1H, m, C$\underline{H}$(3)], 4.34 (1H, dd, *J* = 5.9, 11.8 Hz, methylbenzoate), 4.49 (1H, dd, *J* = 3.5, 11.7, CH$_a\underline{H}_b$ methylbenzoate), 4.71 (1H, br m, N$\underline{H}$), 7.22 (2H, d, *J* = 8.1 Hz, toluoyl Ar C$\underline{H}$), 7.93 (2H, d, *J* = 8.2 Hz, toluoyl Ar C$\underline{H}$); ^{13}C NMR (100 MHz, $CDCl_3$) (**Figure A28**) δ 21.6 (toluoyl $\underline{C}H_3$), 28.4 (Boc $\underline{C}H_3$), 33.3 [$\underline{C}H_2$(4)], 53.2 [$\underline{C}$H(3)], 65.1 ($\underline{C}H_2$ methylbenzoate), 67.2 [$\underline{C}H_2$(5)], 79.9 (Boc $\underline{C}$), 82.9 [$\underline{C}$H(2)], 127.2 (toluoyl Ar $\underline{C}$), 129.1 (toluoyl Ar $\underline{C}$H), 129.8 (toluoyl Ar $\underline{C}$), 143.7 (toluoyl Ar $\underline{C}$), 155.5 ($\underline{C}$=O), 166.5 ($\underline{C}$=O); IR (KBr) (**Figure A31**) ν_{max} 3348.9, 2975.6, 2937.9, 2868.5, 1724.8 (C=O), 1682.0 (C=O), 1609.01, 1528.6, 1432.5, 1369.5, 1271.1, 1172.7, 1108.3, 1077.2, 1021.5, 1001.2, 882.6, 884.9, 753.1, 607.6 cm^{-1}; m.p. 108-110 °C; $[\alpha]_D^{23}$ = +27.9° (*c* = 1.0 g/100 mL, CH_2Cl_2); HRMS (ESI+) (**Figure A32**) calcd for $C_{18}H_{25}NO_5Na$ (M+Na$^+$) 358.1625, found 358.1635.

2.4.1.10 tert-Butyl (2S,3S)-2-(hydroxymethyl)tetrahydrofuran-3-ylcarbamate (11)

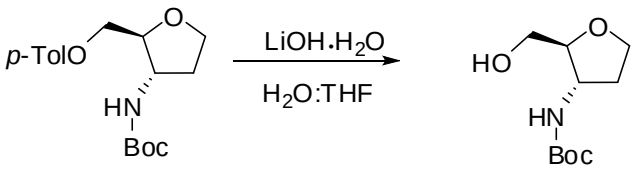

10a **11**

The mixture of **10** (0.39 g, 1.17 mmol) and $LiOH{\cdot}H_2O$ (0.13 g, 3.2 mmol) was dissolved in 1:1 THF:H_2O (4 mL) and stirred at room temperature for overnight. The completion of the reaction was confirmed by TLC analysis (EtOAc:Hexanes 4:1; ninhydrin stain; R_f = 0.33). The excess organic solvent was removed by rotary evaporation and the aqueous residue was extracted with CH_2Cl_2 (3 x 10 mL). The combined organic phases were dried over anhydrous Na_2SO_4 and evaporated to give compound **11** as a white solid (0.23 g, 1.0 mmol, 89% from **4a**). ^{1}H NMR (400 MHz, $CDCl_3$) (**Figure A33**) δ 1.44 (9H, s, Boc CH_3), 1.79 [1H, m, C$\underline{H}_a$$H_b$(4)], 2.29 [1H, dt *J* = 7.5, 14.6 Hz, $CH_a\underline{H}_b$(4)], 2.87 (1H, s, O$\underline{H}$), 3.65-3.69 [3H, m, C$\underline{H}_2$(5), C$\underline{H}$(3)], 3.85-4.00 [2H, m, C$\underline{H}_2$ methylbenzoate, C$\underline{H}$(2)], 4.47 (1H,s, N$\underline{H}$); ^{13}C NMR (100 MHz, $CDCl_3$) (**Figure A34**) δ 28.3 (Boc $\underline{C}H_3$), 33.1 [$\underline{C}H_2$(4)], 52.9 [$\underline{C}$H(3)], 63.1 ($\underline{C}H_2$(5) methylbenzoate), 66.7 [$\underline{C}H_2$(5)], 85.1 [$\underline{C}$H(2)], 155.9 (Boc $\underline{C}$=O); IR (ATR) (**Figure A35**) ν_{max} 3346.8, 2987.4, 2964.1, 2908.1, 2849.5, 1676.0 (C=O), 1522.0, 1363.3, 1300.3, 1239.6, 1160.3, 1097.3, 1073.9, 1015.6, 866.3, 621.2 cm^{-1}; m.p. 85-87 °C; $[\alpha]_D^{23}$ = -11.1° (*c* = 1.0 g/100 mL, CH_2Cl_2); HRMS (ESI+) (**Figure A36**) calcd for $C_{10}H_{19}NO_4Na$ ($M+Na^+$) 240.1206, found 240.1207.

2.4.1.11 Alternate synthesis of tert-butyl (2S,3S)-2-(hydroxymethyl)tetrahydrofuran-3-ylcarbamate (11)

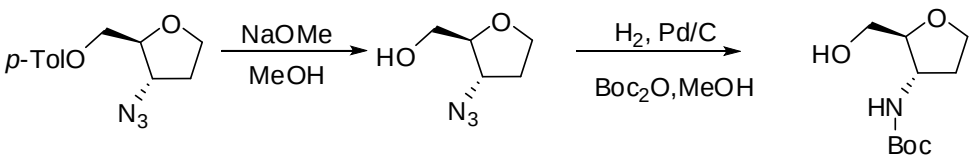

9a **9b** **11**

A solution of **9a** (0.47 g, 1.8 mmol) in dry MeOH (5 mL) was treated with NaOMe (0.31 g, 5.7 mmol). The reaction mixture was stirred at room temperature overnight. The resulting mixture was filtered and evaporated to dryness to afford crude **9b** which was subjected to the next step without purification. A solution of crude **9b** in MeOH (4 mL) was treated with Boc_2O (0.64 g, 2.9 mmol) and Pd/C (20% w/w, 50.1 mg). The reaction flask was flushed with H_2 gas and a H_2 balloon was attached through a rubber septum. The reaction was monitored by TLC analysis (EtOAc:Hexanes 2:3; ninhydrin stain; R_f = 0.46) until completion. It was then filtered through a short plug of celite, concentrated to dryness and purified by column chromatography on silica gel to afford **11** as colorless oil (0.15 g, 39% from **9a**). Spectroscopic data are identical to **11** obtained by the previous procedure.

2.4.1.12 (2S,3S)-3-(tert-Butoxycarbonylamino)tetrahydrofuran-2-carboxylic acid (12)

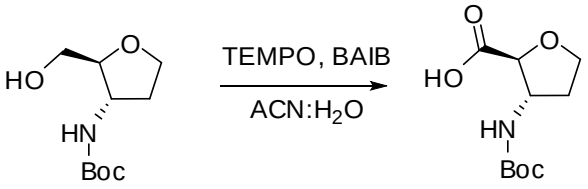

11 **12**

To a solution of **11** (0.27 g, 1.3 mmol) in 1:1 ACN:H_2O was added TEMPO (95 mg, 0.61 mmol) and BIAB (1.13 g, 3.5 mmol). The reaction mixture was stirred overnight at room temperature. The completion of the reaction was controlled by TLC analysis (EtOAc; ninhydrin stain; R_f = 0.17). Then, the resulting solution was basified to pH 8-9 by the addition of solid $NaHCO_3$ and extracted with EtOAc. The collected aqueous phase was acidified to pH 2 with solid $NaHSO_4$ following by EtOAc extraction. The combined organic phases were evaporated to dryness to give **12** as a colorless oil (0.27 g, 93% from **9**). ^{1}H NMR (400 MHz, DMSO-d_6) (**Figure A37**) δ 1.38 (9H, s, Boc CH_3), 1.76 [1H, dt J = 6.3, 12.0 Hz, C$\underline{H}_a$H$_b$(4)], 2.06 [1H, m, CH$_a$$\underline{H}_b$(4)], 3.85-3.89 [2H, m, CH_2(5)], 4.04 [1H, d J = 3.8 Hz, C$\underline{H}$(3)], 4.06-4.14 [1H, br m, C$\underline{H}$ (2)], 7.27 (1H, d J = 6.9 Hz, NH); ^{13}C NMR (100 MHz, DMSO-d_6) (**Figure A38**) δ 28.1 (Boc $\underline{C}H_3$), 31.6 [$\underline{C}H_2$(4)], 54.9 [$\underline{C}$H(3)], 67.1[$\underline{C}H_2$(5)], 77.9 (Boc $\underline{C}$), 81.0 [$\underline{C}$H(2)], 154.9 (Boc $\underline{C}$=O), 172.7 [$\underline{C}$=O (1)]; IR (thin flim) (**Figure A39**) ν_{max} 3328.6, 2972.7, 1710.9 (C=O), 1528.6, 1363.7, 1279.7, 1161.1, 1100.3, 1016.4 cm^{-1}; $[\alpha]_D^{22}$ = +49.1° (c = 1.5 g/100 mL, DMSO); HRMS (ESI+) (**Figure A40**) calcd for $C_{10}H_{17}NO_5Na$ (M+Na$^+$) 254.0999, found 254.0992.

2.4.1.13 (2S,3S)-3-(((9H-Fluoren-9-yl)methoxy)carbonylamino)tetrahydrofuran-2-carboxylic acid (13)

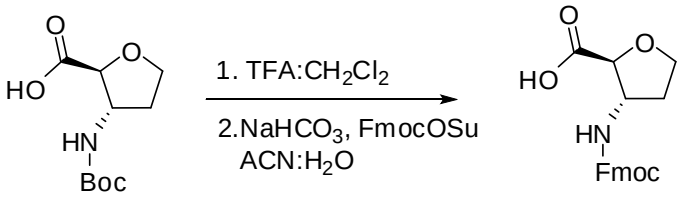

12 **13**

Compound **12** (0.115 g, 0.498 mmol) was dissolved in 1:1 TFA:CH_2Cl_2 (4 mL) and left at room temperature for 30 min. The solvent was evaporated by flushing with N_2. The crude amino acid was dissolved in ACN:H_2O 1:1 (4 mL) and the pH of the solution was adjusted to 8-9 by the addition of solid $NaHCO_3$. Next, FmocOSu (0.143 g, 0.423 mmol) was added in small portions along with more $NaHCO_3$ to maintain the pH at about 8-9. The solution was diluted with water and washed with diethyl ether. The aqueous phase was flushed with N_2 to remove the dissolved ether and acidified to pH 2 with concentrated HCl to give a white suspension. After filtration, the precipitate was air dried to afford compound **13** as a white solid (0.128 g, 73%). ^{1}H NMR (400 MHz, DMSO-d_6) (**Figure A41**) δ 1.79 [1H, td *J* = 6.0, 18.4 Hz, C$\underline{H}_a$H$_b$(4)], 2.09 [1H, td *J* = 7.3, 19.8 Hz, CH$_a\underline{H}_b$(4)], 3.90 [2H, t *J* = 6.8 Hz, C$\underline{H}_2$(5)], 4.09 [1H, m, C$\underline{H}$(3)], 4.12-4.22 [1H, m, CH$_a\underline{H}_b$(2)], 4.22 (1H, t *J* = 6.9 Hz, Fmoc aliphatic C$\underline{H}$), 4.33 (2H, d *J* = 6.4 Hz, Fmoc aliphatic C$\underline{H}_2$); ^{13}C NMR (100 MHz, DMSO-d_6) (**Figure A42**) δ ppm 31.8 [$\underline{C}H_2$(4)], 46.6 (Fmoc aliphatic $\underline{C}$H), 55.3 [$\underline{C}$H(3)], 65.3 (Fmoc aliphatic $\underline{C}H_2$), 67.0 [$\underline{C}H_2$(5)], 81.1 [$\underline{C}$H(2)], 120.0, 125.0, 127.0, 127.5 (Fmoc aromatic $\underline{C}$H), 140.6, 143.7 (Fmoc aromatic $\underline{C}$), 155.5 (Fmoc $\underline{C}$=O), 172.8 [$\underline{C}$=O (1)]; IR (KBr) (**Figure A43**) ν_{max} 3308.4, 3062.4, 2946.6, 2362.1, 2341.8, 1722.5, 1690.7, 1540.2, 1447.6, 1259.6, 1099.4, 732.8 cm^{-1}; m.p. 166-168 °C; $[\alpha]_D^{23}$ = +41.5° (*c* = 1.0 g/100 mL, DMSO); HRMS (ESI+) (**Figure A44**) calcd for $C_{20}H_{19}NO_5Na^+$ (M+Na$^+$) 376.1155, found 376.1180 and calcd for $C_{20}H_{19}NO_5K^+$ (M+K$^+$) 392.0895, found 392.0895.

2.4.1.14 (2S,3S)-Pentafluorophenyl-3-(((9H-fluoren-9-yl)methoxy)carbonylamino)tetrahydrofuran-2-carboxylate (1a)

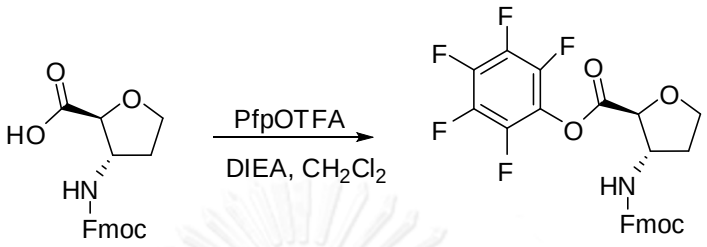

13 **1a**

A suspension of compound **13** (0.22 g, 0.63 mmol) in CH_2Cl_2 (2 mL) was treated with DIEA (600 µL, 3.45 mmol) and PfpOTfa (600 µL, 3.39 mmol) in three portions. The completion of the reaction was monitored by TLC analysis (EtOAc:Hexanes 1:1; R_f = 0.50). The reaction mixture was diluted with CH_2Cl_2 (10 mL), washed with 1 M HCl, saturated $NaHCO_3$ and dried over anhydrous Na_2SO_4. After removal of the solvent, the resulting pink oil was sonicated in hexane to give a white suspension. The Vacuum filtration and drying afforded the product **1a** as a white solid (207 mg, 0.398 mmol, 64% from **13**). ^{1}H NMR (400 MHz, $CDCl_3$) (**Figure A45**) δ 1.91-2.04 [1H, m, CH_aH_b(4)], 2.29-2.43 [1H, br m, CH_aH_b(4)], 4.13-4.25 [3H, m, Fmoc aliphatic CH, CH_2(5)], 4.50 [2H, d *J* = 5.1 Hz, Fmoc aliphatic CH_2], 4.59-4.75 [2H, m, CH(3), CH(2)], 5.06 [1H,d *J* = 5.3, NH], 7.31 (2H, t, *J* = 7.1 Hz, Fmoc aromatic CH), 7.41 (2H, t, *J* = 6.9 Hz, Fmoc aromatic CH), 7.58 (2H, d, *J* = 7.2 Hz, Fmoc aromatic CH), 7.77 (2H, d, *J* = 7.4 Hz, Fmoc aromatic CH); ^{13}C NMR (100 MHz, $CDCl_3$) (**Figure A46**) δ 31.9 [CH_2 (4)], 47.3 (Fmoc aliphatic CH), 56.2 [CH (3)], 66.9 (Fmoc aliphatic CH_2), 68.3 [CH (5)], 81.7[CH (2)], 120.0, 124.9, 127.0, 127.8 (d) (Fmoc aromatic CH), 141.4 (Fmoc aromatic C), 143.7 (d), 155.5 (Fmoc CO), 167.3 [CO (1)]; ^{19}F NMR (376 MHz, $CDCl_3$) (**Figure A47**) δ -161.8 (t *J* = 20.2 Hz), -157.14 (t *J* = 19.9 Hz), -152.4 (d *J* = 18.0 Hz); IR (ATR) (**Figure A48**) ν_{max} 3309.4, 1799.7, 1687.6, 1550.0, 1519.6, 1291.0, 1234.9, 1066.9, 1031.9, 994.6, 761.2, 735.6, 665.6; m.p. = 123-125 °C; $[\alpha]_D^{23}$ = +57.3° (*c* = 1.0 g/100 mL, CH_2Cl_2); HRMS. calcd for $C_{26}H_{18}F_5KNO_4^+$ ($M+K^+$) 542.0788, found 542.0795 (**Figure A49**).

2.4.2 Other intermediates not in the main pathway

2.4.2.1 5-O-Benzoyl-2-deoxy-D-ribose methyl glycoside (4b) (mixture of α and β anomers)

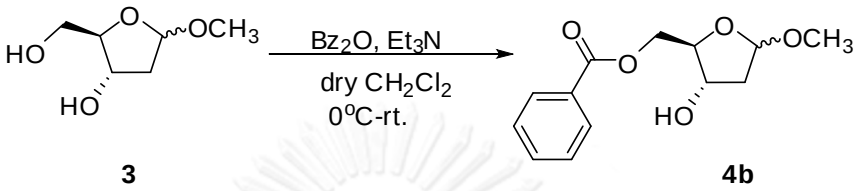

3 **4b**

Diol **3** (1.14 g, 7.66 mmol) was dissolved in dry CH_2Cl_2 (5 mL) and the solution was treated with Et_3N (1.95 mL, 14 mmol). The reaction mixture was stirred at 0 °C under N_2 atmosphere. Then a solution of Bz_2O (1.80 g, 7.95 mmol) in dry CH_2Cl_2 (2 mL) was added to the mixture, and the resulting solution was allowed to warm to room temperature. The progress of the reaction was monitored by TLC analysis; product R_f (product) = 0.40 (EtOAc:Hexanes 1:1). Upon completion, the reaction mixture was extracted with EtOAc (20 mL), saturated solution of $NaHCO_3$ and dried over anhydrous Na_2SO_4. The crude product was purified by column chromatography on silica gel to give compound **4b** as colorless oil (0.98 g, 55% from **3**). ^{1}H NMR spectrum of the product is shown in **Figure A51.**

2.4.2.2 5-O-Benzoyl-3-O-methanesulfonyl-2-deoxy-D-ribose methyl glycoside (5b) (mixture of α and β anomers)

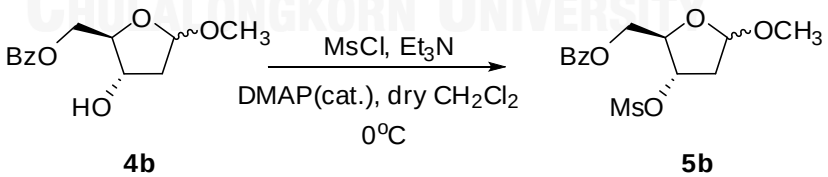

4b **5b**

To a mixture **4b** (0.930 g, 3.69 mmol) and DMAP (98 mg, 0.80 mmol) in dry CH_2Cl_2 (4 mL) at 0 °C under N_2 atmosphere then Et_3N (1.00 mL, 7.17 mmol) and MsCl (0.34 mL, 4.44 mmol) were added dropwise. The reaction was stirred at 0 °C for 30 minutes and was monitored by TLC analysis; R_f = 0.76 (Acetone:CH_2Cl_2 1:4). The reaction was quenched at 0 °C with cold water and EtOAc (15 mL). The organic layer was

extracted with saturated $NaHCO_3$, dried over $NaSO_4$ and evaporated. The crude product was purified by column chromatography to afford compound **5b** as off white solid (1.18 g, 3.56 mmol, 97% from **4b**). ^{1}H NMR spectrum of the product is shown in **Figure A52**.

2.4.2.3 5-O,3-O-Dibenzoyl-2-deoxy-D-ribose methyl glycoside (5c) (mixture of α and β anomers)

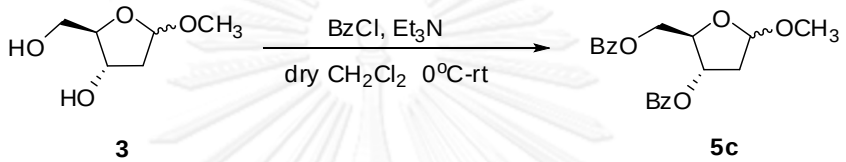

3 **5c**

A solution of crude **3** (prepared from 11.9 mmol of **2**) in anhydrous CH_2Cl_2 (9 mL) was cooled to 0 ºC under N_2 atmosphere and then treated with Et_3N (4.5 mL, 36 mmol), and BzCl (3.0 mL, 26 mmol). The reaction mixture was allowed to warm to room temperature and monitored by TLC (EtOAc:Hexanes 1:9; R_f = 0.40 and 0.50). After completion of the reaction, the resulting mixture was diluted with EtOAc and water. The combined organic extracts were washed with saturated NH_4Cl (40 mL), saturated $NaHCO_3$ (40 mL), dried over anhydrous Na_2SO_4 and evaporated. The crude product (4.64 g) was purified by flash column chromatography on silica gel to afford compound **5c** as a yellow oil (2.88 g, 83% from **2**). ^{1}H NMR spectrum of the product is shown in **Figure A53**.

2.4.2.4 5-O-Benzoyl-3-O-methanesulfonyl-1,2-dideoxy-D-ribose (6b)

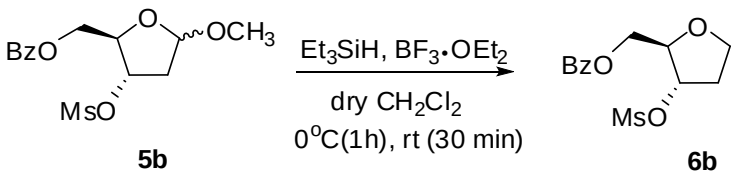

5b **6b**

Compound **5b** (0.706 g, 2.14 mmol) was dried and dissolved in CH_2Cl_2 (2 mL) at 0 ºC under N_2 atmosphere. Et_3SiH (0.75 mL, 4.70 mmol) was added to the cooled

solution, followed by $BF_3{\cdot}OEt_2$ (0.50 mL, 4.05 mmol). The reaction was stirred for 1 h at 0 ºC and then allowed to warm up to room temperature for 30 minutes. The reaction was monitored by TLC analysis (EtOAc:Hexanes 1:1, R_f = 0.40, *p*-anisaldehyde) until completion. The reaction was quenched with saturated $NaHCO_3$ (20 mL) and extracted with CH_2Cl_2 and combined organic phase was dried over $NaSO_4$, filtered and evaporated to give **6b** as yellow oil (0.633 g of crude). ^{1}H NMR (400 MHz, $CDCl_3$) (**Figure A54**) δ 2.30 [2H, ddd *J* = 5.4, 6.6, 7.9 Hz, C$\underline{H}_2$(2)], 3.06 (3H, s, mesyl C$\underline{H}_3$), 3.98 [1H, td *J* = 6.9, 8.7 Hz, C$\underline{H}_a$H$_b$(1)], 4.13 [1H, ddd *J* = 4.6, 6.9, 8.9 Hz, CH$_a\underline{H}_b$(5)], 4.36-4.48 [3H, m, C$\underline{H}_2$(5), C$\underline{H}$(4)], 5.24 [1H, td *J* = 2.3, 4.8 Hz, C$\underline{H}$(3)], 7.45 (2H, t *J* = 7.7 Hz, benzoyl C$\underline{H}$), 7.58 (1H, t *J* = 7.4 Hz, benzoyl C$\underline{H}$), 8.03 (2H, d *J* = 7.1 Hz, benzoyl C$\underline{H}$).

2.4.2.5 ((2R,3R)-3-Hydroxytetrahydrofuran-2-yl)methyl benzoate (7b)

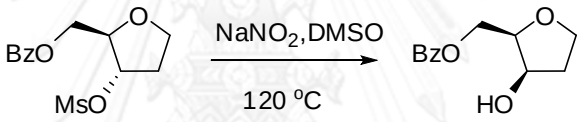

6b **7b**

A solution of compound **6b** (0.28 g, 0.92 mmol) in DMSO (1 mL) was heated with $NaNO_2$ (0.51 g, 7.3 mmol) at 120 ºC for 5 hours. After the reaction was completed as monitored by TLC analysis (Acetone:CH_2Cl_2 1:4; R_f = 0.73), it was cooled down and diluted with water. The aqueous layer was then extracted with CH_2Cl_2 and the combined organic extract was dried over anhydrous Na_2SO_4 and evaporated to dryness. The crude product was purified by column chromatography to give **7b** as a white solid (0.038 g, 18%). ^{1}H NMR (400 MHz, $CDCl_3$) (**Figure A55**) δ 1.99-2.07 [1H, m, C$\underline{H}_a$H$_b$(2)], 2.12-2.23 [1H, m, CH$_a\underline{H}_b$(2)], 2.54 (1H, br s, O$\underline{H}$), 3.87 [1H, dt *J* = 3.9, 8.6 Hz, C$\underline{H}_a$H$_b$(1)], 3.98 [1H, dt *J* = 3.5, 6.1 Hz, C$\underline{H}$(4)], 4.10 [1H, dd *J* = 8.2, 16.0 Hz, CH$_a\underline{H}_b$(1)], 4.40 [2H, dd *J* = 6.1, 11.5 Hz, C$\underline{H}_a$H$_b$(5), CH(3)], 4.74 [1H, dd *J* = 6.3, 11.6 Hz, CH$_a\underline{H}_b$(5)], 7.43 (2H, t *J* = 7.7 Hz, benzoyl C$\underline{H}$), 7.56 (1H, t *J* = 7.3 Hz, benzoyl C$\underline{H}$), 8.04 (2H, d *J* = 7.4 Hz, benzoyl C$\underline{H}$).

2.4.2.6 ((2R,3R)-3-Hydroxy-5-methoxytetrahydrofuran-2-yl)methyl benzoate (7c) (mixture of α and β anomers)

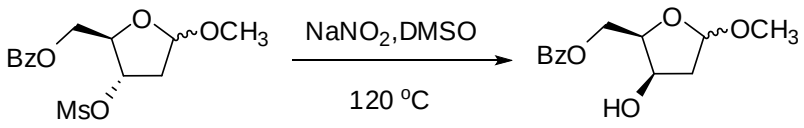

5b **7c**

A solution of **5b** (0.97 g, 2.9 mmol) in DMSO (1.5 mL) was treated with $NaNO_2$ (1.46 g, 21.2 mmol) and stirred at 120 °C overnight. The reaction was monitored by TLC analysis (Acetone:CH_2Cl_2 1:4; R_f = 0.73), and then diluted with water. The aqueous layer was then extracted with CH_2Cl_2 and the combined organic extract was dried over anhydrous Na_2SO_4 and evaporated. The crude product was purified by column chromatography to give **7c** as a colorless wax (0.22 g, 29%). ^{1}H NMR spectrum of the product is shown in **Figure A56**.

2.4.2.7 ((2R,3R)-3-Hydroxy-5-methoxytetrahydrofuran-2-yl)methyl p-methylbenzoate (7d) (mixture of α and β anomers)

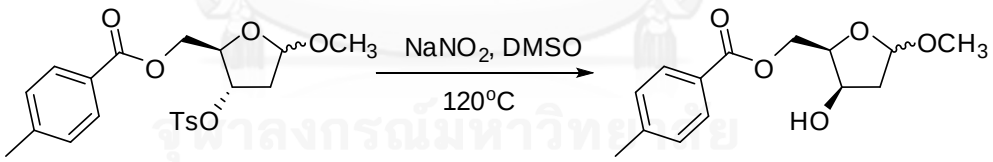

5a **7d**

A solution of compound **5a** (2.42 g, 5.76 mmol) in DMSO (3 mL) was heated with $NaNO_2$ (6.80 g, 98.7 mmol) at 120 °C for 2 hours. After completion of the reaction, as monitored by TLC analysis (EtOAc:Hexanes 1:1, *p*-anisaldehyde stain), the reaction mixture was cooled down and diluted with water. The aqueous layer was then extracted with CH_2Cl_2 and the combined organic extract was dried over anhydrous Na_2SO_4 and evaporated. The crude product was purified by column chromatography to give **7d** as a colorless wax (0.46 g, 30% from **5a**). ^{1}H NMR spectrum of the product is shown in **Figure A57**.

2.4.2.8 ((2R,3R)-3-(Methylsulfonyloxy)tetrahydrofuran-2-yl)methyl benzoate (8c)

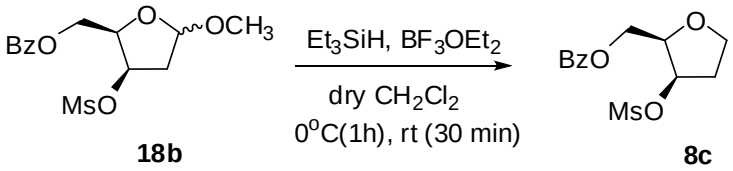

18b **8c**

A solution of compound **18b** (0.32 g, crude from **7c**) in anhydrous CH_2Cl_2 (4 mL) was cooled to 0 °C under N_2 atmosphere and treated with Et_3SiH (0.30 mL, 1.88 mmol), followed by dropwise addition of $BF_3{\bullet}OEt_2$ (0.22 mL, 1.78 mmol). The reaction was stirred at 0 °C for 1 hour and then allowed to warm up to room temperature for 30 minutes. The progress of the reaction was monitored by TLC (EtOAc:Hexanes 1:1; negative *p*-anisaldehyde stain; R_f = 0.40). The reaction mixture was neutralized with saturated $NaHCO_3$ and the aqueous phase was extracted with CH_2Cl_2. The combined organic phase was dried over anhydrous Na_2SO_4 to give compound **8c** as a colorless wax (0.27 g of crude). ^{1}H NMR (400 MHz, $CDCl_3$) (**Figure A58**) δ 2.13-2.23 [1H, m, C$\underline{H}_a$H$_b$(4)], 2.43 [1H, m, CH$_a\underline{H}_b$(4)], 3.02 (3H, s, mesyl C$\underline{H}_3$), 3.96 [1H, dt *J* = 4.9, 8.5 Hz, C$\underline{H}_a$H$_b$(5)], 4.14 [1H, dd *J* = 7.9, 15.8 Hz, CH$_a\underline{H}_b$(5)], 4.28 (1H, dd *J* = 5.3, 10.1 Hz, C$\underline{H}_a$H$_b$ methylbenzoate), 4.46 [2H, d *J* = 5.6 Hz, CH(2), CH$_a\underline{H}_b$ methylbenzoate], 5.67 [1H, br m, CH(3)], 7.46 [2H, t *J* = 7.7 Hz, benzoyl C$\underline{H}$], 7.59 [1H, t *J* = 7.4 Hz, benzoyl C$\underline{H}$], 8.00 [2H, d *J* = 7.4 Hz, benzoyl C$\underline{H}$].

2.4.2.9 ((2S,3S)-3-Azidotetrahydrofuran-2-yl)methyl benzoate (9c)

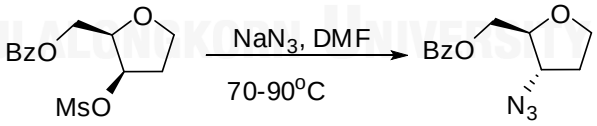

8c **9c**

A solution of **8c** (0.25 g, 0.8 mmol) in DMF (2 mL) was treated with NaN_3 (0.30 g, 4.6 mmol) and then heated at 70 °C. The reaction mixture was monitored by TLC analysis (EtOAc:Hexanes 2:3; R_f = 0.62). Since the reaction was not completed after 2 hours, the temperature was raised to 80 °C for 4 hours and 90 °C for another 3 hours, after which the starting material was completely consumed. The reaction mixture was cooled down, diluted with water and extracted with EtOAc. The

combined organic phase was dried over anhydrous Na_2SO_4, and concentrated to dryness to give compound **9c** as a yellow oil (0.11 g, 54%). ^{1}H NMR (**Figure A59**) (400 MHz, $CDCl_3$) δ 2.03-2.12 [1H, m, C$\underline{H}_a$H$_b$(4)], 2.29 [1H, m, CH$_a\underline{H}_b$(4)], 3.95 [1H, dd *J* = 8.3, 16.0 Hz, C$\underline{H}_a$H$_b$(5)], 4.02-4.19 [3H, m, C$\underline{H}$(3), C$\underline{H}$(2) CH$_a\underline{H}_b$(5)], 4.40 (2H, d *J* = 4.9 Hz, CH_2 methylbenzoate), 7.45 (2H, t *J* = 7.4 Hz, benzoyl C$\underline{H}$), 7.58 (1H, t *J* = 7.2 Hz, benzoyl C$\underline{H}$), 8.05 (2H, d *J* = 7.1 Hz, benzoyl C$\underline{H}$).

2.4.2.10 ((2R,3R)-5-Methoxy-3-(methylsulfonyloxy)tetrahydrofuran-2-yl)methyl benzoate (18b) (mixture of α and β anomers)

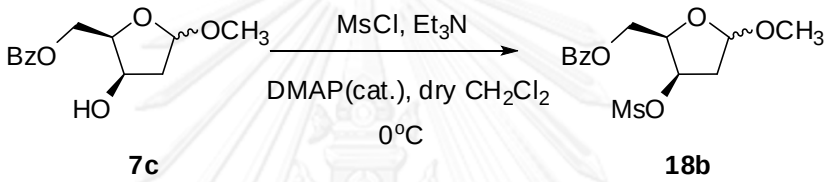

7c **18b**

A solution of **7c** (0.217 g, 0.860 mmol) in anhydrous CH_2Cl_2 (4 mL) was cooled to 0 °C and treated with DMAP (34 mg, 0.28 mmol), Et_3N (0.40 mL, 2.80 mmol) and MsCl (0.20 mL, 2.60 mmol). The completion of the reaction was indicated by TLC analysis (Acetone:CH_2Cl_2 1:4; R_f = 0.76), and it was then poured into cooled water and extracted with EtOAc. The organic layer was extracted with saturated $NaHCO_3$, dried over anhydrous Na_2SO_4 and concentrated to dryness give the crude product (0.32 g). ^{1}H NMR (400 MHz, $CDCl_3$) (**Figure A60**)

2.4.2.11 5-O,3-O-Dibenzoyl-1,2-dideoxy-D-ribose (14)[48]

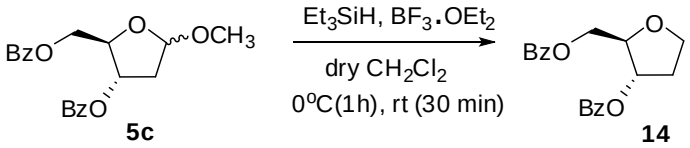

A solution of **5c** (10.26 g, 3.66 mmol) in dried CH_2Cl_2 (5 mL) at 0 °C under N_2 atmosphere was treated with Et_3SiH (3.40 mL, 21.4 mmol) followed by dropwise addition of $BF_3{\cdot}OEt_2$ (2.65 mL, 21.4 mmol). The reaction was stirred at 0 °C for 1 hour and then allowed to warm up to room temperature for 30 minutes. The progress of the reaction was monitored by TLC (EtOAc:Hexanes 1:9; negative *p*-anisaldehyde stain; R_f = 0.40). The reaction mixture was neutralized with saturated $NaHCO_3$ and extracted with CH_2Cl_2. The combined organic phases were dried over anhydrous Na_2SO_4 resulting in yellow oil (3.20 g). The crude product was purified by column chromatography on silica gel to give compound **14** as a colorless oil (2.38 g, 71% from **5c**). ^{1}H NMR (400 MHz, $CDCl_3$) (**Figure A61**) δ ppm 2.21 [1H, tdd *J* = 2.1, 5.0, 8.5 Hz, C$\underline{H}_a$H$_b$(2)], 2.38 [1H, dddd *J* = 6.5, 7.7, 9.8, 14.3 Hz, CH$_a\underline{H}_b$(2)], 4.04 [1H, ddd *J* = 6.2, 8.8, 9.3 Hz, C$\underline{H}_a$H$_b$(1)], 4.31 [1H, dt *J* = 3.0, 8.3 Hz, CH$_a\underline{H}_b$(1)], 4.38 [1H, dt *J* = 2.5, 4.6 Hz, C$\underline{H}_a$H$_b$(5)], 4.52 [2H, t *J* = 4.6 Hz, CH$_a\underline{H}_b$(5), C$\underline{H}$(4)], 5.50 [1H, td *J* = 2.0, 6.1 Hz, C$\underline{H}$(3)], 7.44 (4H, q *J* = 7.4, 7.2 Hz, benzoyl C$\underline{H}$), 7.57 (2H, m, benzoyl, C$\underline{H}$), 8.05 (4H, m, benzoyl C$\underline{H}$).

2.4.2.12 1,2-Dideoxy-D-ribose or (2R,3S)-2-(hydroxymethyl)tetrahydrofuran-3-ol (16)[49]

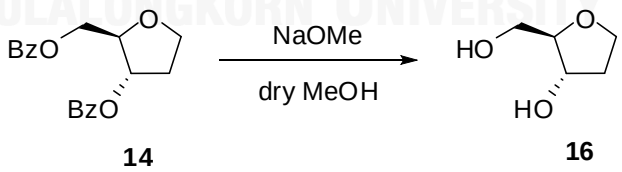

A mixture of **14** (2.29 g, 7.02 mmol) and NaOMe (0.946 g, 17.5 mmol) in dried methanol was heated at 60 °C with stirring under N_2 for 2 hours. The reaction was monitored by TLC analysis (MeOH:CH_2Cl_2 1:9, ceric molybdate stain, R_f = 0.33). After removal of the solvent, the crude product was purified by column chromatography on silica gel to yield **16** as a colorless liquid (0.684 g, 83% from **14**). ^{1}H NMR (400 MHz,

D_2O) (**Figure A62**) δ ppm 1.88 [1H, m, C$\underline{H}_a$H$_b$(2)], 2.11 [1H, dddd *J* = 6.4, 8.4, 9.2, 13.3 Hz, CH$_a\underline{H}_b$(2)], 3.52 [1H, dd *J* = 6.1, 12.1 Hz, C$\underline{H}_a$H$_b$(1)], 3.60 [1H, dd *J* = 4.2, 812.1 Hz, CH$_a\underline{H}_b$(1)], 3.81 [1H, ddd *J* = 3.2, 4.0, 6.1 Hz, C$\underline{H}_a$H$_b$(5)], 3.85-3.99 [2H, m, CH$_a\underline{H}_b$(5), C$\underline{H}$(3)], 4.24 [1H, td *J* = 2.9, 6.0 Hz, C$\underline{H}$(4)].

2.4.2.13 5-O-Benzoyl-1,2-dideoxy-D-ribose (17a)

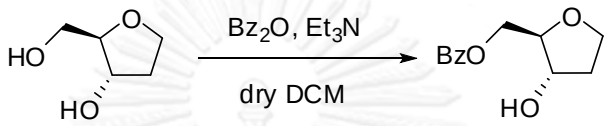

16 **17a**

A solution of compound **16** (0.373 g, 3.15 mmol) in dried CH_2Cl_2 (2 mL) was treated with Et_3N (0.84 mL, 6.0 mmol) at 0 °C followed by the addition of a solution of Bz_2O (0.86 g, 3.8 mmol) in dry CH_2Cl_2 (2 mL). The reaction mixture was stirred at room temperature and monitored by TLC analysis (EtOAc:Hexanes 1:1; R_f = 0.30). After the reaction had reached completion, the resulting solution was diluted with EtOAc, washed with water and saturated $NaHCO_3$, dried over anhydrous Na_2SO_4 and evaporated to give crude product **17a** (0.49 g). Based on ^{1}H-NMR analysis, the crude contains desired product **17a** in acceptable purity (57%) and by-product **14** less than 10%. ^{1}H NMR (400 MHz, $CDCl_3$) (**Figure A63**) δ ppm 1.95 [1H, m, C$\underline{H}_a$H$_b$(2)], 2.20 [1H, tdd *J* = 6.6, 8.4, 16.7 Hz, CH$_a\underline{H}_b$(2)], 3.97-4.13 [3H, m, C$\underline{H}_2$(1), C$\underline{H}$(3)], 4.34-4.40 [2H, m, C$\underline{H}_2$(5), C$\underline{H}$(4)], 7.44 (2H, t *J* = 7.8 Hz, benzoyl C$\underline{H}$), 7.57 (1H, t *J* = 7.4 Hz, benzoyl, C$\underline{H}$), 8.04 (2H, dd *J* = 1.2, 8.3 Hz, benzoyl C$\underline{H}$).

2.4.2.14 5-O-tert-Butyldimethylsilyl-1,2-dideoxy-D-ribose (17b)

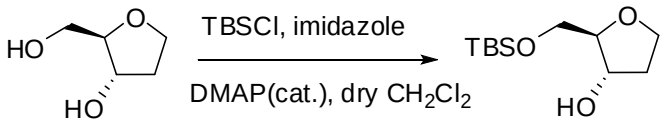

16 **17b**

A solution of diol **16** (0.66 g, 5.57 mmol) in dried CH_2Cl_2 (2 mL) was treated with imidazole (0.40 g, 5.89 mmol) and DMAP (68 mg, 0.55 mmol). The reaction mixture was cooled to 0 °C and then TBSCl (0.803 g, 5.33 mmol) in CH_2Cl_2 (2 mL) was added. The reaction mixture was stirred at room temperature until the reaction reached completion according to TLC analysis (EtOAc:Hexanes 1:1; R_f = 0.50) and then it was diluted with EtOAc and washed with saturated NH_4Cl. The collected organic phase was washed with saturated $NaHCO_3$, dried over anhydrous Na_2SO_4 and evaporated to dryness. The crude product (pink oil, 1.37 g) was purified by column chromatography on silica gel to afford **17b** as a colorless oil (0.836 g, 68% from **16**). ^{1}H NMR (400 MHz, $CDCl_3$) (**Figure A64**) δ ppm 0.64 (6H, s, C$\underline{H}_3$ TBS methyl), 0.89 (9H, s, C$\underline{H}_3$ TBS *t*-butyl), 1.88 [1H, m, C$\underline{H}_a$CH$_b$(2)], 2.14 [1H, tdd *J* = 6.5, 8.3, 16.6 Hz, CH$_a$C$\underline{H}_b$(2)], 3.52 [1H, dd *J* = 7.8, 11.3 Hz, C$\underline{H}_a$H$_b$(1)], 3.75 [2H,m, CH$_a$$\underline{H}_b$(1) and CH(3)], 3.96 [2H, m, C$\underline{H}_2$(5)], 4.32 [1H, td *J* = 3.3, 6.4 Hz, C$\underline{H}$(4)].

2.5 PNA oligomer synthesis & characterization

2.5.1 Unmodified PNA oligomers

The atfcPNA were synthesized manually at 1.5 μmol scale on Tentagel S-RAM resin (Fluka, 0.24 mmol/g) from the four Fmoc-protected pyrrolidinyl PNA monomers (Fmoc-A^{Bz}-OPfp, Fmoc-T-OPfp, Fmoc-C^{Bz}-OPfp, Fmoc-G^{Ibu}-OH) and the activated ATFC spacer **1a** according to the previously published protocol.[8] Deprotection was carried out with 20% piperidine + 2% DBU in DMF (100 μL, 5 min). Pfp-activated monomers were directly coupled to the free amino group on the resin (4 equiv Pfp-activated monomer, 4 equiv HOAt, 4 equiv DIEA in DMF, 30 min single coupling). Free acid monomers (G^{Ibu}) required HATU activation before the coupling (3.9 equiv free acid monomer, 4 equiv HATU, 8 equiv DIEA in DMF, 1 min pre-activation, 30 min single coupling). Capping was performed by 2 μL Ac_2O + 7% DIEA in DMF (30 μL) for 5 min. Lysine (in the form of Fmoc-L-Lys(Boc)-OPfp) was included at the C-termini for comparison with acpcPNA. After completion of the synthesis, the N-terminal Fmoc group was removed and the free amino group of the PNA was capped by acetylation (except for fluorescein labeling, see below). The nucleobase protecting groups was removed by heating with 1:1 aqueous ammonia-dioxane at 60 °C overnight. The resin was washed thoroughly with methanol and dried.

2.5.2 N-terminal fluorescein labeling

The N-Fmoc-deprotected atfcPNA on the resin (0.5 μmol) was reacted with 5(6)-carboxyfluorescein *N*-hydroxysuccinimide ester (2.4 mg) in anhydrous DMF (40 μL) in the dark at room temperature for 3 days. The nucleobase protecting groups was removed by heating with 1:1 aqueous ammonia-dioxane at 60 °C overnight. The resin was washed thoroughly with methanol and dried.

2.5.3 Cleavage from the resin

The atfcPNA after the appropriate N-terminal modification and side-chain deprotection was cleaved from the resin by treatment with pure TFA (500 μL x 30 min x 3). The combined cleavage mixture was evaporated under a stream of nitrogen gas, and the residue was washed with diethyl ether and air-dried to afford the crude PNA.

2.5.4 Purification and characterization

2.5.4.1 MALDI-TOF mass spectrometry

All PNA oligomers were characterized by MALDI-TOF mass spectrometry in linear positive mode. A solution of α-cyano-4-hydroxycinnamic acid was used as the matrix for MALDI-TOF analysis. All samples were prepared by mixing around 1 µL of PNA samples with 10 µL of matrix solution and deposited on MALDI target. The observed masses were compared with the calculated mass obtained from an in-house PNA molecular weight calculator web application developed by Dr. Tirayut Vilaivan (http://www.chemistry.sc.chula.ac.th/pna) and software ChemDraw Ultra 10.0 (CambridgeSoft©).

2.5.4.2 Reverse phase HPLC (separation and polarity identification)

The crude PNA was dissolved in water, purified by reverse phase HPLC using a gradient of water-methanol containing 0.1% TFA with column: ACE 5 A71197, C18-AR, 150x4.6 mm. The gradient system consisted of two solution systems that are solvent A (0.1% trifluoroacetic acid in MilliQ water) and solvent B (0.1% trifluoroacetic acid in methanol). The gradient started from A:B at 90:10 for the first 5 min and then increased linearly to 10:90 over 90 min. The peaks were monitored at by UV absorbance at 260 and 300 nm (445 nm for modified fluorescein PNA). Fractions containing the pure PNA (according to MALDI-TOF MS analysis) were combined and freeze dried to obtain the purified PNA. For polarity identification applied Vertisep UPS, 3µ particle size, 50 x 4.6 mm with gradient started from A:B at 90:10 first 5 min and then increased linearly to 10:90 over 35 min.

2.5.4.3 Determination of concentration

Concentrations of the oligomers were determined by UV absorption at 260 nm at 20 ºC in 10 mM phosphate buffer pH 7 using the following extinction coefficients (ε): 8.8 $mL \cdot \mu mol^{-1} \cdot cm^{-1}$ (T), 10.8 $mL \cdot \mu mol^{-1} \cdot cm^{-1}$ (A), 7.4 $mL \cdot \mu mol^{-1} \cdot cm^{-1}$ (C), 11.5 $mL \cdot \mu mol^{-1} \cdot cm^{-1}$ (G) and 20.9 $mL \cdot \mu mol^{-1} \cdot cm^{-1}$ (Fluorescein). Extinction coefficients (ε) of PNAs were calculated from sum of individual extinction coefficients (ε) of the nucleobase and fluorophore.

2.6 Experimental procedures for PNA property studies

2.6.1 UV-melting experiment

A 1 cm cell path length cuvette was used in all experiments. All of samples were prepared by mixing a stoichiometric amount of each strand (1 μM) in a 10 mM sodium phosphate buffer at pH 7, optionally with 100 mM NaCl. The melting experiments were performed by measuring the change in the absorbance at 260 nm as a function of temperature. The A_{260} was recorded at temperatures ranging from 20-90 ºC (block temperature) with a temperature ramp of 1 ºC/min. The temperature was corrected by applying a linear equation obtained from a measured temperature versus block temperature.[50] The recorded spectra were normalized and smoothed using a five-point adjacent averaging algorithm using KaliedaGraph 4.0 (Synergy Software) and analysis of the data was performed on a PC compatible computer using Microsoft Excel (Microsoft Corporation). The melting transitions were determined from maxima of the first derivative plot of the absorbance-temperature profile. T_m values obtained from independent experiments were accurate to within ± 0.5 $^{\circ}$C. Correct temperature and normalized absorbance are defined as follows.

$$\text{Correct Temp.} = (0.9696 \times T_{block}) - 0.6068$$

$$\text{Normalized Abs.} = Abs_{obs}/Abs_{init}$$

2.6.2 CD spectroscopy

CD spectra were recorded at 20 ºC via a 1 cm cell path length cuvette. The samples were prepared as in **2.6.1**. For PNA T9 spectra represent an average of 4 scans, recorded from 400 to 200 nm at the rate of 200 nm/min. The CD scan at different temperature was recorded from 20-90 ºC with 10 ºC temperature interval (ramping rate 2 ºC /min). For PNA mix-base spectra represent an average of 4 scans, recorded from 400 to 200 nm at the rate of 100 nm/min (mixing amount of each stand = 2.5 μM). All spectra were processed using Microsoft Excel and OriginPro7G (OriginLab Corporation) and were baseline subtracted.

2.6.3 UV-titration

To a solution containing the PNA (2 μM) and 10 mM sodium phosphate buffer pH 7.0 (800 μL) in a 1 cm cell path length cuvette was titrated with a concentrated stock solution of DNA (40 μM in sodium phosphate buffer pH 7.0, 5 μL for each addition). The A_{260} were measured at 25 °C at 260 nm (averaged 3 times). More DNA stocks were added until a total volume of 200 μL (4 equiv. of DNA) has been added. The stoichiometry was determined by the inflection point of a plot between the ratio of observed A260/calculated A260 as a function of %mol of DNA in the reaction.[50]

$$\text{Calcd. } A_{260} = \frac{[OD_{260}(PNA)\times V_{PNA}] + [OD_{260}(DNA)\times V_{DNA}]}{V_{PNA} + V_{DNA}}$$

$$\text{Ratio of PNA:DNA} = \frac{\varepsilon_{DNA}\times OD_{260}(PNA)\times V_{PNA}}{\varepsilon_{PNA}\times OD_{260}(DNA)\times V_{DNA}}$$

$$\text{\% mol of DNA} = \frac{1}{1 + \text{Ratio of PNA:DNA}}$$

2.6.4 Fluorescence spectroscopy to determine non-specific interaction with hydrophobic materials

Non-specific adsorption of fluorescein-modified acpcPNA and atfcPNA were compared by fluorescence measurement. The PNA samples were prepared at 0.05 μM in 10 mM sodium phosphate buffer pH 7.0 (1000 μL) at 25 °C. The solution was transferred back and forth between the cuvette and a 1.5 mL polypropylene microcentrifuge tube, and the fluorescence spectra were recorded after each transfer until no further change was observed. The excitation wavelength was fixed at 480 nm, slit widths 5 nm and the PMT voltage was set to high.

CHAPTER III

RESULTS AND DISCUSSIONS

3.1 ATFC spacer synthesis

In order to synthesize the acpcPNA analogue with replacement of the cyclopentane ring in the ACPC spacer with the tetrahydrofuran ring (**Figure 3.1**), a tetrahydrofuran-derived amino acid (from now on will be referred to as aminotetrahydrofurancarboxylic acid or ATFC) is required. The amino group of ATFC has to be protected with the base-labile Fmoc group in order to be used with other Fmoc-protected acpcPNA monomers (A, T, C and G) in Fmoc-solid phase peptide synthesis. In addition, the carboxyl group should be activated in order to facilitate the amide bond formation. Pentafluorophenyl (Pfp) ester was chosen similar to the ACPC spacer and other acpcPNA monomers because Pfp esters are usually stable, crystalline solid that react readily with amines. As a result, possible target molecules are **1a** or **1b** (**Figure 3.2**). The relative and absolute configurations of the ATFC spacers should correspond to those of the ACPC spacer, *i.e. trans*-(1*S*,2*S*), as shown below.

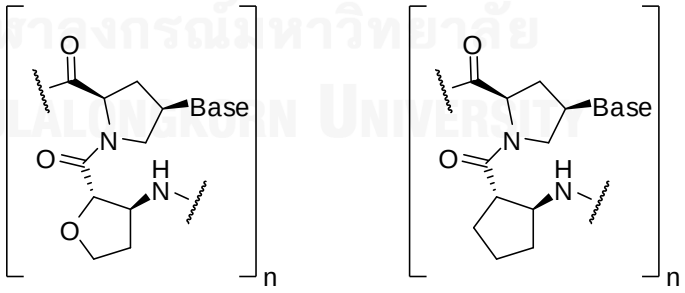

Figure 3.1 Structures of atfcPNA and acpcPNA

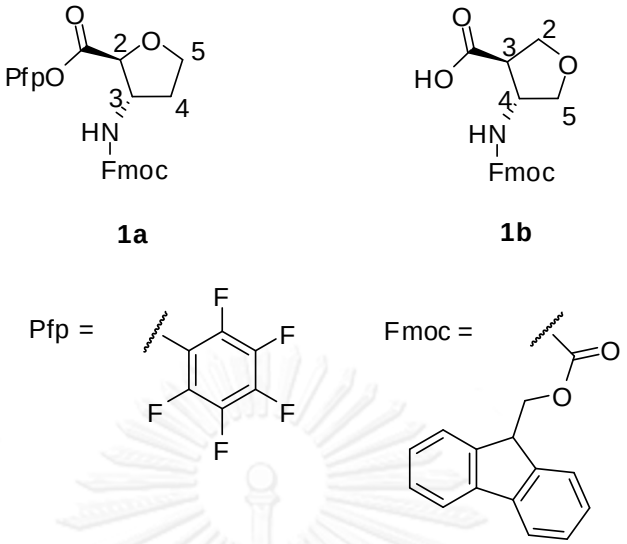

1a **1b**

Figure 3.2 Structures of compounds **1a** and **1b**

3.1.1 Planning and retro-synthesis

In this research, the target **1a** was chosen because it was proposed to be readily synthesized starting from the commercially available 2-deoxy-D-ribose (**2**). This should involve a series of functional group transformation involving (not necessarily in the order shown, protection may be required along the synthesis pathway) i) reduction of the anomeric position (CH-OH to CH_2) ii) substitution of the 3-OH group by a suitable nitrogen nucleophile with retention of configuration iii) oxidation of the CH_2OH group to a carboxylic acid and iv) protection of the nitrogen function and activation of the carboxyl group. These steps can be summarized as shown in **Figure 3.3**. Although relatively straightforward, the reaction sequence had not been performed in the literature and this particular enantiomer of compound **1a**, as well as its other derivatives with protected or unprotected amino and/or carboxyl groups, are unknown.

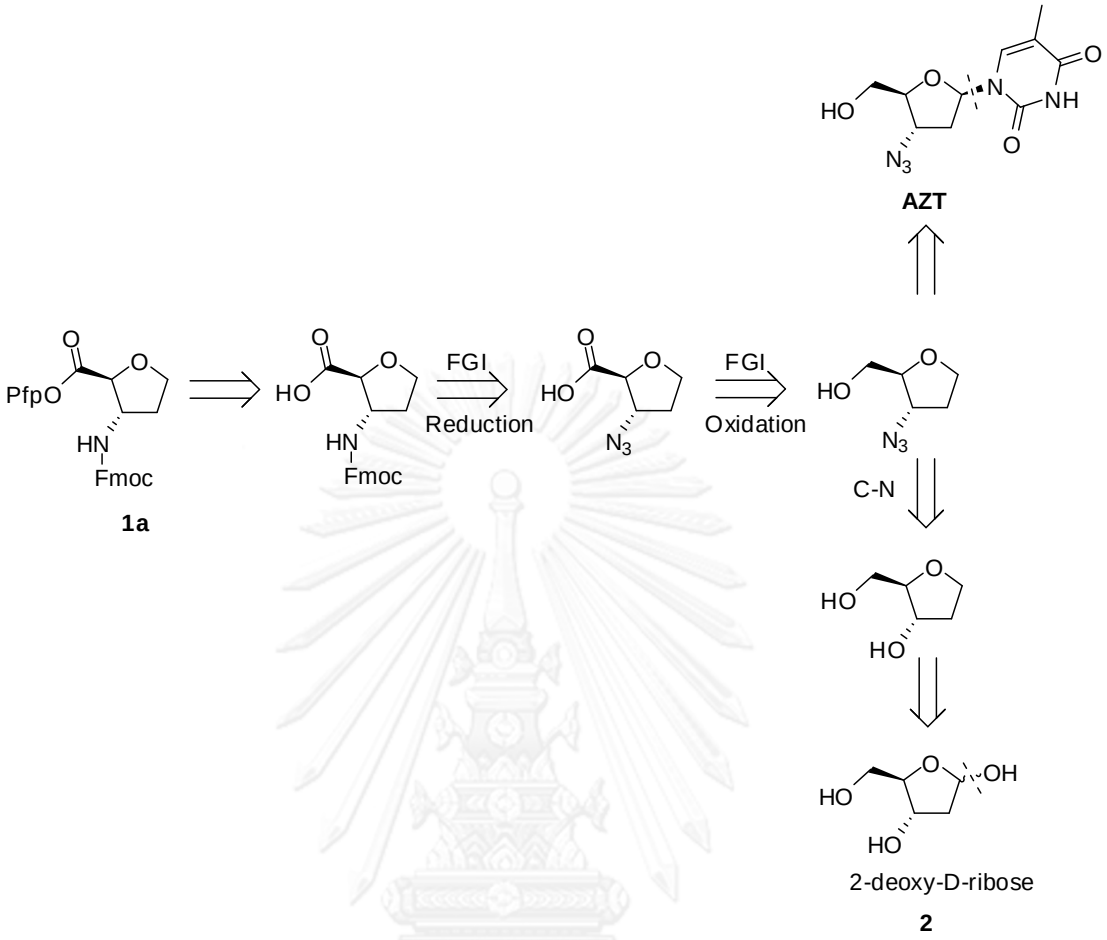

Figure 3.3 Possible planing to synthesize *SS*-ATFC spacer

In another plausible alternative plan (**Figure 3.3**), the commercially available anti-HIV drug azidothymidine (AZT or zidovidine) could be used as the starting material as it contains the nitrogen functional group in the required configuration. The tasks required to convert AZT to **1a** will be similar to the above-mentioned synthetic plan starting from deoxyribose (**2**), but the step ii) (substitution of the 3-OH group by a suitable nitrogen nucleophile with retention of configuration) should be changed to a reductive dethymination (**Figure 3.3**) Although the acid-catalyzed dethymination of persilylated thymidine derivatives is already known in the literature,[51-54] the analogous reaction with AZT is unknown. The challenge for this route is therefore to develop a selective method to perform this step without affecting the azide group.

3.1.2 Synthesis of the ATFC derivative 1a starting from 2-deoxy-D-ribose (2)

3.1.2.1 Protection of anomeric hydroxyl group

Reduction of the anomeric position of sugars, including 2-deoxy-D-ribose (**2**), had been performed on the corresponding methylglycosides in the presence of a Lewis acid and a hydrosilane reducing agent such as $BF_3{\cdot}Et_2O/Et_3SiH$.[48] The synthesis should therefore start with formation of the methylglycoside of 2-deoxy-D-ribose (**2**). In principle, methylglycoside could be formed by treatment of **2** with methanol in the presence of an acid catalyst, which subsequently generate a stabilized oxocarbenium ion that would subsequently be attacked by methanol. Since the reaction involves an equilibrium between methanol and water, anhydrous acid and large excess of methanol should be used to drive the equilibrium forward. At the beginning, the use of in situ generated methanolic HCl by addition of trimethylsilyl chloride (TMSCl) to a solution 2-deoxy-D-ribose (**2**) in methanol was attempted.[55] However, large excess of TMSCl was required and the excess HCl was difficult to remove and caused undesired reactions,[48] the use of methanesulfonic acid (MSA) as a more easily handled acid catalyst was next explored.[56]

The reaction was initially performed in the presence of catalytic amount of methanesulfonic acid (2×0.02 equiv.) for 30 minutes as described in the literature.[56] After quenching by DMAP and adjusted pH to 9,[56] followed by immediate protection with excess benzoyl chloride in the presence of Et_3N to facilitate the product analysis and purification, a major product **19** was obtained as a white solid after purification by column chromatography (hexanes: EtOAc 1:9). ^{1}H and ^{13}C NMR analyses suggested that the isolated product **19** contained no methyl group. Integration of the aromatic region indicated that it was a tribenzoate derivative of deoxyribose. A question remained whether the isolated product is in the desired furanose (five-membered) or undesired pyranose (six-membered) form, which should show similar ^{1}H NMR splitting pattern (**Figure 3.4**). However, all proton and carbon resonances were successfully assigned by 2D NMR techniques (^{1}H-^{1}H COSY, ^{1}H-^{13}C HSQC and ^{1}H-^{13}C HMBC). Based on the high field resonance of the CH_2 protons (C5, 60.3 ppm), it can be concluded that the product is the undesired pyranose form (**19b**) (**Figure 3.5**).[57]

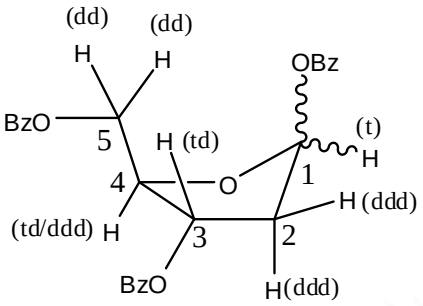

5-membered ring

19a

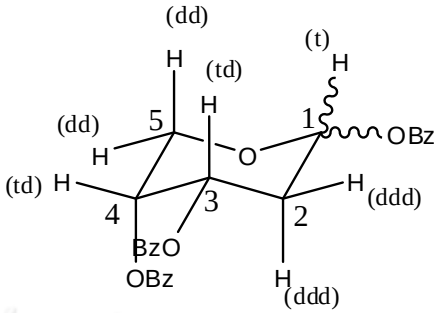

6-membered ring

19b

Figure 3.4 Predicted ^{1}H NMR splitting pattern of the five and six membered ring.

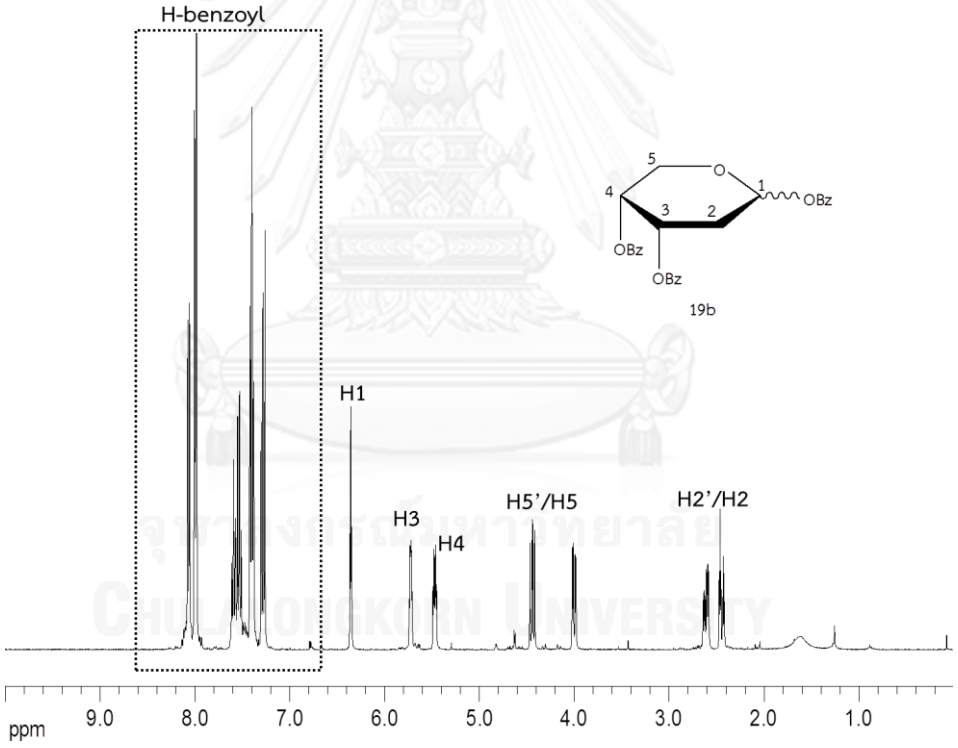

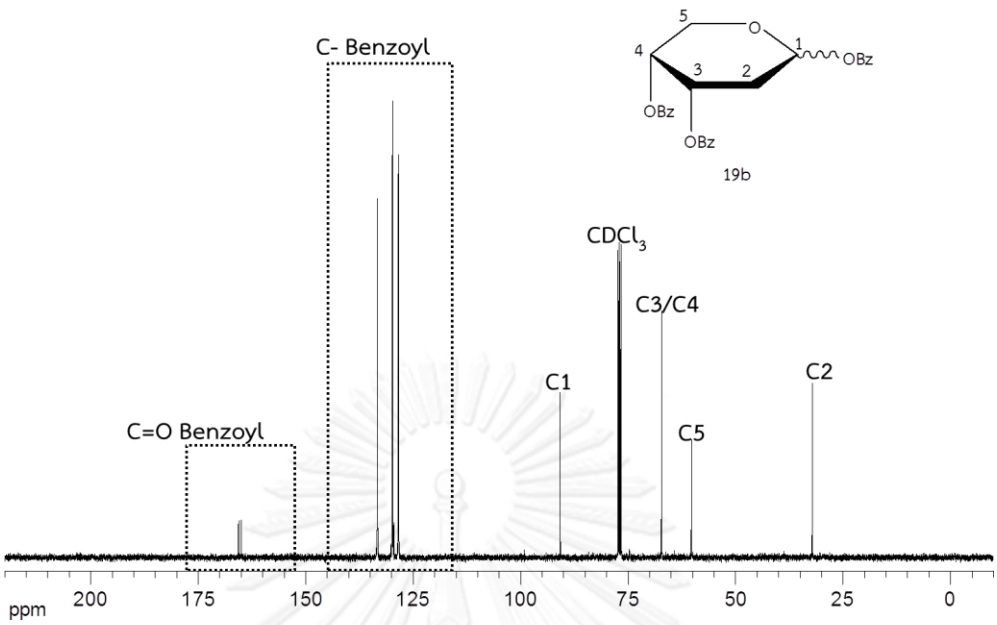

Figure 3.5 ^{1}H NMR ($CDCl_3$, 400 MHz) and ^{13}C NMR ($CDCl_3$, 100 MHz) of tribenzoate derivative of deoxyribopyranose (**19b**)

When the reaction time was extended to overnight, a different product was obtained following a similar work-up procedure and perbenzoylation to give **5c**. However, the NMR was very complicated due to the presence of anomeric as well as furanose and pyranose mixtures. To reduce the complexity of the spectra, the crude perbenzoylated product **5c** was further reduced by $BF_3{\cdot}Et_2O/Et_3SiH$.[48] After the reduction, the ^{1}H, ^{13}C as well as 2D NMR analyses (**Figures A65-A67**) suggested that it was a 1.5:1 mixture of the dibenzoylated furanose (**14**) and pyranose (**15**) forms of 1,2-dideoxy-D-ribose (**Figure 3.6, 3.7**).

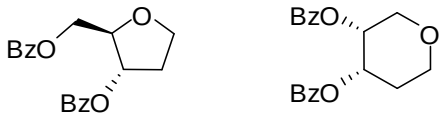

14 **15**

Figure 3.6 Structures of **14** and **15**

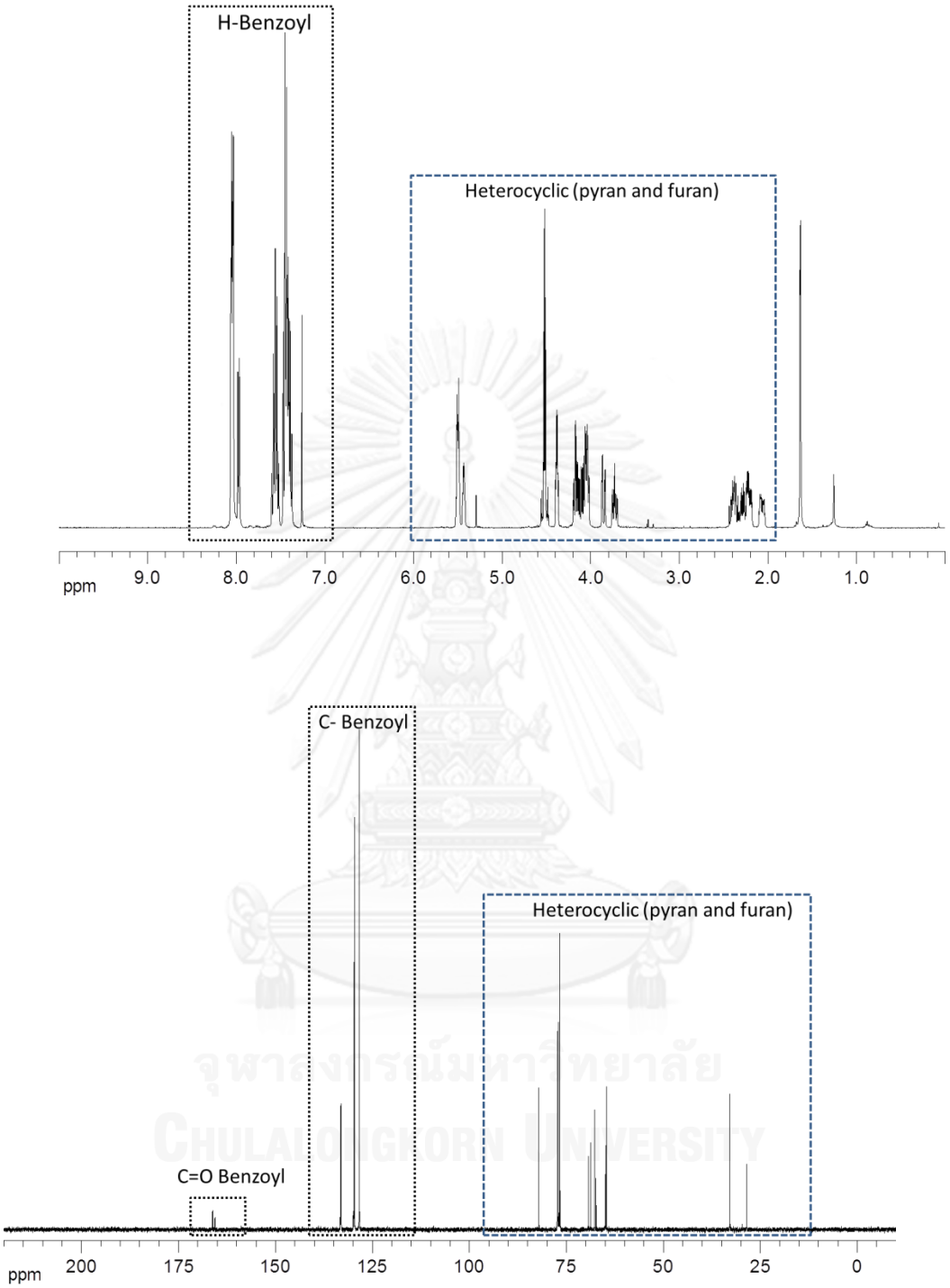

Figure 3.7 ^{1}H (400 MHz, $CDCl_3$) (top) and ^{13}C NMR (100 MHz, $CDCl_3$) (bottom) of the mixture of dibenzoylated 1,2-dideoxy-D-ribofuranose (**14**) and dibenzoylated 1,2-dideoxy-D-ribopyranose (**15**)

Analyses of the heavily overlapping aliphatic protons required a combination of 2D techniques including ^{1}H-^{1}H COSY (revealed the connectivity of protons through *J*-couplings), ^{1}H-^{13}C HSQC (revealed the connectivity of protons and ^{13}C that directly connects to each other) and ^{1}H-^{13}C HMBC (revealed the connectivity of protons and ^{13}C that are two to three bonds apart). The results are as shown in **Figures 3.8** to **3.11**.

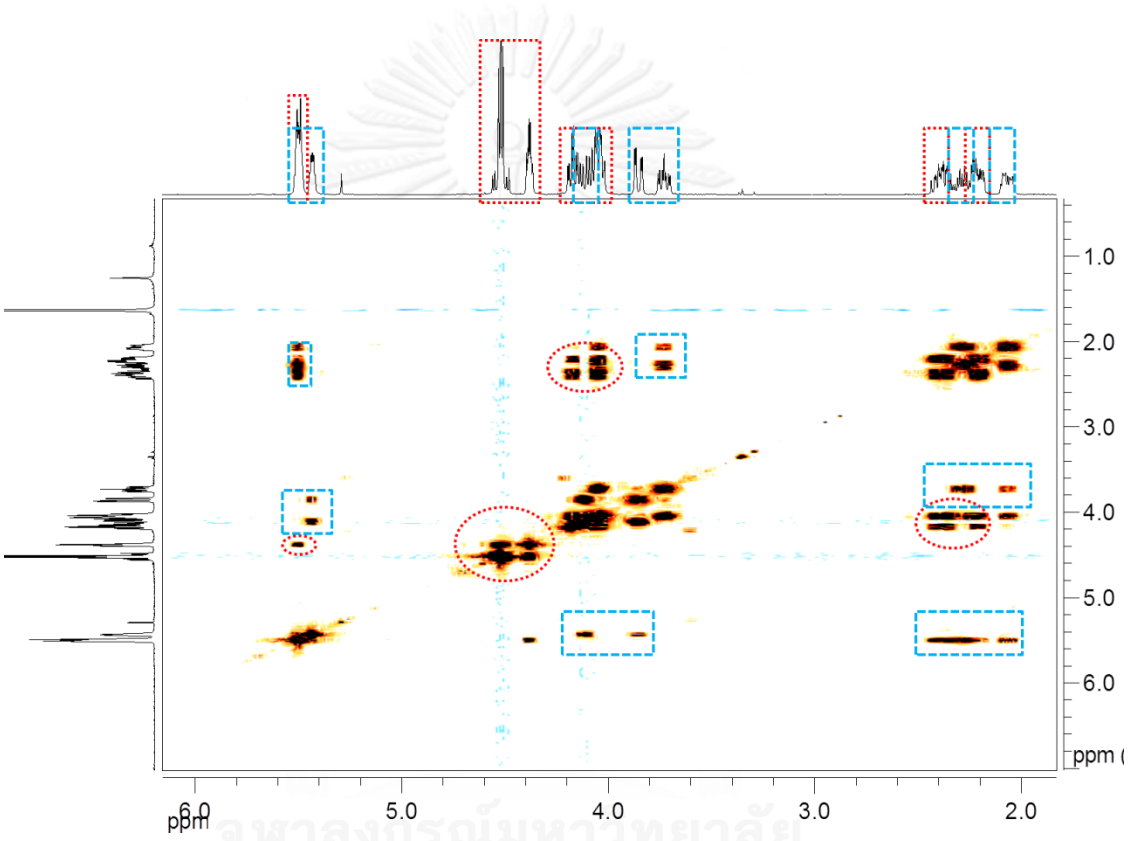

Figure 3.8 ^{1}H-^{1}H COSY NMR spectrum (400 MHz, $CDCl_3$) of the mixture of dibenzoylated 1,2-dideoxy-D-ribofuranose (**14**) (red boxes) and dibenzoylated 1,2-dideoxy-D-ribopyranose (**15**) (blue boxes)

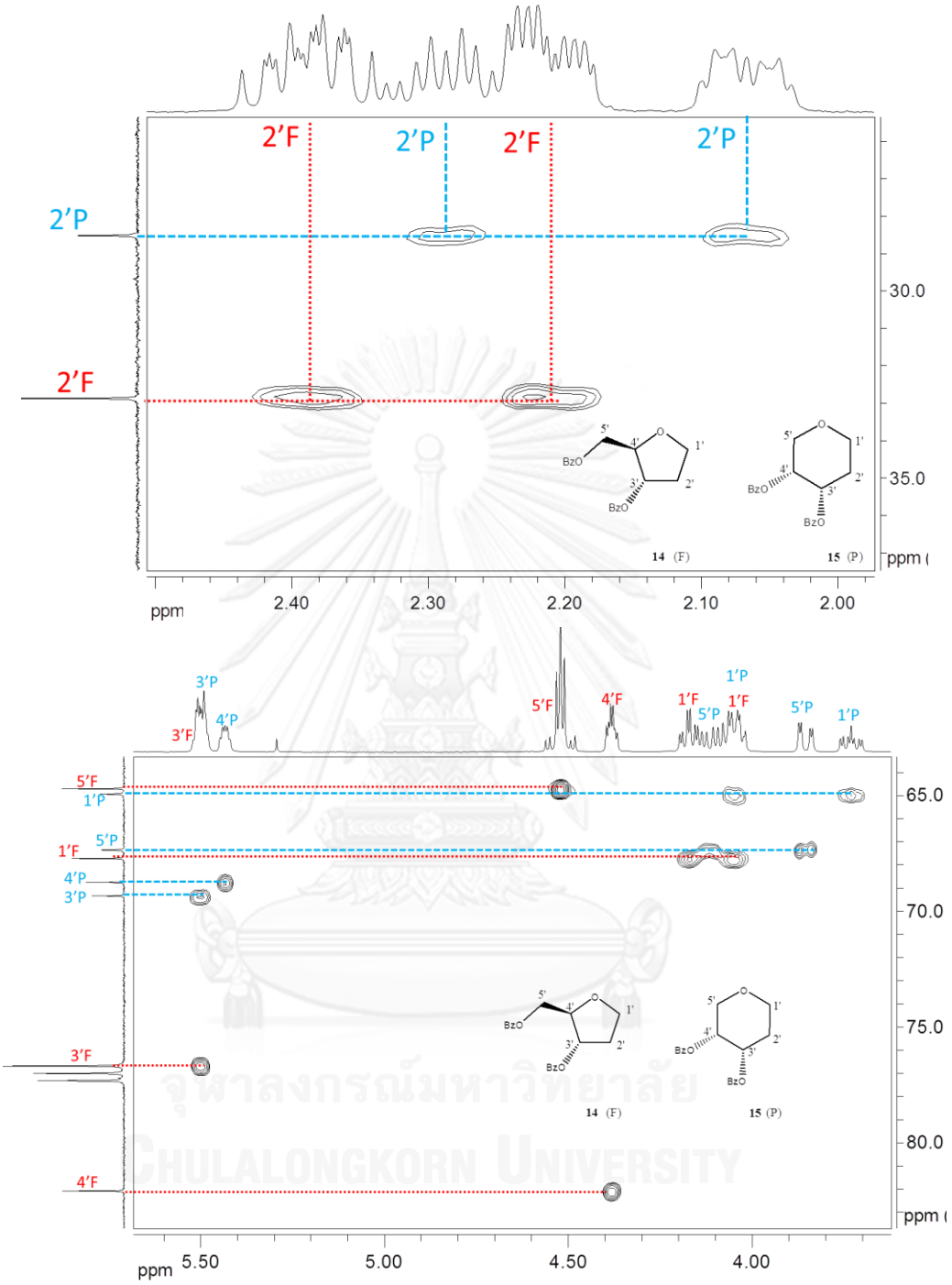

Figure 3.9 ^{1}H-^{13}C HSQC spectrum (400 MHz, $CDCl_3$) of the mixture of dibenzoylated 1,2-dideoxy-D-ribofuranose (**14**) (red) and dibenzoylated 1,2-dideoxy-D-ribopyranose (**15**) (blue)

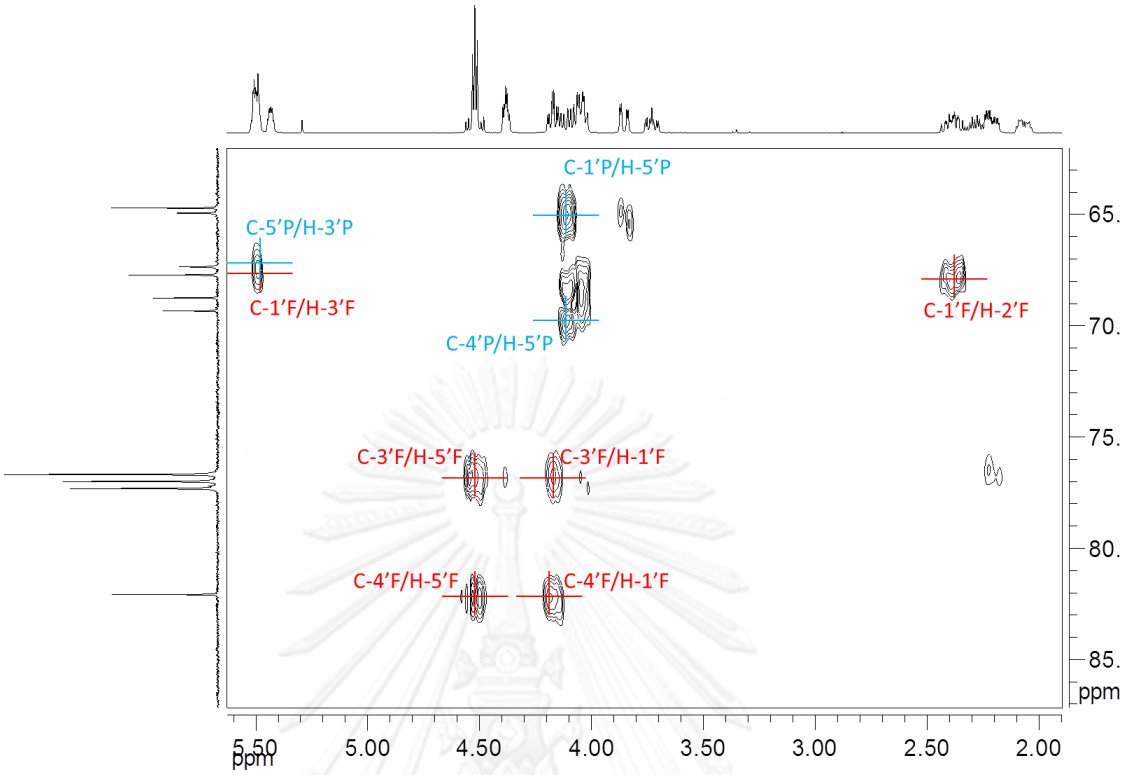

Figure 3.10 ^{1}H-^{13}C HMBC spectrum (400 MHz, $CDCl_3$) of the mixture of dibenzoylated 1,2-dideoxy-D-ribofuranose (**14**) (red) and dibenzoylated 1,2-dideoxy-D-ribopyranose (**15**) (blue)

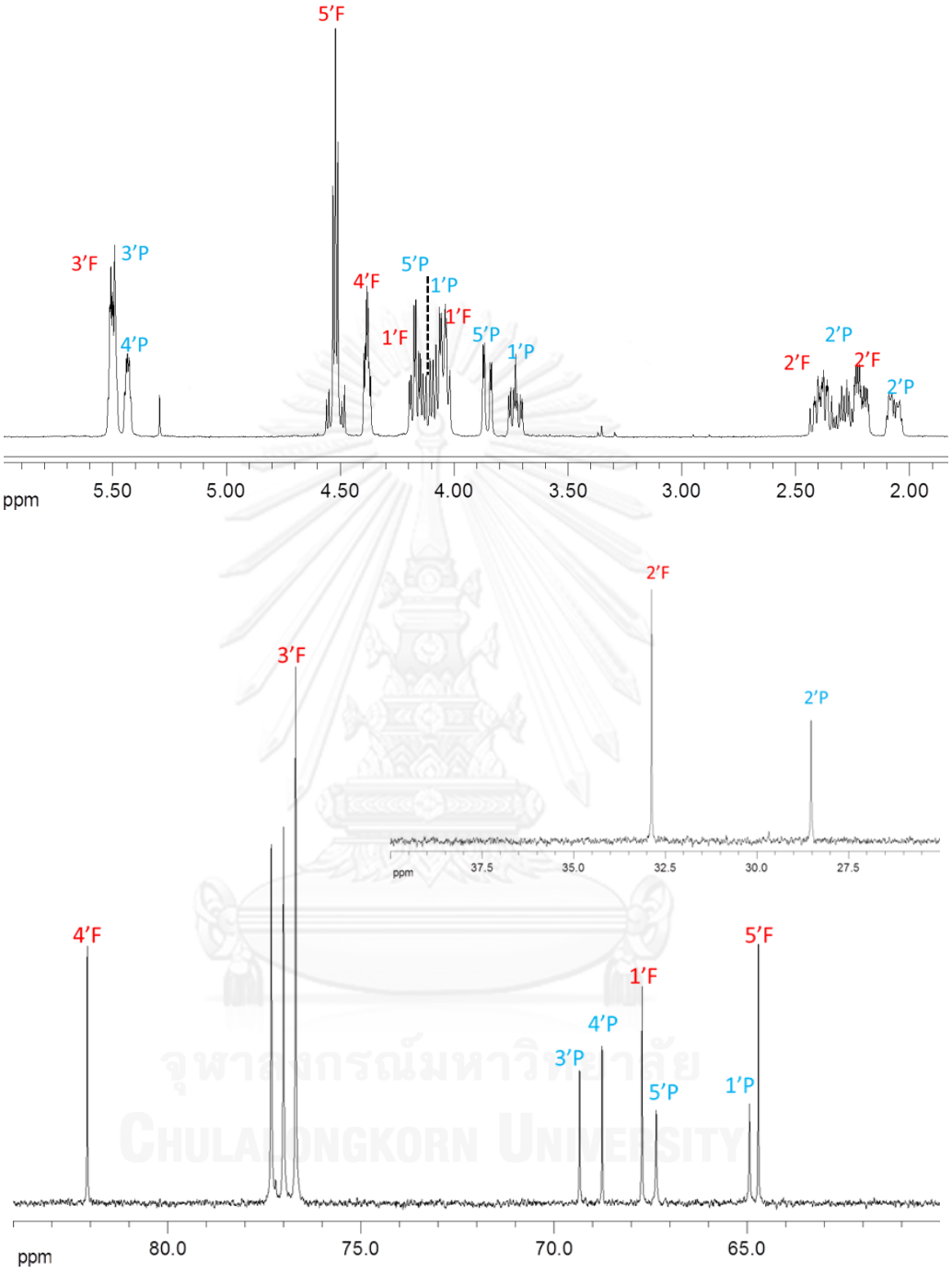

Figure 3.11 ^{1}H (400 MHz, $CDCl_3$) (top) and ^{13}C NMR (100 MHz, $CDCl_3$) (bottom) of the mixture of dibenzoylated 1,2-dideoxy-D-ribofuranose (**14**, red) and dibenzoylated 1,2-dideoxy-D-ribopyranose (**15**, blue) with full assignment (expansion of the aliphatic region only)

Accordingly, it was concluded that the formation of the methylglycoside **3** was successful under the new condition, but the methylglycoside in the furanose and pyranose forms were obtained in almost equal amounts. This was thought to be the result of equilibration between the furanose and pyranose forms of the 2-deoxyribose. The longer reaction time probably facilitates the formation of the more thermodynamically stable pyranose form. As a result, the reaction time was shortened by increasing the amount of the acid catalyst (0.05 equiv) in the next experiments and the reaction was stopped as soon as the starting material was completely consumed (approximately 1 h). Under this modified condition, the furanose dibenzoate **14** was obtained as the major product (>80% purity of the crude reaction mixture, 40% yield of the pure **14** was isolated by column chromatography) (**Figure 3.12**) after quenching, perbenzoylation and reduction as described above. Therefore this condition was chosen for the synthesis of the furanose form (**3**) of the methylglycoside of 2-deoxy-D-ribose. Due to its high water solubility, the methylglycoside (**3**) was not isolated but was used directly for the next steps.

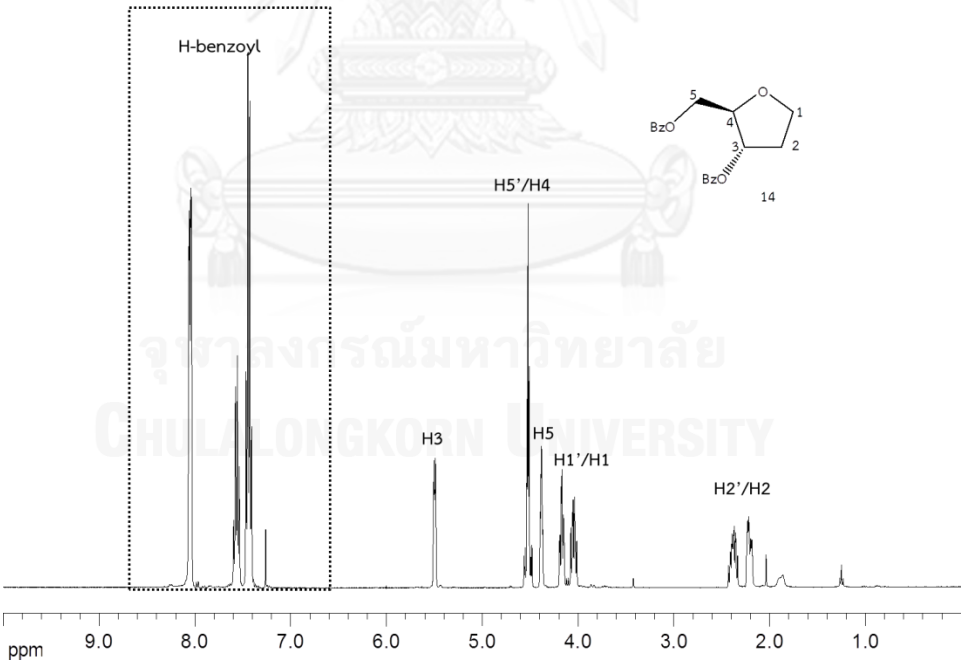

Figure 3.12 ^{1}H NMR ($CDCl_3$, 400 MHz) spectrum of dibenzoylated 1,2-dideoxy-D-ribofuranose (**14**) prepared under the modified condition after purified by column chromatography

3.1.2.2 Selective protection of the primary alcohol functional group of 2-deoxy-D-ribose methylglycoside

In order to achieve the subsequent selective substitution of the 3-OH group (2° alcohol) without competing reaction at the 5-OH group (1° alcohol), the primary alcohol functional group of the methylglycoside (**3**) must be first selectively protected following the literature procedure.[58] The benzoyl and *p*-toluoyl groups were tested under various conditions. Since protection by *p*-toluoyl chloride in CH_2Cl_2 in the presence of pyridine as a base gave the best yield of 67% yield of the desired mono-protected product (**4a**) (**Figures A2** and **A3**) after chromatographic purification, it was chosen as the optimized protection condition (see **Table 3.1**). This mono-protected product could in principle be reduced at the anomeric position before or after the reaction at the 3-position, which will be described in the next section.

Table 3.1 Optimization of primary alcohol protection of diol (**3**)

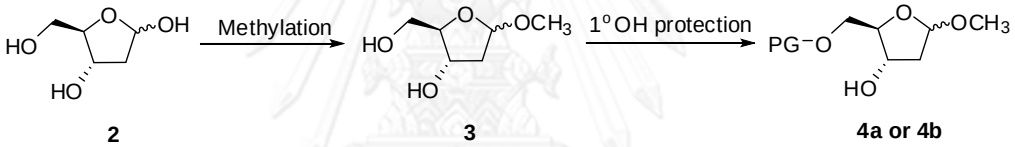

2 **3** **4a or 4b**

Protecting group	Conditions	Scale (mmol)	Yield (%)
benzoyl	benzoyl anhydride (1.2 equiv), Et_3N (2 equiv), CH_2Cl_2 (dry), 0 °C-rt	5.0	52[a]
benzoyl	benzoyl anhydride (1.1 equiv), Et_3N (2 equiv), CH_2Cl_2 (dry), 0 °C-rt	7.7	55[a]
p-toluoyl	*p*-toluoyl chloride (1.1 equiv), Et_3N (2 equiv), CH_2Cl_2 (dry), 0 °C-rt	4.2	45[a]
p-toluoyl	*p*-toluoyl chloride (1.1 equiv), Et_3N (2 equiv), CH_2Cl_2 (dry), 0 °C-rt	44.8	48[a]
benzoyl	benzoyl anhydride (1.1 equiv), Et_3N (2 equiv), CH_2Cl_2 (dry), 0 °C-rt	11.5	29[b]
p-toluoyl	*p*-toluoyl chloride (1.2 equiv) , pyridine (3 equiv), CH_2Cl_2 (dry), 0 °C	85	67[b]

[a]The methylglycoside **3** was isolated and partially purified by column chromatography before the protection. The yield was calculated from **3**. [b]The methylglycoside **3** was not isolated. The yield was calculated from 2-deoxy-D-ribose (**2**).

3.1.2.3 Reduction at the anomeric position

Removal of the anomeric methoxy group could be accomplished by using Et_3SiH and $BF_3{\cdot}OEt_2$ according to the literature procedure,[48] which was previously applied to 2-deoxyribose derivatives with the 3- and 5-OH groups were fully protected [59]. To test the condition, the reduction was first attempted with the perbenzoylated methylglycoside **5c** to avoid possible interference from the unprotected 3'-OH group. The reaction was successful to give compound **14** in 80-90% yields from **5c**. ^{1}H NMR analysis showed disappearance of two singlets due to the anomeric methoxy groups of **5c** (α/β, ~3.20–3.40 ppm) (**Figure A53**) with concomitant decrease in spectral complexity (**Figure 3.12**). Deprotection of this model compound **14** using NaOMe/MeOH gave the parent diol 1,2-dideoxy-D-ribose (**16**) (**Figure A62**) in 80% yield.[49] Selective re-protections of the 5-position of the diol **16** with benzoyl group or TBDMS group to give compounds **17a** or **17b** were attempted (**Table 3.2**, **Figure A63** and **A64**). Although the mono-protection was possible with both protecting groups, these routes are quite wasteful because of multiple protection/deprotection sequences. As a result, alternative protection schemes of the 3'-OH group in **4a** (**Figure A2** and **A3**) or **4b** (**Figure A51**) were next explored.

Table 3.2 Optimization of primary alcohol protection of diol (**16**)

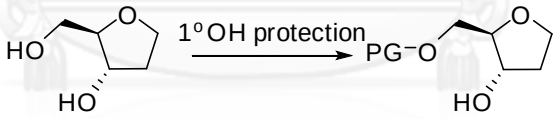

16 **17a or 17b**

Protecting group	Conditions	Yield (%)
benzoyl	benzoyl anhydride, Et_3N, CH_2Cl_2 (dry), 0 °C-rt	67
t-butyldimethylsilyl	*t*-butyldimethylsilyl chloride, imidazole, DMAP, CH_2Cl_2 (dry), 0 °C-rt	68

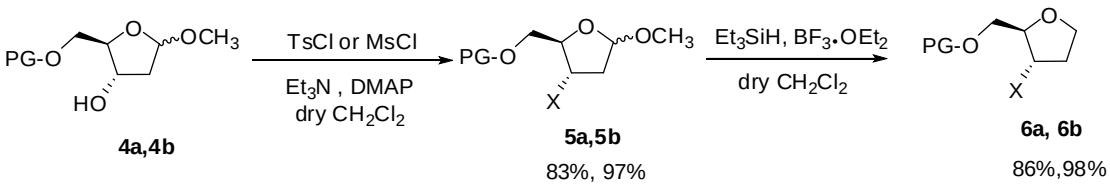

Figure 3.13 Synthesis pathway of **6a** and **6b**

Since the stereochemistry of the 3-OH group must be eventually inverted by S_N2 reaction with an oxygen nucleophile,[60, 61] it was envisioned that the 3-OH group in **4a** and **4b** could be "protected" with a sulfonate ester such as tosylate (**5a**) or mesylate (**5b**) ester before performing the anomeric reduction. Both **5a** and 5**b** were successfully reduced to **6a** (tosylate) and **6b** (mesylate) in 86 and 98 % yields (**Figure 3.13**, **Figure A9** and **A10** for **6a** and **Figure A54**), confirming that the sulfonate ester is compatible with this reduction procedure. The proposed mechanism of the reduction is shown in **Figure 3.14**, which proposed the activation by BF_3 and reduction by silane although the exact details cannot be specified without further investigation.[62]

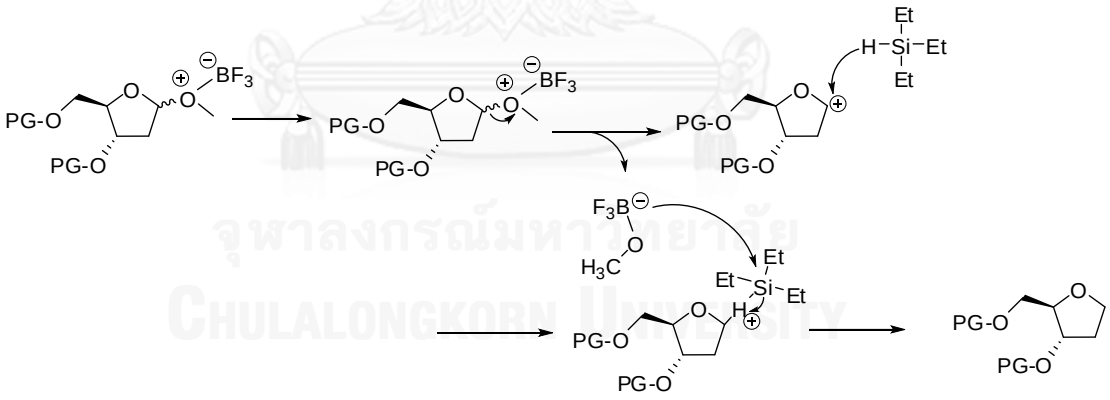

Figure 3.14 A possible mechanism of the reduction of methylglycosides with hydrosilane [62]

3.1.2.4 Inversion of stereochemistry at the 3-position

After the successful anomeric reduction was achieved, the next key step involved a nucleophilic substitution of the secondary -OH group at the 3-position with a nitrogen nucleophile with retention of stereochemistry. However, S_N2 type nucleophilic displacement of the OH group should normally give the undesired stereochemically inverted product. A double inversion strategy was therefore applied, whereby the stereochemistry of the 3-OH group was first inverted. Mitsunobu reaction in the presence of an oxygen nucleophile such as formic acid or acetic acid followed by hydrolysis, is one of the most frequently employed methods for stereochemical inversion of 2º OH group.[63] Alternatively, in the presence of MeOTs or MSA,[60] the stereochemical inversion and sulfonylation was achieved in a single reaction. This reaction was attempted with the model compounds **17a**, **17b** and **4b** (conditions 1: MeOTs, PPh_3, DIAD, THF; conditions 2: MSA, PPh_3, DIAD, toluene[60]). Unfortunately, none of these reactions was successful. In the best cases, only impure products were obtained in very low yield.

Another obvious alternative to the Mitsunobu reaction was to first convert the alcohol to a good leaving group such as a mesylate or tosylate, followed by a nucleophilic substitution with an oxygen nucleophile. One relatively overlooked as a nucleophile for stereochemical inversion of OH groups is nitrite ion.[60, 61] It had been successfully used in stereochemical inversion of various alcohols including carbohydrate derivatives.[60, 61, 64-66] The nucleophilic substitution reactions of **6a** (dideoxy, 3-tosylate), **6b** (dideoxy, 3-mesylate) or **5a** (methylglycoside, tosylate), **5b** (methylglycoside, mesylate) with sodium nitrite in a polar aprotic solvent (DMF or DMSO) were attempted. The tosylate and mesylate derivatives of methylglycoside (**5a** and **5b**) were obtained by treatment of the monoprotected alcohols (**4a** or **4b**) with mesyl chloride or tosyl chloride in the presence of catalytic DMAP, Et_3N/CH_2Cl_2 to give the desired products in 83 and 97 % yield (**Figure 3.13**), respectively. Gratifyingly, the reaction of **6a** and **6b** with excess of $NaNO_2$ in DMF or DMSO at 120 ºC yielded the expected inversion products **7a** and **7b** (**Figure A55**) as confirmed by ^{1}H NMR albeit in rather poor yield. The ^{1}H signals due to the mesyl or tosyl groups disappeared in the products. Moreover, the ^{1}H NMR spectrum of the compound **7b** resembled the monoprotected alcohols (**17a**), but significant differences in chemical shifts and coupling constants were observed as shown in **Figure 3.15**.

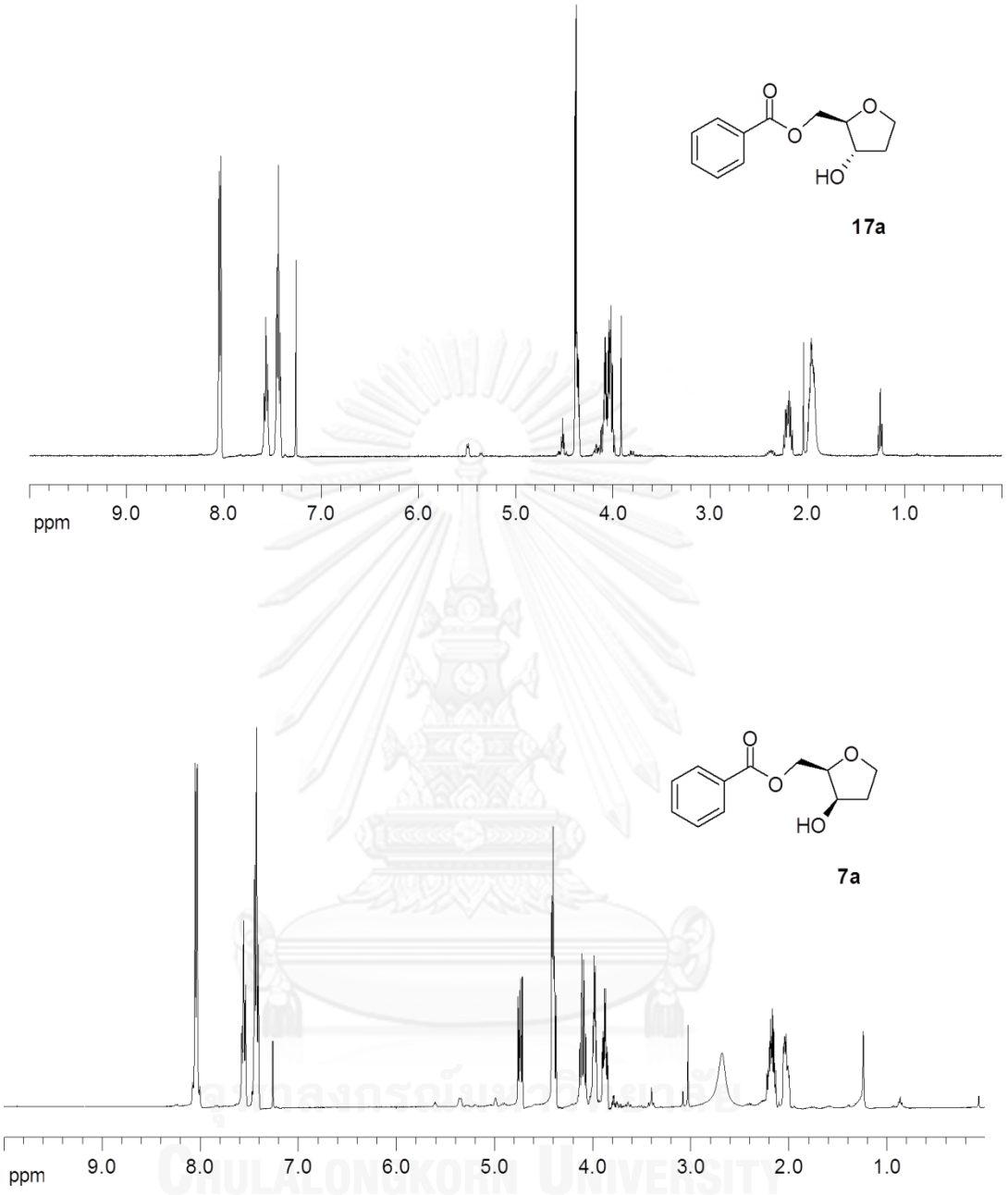

Figure 3.15 Comparision of ^{1}H NMR spectra between **7a** and **17a** ($CDCl_3$, 400 MHz)

The reaction condition was next optimized as shown in **Tables 3.3** and **3.4** The dideoxyribose derivatives **6a** and **6b** (**Table 3.4**) gave better results compared to the methylglycosides **4a** and **4b** (**Table 3.3**), which may be due to the instability of the methylglycosides at high temperature required to achieve the substitution reaction.

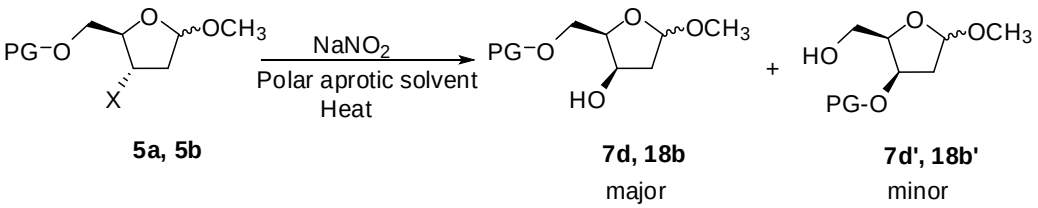

5a, 5b **7d, 18b** major **7d', 18b'** minor

Table 3.3 Optimization of the S_N2 inversion with nitrite (with methoxy group at the anomeric position)

Leaving group (X)	$NaNO_2$ (Equiv.)	Solvent	Time (h.)	Scale (mmol)	% yield (combined)[a]	% yield[b]
Mesylate	1.5	DMF	6	1.58	38	24
Mesylate	5	DMSO	4	2.95	29	20
Tosylate	26	DMSO	3	5.76	30	25

[a]Combined yield of the expected product (**5a**, **5b**) and migrated product (**5a'**, **5b'**) and purified by column chromatography. [b]Yield of the expected product (**5a**, **5b**) based on the combined yield and ^{1}H NMR analysis.

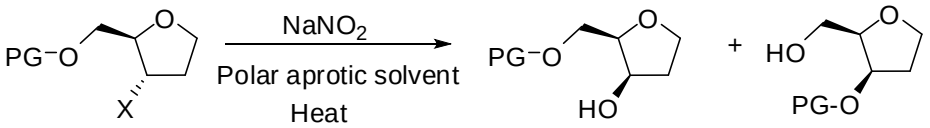

6a, 6b **7a, 7b** **7a, 7b**

Table 3.4 Optimization of the S_N2 inversion with nitrite (without methoxy group at the anomeric position)

Leaving group (X)	$NaNO_2$ (Equiv.)	Solvent	Time (h.)	Scale (mmol)	% yield (combined)[a]	% yield[b]
Mesylate	1.5	DMF	14	1.05	17	15
Mesylate	5	DMSO	5	0.92	18	17
Tosylate	10	DMSO	5	10.2	60	N.D.
Tosylate	10	DMSO	3.5	5.08	57	47
Tosylate	5	DMSO	1.5	1.29	54	N.D. (30)
Tosylate	5	DMSO	1.5	1.80	43	34 (28)
Tosylate	5	DMSO	5	2.78	63	32 (28)
Tosylate	5	DMSO	5	2.06	51	38 (26)
Tosylate	5	DMSO	5	4.51	52	37

[a]Combined yield of the expected product (**7a**, **7b**) and migrated product (**7a'**, **7b'**) and purified by column chromatography.

[b]Yield of the expected product (**7a**, **7b**) based on the combined yield and ^{1}H NMR analysis. Yield in parenthesis refers to purified yield via reaction with Bz_2O followed by column chromatography (*vide infra*).

In some instances, significant migration of the *p*-toluoyl group from the primary OH to the (inverted) secondary OH positions was observed in a range between 25 to 50% (3:1 to 1:4 of **7a**:**7a'**) due to their close proximity. This migration occurs quite readily in 3-OH inverted compounds like **7a** because the inverted 3-OH group became on the same face as the *p*-toluoyl group at the 5-OH, which facilitate the intramolecular nucleophilic attack (**Figure 3.16**). The migration was probably accelerated by the high temperature required for the substitution reaction. Moreover, this migration was observed even when the product **7a** was isolated in pure form and kept for a prolonged period. Due to the similar polarity, this contaminated *p*-toluoyl-migrated byproduct could not be isolated by chromatography. Fortunately, the sterically congested inverted 3-OH group is much less reactive than the free 5-OH group. Hence, reaction of the mixture with Bz_2O/Et_3N in CH_2Cl_2 gave a 5-benzoyl/3-toluoyl protected dideoxyribose (**22**), which could be easily removed from the unreacted **7a** by column chromatography.

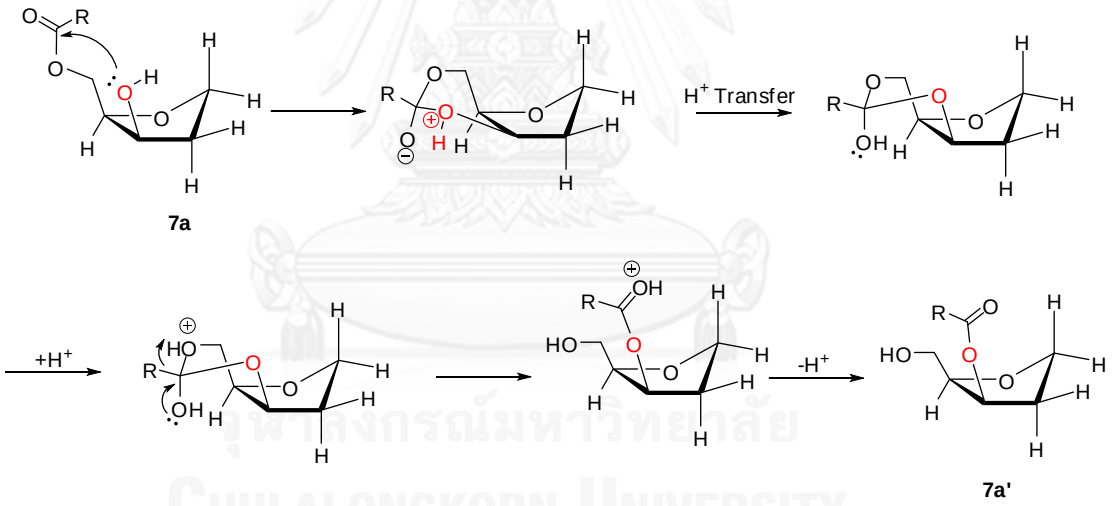

Figure 3.16 Intramolecular nucleophilic attack of **7a** to **7a'**

The best product yield was obtained from the reaction of the tosylate derivative (**6a**) and 5 equiv. of $NaNO_2$ in DMSO at 120 °C for 5 h. Using DMF as solvent was less preferred since the product was contaminated by unidentified impurities possibly due to decomposition of DMF at high temperature. The mechanism of this reaction is illustrated in **Figure 3.17**.

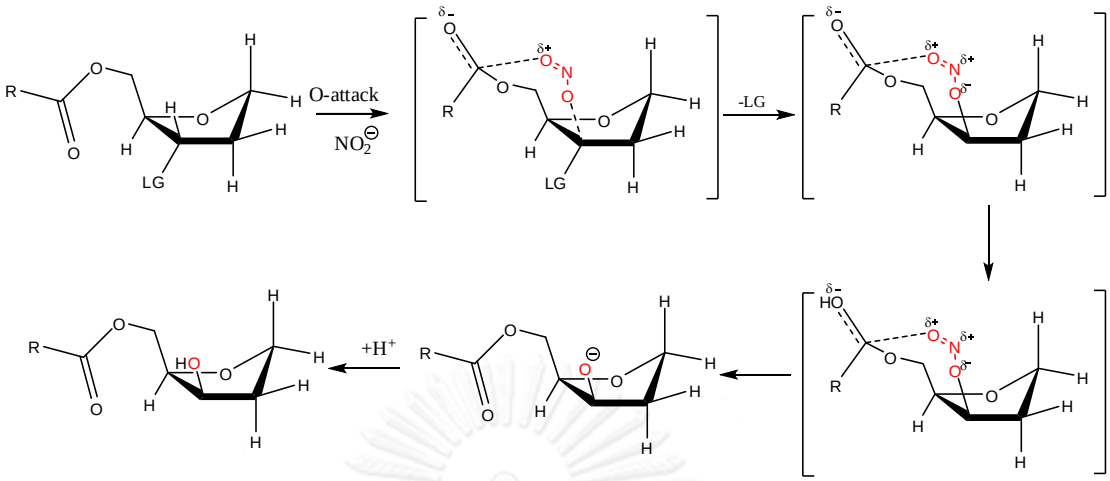

Figure 3.17 Mechanism of inversion reaction with nitrite [67]

3.1.3 Functional group manipulation (azidation, reduction, oxidation)

According to the retrosynthesis plan (**Figure 3.3**), the inverted 3-OH group must be replaced with a suitable nitrogen nucleophile (azide was chosen in this case). The 2° OH group at the position 3 of the key intermediate **7a** was first activated followed by S_N2 reaction with NaN_3. The remaining steps are straightforward functional group manipulations (azide reduction, nitrogen protection, oxidation and protecting groups exchange).

3.1.3.1 Conversion of the secondary alcohol to a good leaving group

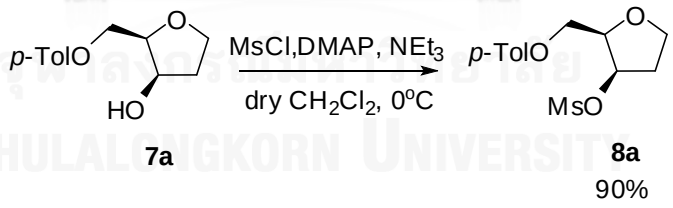

7a **8a** 90%

Figure 3.18 Synthesis of **8a**

To allow substitution, the 2° OH group at the position 3 of the key intermediate **7a** needed to be activated. Unexpectedly, all attempts to put a tosyl group to the 3-OH of compound **7a** under standard condition ($TsCl/Et_3N$, cat. DMAP in dry CH_2Cl_2) failed. Since acetylation of **7a** proceeded normally to give the acetate **18** in good yield, the difficulty in tosylation was attributed to steric effect around the 3-OH group. On the other hand, mesylation under the similar condition (3 equiv. $MsCl/Et_3N$, cat. DMAP in dry CH_2Cl_2) proceeded readily at 0 °C to give the mesylate

8a in 90% yield (**Figure 3.18**). The characteristic singlet at 3.04 ppm with an integration of 3 protons in ^{1}H NMR and a CH_3 signal at 38.5 ppm in ^{13}C NMR spectrum of **8a** (**Figures A19** and **A20**) confirmed the successful mesylation.

3.1.3.2 Azidation

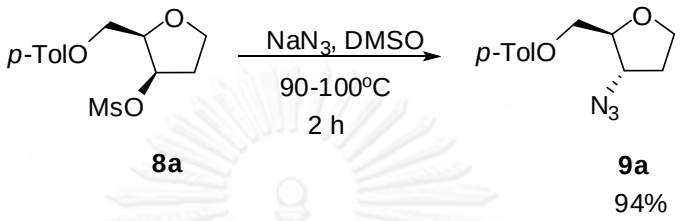

8a **9a**
94%

Figure 3.19 Synthesis of **9a**

With the mesylate **8a** in hands, the next step was the introduction of the azide group by S_N2 reaction with sodium azide in a polar aprotic solvent. Reaction of **8a** with 5 equivalents of NaN_3 in DMSO at 80 ºC for 24 h gave the expected azide **9a** (**Figures A23** and **A24**) in 64% yield. An improved yield (94%) was achieved (**Figure 3.19**) when the temperature was increased to 90–100 ºC and reaction time was shortened (2 h).

3.1.3.3 Reduction of azido to amino group

One of the most common methods to reduce azido to amino group is hydrogenation with H_2 gas over Pd/charcoal catalyst.[43] Since a newly generated amino group is highly reactive and very polar, it is preferable to protect this amino group as soon as it is formed. This could be achieved in a one-pot fashion by hydrogenation of the azide **9a** in the presence of Boc_2O to give a Boc-protected amine **10** (**Figures A28-A30**). The Boc group was chosen because of its stability, compatibility with the remaining reaction sequences and ease to remove by acid treatment. The product **10** was obtained in 80-94% yield as a white solid. ^{1}H NMR analysis showed a singlet at 1.44 ppm with an integration of 9H characteristic of Boc C$\underline{H}_3$. ^{13}C NMR also confirmed the presence of the Boc $\underline{C}H_3$, $\underline{C}$ and $\underline{C}O$ at 28.4, 79.9 and 155.5 ppm respectively (**Figures A27-A30**). The *p*-toluoyl group in **10** was next removed by $LiOH{\cdot}H_2O$ in THF to give the Boc-protected aminoalcohol **11** (**Figures A33** and **A34**) in 89-91% yield (**Figure 3.20**).

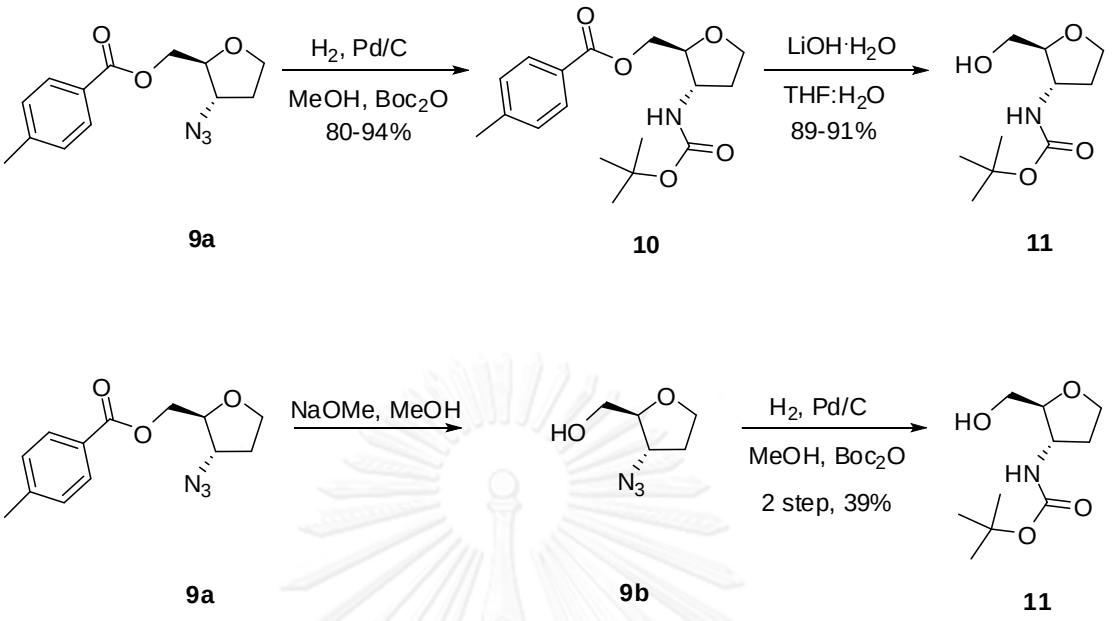

Figure 3.20 Reduction of azido group to amino and subsequent protection with Boc in one-pot reaction

In an alternative reaction sequence, the p-toluoyl group in **9a** was first removed by NaOMe/MeOH to give the azido alcohol **9b**, which was subsequently reduced by hydrogenation in the presence of Boc_2O to give the same compound **11** in 39% yield (from **9a**). Since the total yield of **11** from **9a** by the deprotection-reduction approach was rather poor, the reduction-deprotection approach described above which gave 71-86% overall yield of **11** was chosen as the preferred method.

3.1.3.4 Oxidation of primary alcohol to carboxylic acid

Several methods for oxidation of primary alcohol to carboxylic acid are available.[68] A TEMPO-mediated oxidation was chosen because of its high efficiency under mild reaction condition. In addition, it does not produce toxic heavy metal wastes. Several co-oxidants have been successfully used in combination with catalytic amounts of TEMPO for oxidation of primary alcohols.[69] The choice of the oxidant and reaction conditions can determine whether the oxidation of a 1° alcohol will stop at the aldehyde stage or proceed further to carboxylic acid.[70] In this case, the hypervalent iodine reagent bis-acetoxyiodobenzene (BAIB) was used as the oxidant in preference to the more commonly used $NaClO/NaClO_2$ combination because this condition was successfully used for the previous report on preparation of nucleoside-5'-carboxylic acids.[71]

Oxidation of the primary alcohol group in compound **11** with BAIB (3 equiv.) in the presence of TEMPO (0.2 equiv.) in a 1:1 mixture of ACN and water proceeded to give the Boc-protected amino acid **12** in 74-93% yield (**Figure 3.21**). The reaction mechanism was depicted in **Figure 3.22**. The disappearance of the 5-CH_2 signals from ^{1}H NMR spectrum (**Figure A37**) and the presence of a C=O resonance at 172.7 ppm in ^{13}C NMR spectrum of **12** (**Figure A37**) confirmed the success of oxidation.

Figure 3.21 TEMPO-BAIB oxidation of primary alcohols to carboxylic acids[69, 71]

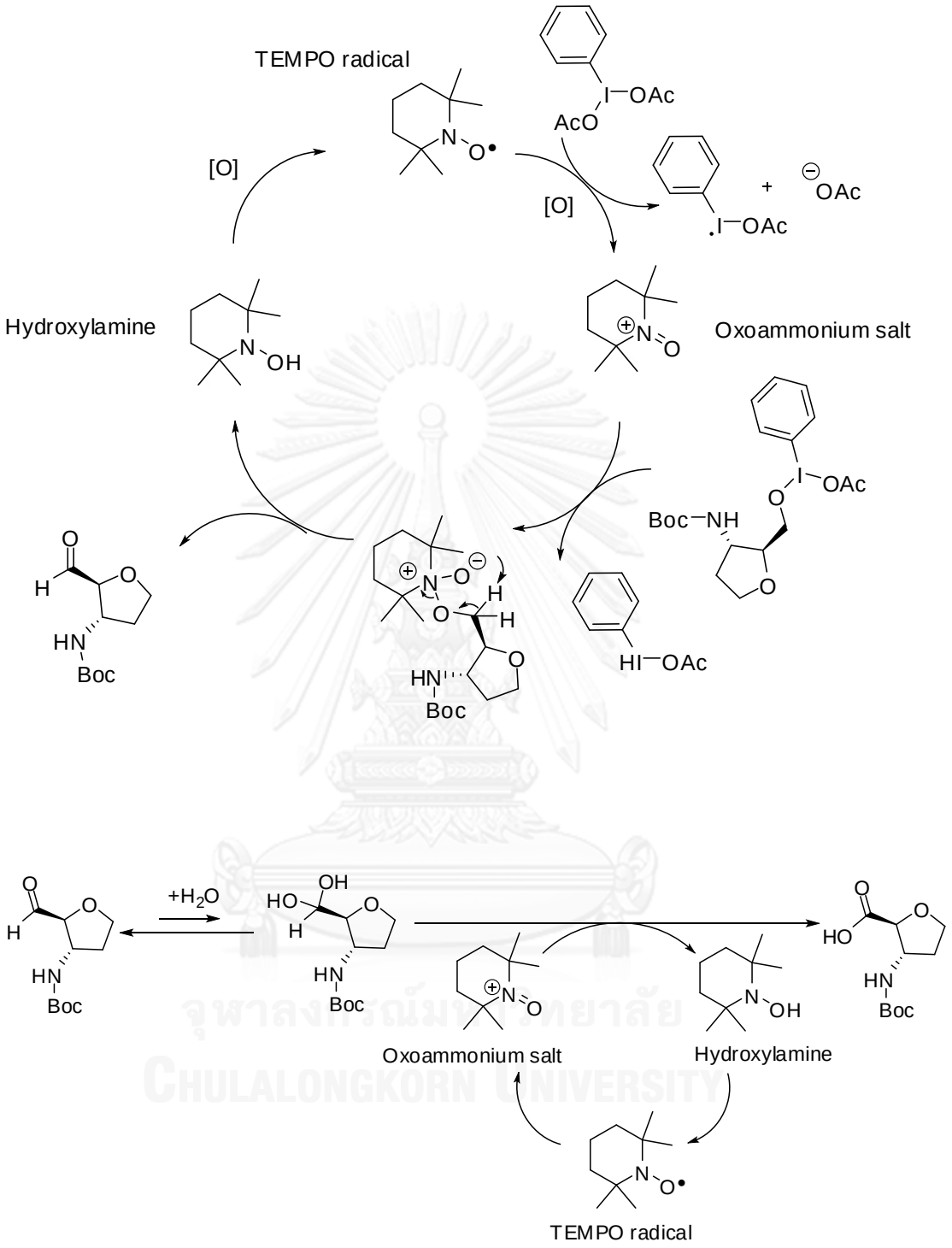

Figure 3.22 Mechanism of TEMPO-BAIB oxidation of a 1° alcohol [69]

3.1.4 Protection and activation

The Boc-protected β-amino acid **12** was then converted to the desired synthetic target **1a** as follows.

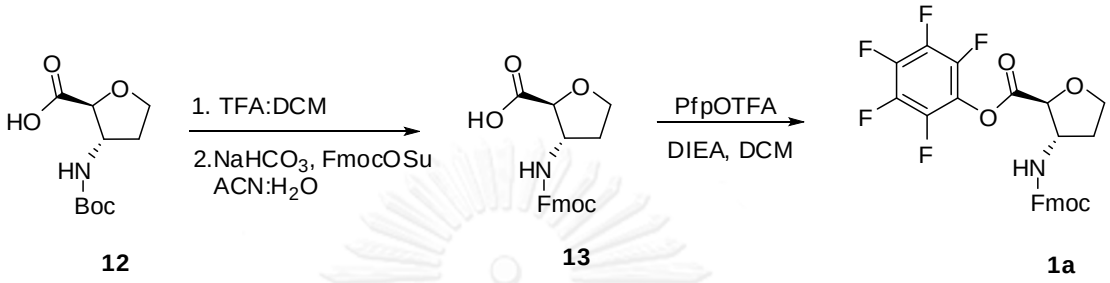

12 **13** **1a**

Figure 3.23 Synthesis of **1a** from **12**

3.1.4.1 Fmoc protection

Compound **12** (**Figure 3.23**) was treated with a mixture of TFA and CH_2Cl_2 (1:1, 30 minutes) to remove the Boc group. Without isolation of the free amino acid, the amino group was further protected with Fmoc under standard conditions (FmocOSu, aq $NaHCO_3$-ACN) [16] to give the desired Fmoc-protected amino acid **13** in 73% yield. ^{1}H NMR analysis showed several signals which are characteristic of the Fmoc group in the aromatic region at 7.33 (triplet), 7.37 (triplet), 7.69 (doublet), 7.74 (doublet) and 7.89 (doublet) ppm (**Figure A41**). ^{13}C NMR showed signals of Fmoc aliphatic CH at 46.6 ppm, Fmoc aliphatic CH_2 at 65.3 ppm, Fmoc aromatic CH at 120.0, 121.2, 125.0 and 126.9 ppm, Fmoc aromatic C at 140.6 and 143.7 ppm, and Fmoc CO at 155.4 ppm (**Figure A42**).

3.1.4.2 Activation of the carboxyl group

Finally, the pentafluorophenyl ester **1a** (**Figures A45** and **46**) was obtained as a white solid in 55-64 % yield by reaction of the acid **13** with pentafluorophenyl trifluoroacetate (PfpOTfa) in the presence of *N*,*N*-diisopropylethylamine (DIEA). The lowered polarity of **1a** compared to the acid **13**, as well as the ^{19}F NMR spectrum clearly confirmed its successful synthesis (**Figure A47**). The mechanism is as shown in **Figure 3.24**.

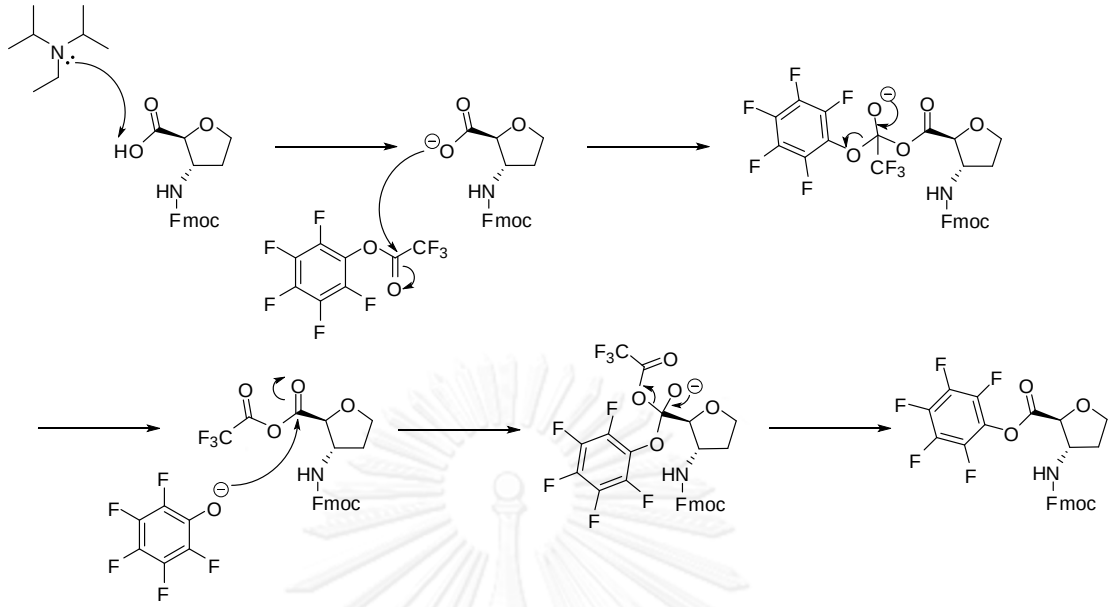

Figure 3.24 Mechanism of carboxyl group activation by PfpOTfa

3.1.5 Summary of the synthesis plan and alternative reaction sequences

The reaction sequence from 2-deoxy-D-ribose (**2**) to the target molecule **1a** can be summarized in **Figure 3.25**. The overall yield of **1a** was 3% over 13 steps from **2**. Although the synthesis was straightforward and produced the desired product, the reaction sequence is lengthy and not very efficient, especially during the conversion from **6a** to **7a**. Another alternative synthetic plan starting from AZT as mentioned earlier (**Figure 3.3**) was considered since AZT already have the azide functional group with the correct stereochemistry at the C3 position. Unfortunately, all attempts to eliminate the thymine moiety from AZT by treatment with hexamethyldisilazane (HMDS) in the presence of various acidic catalysts (MSA, ammonium sulfate) with or without protection of the 5-OH group and before or after reduction of the azide group were not yet successful.[72]

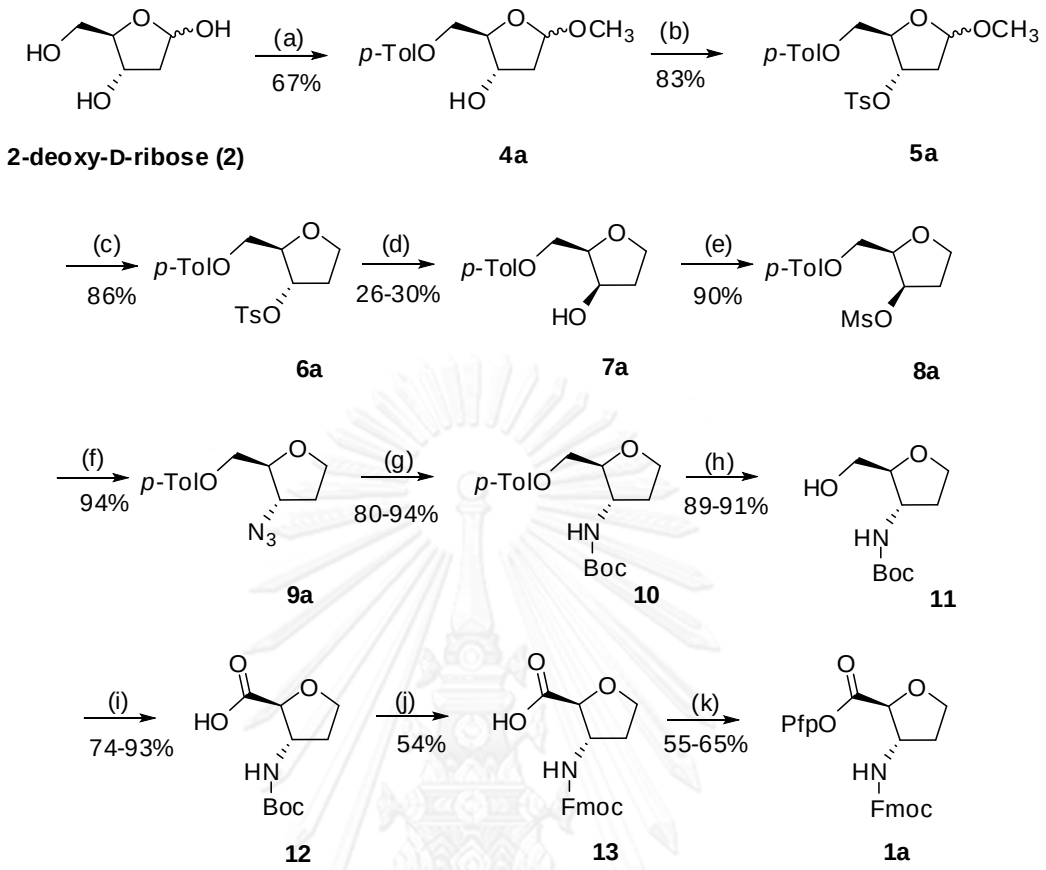

Figure 3.25 Summary of the chosen synthetic plan for compound **1a**.

Reagent and conditions: (a) i) methanesulfonic acid, MeOH, rt, 30 min, ii) *p*-toluoyl chloride, pyridine, CH_2Cl_2, 0 °C, 67%; (b) *p*-TsCl, DMAP (cat), Et_3N, CH_2Cl_2, 0 °C to rt, 83%; (c) Et_3SiH, $BF_3{\cdot}OEt_2$, 0 °C to rt, 86%; (d) $NaNO_2$, DMSO, 120 °C, 26-30%; (e) MsCl, DMAP (cat), Et_3N, CH_2Cl_2, 0 °C, 90%; (f) NaN_3, DMSO, 90-100 °C, 94% ; (g) Pd/C, H_2 (1 atm), Boc_2O, MeOH, 80-94%; (h) LiOH, THF:H_2O (1:1), rt, 89-91%; (i) TEMPO (cat), BAIB, ACN:H_2O (1:1), rt, 74-93%; (j) i) TFA:CH_2Cl_2 (1:1), (ii) FmocOSu, $NaHCO_3$, ACN:H_2O (1:1), pH 8, rt, 73%; (k) PfpOTfa, DIEA, CH_2Cl_2, 55-64%.

3.2 PNA oligomer synthesis and characterization

The atfcPNA were synthesized by Fmoc solid phase peptide synthesis analogously to acpcPNA.[13] The scale of the synthesis was 1.5 μmol. One homothymine and one mix base sequences were synthesized in order to compare the DNA binding affinities with the corresponding acpcPNA sequences. For the mix sequence, a fluorescein label was also introduced at the *N*-terminus to investigate the advantage of atfcPNA in decreasing the non-specific interactions previously observed with acpcPNA. All atfcPNA were purified to >90% purity by reverse phase HPLC and gave the expected masses (MALDI-TOF). The synthesis and characterization data of all atfcPNAs are summarized in **Table 3.5**. It should be noted that the retention time of atfcPNA are significantly shorter than the corresponding acpcPNA with the same sequence (T9 atfcPNA: 30.6 min; T9 acpcPNA: 33.3 min), indicating that atfcPNA is more hydrophilic than acpcPNA (the different of molecular weight was negligible).

Table 3.5 Characterization data of atfcPNA

PNA sequences	t_R[a] (min)	Yield (%)	Mol. Wt. (calcd)	Mol. Wt.[b] (found)
Ac-TTTTTTTTT-$LysNH_2$	30.6	44	3197.19[c] 3219.18[d] 3235.29[e]	3193.52[c] 3215.84[d] 3231.56[e]
Ac-GTAGATCACT-$LysNH_2$	25.1	22	3578.56[c]	1789.78,[f] 3578.33[c]
Flu-GTAGATCACT-$LysNH_2$	28.5, 29.3	15	3893.82	1947.40,[f] 3893.27

[a]Reverse phase HPLC: C-18 column 3 μ particle size 4.6 x 50 mm; gradient of water-methanol containing 0.1% TFA, monitoring by UV absorbance at 260 nm. [b]MALDI-TOF mass spectrometry in linear positive ion mode using α-cyano-4-hydroxycinnamic acid (CCA) as a matrix. [c]$[M+H]^+$, [d]$[M+Na]^+$, [e]$[M+K]^+$ and [f]$[M+H]^{2+}$

3.3 DNA and RNA binding properties of atfcPNA

DNA bases absorb UV light at 260 nm. Hypochromism is generally observed upon base pairing in DNA duplexes. As a result, heating of a DNA duplex result in its dissociation accompanied with a slight increase (*ca*. 10%) in the absorbance at 260

nm. The plot between UV absorption and temperature gives a sigmoidal curve called a melting curve. The temperature at the midpoint of the melting curve (T_m, obtained from the maxima of the first derivative plot) can be used as a parameter to estimate the stability of the duplex. The higher T_m, the more stable is the duplex.

3.3.1 Hybridization of homothymine atfcPNA sequence

3.3.1.1 UV-T_m (melting temperature)

The ability of atfcPNA to recognize its complementary single stranded DNA was first investigated by UV-melting experiment. Four DNA sequences were used as the counter-strand: d(AAAAXAAAA), X = A, C, G and T. The T_m values are summarized in **Table 3.6**. The corresponding T_m values for acpcPNA hybrids with the same sequences taken from literature[13, 17] are also included for comparison. It can be seen that the T_m values of homothymine atfc-DNA hybrids are considerably lower than those of acpcPNA-DNA hybrids, both in the absence and presence of salt (NaCl). This may be due to the unfavorable interactions between lone pair of oxygen atom in *SS*-ATFC spacer and phosphodiesters backbone of DNA, or the inability of the THF ring in atfcPNA to adopt exactly the same conformation as the cyclopentane ring in acpcPNA. Nevertheless the pairing between atfcPNA and DNA is specific as shown by a marked decrease of the T_m values (19.3 to >40 °C). Again, the specificity appeared to be less than that of acpcPNA as shown by smaller Tm differences.

Table 3.6 The thermal stability of PNA sequence: Ac-TTTTTTTT-LysNH_2 and DNA

Entry	DNA sequences	T_m (°C) atfcPNA	ΔT_m (°C)[c] atfcPNA	T_m (°C)[d] acpcPNA	ΔT_m (°C)[c] acpcPNA
1[a]	5'-AAAAAAAAA-3'	64.1	-	>80	-
2[b]	5'-AAAAAAAAA-3'	60.3	-	72.5	-
3[a]	5'-AAAA<u>C</u>AAAA-3'	44.8	19.3	47.7	29.1
4[a]	5'-AAAA<u>G</u>AAAA-3'	<20	>40	39.0	37.8
5[a]	5'-AAAA<u>T</u>AAAA-3'	41.8	22.3	47.6	29.2

[a]Conditions: 1.0 μM PNA, 1.0 μM DNA, 10 mM sodium phosphate buffer pH 7.0, 0 mM NaCl. [b]Conditions: 1.0 μM PNA, 1.0 μM DNA, 10 mM sodium phosphate buffer pH 7.0, 100 mM NaCl. Heating rate 1 °C/1 min. [c]T_m(complementary) - T_m(mismatch). [d]The data were taken from reference[17].

3.3.1.2 UV-Titration

Since homothymine (homopurine) PNA or DNA can bind to homopyrimidine DNA to form either duplexes or triplexes,[4] the stoichiometry of the interaction between homothymine atfcPNA and homoadenine DNA was determined by UV-titration. The ratio between atfcPNA and complementary DNA was determined to be 1:1 (**Figure 3.26**). This means that homothymine atfcPNA forms only 1:1 hybrid with DNA, which is similar to acpcPNA.[12]

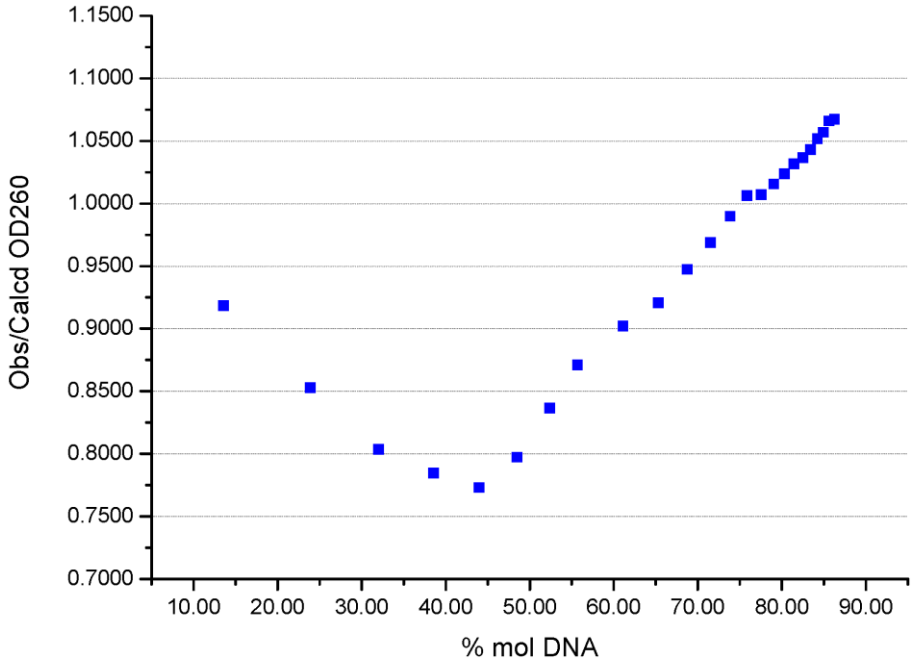

Figure 3.26 UV-Titation plot show the ratio of observed Abs_{260}/calculated Abs_{260} and mole fraction of DNA d(AAAAAAAAA). The titration was performed at initial concentration of PNA (Ac-TTTTTTTTT-LysNH_2) = 2 μM in 10 mM sodium phosphate buffer pH 7.0, 25 °C without NaCl.

3.3.1.3 CD spectroscopy

CD spectroscopy can be used to monitor the conformational change of chiral macromolecules such as proteins and DNA. It has also been applied for studying the interaction of PNA and DNA. The CD spectrum of a 1:1 mixture between the homothymine atfcPNA and its complementary DNA was significantly different from the sum CD spectra of each component. This clearly indicates that the homothymine

atfcPNA forms a hybrid with DNA, resulting in a conformational change to give a strong CD signal (**Figure 3.27**). The temperature dependent CD spectroscopy (**Figure 3.28** (**A**)) showed that the CD signal changes with temperatures. The most obvious change can be seen at 248 nm, whereby the magnitude of the negative band decreased as the temperature increased. A plot between the CD signal at 248 nm and temperature gave an S-curve as shown in **Figure 3.28** (**B**). From this sigmoidal CD melting curve, a T_m of 60 °C was obtained, which is in good agreement with the value obtained from the UV melting curve.

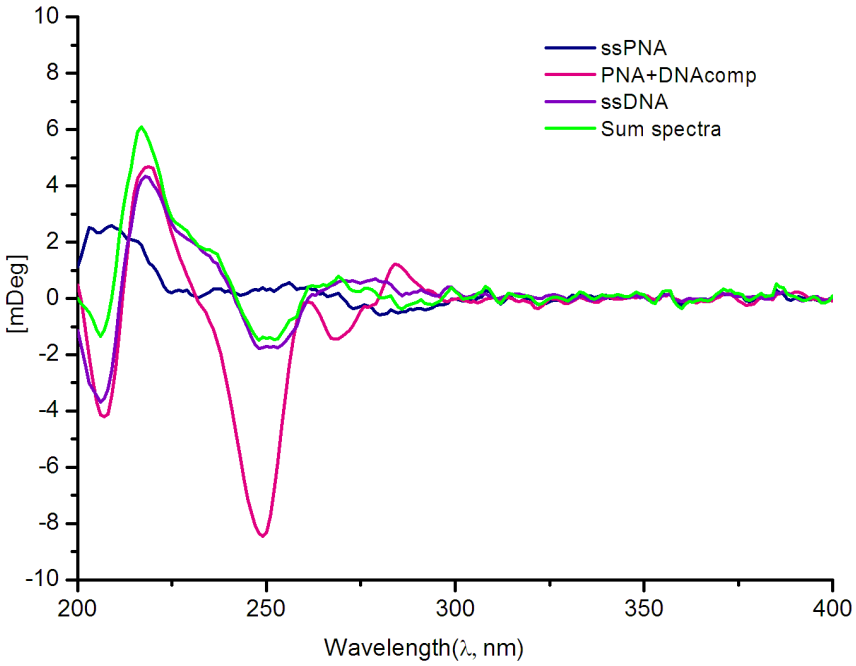

Figure 3.27 CD spectra of atfcPNA sequence: Ac-TTTTTTTTT- $LysNH_2$ (ssPNA), DNA 5'-AAAAAAAAA-3'(ssDNA), PNA/DNA hybrid(PNA+compDNA) and sum spectra.

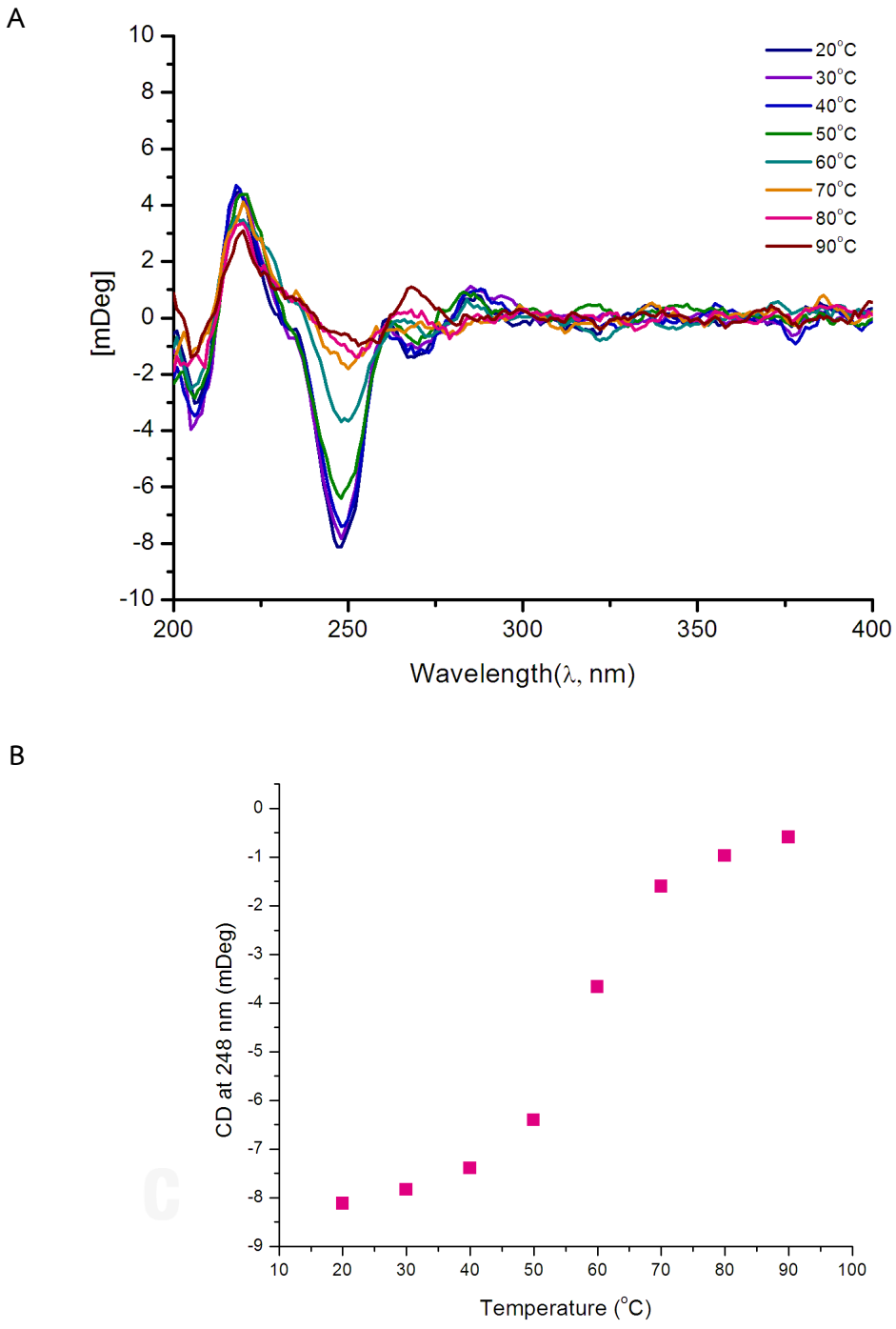

Figure 3.28 (**A**) CD spectra of hybrid of homothymine atfcPNA and complementary DNA at different temperature and (**B**) Change of the CD signal at 248 nm as a function of themperature. Conditions: 10 mM sodium phosphate buffer pH 7.0 and [PNA] = [DNA] = 1 μM.

3.3.2 Hybridization of mix base atfcPNA

3.3.2.1 UV-T_m (melting temperature)

The mix base atfcPNA Ac-GTAGATCACT-LysNH_2 was chosen as a representative sequence to investigate the interactions with DNA and RNA. Unlike the homothymine sequence, the binding of mix base atfcPNA and DNA/RNA may occur in either parallel or antiparallel fashions. The direction of the binding was therefore investigated by UV melting experiments using DNA/RNA targets that can form complementary hybrids with the PNA in only one direction. T_m values of the corresponding acpcPNA hybrids[13] are also included for comparison. As shown in **Table 3.7**, the atfcPNA binds to DNA and RNA exclusively in antiparallel fashion similar to acpcPNA.

Table 3.7 The thermal stability of PNA sequence: Ac-GTAGATCACT-LysNH_2 and DNA/RNA[a]

Entry	DNA/RNA sequences	T_m (°C)[a] atfcPNA	T_m (°C)[b] acpcPNA	Comment
1	5'-AGTGATCTAC-3'	52.5	53.3	antiparallel
2	5'-CATCTAGTGA-3'	<20	<20	parallel
3	5'-AGUGAUCUAC-3'	36.0	42.3	antiparallel
4	5'- CAUCUAGUGA -3'	<20	<20	parallel

[a]Conditions: 1.0 μM PNA, 1.0 μM DNA, 10 mM sodium phosphate buffer pH 7.0, 100 mM NaCl. Heating rate 1 °C/1 min. [b]Data were taken from reference[17] under identical conditions.

Unlike the homothymine case, the thermal stability of the mix-base atfcPNA-DNA hybrid was similar to the corresponding acpcPNA-DNA hybrid. With the limited data available at present, this sequence-dependent stability of atfcPNA hybrids cannot be satisfactorily explained. The atfcPNA-RNA hybrid showed a lower T_m than the corresponding atfcPNA-DNA as well as acpcPNA-RNA hybrids. This indicates that atfcPNA does not form stable hybrid with RNA, although the hybrid formation with RNA was possible only in antiparallel fashion like with DNA.

To further investigate the specificity of mix base atfcPNA compared to acpcPNA, the T_m values of PNA hybrids with various DNA consisting of a single mismatched base at the middle position of the sequence were determined (**Table 3.8**). Gratifyingly, the specificity in the mix base sequence was very similar to acpcPNA[13] as shown by the ΔT_m values in the same range (~24 to 29 °C). This is again in contrast to the homothymine sequence, and cannot yet be explained using the data available.

Table 3.8 The thermal stability of PNA sequence: Ac-GTAGATCACT-LysNH_2 and antiparallel DNA

Entry	DNA sequences	T_m (°C)[a] atfcPNA	ΔT_m (°C)[b] atfcPNA	T_m (°C)[c] acpcPNA	ΔT_m (°C)[b] acpcPNA
1	5'-AGTGATCTAC-3'	56.4	-	57.0	-
2	5'-AGTGATCTAC-3'	52.5	-	53.3	-
3	5'-AGTGCTCTAC-3'	23.4	29.1	23.8	29.4
4	5'-AGTGGTCTAC-3'	23.4	29.1	23.9	29.3
5	5'-AGTGTTCTAC-3'	25.4	27.1	29.4	23.8

[a]Conditions: 1.0 μM PNA, 1.0 μM DNA, 10 mM sodium phosphate buffer pH 7.0, 100 mM NaCl (except entry 1, without NaCl). Heating rate 1 °C/1 min. [b]T_m(complementary) - T_m(mismatch). [c]Data were taken from reference[17] under identical conditions.

3.3.2.2 CD spectroscopy

CD spectra of the mix sequence atfcPNA and antiparallel RNA/DNA were significantly different from the sum spectra. In both cases, a strong negative band around 200-225 nm was observed. The RNA hybrid showed a positive band near 250 nm and more negative about 270 nm, but the DNA hybrid showed only one negative band near 260 nm. This suggests subtle difference between the conformations of the antiparallel RNA and DNA hybrids of atfcPNA.

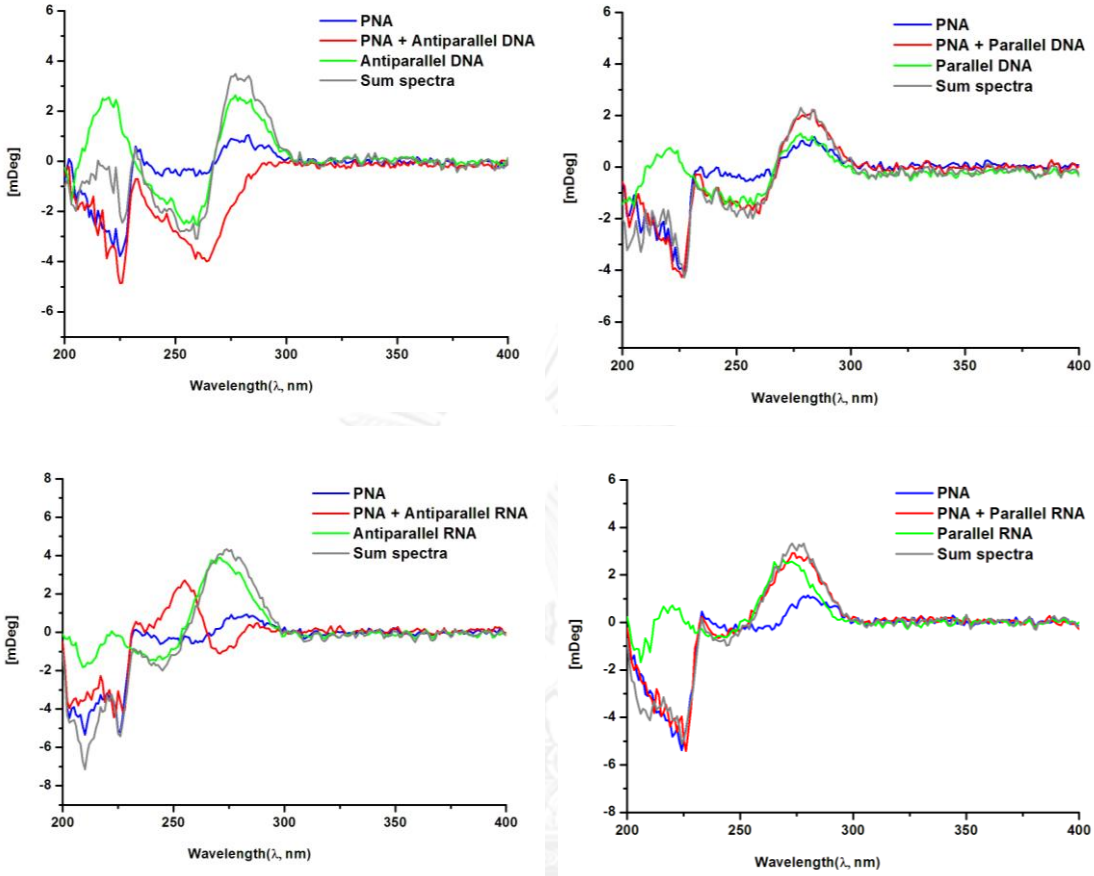

Figure 3.29 CD spectra of atfcPNA Ac-GTAGATCACT-LysNH$_2$, DNA 5'-AGTGATCTAC-3', their 1:1 mixture and the sum of DNA and PNA spectra. The experiments were conducted at [PNA] = [DNA] = 2.5 μM in 10 mM sodium phosphate buffer (pH 7.0), 100 mM NaCl at 20 °C.

3.4 Non-specific interaction with hydrophobic materials

Many applications of PNA required labeling with one or more fluorophores. Most organic fluorophores are hydrophobic molecules with extensive aromatic system or π-conjugation. Attachment of these fluorophores tends to increase the hydrophobicity of the molecule, which may lead to undesired non-specific interactions with hydrophobic material. This situation is indeed observed with many dye-labeled acpcPNA which could adsorb readily on plastic tubes.

In order to test whether the atfcPNA can solve this problem, the mix base atfcPNA was first labeled with fluorescein at the N-terminus. This fluorescein labeled atfcPNA showed slightly lowered thermal stability compared to the unlabeled atfcPNA (T_m atfcPNA with label: 45.7; without label: 52.5 °C, in 10 mM sodium

phosphate + 100 mM NaCl). This behavior was also observed in acpcPNA (T_m acpcPNA with label: 46.7; without label: 53.3 °C, in 10 mM sodium phosphate + 100 mM NaCl) and could be explained by the destabilization of the PNA-DNA duplexes due to the steric bulkiness and negative charge on the fluorescein label.

Next, the non-specific adsorption of the fluorescein-labeled atfcPNA and fluorescein-labeled acpcPNA were compared using fluorescence spectroscopy. The solution of the labeled PNA (50 nM in 10 mM sodium phosphate buffer pH 7.0, 1000 µL) was first measured the fluorescence spectra (λ_{ex} 480 nm, slid widths 5 nm, 25 °C) and transferred back and forth between the cuvette and a plastic microcentrifuge tube (the same cuvette and tube was used for each PNA). The fluorescence spectra were measured until no further change was observed.

Obviously, the signal of the fluorescein-labeled acpcPNA was decreased by almost 20% in the first transfer and after the 6th transfer, the remained signal was only slightly above 50% of the original value (**Figure 3.30**). This suggests a significant adsorption of the fluorescein-labeled acpcPNA by the plastic tube. On the other hand, the signal does not significantly change (within the experimental limit) after repeated transfer (**Figure 3.30**). These preliminary results showed the potential benefit of the ATFC spacer in decreasing non-specific interactions of acpcPNA. Since the mix sequence atfcPNA showed very similar hybridization properties to acpcPNA, it is expected that partial or total replacement ACPC residues will remove the non-specific interactions of acpcPNA without decreasing its DNA binding affinities.

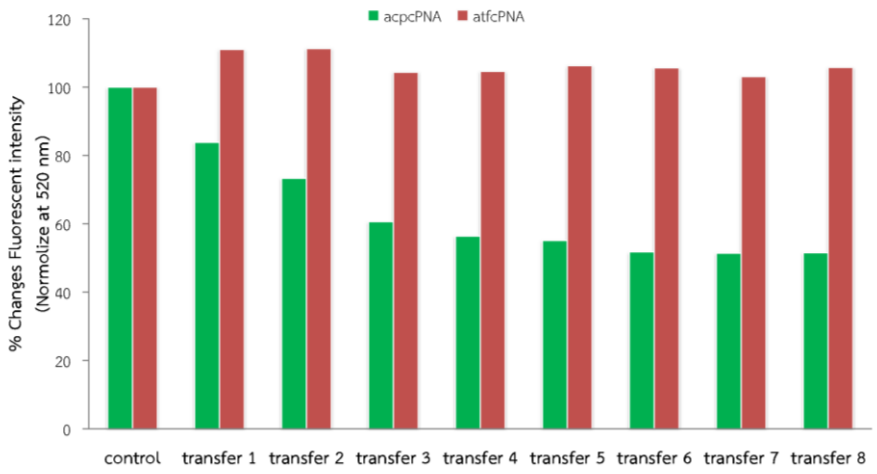

Figure 3.30 Comparison of normalized fluorescence emission (at 520 nm) of fluorescein labeled mix base acpcPNA (green) and atfcPNA (red) after transferring to a plastic microcentrifuge tube and back to the quartz cuvette.

CHAPTER IV

CONCLUSION

A novel cyclic β-amino acid with a hydrophilic tetrahydrofuran ring named (2*S*,3*S*)-3-aminotetrahydrofuran-2-carboxylic acid (*SS*-ATFC) was successfully synthesized through a 13-step reaction sequence in 3% overall yield starting from 2-deoxy-D-ribose (**2**). The synthesis started from conversion of the deoxyribose into the corresponding methyl glycoside (**3**) followed by protections of the 5-OH with a *p*-toluoyl and the 3-OH with tosyl groups to give compound **4a**. Anomeric reduction of **4a** gave the fully protected 1,2-dideoxy-D-ribose, which was further substituted at the position 3 with sodium nitrite to give the 3-OH-inverted epimer of 1,2-dideoxy-D-ribose **7a**. Activation of the 3-OH group by mesylation, followed by azide substitution, reduction, oxidation and straightforward protecting groups manipulation gave the desired Fmoc-protected and C-activated *SS*-ATFC derivative **1a**. The compound **1a** was used, in combination of the four pyrrolidinyl PNA monomer (A^{Bz}, T, C^{Bz}, G^{Ibu}), to synthesize two new tetrahydrofuran-containing pyrrolidinyl PNA oligomers with (atfcPNA) (T9 and mix base 10mer) by Fmoc-solid phase peptide synthesis.

All atfcPNAs were purified by reversed phase HPLC and characterized by MALDI-TOF mass spectrometry. The hybridization properties with oligonucleotides were studied by UV-T_m and CD spectroscopy and compared to the benchmark acpcPNA with the same sequence under identical conditions. In case of homothymine sequence (T9), atfcPNA showed considerably lower affinity to complementary DNA when compared to acpcPNA. UV titration of the homothymine atfcPNA and its complementary DNA suggested the formation of a 1:1 hybrid similar to acpcPNA. In the case of mix sequence acfcPNA, the binding affinity and specificity was very similar to acpcPNA.

The lower hydrophobicity of the new atfcPNA than acpcPNA was confirmed by reverse phase HPLC analysis. Fluorescence spectroscopy was employed to observe the non-specific interaction with hydrophobic materials, which clearly confirmed that atfcPNA have much reduced affinity to polypropylene plastic tubes when compared to the acpcPNA.

REFERENCES

1. Nielsen, P.E., Egholm, M., Berg, R.H.,Buchardt, O. Sequence-selective recognition of DNA by strand displacement with a thymine-substituted polyamide. *Science*, **1991**, *254*, 1497-1500.
2. Nielsen, P.E.,Haaima, G. Peptide nucleic acid (PNA). A DNA mimic with a pseudopeptide backbone. *Chemical Society Reviews*, **1997**, *26*, 73-78.
3. Ray, A.,Nordén, B. Peptide nucleic acid (PNA): its medical and biotechnical applications and promise for the future. *The FASEB Journal*, **2000**, *14*, 1041-1060.
4. Nielsen, P.E. Peptide Nucleic Acids (PNA) in chemical biology and drug discovery. *Chemistry & Biodiversity*, **2010**, *7*, 786-804.
5. Lowe, G.,Vilaivan, T. Amino acids bearing nucleobases for the synthesis of novel peptide nucleic acids. *Journal of the Chemical Society, Perkin Transactions 1*, **1997**, 539-546.
6. Lowe, G., Vilaivan, T.,Westwell, M.S. Hybridization studies with chiral peptide nucleic acids. *Bioorganic Chemistry*, **1997**, *25*, 321-329.
7. Lowe, G.,Vilaivan, T. Dipeptides bearing nucleobases for the synthesis of novel peptide nucleic acids. *Journal of the Chemical Society, Perkin Transactions 1*, **1997**, 547-554.
8. Vilaivan, T., Khongdeesameor, C., Harnyuttanakorn, P., Westwell, M.S.,Lowe, G. Synthesis and properties of chiral peptide nucleic acids with a N-aminoethyl-D-proline backbone. *Bioorganic & Medicinal Chemistry Letters*, **2000**, *10*, 2541-2545.
9. Vilaivan, T., Suparpprom, C., Harnyuttanakorn, P.,Lowe, G. Synthesis and properties of novel pyrrolidinyl PNA carrying β-amino acid spacers. *Tetrahedron Letters*, **2001**, *42*, 5533-5536.
10. Vilaivan, T.,Lowe, G. A novel pyrrolidinyl PNA showing high sequence specificity and preferential binding to DNA over RNA. *Journal of the American Chemical Society*, **2002**, *124*, 9326-9327.
11. Vilaivan, T., Suparpprom, C., Duanglaor, P., Harnyuttanakorn, P.,Lowe, G. Synthesis and nucleic acid binding studies of novel pyrrolidinyl PNA carrying an N-amino-N-methylglycine spacer. *Tetrahedron Letters*, **2003**, *44*, 1663-1666.
12. Suparpprom, C., Srisuwannaket, C., Sangvanich, P.,Vilaivan, T. Synthesis and oligodeoxynucleotide binding properties of pyrrolidinyl peptide nucleic acids

bearing prolyl-2-aminocyclopentanecarboxylic acid (ACPC) backbones. *Tetrahedron Letters*, **2005**, *46*, 2833-2837.

13. Vilaivan, T.,Srisuwannaket, C. Hybridization of pyrrolidinyl peptide nucleic acids and DNA: selectivity, base-pairing specificity, and direction of binding. *Organic Letters*, **2006**, *8*, 1897-1900.
14. Ananthanawat, C., Vilaivan, T., Mekboonsonglarp, W.,Hoven, V.P. Thiolated pyrrolidinyl peptide nucleic acids for the detection of DNA hybridization using surface plasmon resonance. *Biosensors & Bioelectronics*, **2009**, *24*, 3544-3549.
15. Boonlua, C., Vilaivan, C., Wagenknecht, H.A.,Vilaivan, T. 5-(Pyren-1-yl)uracil as a base-discriminating fluorescent nucleobase in pyrrolidinyl peptide nucleic acids. *Chemistry - An Asian Jounal*, **2011**, *6*, 3251-3259.
16. Taechalertpaisarn, J., Sriwarom, P., Boonlua, C., Yotapan, N., Vilaivan, C.,Vilaivan, T. DNA-, RNA- and self-pairing properties of a pyrrolidinyl peptide nucleic acid with a (*2′R*,4′*S*)-prolyl-(1*S*,2*S*)-2-aminocyclopentanecarboxylic acid backbone. *Tetrahedron Letters*, **2010**, *51*, 5822-5826.
17. Vilaivan, C., Srisuwannaket, C., Ananthanawat, C., Suparpprom, C., Kawakami, J., Yamaguchi, Y., Tanaka, Y.,Vilaivan, T. Pyrrolidinyl peptide nucleic acid with alpha/beta-peptide backbone: A conformationally constrained PNA with unusual hybridization properties. *Artificial DNA:PNA & XNA*, **2011**, *2*, 50-59.
18. Reenabthue, N., Boonlua, C., Vilaivan, C., Vilaivan, T.,Suparpprom, C. 3-Aminopyrrolidine-4-carboxylic acid as versatile handle for internal labeling of pyrrolidinyl PNA. *Bioorganic & Medicinal Chemistry Letters*, **2011**, *21*, 6465-6469.
19. Mansawat, W., Vilaivan, C., Balazs, A., Aitken, D.J.,Vilaivan, T. Pyrrolidinyl peptide nucleic acid homologues: effect of ring size on hybridization properties. *Organic Letters*, **2012**, *14*, 1440-1443.
20. Gildea, B.D., Casey, S., MacNeill, J., Perry-O'Keefe, H., Sørensen, D.,Coull, J.M. PNA solubility enhancers. *Tetrahedron Letters*, **1998**, *39*, 7255-7258.
21. Fader, L.D., Myers, E.L.,Tsantrizos, Y.S. Synthesis of novel analogs of aromatic peptide nucleic acids (APNAs) with modified conformational and electrostatic properties. *Tetrahedron*, **2004**, *60*, 2235-2246.
22. Merino, P., Tejero, T., Matés, J., Chiacchio, U., Corsaro, A.,Romeo, G. 3-(Aminomethyl)-2-(carboxymethyl)isoxazolidinyl nucleosides: building blocks for peptide nucleic acid analogues. *Tetrahedron: Asymmetry*, **2007**, *18*, 1517-1520.

23. Hudson, R.H.E., Liu, Y.,Wojciechowski, F. Hydrophilic modifications in peptide nucleic acid — Synthesis and properties of PNA possessing 5-hydroxymethyluracil and 5-hydroxymethylcytosine. *Canadian Journal of Chemistry*, **2007**, *85*, 302-312.
24. Sahu, B., Sacui, I., Rapireddy, S., Zanotti, K.J., Bahal, R., Armitage, B.A.,Ly, D.H. Synthesis and characterization of conformationally preorganized, (R)-diethylene glycol-containing gamma-peptide nucleic acids with superior hybridization properties and water solubility. *The Journal of Organic Chemistry*, **2011**, *76*, 5614-5627.
25. Appella, D.H., Christianson, L.A., Klein, D.A., Powell, D.R., Huang, X., Barchi, J.J.,Gellman, S.H. Residue-based control of helix shape in β-peptide oligomers. *Nature*, **1997**, *387*, 381-384.
26. Martinek, T.A., Toth, G.K., Vass, E., Hollosi, M.,Fulop, F. cis-2-aminocyclopentanecarboxylic acid oligomers adopt a sheetlike structure: switch from helix to nonpolar strand. *Angewandte Chemie International Edition in English*, **2002**, *41*, 1718-1721.
27. Hill, D.J., Mio, M.J., Prince, R.B., Hughes, T.S.,Moore, J.S. A field guide to foldamers. *Chemical Reviews*, **2001**, *101*, 3893-4012.
28. Horne, W.S.,Gellman, S.H. Foldamers with heterogeneous backbones. *Accounts of Chemical Research*, **2008**, *41*, 1399-1408.
29. Cheng, R.P., Gellman, S.H.,DeGrado, W.F. β-Peptides:β From structure to function. *Chemical Reviews*, **2001**, *101*, 3219-3232.
30. Goodman, C.M., Choi, S., Shandler, S.,DeGrado, W.F. Foldamers as versatile frameworks for the design and evolution of function. *Nature Chemical Biology*, **2007**, *3*, 252-262.
31. Wang, X., Espinosa, J.F.,Gellman, S.H. 12-Helix formation in aqueous solution with short β-Peptides containing pyrrolidine-based Residues. *Journal of the American Chemical Society*, **2000**, *122*, 4821-4822.
32. Seebach, D., Beck, A.K.,Bierbaum, D.J. The world of beta- and gamma-peptides comprised of homologated proteinogenic amino acids and other components. *Chemistry & Biodiverity*, **2004**, *1*, 1111-239.
33. Pandey, S.K., Jogdand, G.F., Oliveira, J.C.A., Mata, R.A., Rajamohanan, P.R.,Ramana, C.V. Synthesis and structural characterization of homochiral homo-oligomers of parent cis- and trans-furanoid-β-amino acids. *Chemistry - A European Journal*, **2011**, *17*, 12946-12954.

34. Park, K.-H.,Kurth, M.J. Cyclic amino acid derivatives. *Tetrahedron*, **2002**, *58*, 8629-8659.
35. Chakraborty, T.K., Srinivasu, P., Tapadar, S.,Mohan, B.K. Sugar amino acids in designing new molecules. *Glycoconjugate Jounal*, **2005**, *22*, 83-93.
36. Risseeuw, M.D.P., Overhand, M., Fleet, G.W.J.,Simone, M.I. A compendium of sugar amino acids (SAA): scaffolds, peptide- and glyco-mimetics. *Tetrahedron: Asymmetry*, **2007**, *18*, 2001-2010.
37. Rjabovs, V.,Turks, M. Tetrahydrofuran amino acids of the past decade. *Tetrahedron*, **2013**, *69*, 10693-10710.
38. Risseeuw, M., Overhand, M., Fleet, G.W.,Simone, M.I. A compendium of cyclic sugar amino acids and their carbocyclic and heterocyclic nitrogen analogues. *Amino Acids*, **2013**, *45*, 613-689.
39. Barker, S.F., Angus, D., Taillefumier, C., Probert, M.R., Watkin, D.J., Watterson, M.P., Claridge, T.D.W., Hungerford, N.L.,Fleet, G.W.J. cis- and trans-3-Azido-oxetane-2-carboxylate scaffolds: hexamers of oxetane cis-β-amino acids. *Tetrahedron Letters*, **2001**, *42*, 4247-4250.
40. Claridge, T.D.W., Goodman, J.M., Moreno, A., Angus, D., Barker, S.F., Taillefumier, C., Watterson, M.P.,Fleet, G.W.J. 10-Helical conformations in oxetane β-amino acid hexamers. *Tetrahedron Letters*, **2001**, *42*, 4251-4255.
41. Chandrasekhar, S., Reddy, M.S., Jagadeesh, B., Prabhakar, A., Ramana Rao, M.H.,Jagannadh, B. Formation of a stable 14-helix in short oligomers of furanoid cis-beta-sugar-amino acid. *Journal of the American Chemical Society*, **2004**, *126*, 13586-13587.
42. Giri, A.G., Jogdand, G.F., Rajamohanan, P.R., Pandey, S.K.,Ramana, C.V. Synthesis and structural characterization of homochiral homo-oligomers of cis-γ-methoxy-substituted cis- and trans-furanoid-β-Amino Acids. *European Journal of Organic Chemistry*, **2012**, *2012*, 2656-2663.
43. Chandrasekhar, S., Pavan Kumar Reddy, G., Udaya Kiran, M., Nagesh, C.,Jagadeesh, B. Nucleoside derived amino acids (NDA) in foldamer chemistry: synthesis and conformational studies of homooligomers of modified AZT. *Tetrahedron Letters*, **2008**, *49*, 2969-2973.
44. Threlfall, R., Davies, A., Howarth, N.M., Fisher, J.,Cosstick, R. Peptides derived from nucleoside [small beta]-amino acids form an unusual 8-helix. *Chemical Communications*, **2008**, 585-587.

45. Gogoi, K.,Kumar, V.A. Chimeric ([small alpha]-amino acid + nucleoside-[small beta]-amino acid)n peptide oligomers show sequence specific DNA/RNA recognition. *Chemical Communications*, **2008**, 706-708.
46. Siriwardena, A., Pulukuri, K.K., Kandiyal, P.S., Roy, S., Bande, O., Ghosh, S., Garcia Fernández, J.M., Ariel Martin, F., Ghigo, J.-M., Beloin, C., Ito, K., Woods, R.J., Ampapathi, R.S.,Chakraborty, T.K. Sugar-modified foldamers as conformationally defined and biologically distinct glycopeptide mimics. *Angewandte Chemie International Edition*, **2013**, *52*, 10221-10226.
47. Sharma, G.V.M., Ravindranath, H., Bhaskar, A., Jeelani Basha, S., Gurava Reddy, P.R.G., Sirisha, K., Sarma, A.V.S.,Hofmann, H.-J. Design and study of peptides containing 1:1 left- and right-handed helical patterns from aminopyrancarboxylic acids. *European Journal of Organic Chemistry*, **2014**, DOI: 10.1002/ejoc.201402123.
48. Takeshita, M., Chang, C.N., Johnson, F., Will, S.,Grollman, A.P. Oligodeoxynucleotides containing synthetic abasic sites. Model substrates for DNA polymerases and apurinic/apyrimidinic endonucleases. *Journal of Biological Chemistry*, **1987**, *262*, 10171-10179.
49. Martinez-Montero, S., Fernandez, S., Sanghvi, Y.S., Gotor, V.,Ferrero, M. An expedient biocatalytic procedure for abasic site precursors useful in oligonucleotide synthesis. *Organic & Biomolecular Chemistry*, **2011**, *9*, 5960-5966.
50. Ngamviriyavong, P., *Synthesis of peptide nucleic acid containing aminoethyllinkers* in *Chemistry*. 2004, Chulalongkorn University. p. 143.
51. Serebryany, V., Karpeisky, A., Matulic-Adamic, J.,Beigelman, L. Synthesis of 1,4-Anhydro-2-deoxy-d-ribitol Derivatives from Thymidine Using Improved Preparation of Furanoid Glycals. *Synthesis*, **2002**, 1652-1654.
52. Serebryany, V.,Beigelman, L. Synthesis of 1,4-anhydro-2-deoxy-D-ribitol derivatives from thymidine. *Nucleosides Nucleotides Nucleic Acids*, **2003**, *22*, 1305-1307.
53. Aly, Y.L.,Pedersen, E.B. Synthesis of a new furanoid glycal auxiliary. *Monatshefte für Chemie*, **2005**, *136*, 1641-1644.
54. Singh, I.,Seitz, O. Diastereoselective synthesis of β-aryl-C-nucleosides from 1,2-anhydrosugars. *Organic Letters*, **2006**, *8*, 4319-4322.
55. Larsen, C.H., Ridgway, B.H., Shaw, J.T.,Woerpel, K.A. A stereoelectronic model to explain the highly stereoselective reactions of nucleophiles with five-

membered-ring oxocarbenium Ions. *Journal of the American Chemical Society*, **1999**, *121*, 12208-12209.

56. Rabi Jaime, A., *Methods of manufacture of 2'-deoxy-beta-L-nucleosides*. 2004.
57. Pedersen, C., Diehl, H.W.,Fletcher, H.G. 2-Deoxy-D-ribose. III. The anomeric 1,3,4-Tri-O-benzoyl-2-deoxy-D-riboses, the anomeric 1,3,5-Tri-O-benzoyl-2-deoxy-D-riboses and certain other derivatives1. *Journal of the American Chemical Society*, **1960**, *82*, 3425-3428.
58. Chong, Y., Gumina, G., Mathew, J.S., Schinazi, R.F.,Chu, C.K. L-2‘,3‘-Didehydro-2‘,3‘-dideoxy-3‘-fluoronucleosides: Synthesis, Anti-HIV Activity, Chemical and Enzymatic Stability, and Mechanism of Resistance. *Journal of Medicinal Chemistry*, **2003**, *46*, 3245-3256.
59. James L. Fry, Steven B. Silverman,Orfanopoulo, M. Reduction of ketones to hydrocarbons with triethylsilane: m-nitroethylbenzene. *Organic Syntheses*, **1981**, *60*, 108.
60. Guo, X., Liu, C., Zheng, L., Jiang, S.,Shen, J. Novel exocyclic nucleoside related to clitocine: a convergent synthesis of 3′-Azido-2′,3′-dideoxy clitocine. *Synlett*, **2010**, 1959-1962.
61. McGeary, R.P., Rasoul Amini, S., Tang, V.W.,Toth, I. Nucleophilic substitution reactions of pyranose polytosylates. *The Journal of Organic Chemistry*, **2004**, *69*, 2727-2730.
62. Gevorgyan, V., Rubin, M., Benson, S., Liu, J.-X.,Yamamoto, Y. A novel $B(C_6F_5)_3$-catalyzed reduction of alcohols and cleavage of aryl and alkyl ethers with hydrosilanes. *The Journal of Organic Chemistry*, **2000**, *65*, 6179-6186.
63. Swamy, K.C., Kumar, N.N., Balaraman, E.,Kumar, K.V. Mitsunobu and related reactions: advances and applications. *Chemical Reviews*, **2009**, *109*, 2551-2651.
64. Dong, H., Pei, Z.,Ramström, O. Stereospecific ester activation in nitrite-mediated carbohydrate epimerization. *The Journal of Organic Chemistry*, **2006**, *71*, 3306-3309.
65. Kornblum, N., Blackwood, R.K.,Mooberry, D.D. The Reaction of aliphatic nitro compounds with nitrite esters1,2. *Journal of the American Chemical Society*, **1956**, *78*, 1501-1504.
66. Rainer, A., Karl, D., Robert, W.L.,Arnold, E.S. Carbohydrate triflates: reaction with nitrite, leading directly to epi-hydroxy compounds. *Carbohydrate Research*, **1983**, *118*, C5-C6.

67. Dong, H., Rahm, M., Thota, N., Deng, L., Brinck, T.,Ramstrom, O. Control of the ambident reactivity of the nitrite ion. *Organic & Biomolecular Chemistry*, **2013**, *11*, 648-653.
68. March, J.,Smith, M.B., *March's advanced organic chemistry : reactions, mechanisms and structure*. sixth ed. 2007: Hoboken, N.J : Wiley.
69. Tojo, G.,Fernandez, M.I., *Oxidation of primary alcohols to carboxylic acids*. Basic Reactions in Organic Synthesis. Vol. XV. 2007: Springer.
70. Dettwiler, J.E.,Lubell, W.D. Serine as chiral educt for the practical synthesis of enantiopure N-protected beta-hydroxyvaline. *The Journal of Organic Chemistry*, **2003**, *68*, 177-179.
71. Epp, J.B.,Widlanski, T.S. Facile preparation of nucleoside-5‘-carboxylic acids. *The Journal of Organic Chemistry*, **1998**, *64*, 293-295.
72. Larsen, E., Jørgensen, P.T., Sofan, M.A.,Pedersen, E.B. A new and easy synthesis of silylated furanoid glycals in one step from nucleosides. *Synthesis*, **1994**, 1037-1038.

APPENDIX

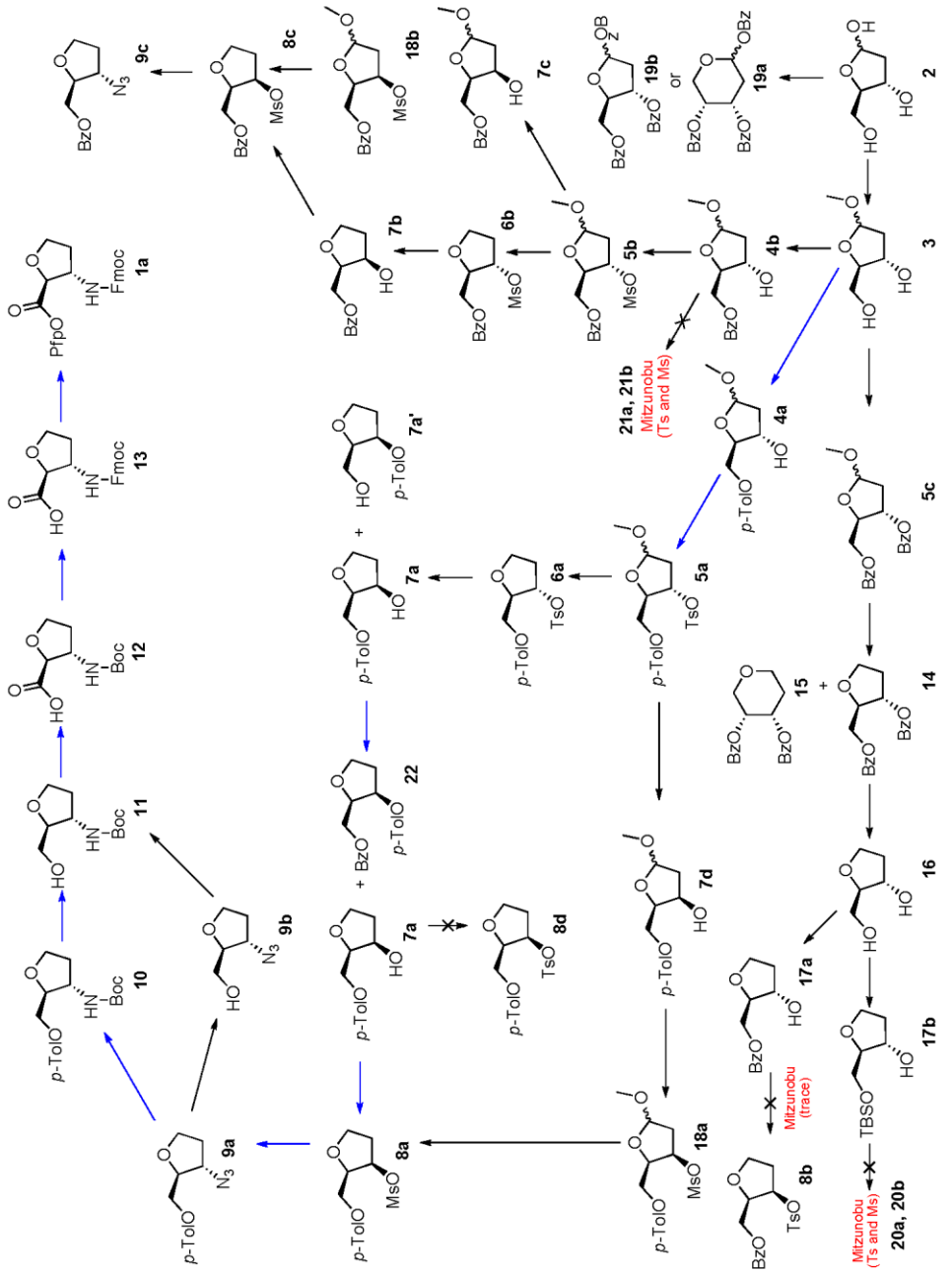

Figure A1 Summary of synthesis of ATFC spacer (including the main pathway and other miscellaneous intermediates)

Characterization data of ATFC spacer and intermediates

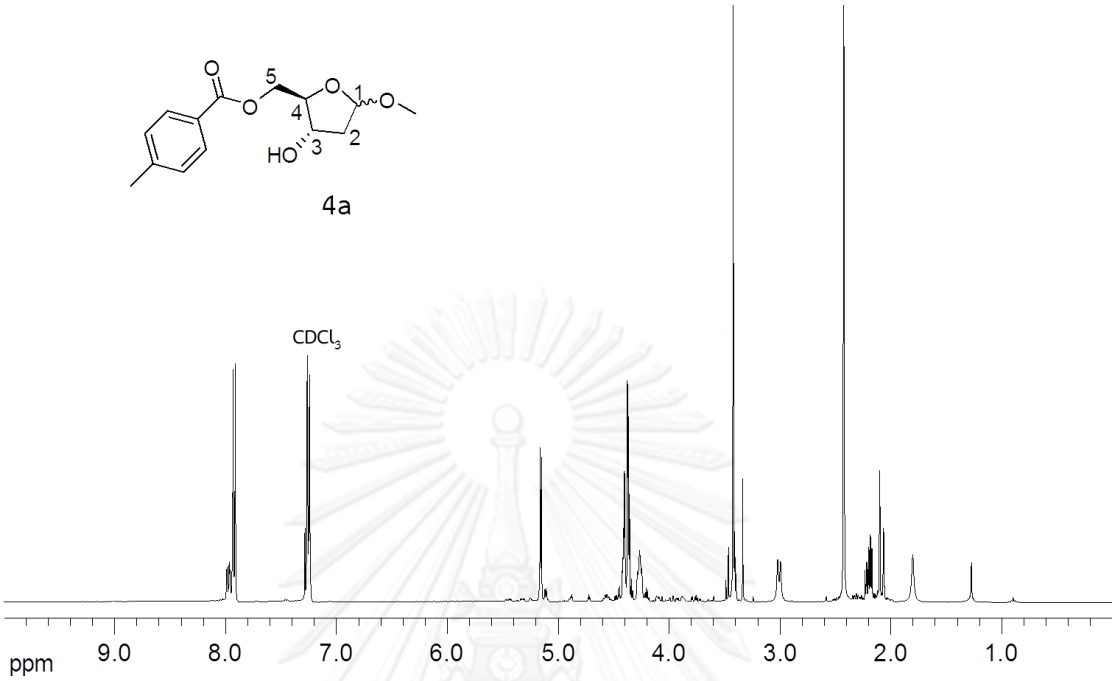

Figure A2 ^{1}H NMR spectrum of 5-*O*-*p*-toluoyl-2-deoxy-D-ribose methyl glycoside (mixture of α and β anomers) (**4a**)

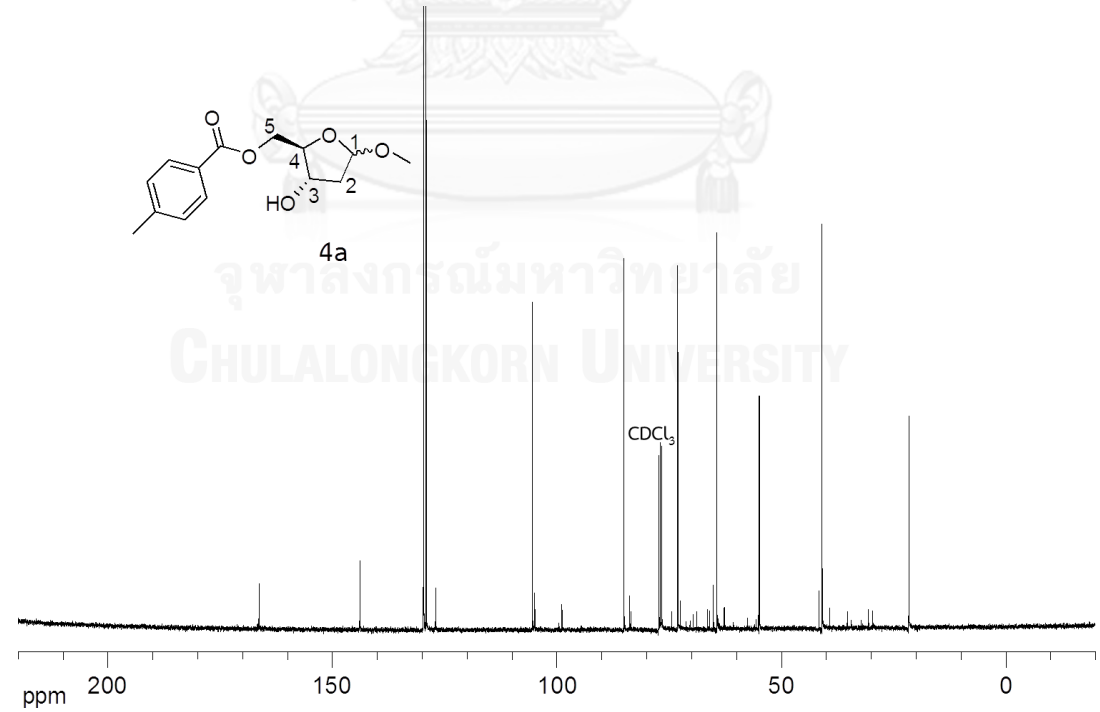

Figure A3 ^{13}C NMR spectrum (100 MHz, $CDCl_3$) of 5-*O*-*p*-toluoyl-2-deoxy-D-ribose methyl glycoside (mixture of α and β anomers) (**4a**)

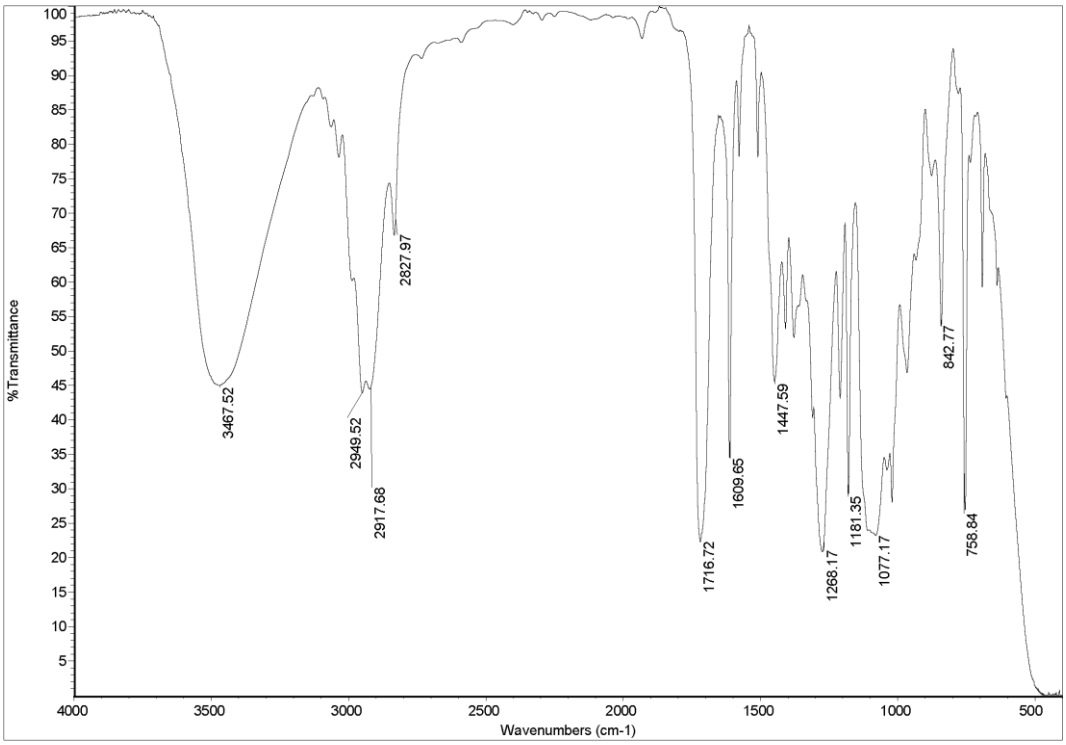

Figure A4 IR spectrum (thin flim) of 5-*O*-*p*-toluoyl-2-deoxy-D-ribose methyl glycoside (mixture of α and β anomers) (**4a**)

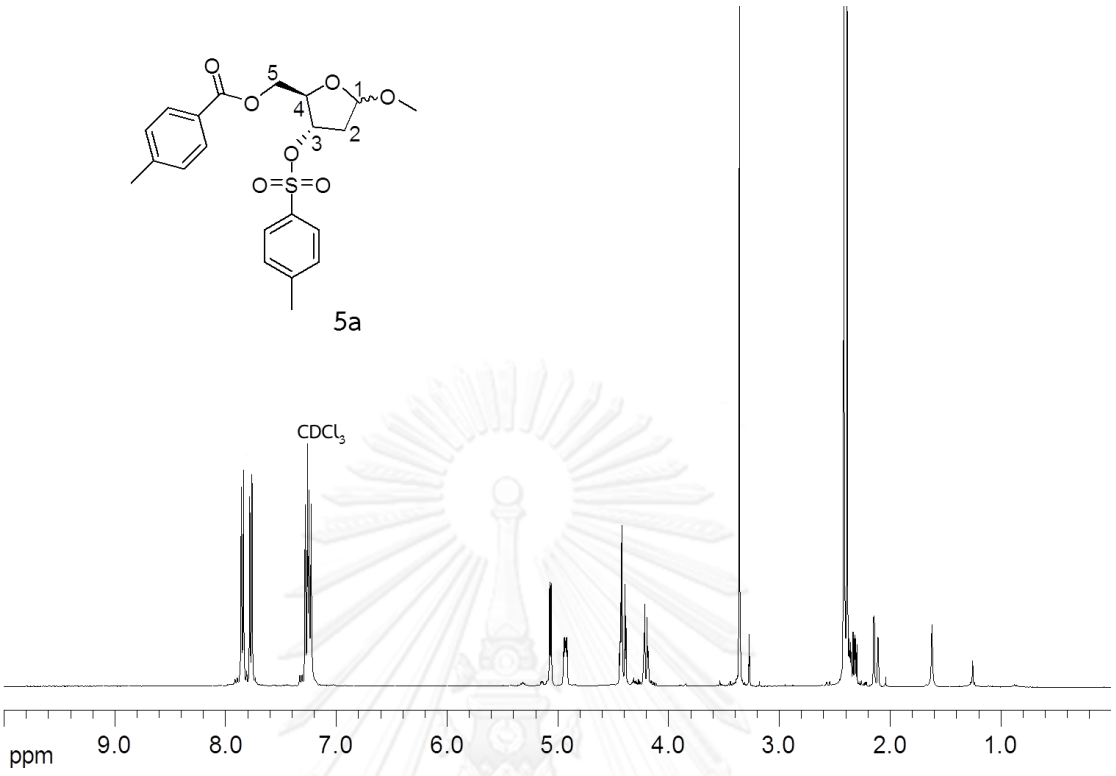

Figure A5 ^{1}H NMR spectrum (400 MHz, $CDCl_3$) of 5-*O*-*p*-toluoyl-3-*O*-tosyl-2-deoxy-D-ribose methyl glycoside (mixture of α and β anomers) (**5a**)

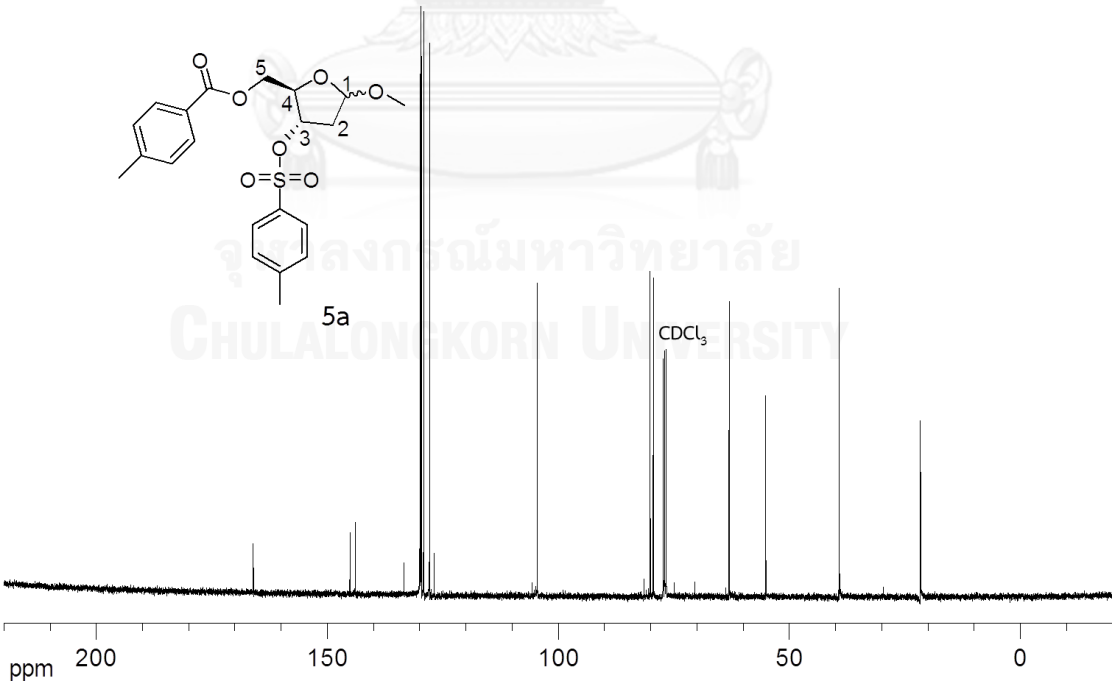

Figure A6 ^{13}C NMR spectrum (100 MHz, $CDCl_3$) of 5-*O*-*p*-toluoyl-3-*O*-tosyl-2-deoxy-D-ribose methyl glycoside (mixture of α and β anomers) (**5a**)

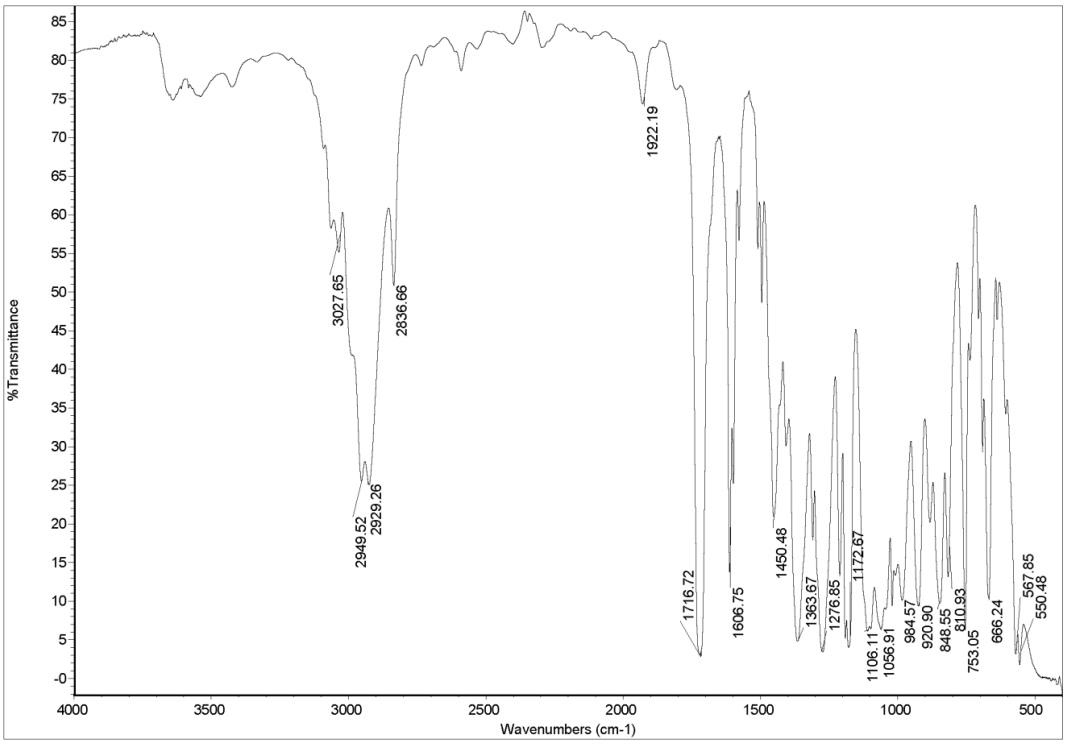

Figure A7 IR spectrum (thin film) of 5-*O*-*p*-toluoyl-3-*O*-tosyl-2-deoxy-D-ribose methyl glycoside (mixture of α and β anomers) (**5a**)

Mass Spectrum List Report

Analysis Info

Analysis Name	OSCUPN561014001.d	Acquisition Date	10/15/2013 11:28:52 AM
Method	MKE_tune_wide_20130204.m	Operator	Administrator
Sample Name	OpTol-oTs-OMe	Instrument	micrOTOF 72
	OpTol-oTs-OMe		

Acquisition Parameter

Source Type	ESI	Ion Polarity	Positive	Set Corrector Fill	75 V
Scan Range	n/a	Capillary Exit	200.0 V	Set Pulsar Pull	398 V
Scan Begin	50 m/z	Hexapole RF	300.0 V	Set Pulsar Push	380 V
Scan End	3000 m/z	Skimmer 1	45.0 V	Set Reflector	1300 V
		Hexapole 1	25.0 V	Set Flight Tube	9000 V
				Set Detector TOF	1910 V

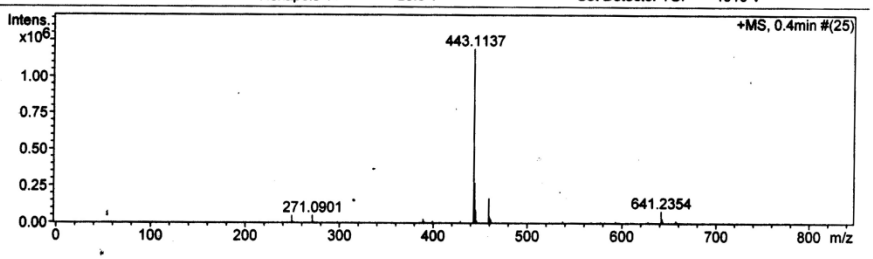

#	m/z	I	I %	S/N	FWHM	Res.
1	249.1083	47512	4.0	146.8	0.0429	5806
2	250.1114	7908	0.7	24.2	0.0443	5644
3	271.0901	48713	4.1	153.1	0.0444	6103
4	272.0937	7654	0.6	23.8	0.0449	6065
5	389.1052	25926	2.2	84.6	0.0599	6494
6	390.1076	6179	0.5	19.8	0.0573	6804
7	399.1817	11796	1.0	38.1	0.0708	5634
8	429.0974	10027	0.8	32.0	0.0653	6573
9	443.1137	1189437	100.0	3845.5	0.0711	6233
10	444.1169	270132	22.7	872.7	0.0693	6408
11	445.1134	88892	7.5	286.7	0.0673	6617
12	446.1151	14904	1.3	47.6	0.0684	6521
13	459.0866	165935	14.0	533.7	0.0709	6474
14	460.0893	36961	3.1	118.4	0.0682	6750
15	461.0906	24356	2.0	77.8	0.0772	5971
16	462.0943	5103	0.4	15.8	0.0771	5992
17	537.2099	9787	0.8	30.2	0.0855	6280
18	567.2786	3921	0.3	11.8	0.0980	5786
19	577.1829	5233	0.4	16.0	0.0932	6193
20	593.1779	9384	0.8	29.5	0.0961	6171
21	627.2251	7718	0.6	24.4	0.1081	5800
22	628.2320	4047	0.3	12.4	0.1211	5186
23	631.1080	4559	0.4	14.1	0.1052	6000
24	641.2354	80428	6.8	263.9	0.0995	6445
25	642.2387	29038	2.4	94.8	0.1019	6303
26	643.2333	7985	0.7	25.5	0.1074	5990
27	657.2090	15155	1.3	49.4	0.1030	6382
28	658.2110	5556	0.5	17.6	0.1117	5892
29	791.2874	4845	0.4	16.8	0.1275	6208
30	2352.7547	4837	0.4	17.8	0.0876	26861

Bruker Daltonics DataAnalysis 3.3 printed: 10/15/2013 12:04:29 PM Page 1 of 1

Figure A8 HRMS spectrum of 5-*O*-*p*-toluoyl-3-*O*-tosyl-2-deoxy-D-ribose methyl glycoside (mixture of α and β anomers) (**5a**)

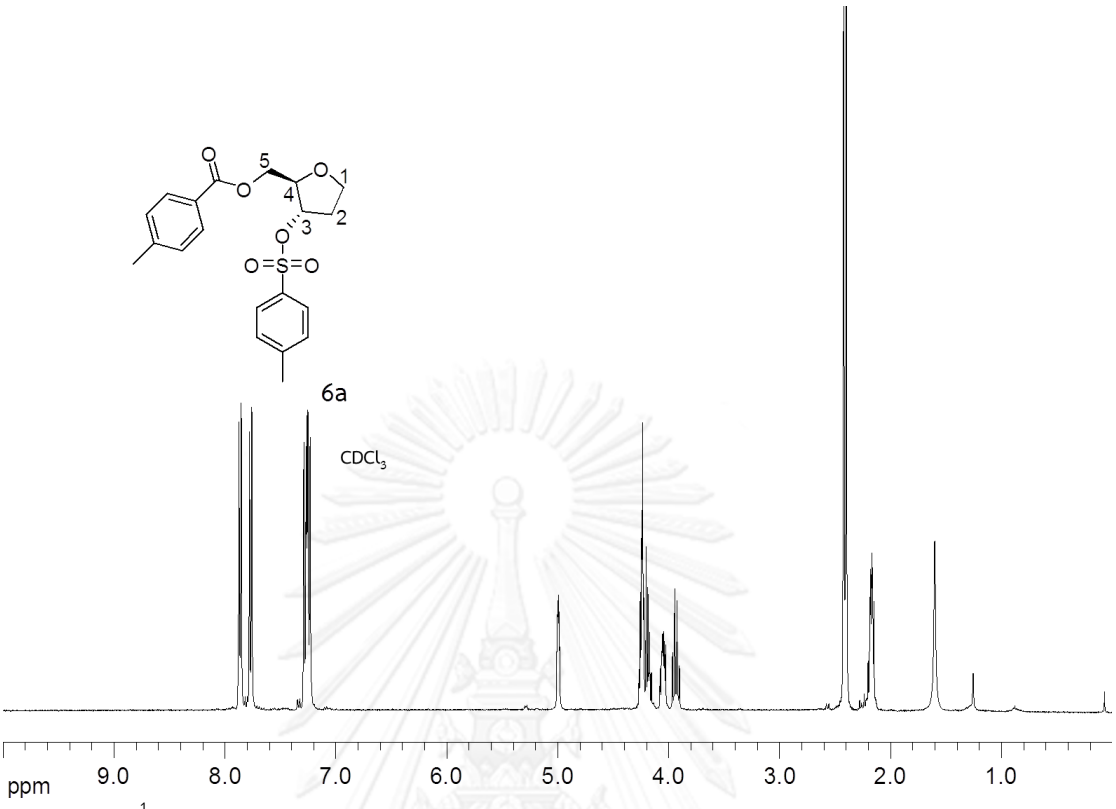

Figure A9 ^{1}H NMR spectrum (400 MHz, $CDCl_3$) of 5-*O*-*p*-toluoyl-3-*O*-tosyl-1,2-dideoxy-D-ribose (**6a**)

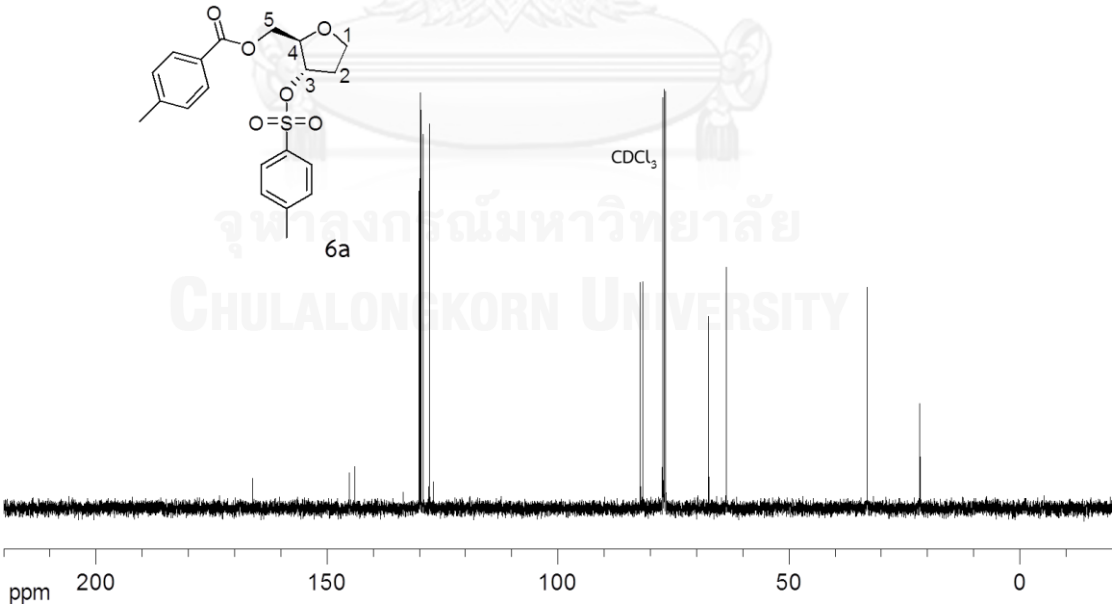

Figure A10 ^{13}C NMR spectrum (100 MHz, $CDCl_3$) of 5-*O*-*p*-toluoyl-3-*O*-tosyl-1,2-dideoxy-D-ribose (**6a**)

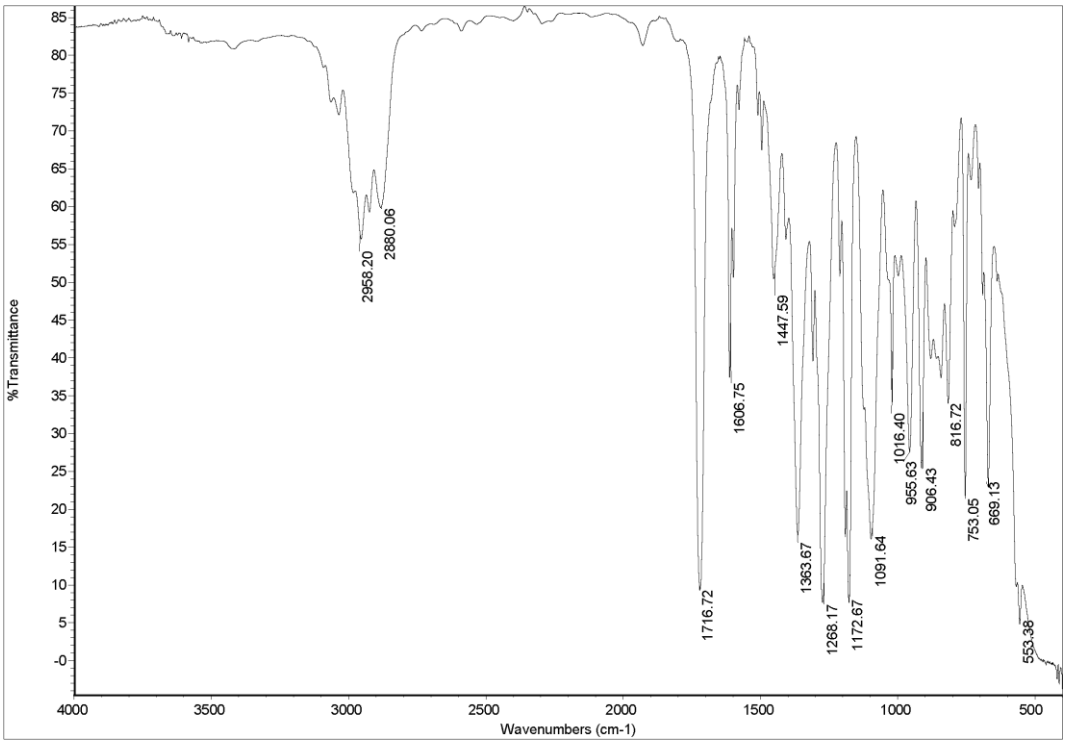

Figure A11 IR spectrum (thin flim) of 5-*O*-*p*-toluoyl-3-*O*-tosyl-1,2-dideoxy-D-ribose (**6a**)

Mass Spectrum List Report

Analysis Info

Analysis Name	OSCUPN561014002.d	Acquisition Date	10/15/2013 11:34:05 AM
Method	MKE_tune_wide_20130204.m	Operator	Administrator
Sample Name	OpTol-OTs	Instrument	micrOTOF 72
	OpTol-OTs		

Acquisition Parameter

Source Type	ESI	Ion Polarity	Positive	Set Corrector Fill	75 V
Scan Range	n/a	Capillary Exit	200.0 V	Set Pulsar Pull	398 V
Scan Begin	50 m/z	Hexapole RF	300.0 V	Set Pulsar Push	380 V
Scan End	3000 m/z	Skimmer 1	45.0 V	Set Reflector	1300 V
		Hexapole 1	25.0 V	Set Flight Tube	9000 V
				Set Detector TOF	1910 V

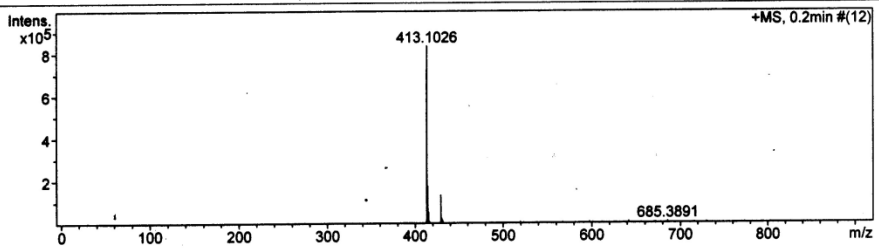

#	m/z	I	I %	S/N	FWHM	Res.
1	274.2694	5765	0.7	17.0	0.0465	5902
2	413.1026	835210	100.0	2609.0	0.0667	6189
3	414.1048	175402	21.0	547.6	0.0648	6393
4	415.1028	55256	6.6	172.2	0.0661	6279
5	416.1039	9524	1.1	29.3	0.0664	6264
6	429.0758	133612	16.0	418.0	0.0660	6501
7	430.0785	27553	3.3	85.8	0.0680	6324
8	431.0757	18140	2.2	56.3	0.0679	6350
9	443.3318	5487	0.7	16.7	0.0678	6542
10	487.3579	6114	0.7	18.7	0.0734	6642
11	493.3120	6095	0.7	18.7	0.0760	6489
12	519.0977	9075	1.1	28.2	0.0778	6675
13	523.2523	5458	0.7	16.7	0.0866	6044
14	537.3373	6618	0.8	20.4	0.0798	6737
15	567.2808	7598	0.9	23.3	0.0880	6444
16	581.3617	6260	0.7	19.0	0.0946	6147
17	597.3348	9029	1.1	27.6	0.0931	6417
18	601.0841	6375	0.8	19.2	0.0928	6479
19	611.3096	6318	0.8	19.0	0.1014	6027
20	625.3862	6737	0.8	20.2	0.0898	6967
21	627.2806	5560	0.7	16.5	0.1071	5856
22	641.3631	10384	1.2	31.5	0.0966	6642
23	655.3414	5459	0.7	16.1	0.1153	5685
24	671.3066	7290	0.9	21.7	0.1138	5900
25	685.3891	10488	1.3	31.4	0.1104	6209
26	715.3321	6727	0.8	19.7	0.1184	6043
27	729.4145	7819	0.9	22.9	0.1164	6266
28	761.2891	5956	0.7	17.8	0.1489	5113
29	773.4422	5676	0.7	17.3	0.1193	6481
30	803.2167	6247	0.7	19.9	0.1517	5294

Bruker Daltonics DataAnalysis 3.3 printed: 10/15/2013 12:05:26 PM Page 1 of 1

Figure A12 HRMS spectrum of 5-*O*-*p*-toluoyl-3-*O*-tosyl-1,2-dideoxy-D-ribose (**6a**)

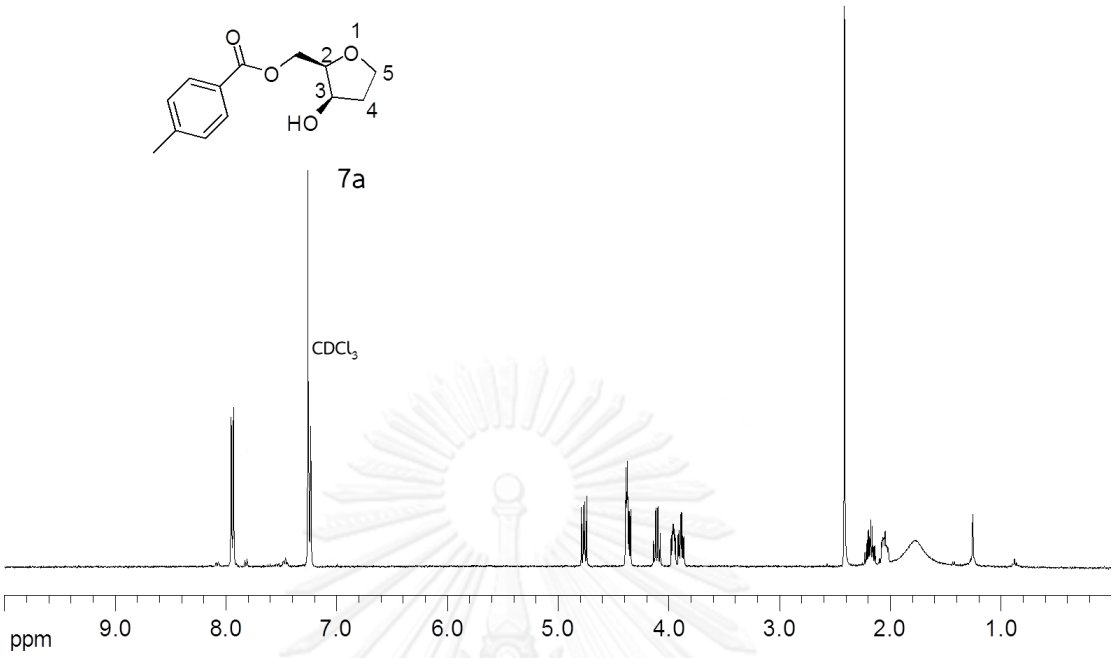

Figure A13 ^{1}H NMR spectrum (400 MHz, $CDCl_3$) of ((2*R*,3*R*)-3-hydroxytetrahydrofuran-2-yl)methyl-4-methylbenzoate (**7a**)

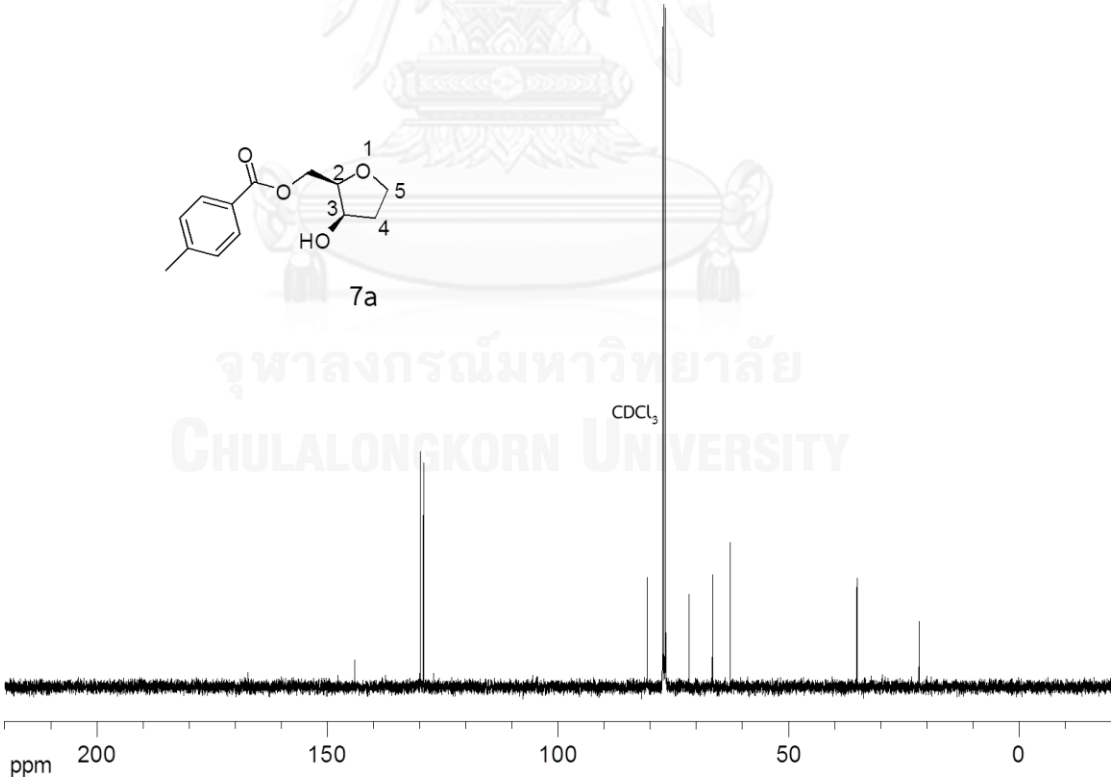

Figure A14 ^{13}C NMR spectrum (100 MHz, $CDCl_3$) of ((2*R*,3*R*)-3-hydroxytetrahydrofuran-2-yl)methyl-4-methylbenzoate (**7a**)

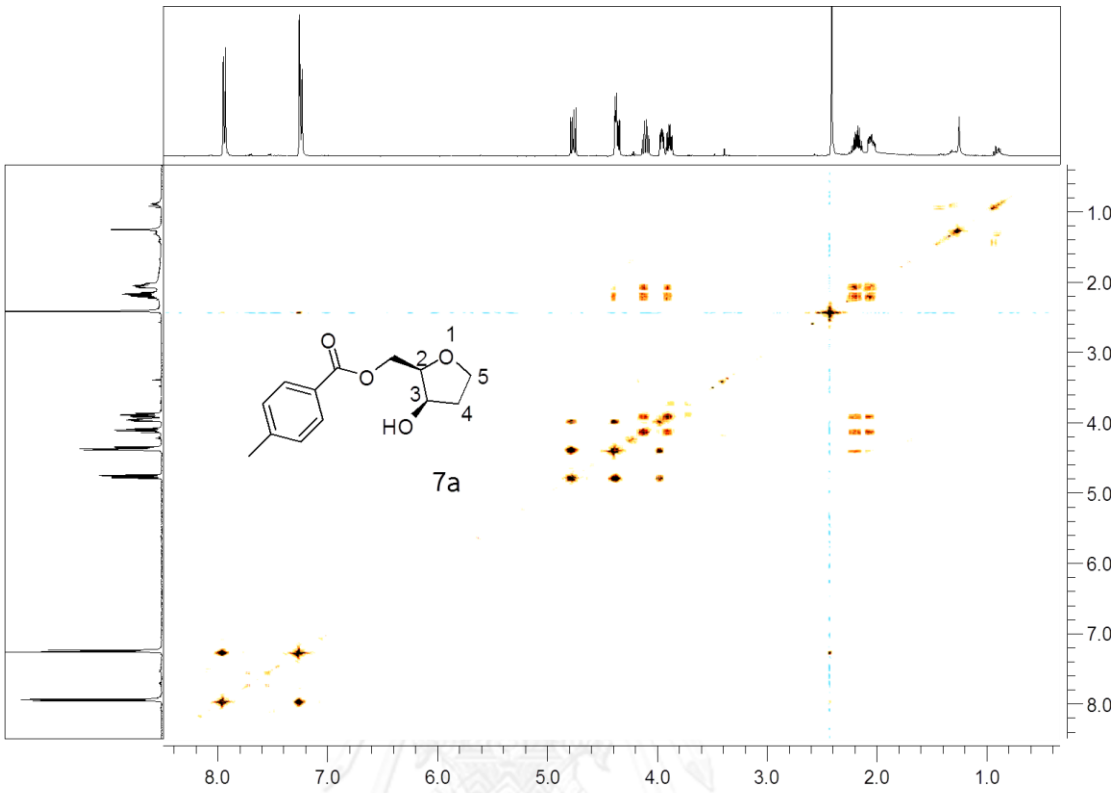

Figure A15 ^{1}H-^{1}H COSY NMR spectrum ($CDCl_3$) of ((2*R*,3*R*)-3-hydroxytetrahydrofuran-2-yl)methyl-4-methylbenzoate (**7a**)

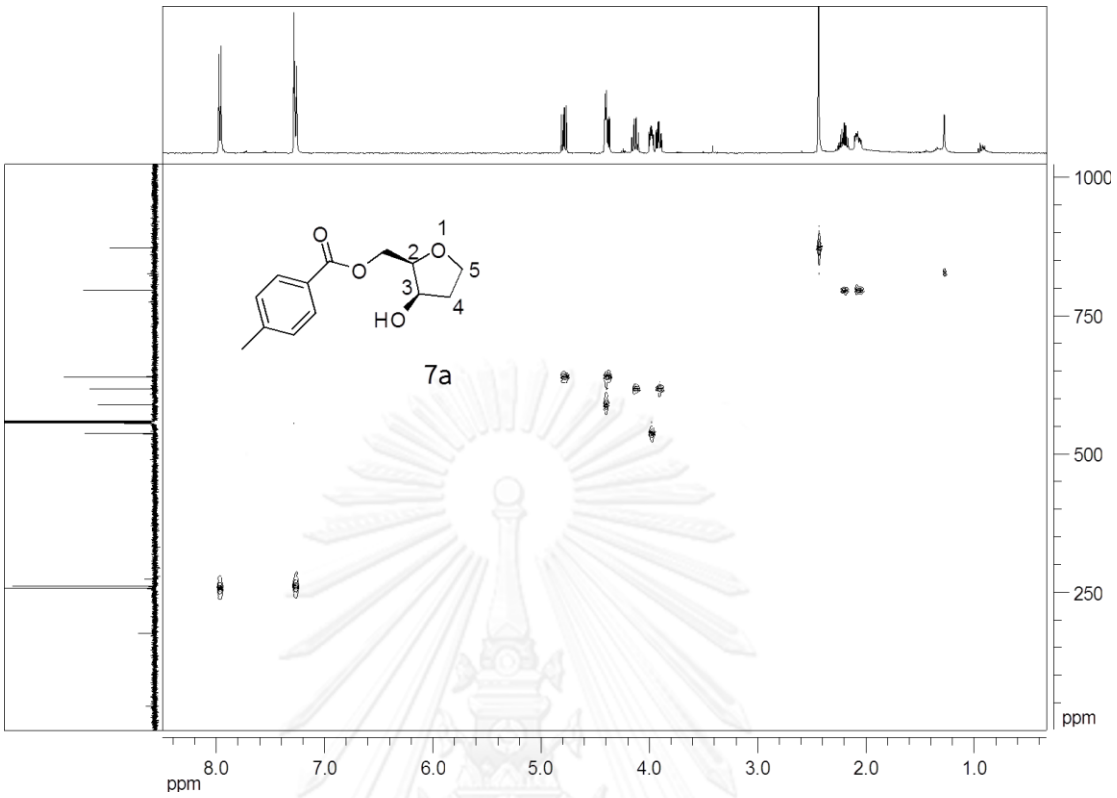

Figure A16 ^{1}H-^{13}C HSQC NMR spectrum ($CDCl_3$) of ((2*R*,3*R*)-3-hydroxytetrahydrofuran-2-yl)methyl-4-methylbenzoate (**7a**)

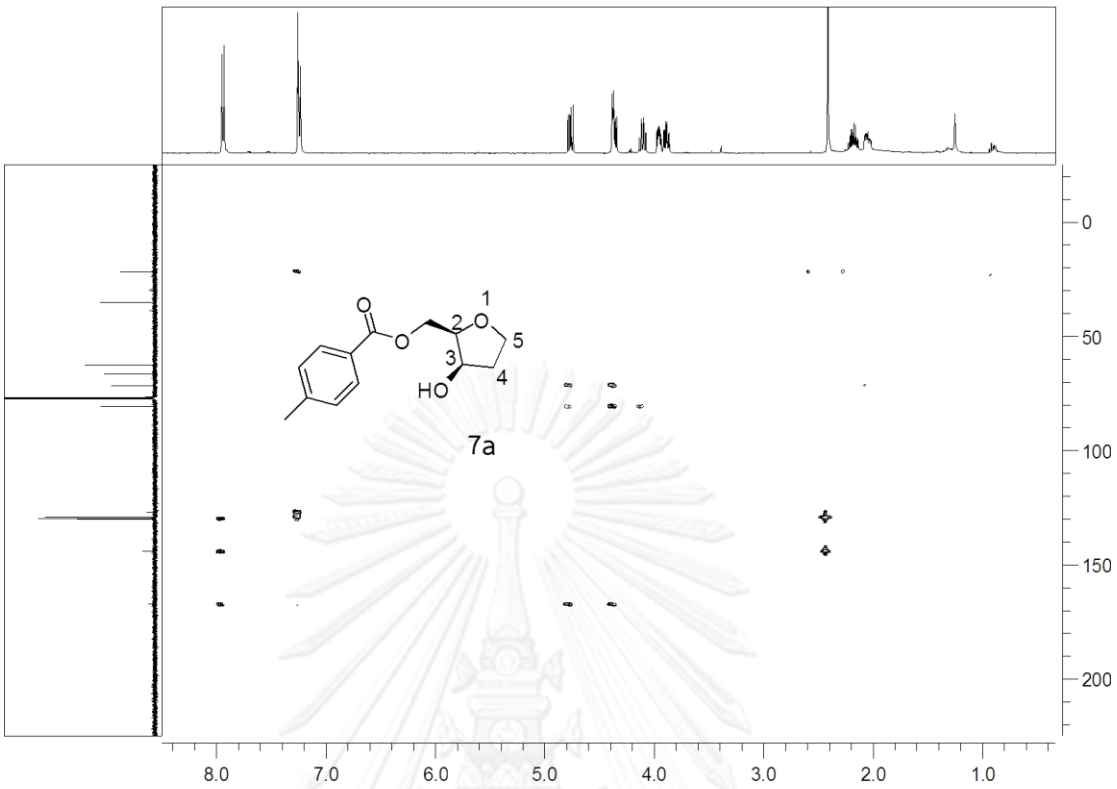

Figure A17 ^{1}H-^{13}C HMBC NMR spectrum ($CDCl_3$) of ((*2R*,*3R*)-3-hydroxytetrahydrofuran-2-yl)methyl-4-methylbenzoate (**7a**)

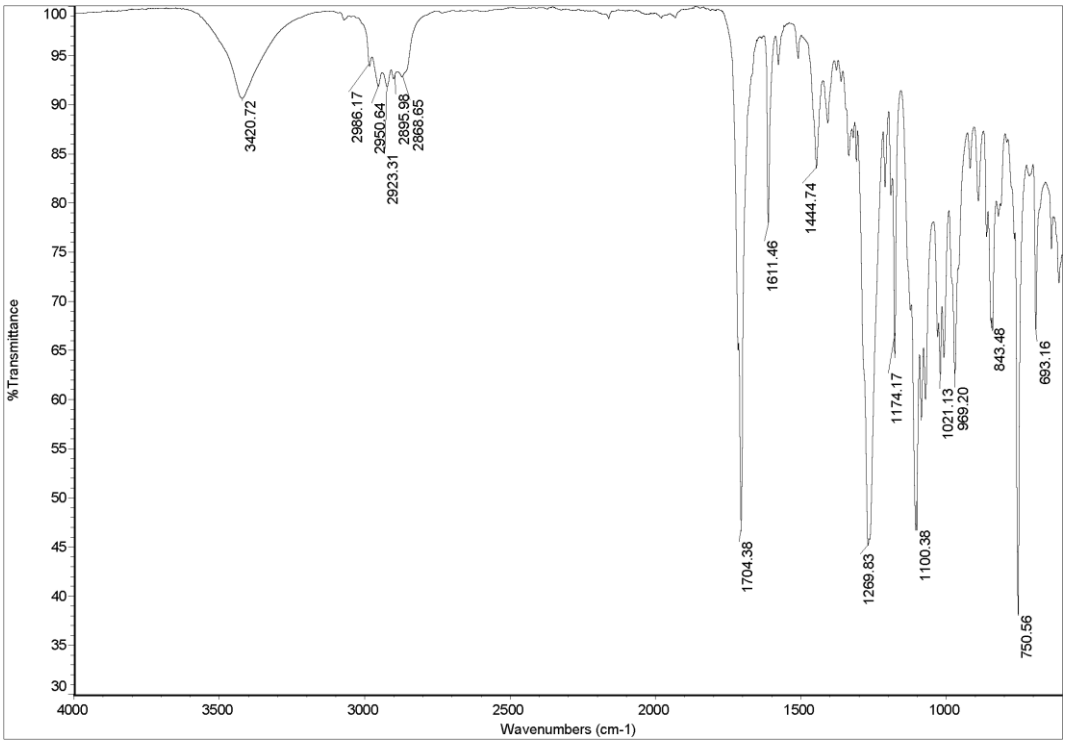

Figure A18 IR spectrum (ATR) of ((2*R*,3*R*)-3-hydroxytetrahydrofuran-2-yl)methyl-4-methylbenzoate (**7a**)

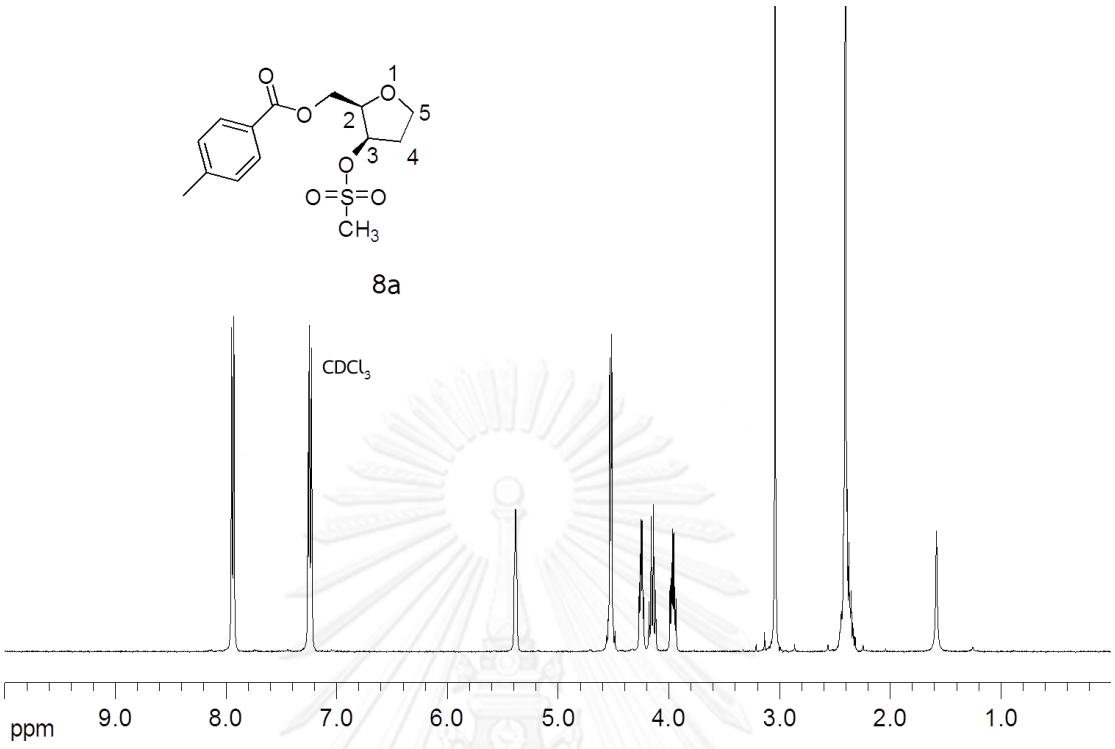

Figure A19 ^{1}H NMR spectrum (400 MHz, $CDCl_3$) of ((2*R*,3*R*)-3-(methylsulfonyloxy)tetrahydrofuran-2-yl)methyl 4-methylbenzoate (**8a**)

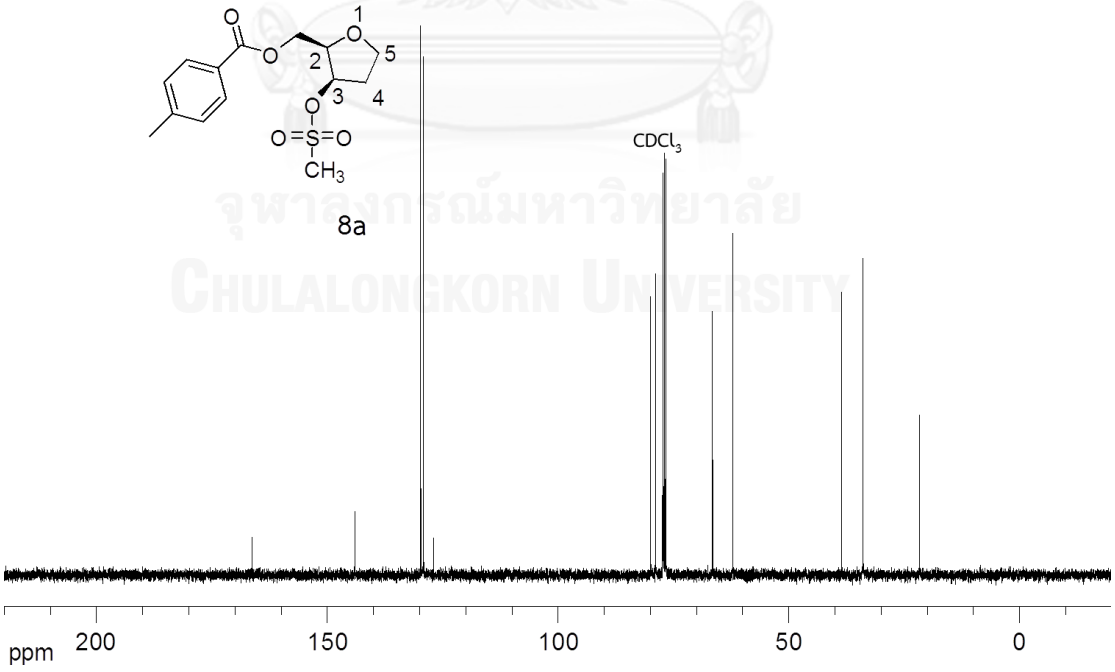

Figure A20 ^{13}C NMR spectrum (100 MHz, $CDCl_3$) of ((2*R*,3*R*)-3-(methylsulfonyloxy)tetrahydrofuran-2-yl)methyl 4-methylbenzoate (**8a**)

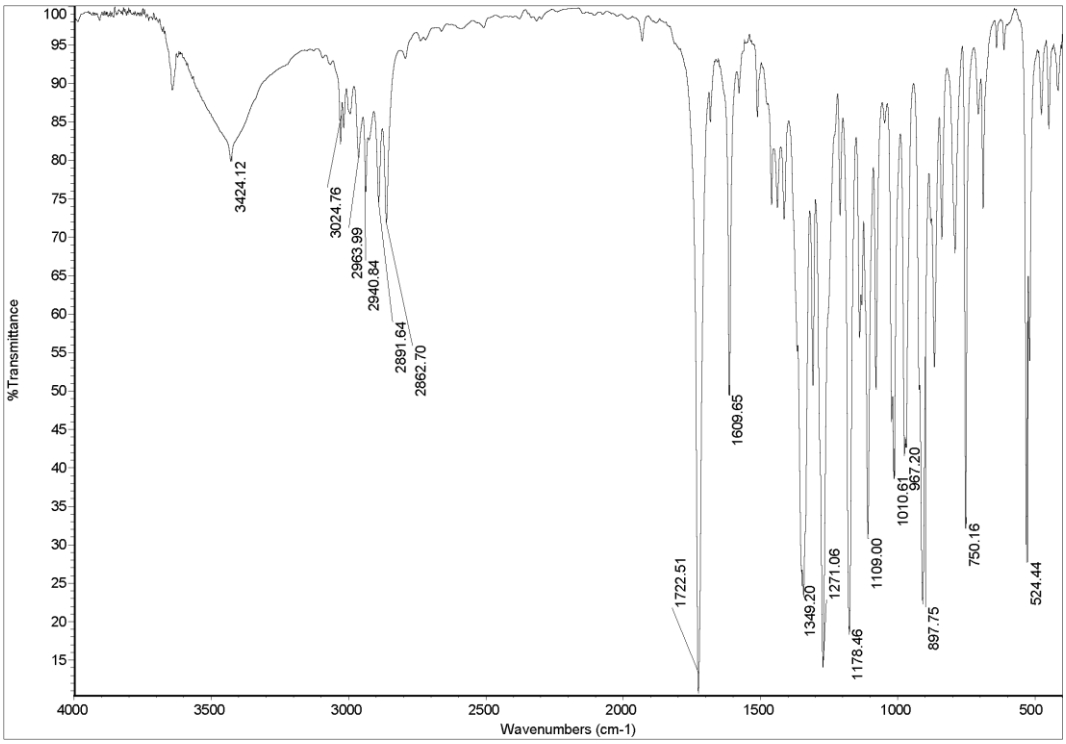

Figure A21 IR spectrum (KBr) of ((2*R*,3*R*)-3-(methylsulfonyloxy)tetrahydrofuran-2-yl)methyl 4-methylbenzoate (**8a**)

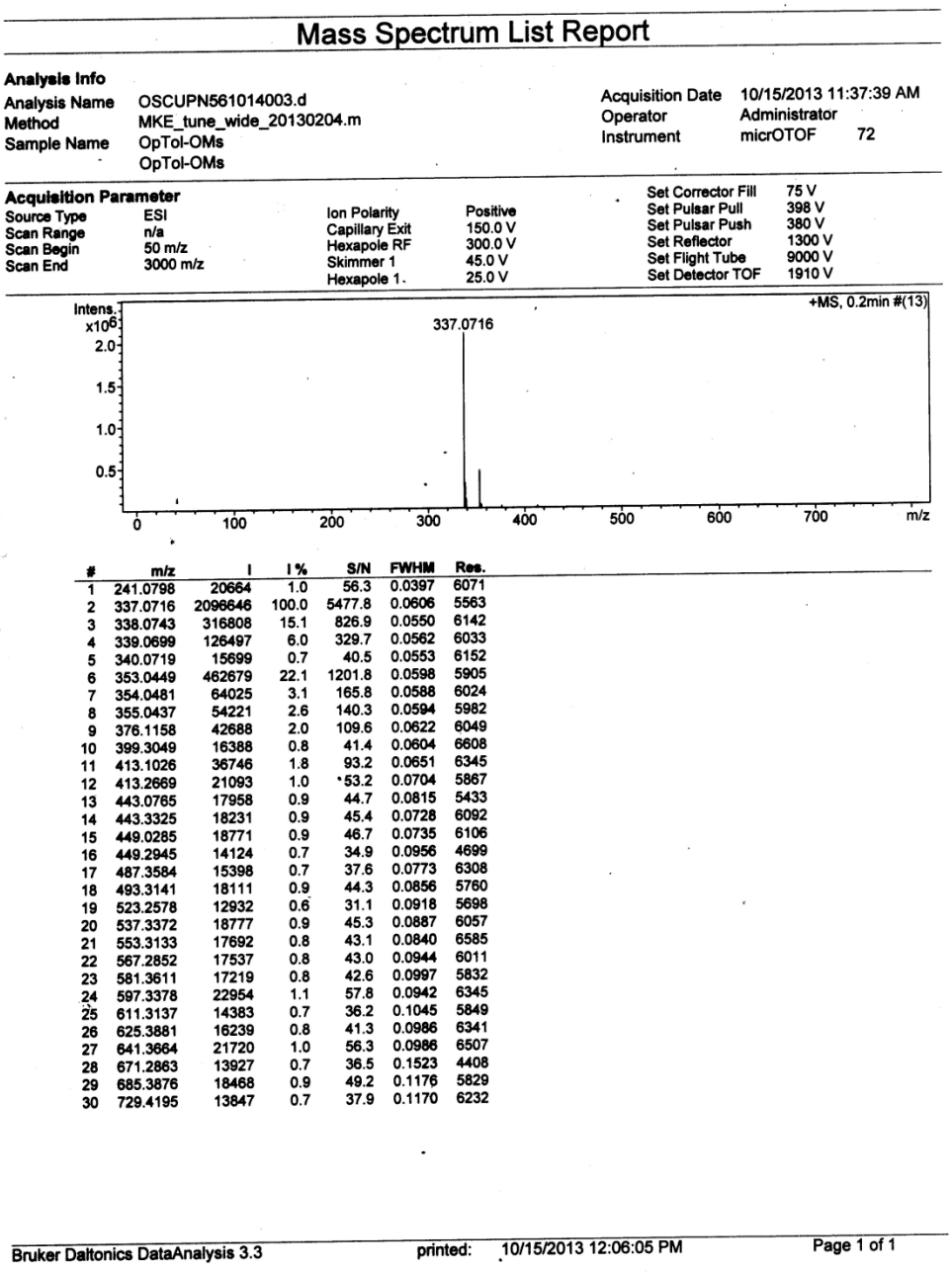

Mass Spectrum List Report

Analysis Info

Analysis Name	OSCUPN561014003.d	Acquisition Date	10/15/2013 11:37:39 AM
Method	MKE_tune_wide_20130204.m	Operator	Administrator
Sample Name	OpTol-OMs	Instrument	micrOTOF 72
	OpTol-OMs		

Acquisition Parameter

Source Type	ESI	Ion Polarity	Positive	Set Corrector Fill	75 V
Scan Range	n/a	Capillary Exit	150.0 V	Set Pulsar Pull	398 V
Scan Begin	50 m/z	Hexapole RF	300.0 V	Set Pulsar Push	380 V
Scan End	3000 m/z	Skimmer 1	45.0 V	Set Reflector	1300 V
		Hexapole 1	25.0 V	Set Flight Tube	9000 V
				Set Detector TOF	1910 V

#	m/z	I	I %	S/N	FWHM	Res.
1	241.0798	20664	1.0	56.3	0.0397	6071
2	337.0716	2096646	100.0	5477.8	0.0606	5563
3	338.0743	316808	15.1	826.9	0.0550	6142
4	339.0699	126497	6.0	329.7	0.0562	6033
5	340.0719	15699	0.7	40.5	0.0553	6152
6	353.0449	462679	22.1	1201.8	0.0598	5905
7	354.0481	64025	3.1	165.8	0.0588	6024
8	355.0437	54221	2.6	140.3	0.0594	5982
9	376.1158	42688	2.0	109.6	0.0622	6049
10	399.3049	16388	0.8	41.4	0.0604	6608
11	413.1026	36746	1.8	93.2	0.0651	6345
12	413.2669	21093	1.0	53.2	0.0704	5867
13	443.0765	17958	0.9	44.7	0.0815	5433
14	443.3325	18231	0.9	45.4	0.0728	6092
15	449.0285	18771	0.9	46.7	0.0735	6106
16	449.2945	14124	0.7	34.9	0.0956	4699
17	487.3584	15398	0.7	37.6	0.0773	6308
18	493.3141	18111	0.9	44.3	0.0856	5760
19	523.2578	12932	0.6	31.1	0.0918	5698
20	537.3372	18777	0.9	45.3	0.0887	6057
21	553.3133	17692	0.8	43.1	0.0840	6585
22	567.2852	17537	0.8	43.0	0.0944	6011
23	581.3611	17219	0.8	42.6	0.0997	5832
24	597.3378	22954	1.1	57.8	0.0942	6345
25	611.3137	14383	0.7	36.2	0.1045	5849
26	625.3881	16239	0.8	41.3	0.0986	6341
27	641.3664	21720	1.0	56.3	0.0986	6507
28	671.2863	13927	0.7	36.5	0.1523	4408
29	685.3876	18468	0.9	49.2	0.1176	5829
30	729.4195	13847	0.7	37.9	0.1170	6232

Bruker Daltonics DataAnalysis 3.3 printed: 10/15/2013 12:06:05 PM Page 1 of 1

Figure A22 HRMS spectrum of ((2*R*,3*R*)-3-(methylsulfonyloxy)tetrahydrofuran-2-yl)methyl 4-methylbenzoate (**8a**)

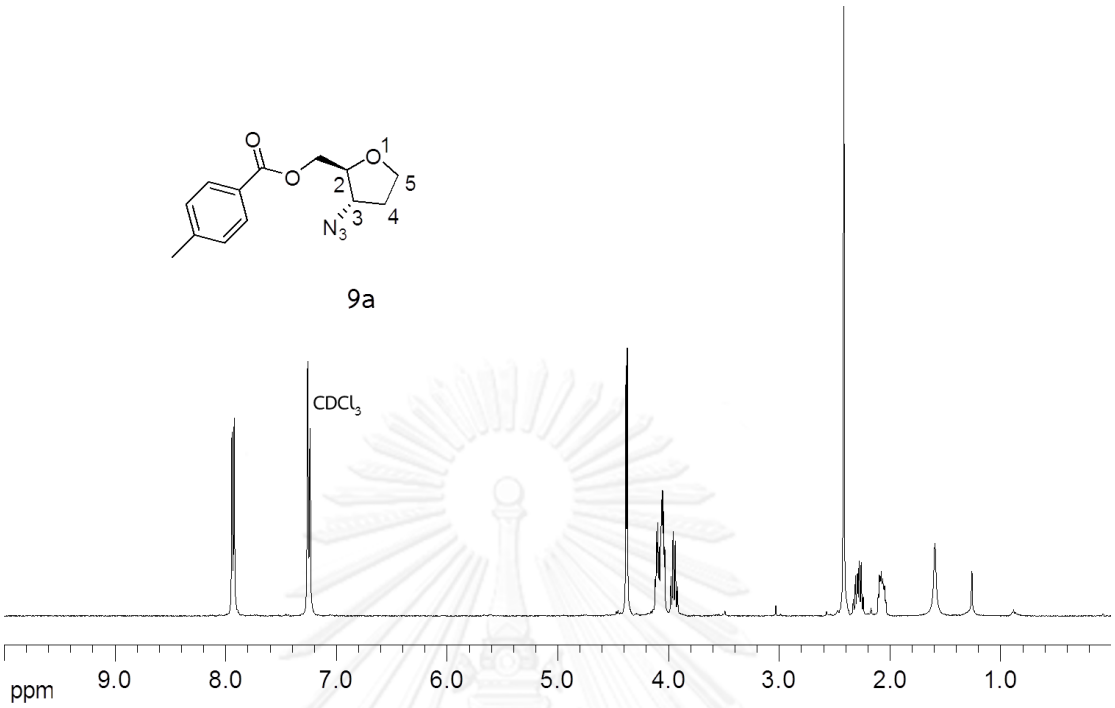

Figure A23 ^{1}H NMR spectrum (400 MHz, $CDCl_3$) of ((2*R*,3*R*)-3azidotetrahydrofuran-2-yl)methyl 4-methylbenzoate (**9a**)

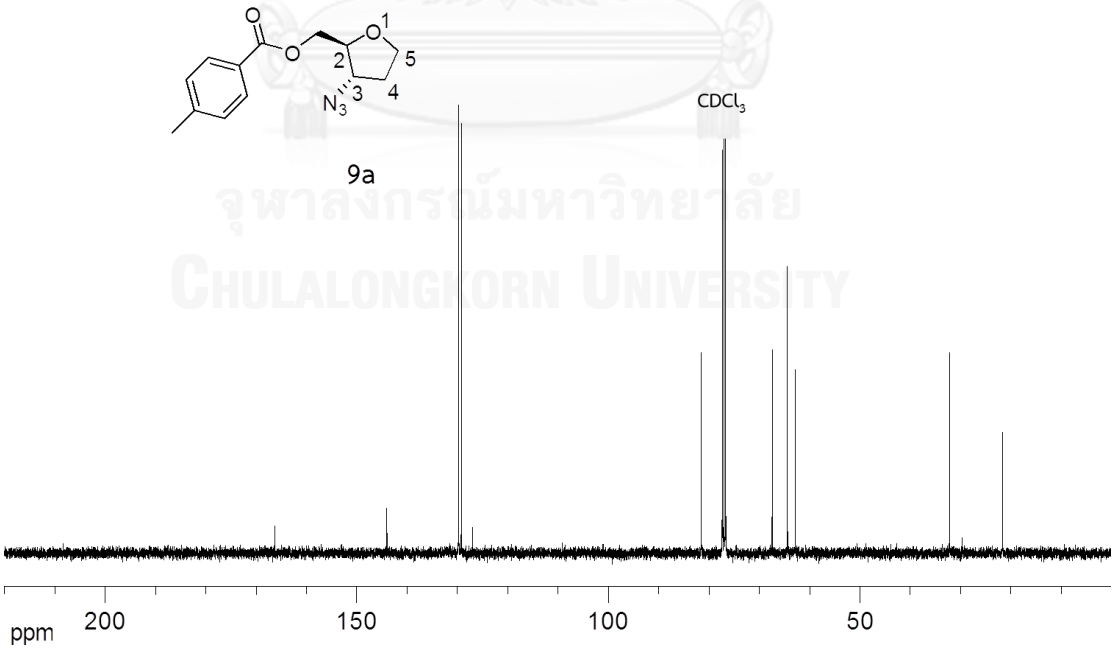

Figure A24 ^{13}C NMR spectrum (100 MHz, $CDCl_3$) of ((2*S*,3*S*)-3-azidotetrahydrofuran-2-yl)methyl-4-methylbenzoate (**9a**)

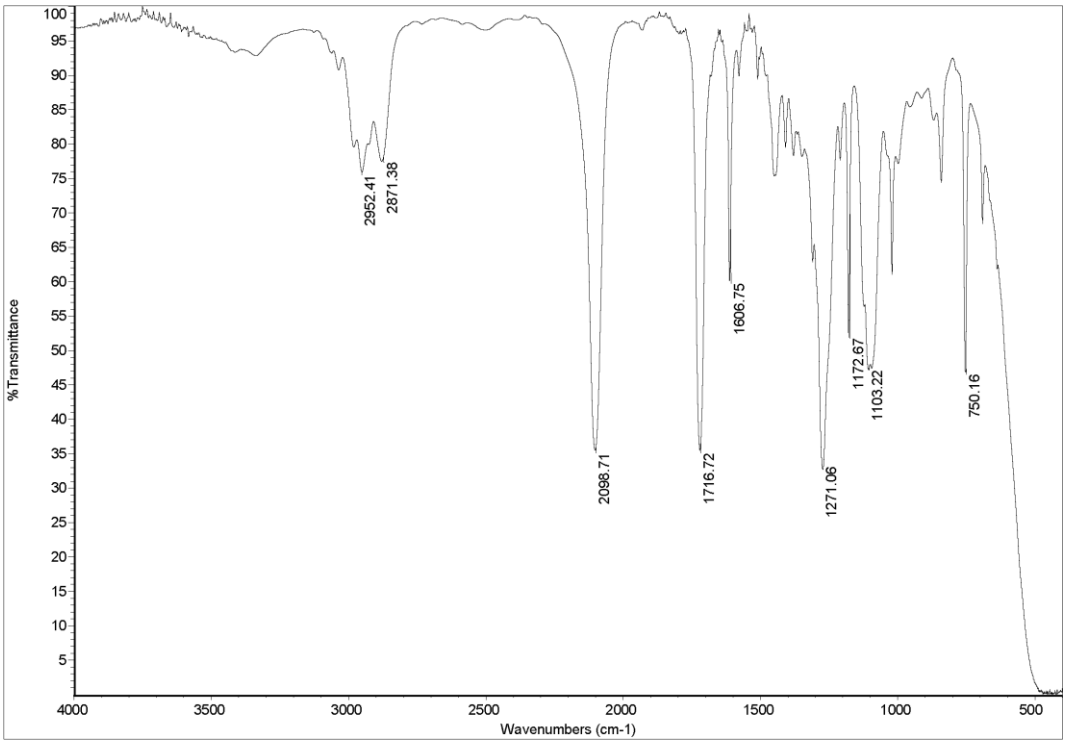

Figure A25 IR spectrum (thin flim) of ((2*S*,3*S*)-3-azidotetrahydrofuran-2-yl)methyl 4-methylbenzoate (**9a**)

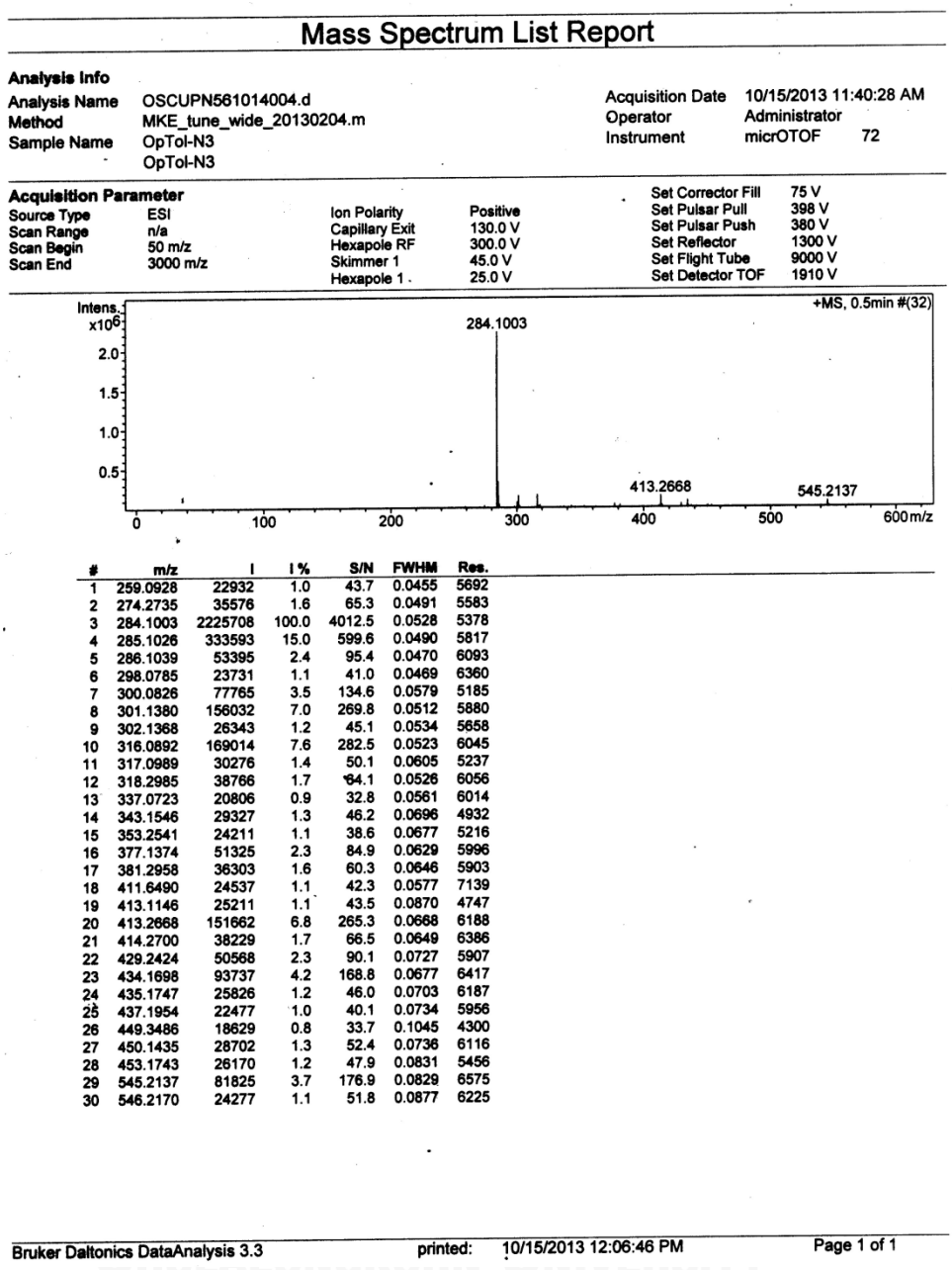

Mass Spectrum List Report

Analysis Info

Analysis Name	OSCUPN561014004.d	Acquisition Date	10/15/2013 11:40:28 AM
Method	MKE_tune_wide_20130204.m	Operator	Administrator
Sample Name	OpTol-N3	Instrument	micrOTOF 72
	OpTol-N3		

Acquisition Parameter

Source Type	ESI	Ion Polarity	Positive	Set Corrector Fill	75 V
Scan Range	n/a	Capillary Exit	130.0 V	Set Pulsar Pull	398 V
Scan Begin	50 m/z	Hexapole RF	300.0 V	Set Pulsar Push	380 V
Scan End	3000 m/z	Skimmer 1	45.0 V	Set Reflector	1300 V
		Hexapole 1	25.0 V	Set Flight Tube	9000 V
				Set Detector TOF	1910 V

#	m/z	I	I %	S/N	FWHM	Res.
1	259.0928	22932	1.0	43.7	0.0455	5692
2	274.2735	35576	1.6	65.3	0.0491	5583
3	284.1003	2225708	100.0	4012.5	0.0528	5378
4	285.1026	333593	15.0	599.6	0.0490	5817
5	286.1039	53395	2.4	95.4	0.0470	6093
6	298.0785	23731	1.1	41.0	0.0469	6360
7	300.0826	77765	3.5	134.6	0.0579	5185
8	301.1380	156032	7.0	269.8	0.0512	5880
9	302.1368	26343	1.2	45.1	0.0534	5658
10	316.0892	169014	7.6	282.5	0.0523	6045
11	317.0989	30276	1.4	50.1	0.0605	5237
12	318.2985	38766	1.7	64.1	0.0526	6056
13	337.0723	20806	0.9	32.8	0.0561	6014
14	343.1546	29327	1.3	46.2	0.0696	4932
15	353.2541	24211	1.1	38.6	0.0677	5216
16	377.1374	51325	2.3	84.9	0.0629	5996
17	381.2958	36303	1.6	60.3	0.0646	5903
18	411.6490	24537	1.1	42.3	0.0577	7139
19	413.1146	25211	1.1	43.5	0.0870	4747
20	413.2668	151662	6.8	265.3	0.0668	6188
21	414.2700	38229	1.7	66.5	0.0649	6386
22	429.2424	50568	2.3	90.1	0.0727	5907
23	434.1698	93737	4.2	168.8	0.0677	6417
24	435.1747	25826	1.2	46.0	0.0703	6187
25	437.1954	22477	1.0	40.1	0.0734	5956
26	449.3486	18629	0.8	33.7	0.1045	4300
27	450.1435	28702	1.3	52.4	0.0736	6116
28	453.1743	26170	1.2	47.9	0.0831	5456
29	545.2137	81825	3.7	176.9	0.0829	6575
30	546.2170	24277	1.1	51.8	0.0877	6225

Bruker Daltonics DataAnalysis 3.3 printed: 10/15/2013 12:06:46 PM Page 1 of 1

Figure A26 HRMS spectrum of ((2*S*,3*S*)-3-azidotetrahydrofuran-2-yl)methyl 4-methylbenzoate (**9a**)

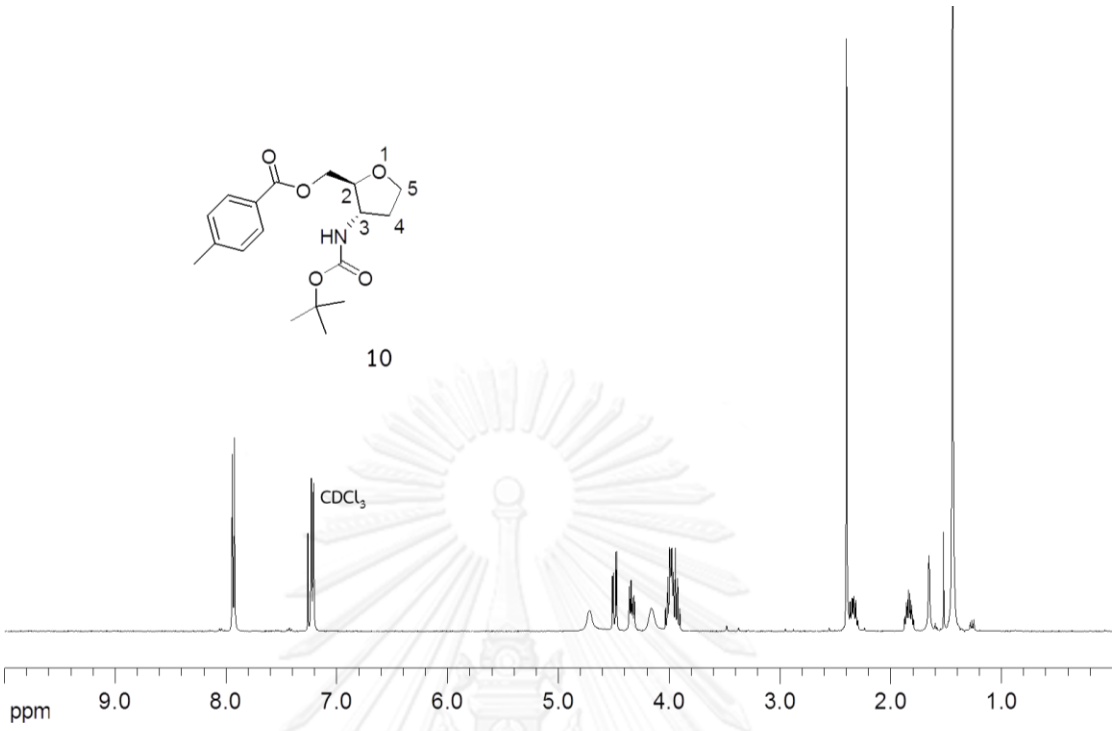

Figure A27 ^{1}H NMR spectrum (400 MHz, $CDCl_3$) of ((2*S*,3*S*)-3-(*tert*-butoxycarbonylamino)tetrahydrofuran-2-yl)methyl 4-methylbenzoate (**10**)

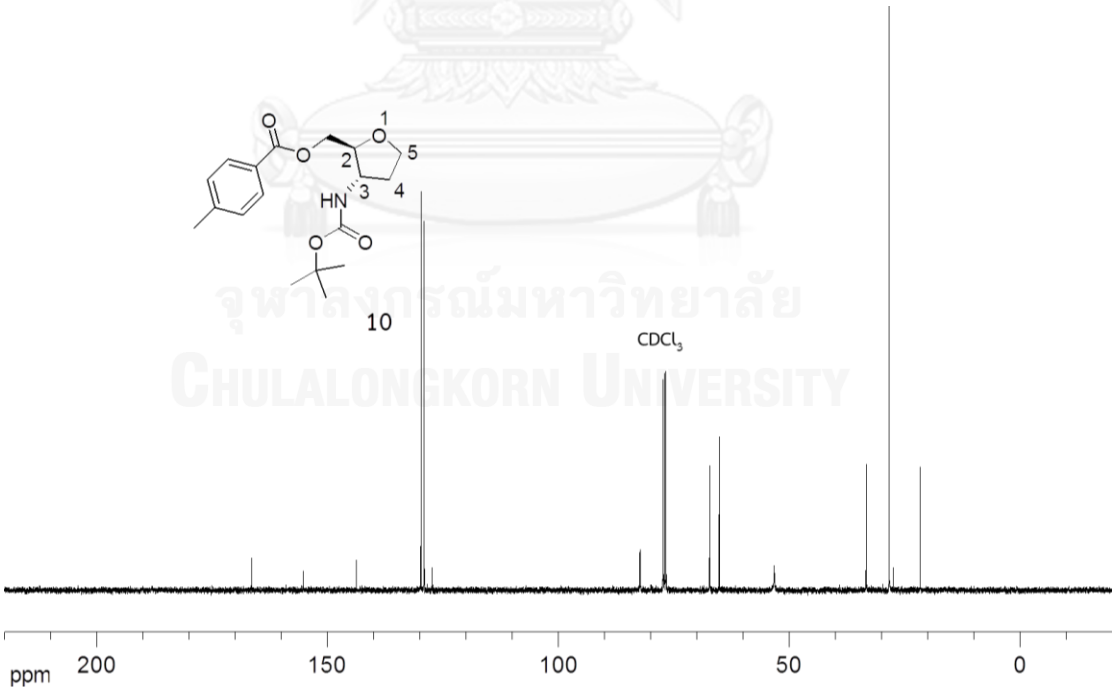

Figure A28 ^{13}C NMR spectrum (100 MHz, $CDCl_3$) of ((2*S*,3*S*)-3-(*tert*-butoxycarbonylamino)tetrahydrofuran-2-yl)methyl 4-methylbenzoate (**10**)

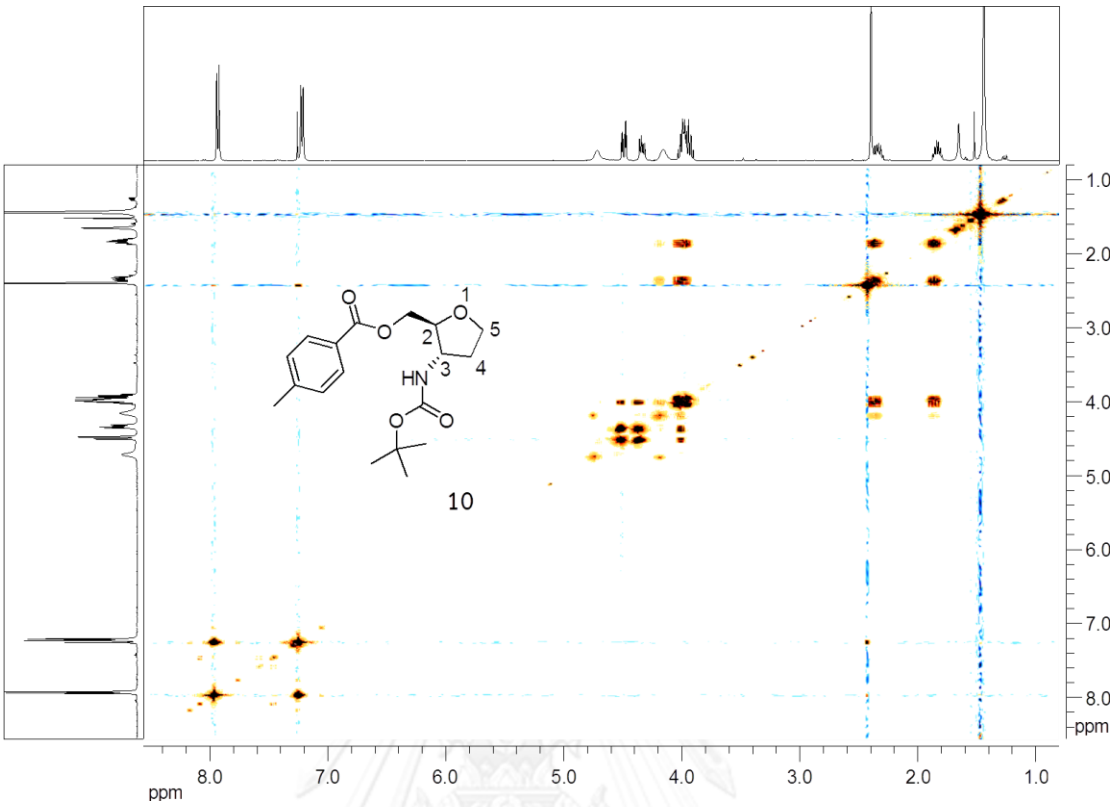

Figure A29 ^{1}H-^{1}H COSY NMR spectrum ($CDCl_3$) of ((2*S*,3*S*)-3-(*tert*-butoxycarbonylamino)tetrahydrofuran-2-yl)methyl 4-methylbenzoate (**10**)

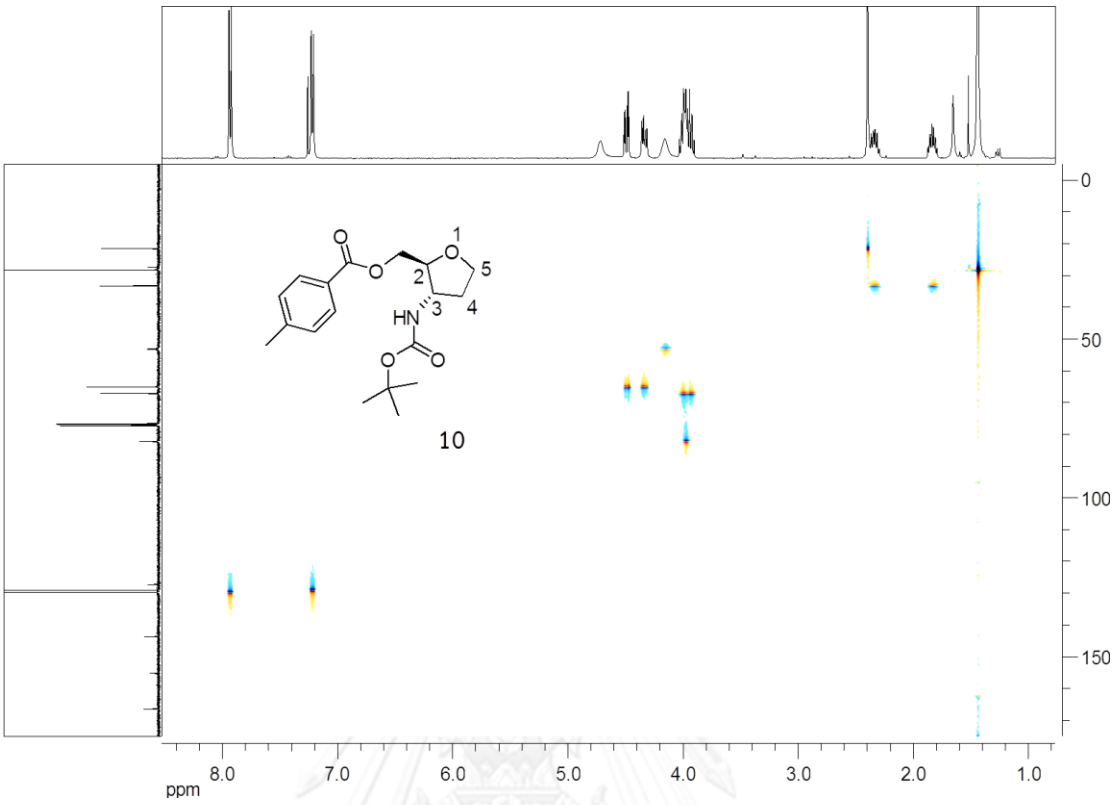

Figure A30 ^{1}H-^{13}C HSQC NMR spectrum ($CDCl_3$) of ((2*S*,3*S*)-3-(*tert*-butoxycarbonylamino)tetrahydrofuran-2-yl)methyl 4-methylbenzoate (**10**)

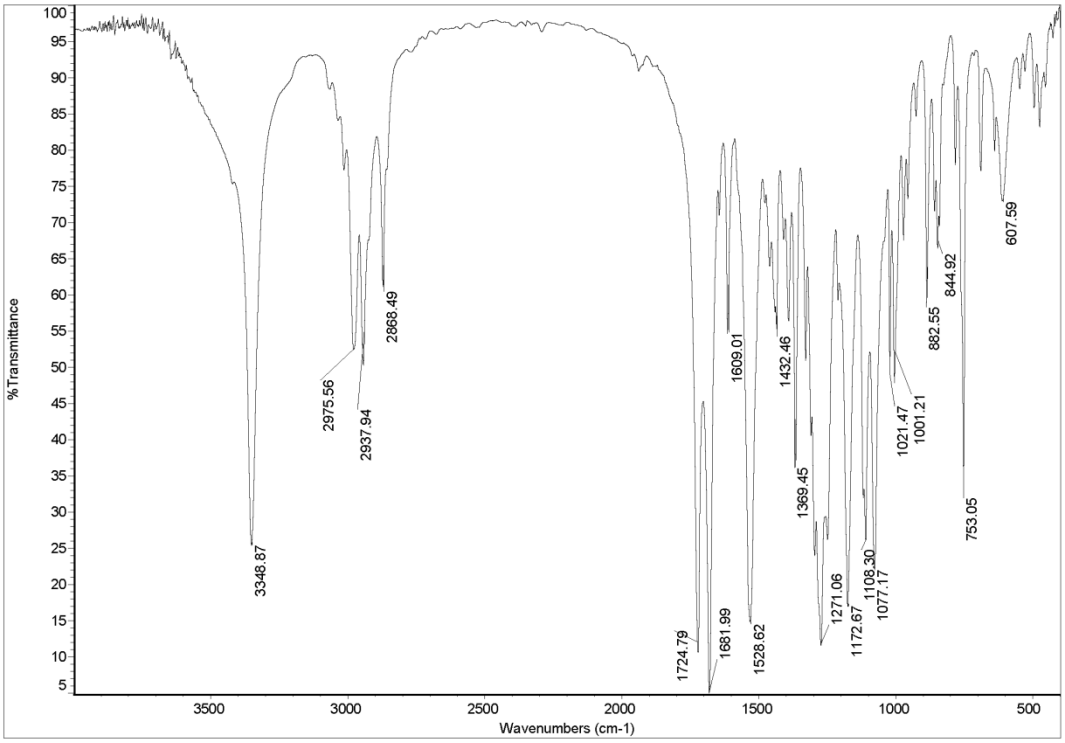

Figure A31 IR spectrum (KBr) of ((2*S*,3*S*)-3-(*tert*-butoxycarbonylamino)tetrahydrofuran-2-yl)methyl 4-methylbenzoate (**10**)

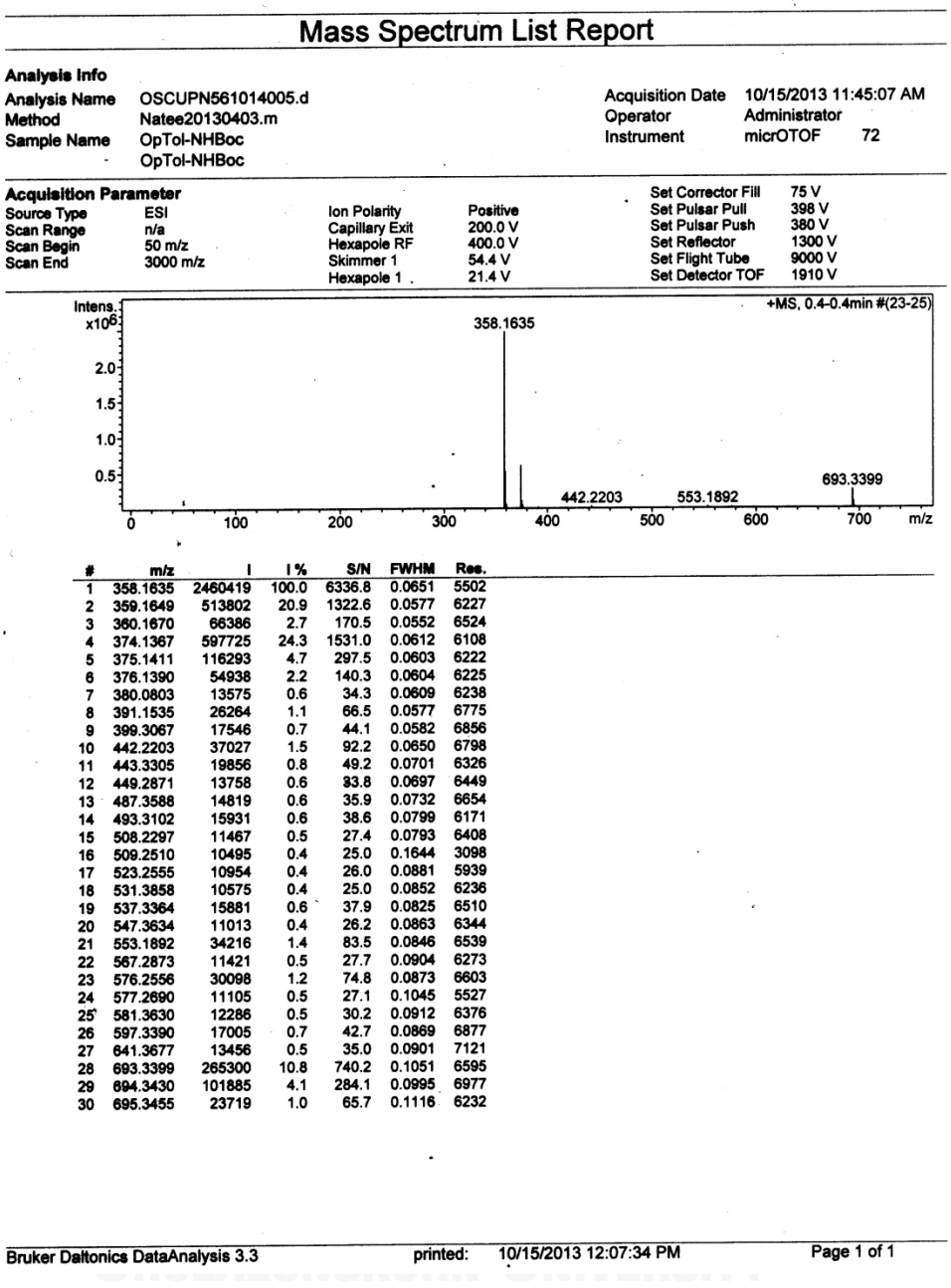

Mass Spectrum List Report

Analysis Info

Analysis Name	OSCUPN561014005.d	Acquisition Date	10/15/2013 11:45:07 AM
Method	Natee20130403.m	Operator	Administrator
Sample Name	OpTol-NHBoc	Instrument	micrOTOF 72
	OpTol-NHBoc		

Acquisition Parameter

Source Type	ESI	Ion Polarity	Positive	Set Corrector Fill	75 V
Scan Range	n/a	Capillary Exit	200.0 V	Set Pulsar Pull	398 V
Scan Begin	50 m/z	Hexapole RF	400.0 V	Set Pulsar Push	380 V
Scan End	3000 m/z	Skimmer 1	54.4 V	Set Reflector	1300 V
		Hexapole 1	21.4 V	Set Flight Tube	9000 V
				Set Detector TOF	1910 V

#	m/z	I	I %	S/N	FWHM	Res.
1	358.1635	2460419	100.0	6336.8	0.0651	5502
2	359.1649	513802	20.9	1322.6	0.0577	6227
3	360.1670	66386	2.7	170.5	0.0552	6524
4	374.1367	597725	24.3	1531.0	0.0612	6108
5	375.1411	116293	4.7	297.5	0.0603	6222
6	376.1390	54938	2.2	140.3	0.0604	6225
7	380.0803	13575	0.6	34.3	0.0609	6238
8	391.1535	26264	1.1	66.5	0.0577	6775
9	399.3067	17546	0.7	44.1	0.0582	6856
10	442.2203	37027	1.5	92.2	0.0650	6798
11	443.3305	19856	0.8	49.2	0.0701	6326
12	449.2871	13758	0.6	33.8	0.0697	6449
13	487.3588	14819	0.6	35.9	0.0732	6654
14	493.3102	15931	0.6	38.6	0.0799	6171
15	508.2297	11467	0.5	27.4	0.0793	6408
16	509.2510	10495	0.4	25.0	0.1644	3098
17	523.2555	10954	0.4	26.0	0.0881	5939
18	531.3858	10575	0.4	25.0	0.0852	6236
19	537.3364	15881	0.6	37.9	0.0825	6510
20	547.3634	11013	0.4	26.2	0.0863	6344
21	553.1892	34216	1.4	83.5	0.0846	6539
22	567.2873	11421	0.5	27.7	0.0904	6273
23	576.2556	30098	1.2	74.8	0.0873	6603
24	577.2690	11105	0.5	27.1	0.1045	5527
25	581.3630	12286	0.5	30.2	0.0912	6376
26	597.3390	17005	0.7	42.7	0.0869	6877
27	641.3677	13456	0.5	35.0	0.0901	7121
28	693.3399	265300	10.8	740.2	0.1051	6595
29	694.3430	101885	4.1	284.1	0.0995	6977
30	695.3455	23719	1.0	65.7	0.1116	6232

Bruker Daltonics DataAnalysis 3.3 printed: 10/15/2013 12:07:34 PM Page 1 of 1

Figure A32 HRMS spectrum of ((2*S*,3*S*)-3-(*tert*-butoxycarbonylamino)tetrahydrofuran-2-yl)methyl 4-methylbenzoate (**10**)

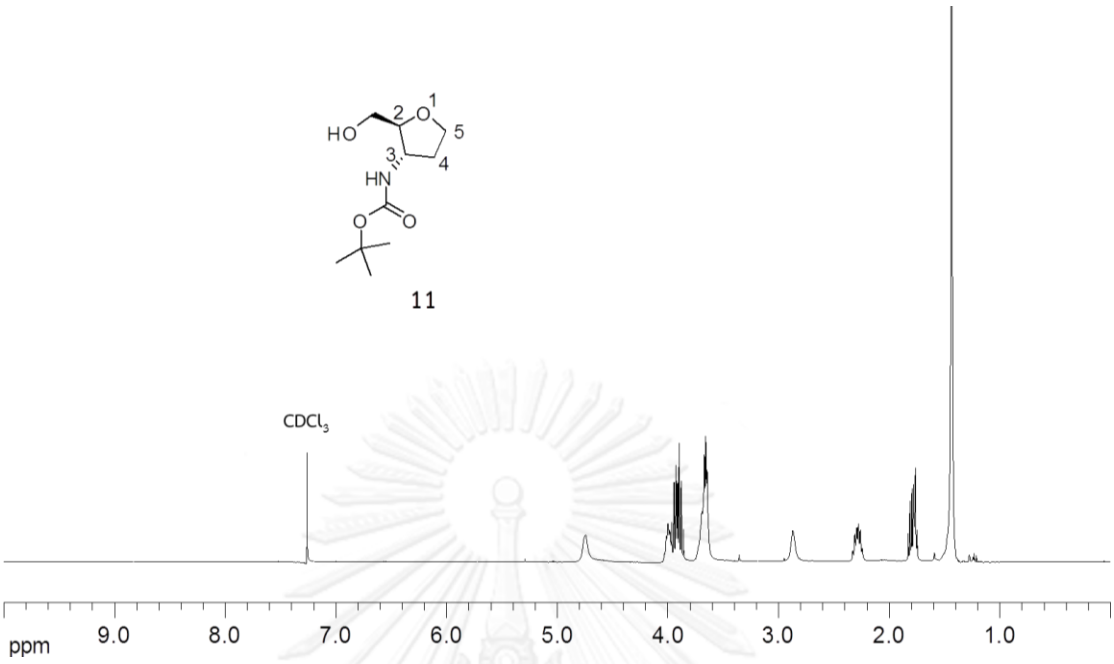

Figure A33 ^{1}H NMR spectrum (400 MHz, $CDCl_3$) of *tert*-butyl (2*S*,3*S*)-2-(hydroxymethyl)tetrahydrofuran-3-ylcarbamate (**11**)

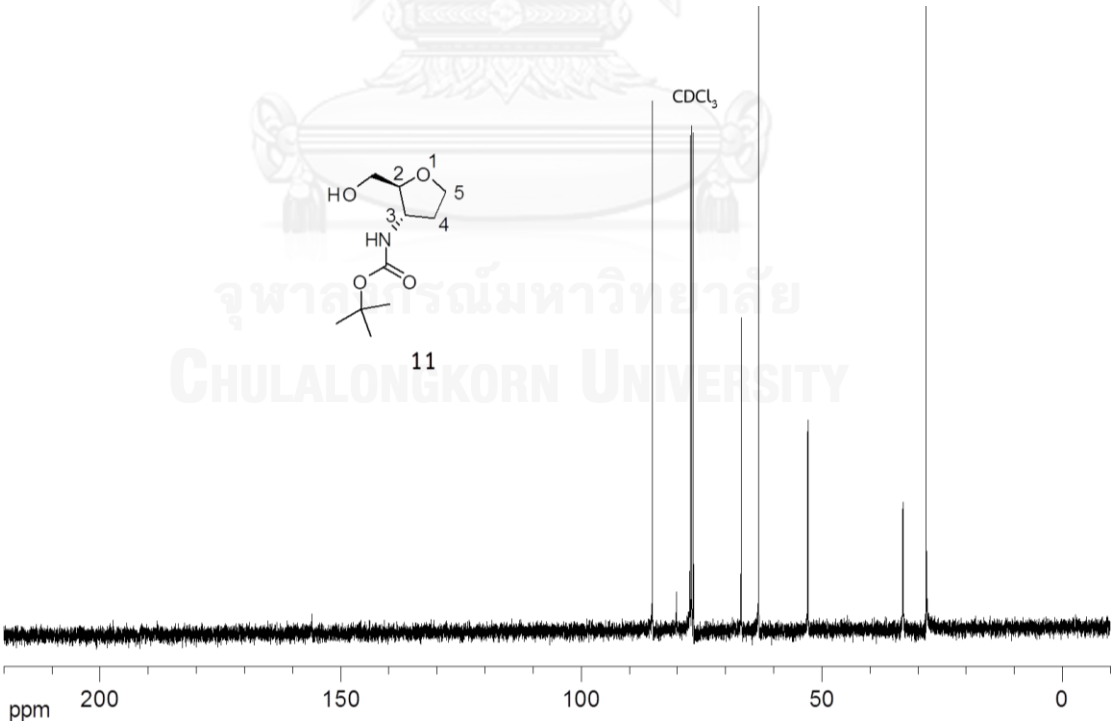

Figure A34 ^{13}C NMR (100 MHz, $CDCl_3$) of *tert*-butyl (2*S*,3*S*)-2-(hydroxymethyl)tetrahydrofuran-3-ylcarbamate (**11**)

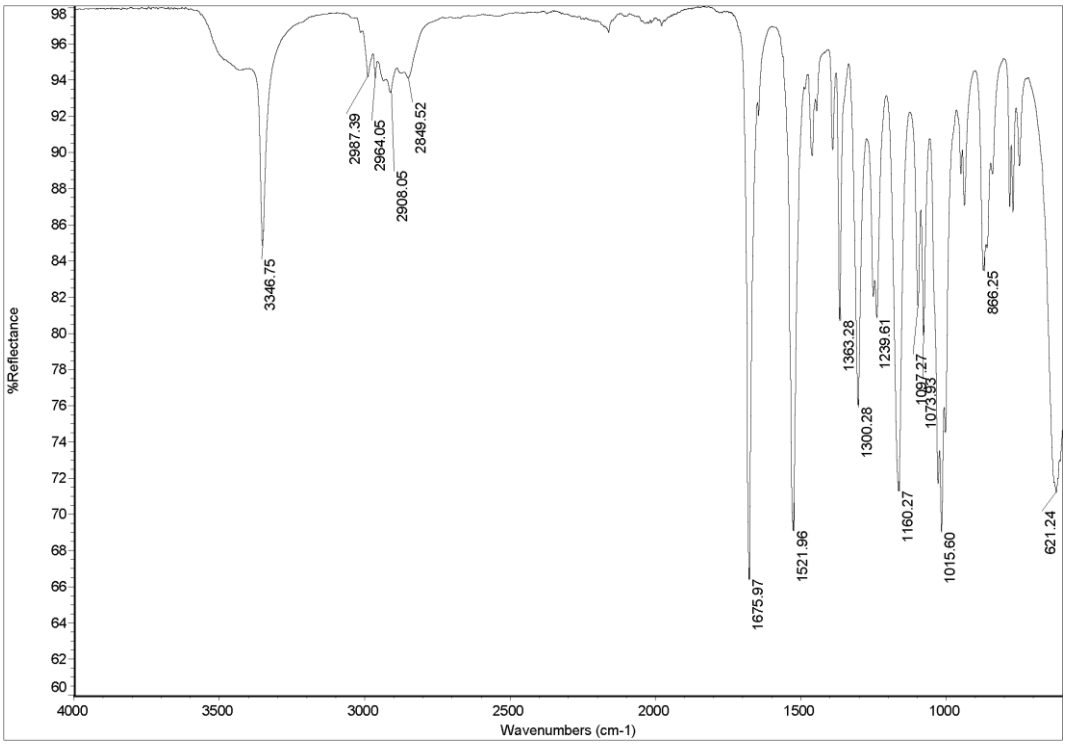

Figure A35 IR spectrum (ATR) of *tert*-butyl (2*S*,3*S*)-2-(hydroxymethyl)tetrahydrofuran-3-ylcarbamate (**11**)

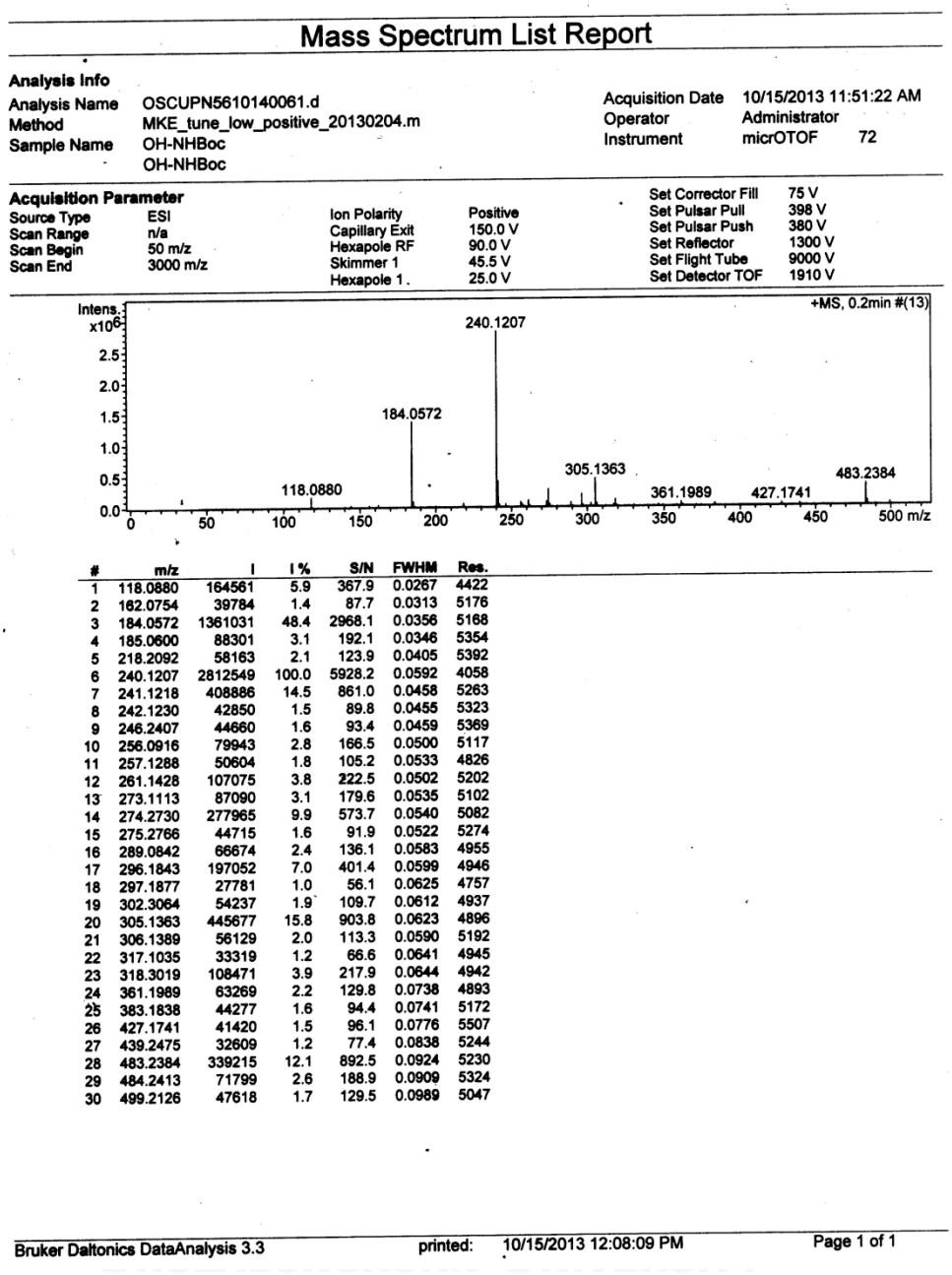

Mass Spectrum List Report

Analysis Info

Analysis Name	OSCUPN5610140061.d	Acquisition Date	10/15/2013 11:51:22 AM
Method	MKE_tune_low_positive_20130204.m	Operator	Administrator
Sample Name	OH-NHBoc	Instrument	micrOTOF 72
	OH-NHBoc		

Acquisition Parameter

Source Type	ESI	Ion Polarity	Positive	Set Corrector Fill	75 V
Scan Range	n/a	Capillary Exit	150.0 V	Set Pulsar Pull	398 V
Scan Begin	50 m/z	Hexapole RF	90.0 V	Set Pulsar Push	380 V
Scan End	3000 m/z	Skimmer 1	45.5 V	Set Reflector	1300 V
		Hexapole 1	25.0 V	Set Flight Tube	9000 V
				Set Detector TOF	1910 V

#	m/z	I	I %	S/N	FWHM	Res.
1	118.0880	164561	5.9	367.9	0.0267	4422
2	162.0754	39784	1.4	87.7	0.0313	5176
3	184.0572	1361031	48.4	2968.1	0.0356	5168
4	185.0600	88301	3.1	192.1	0.0346	5354
5	218.2092	58163	2.1	123.9	0.0405	5392
6	240.1207	2812549	100.0	5928.2	0.0592	4058
7	241.1218	408886	14.5	861.0	0.0458	5263
8	242.1230	42850	1.5	89.8	0.0455	5323
9	246.2407	44660	1.6	93.4	0.0459	5369
10	256.0916	79943	2.8	166.5	0.0500	5117
11	257.1288	50604	1.8	105.2	0.0533	4826
12	261.1428	107075	3.8	222.5	0.0502	5202
13	273.1113	87090	3.1	179.6	0.0535	5102
14	274.2730	277965	9.9	573.7	0.0540	5082
15	275.2766	44715	1.6	91.9	0.0522	5274
16	289.0842	66674	2.4	136.1	0.0583	4955
17	296.1843	197052	7.0	401.4	0.0599	4946
18	297.1877	27781	1.0	56.1	0.0625	4757
19	302.3064	54237	1.9	109.7	0.0612	4937
20	305.1363	445677	15.8	903.8	0.0623	4896
21	306.1389	56129	2.0	113.3	0.0590	5192
22	317.1035	33319	1.2	66.6	0.0641	4945
23	318.3019	108471	3.9	217.9	0.0644	4942
24	361.1989	63269	2.2	129.8	0.0738	4893
25	383.1838	44277	1.6	94.4	0.0741	5172
26	427.1741	41420	1.5	96.1	0.0776	5507
27	439.2475	32609	1.2	77.4	0.0838	5244
28	483.2384	339215	12.1	892.5	0.0924	5230
29	484.2413	71799	2.6	188.9	0.0909	5324
30	499.2126	47618	1.7	129.5	0.0989	5047

Bruker Daltonics DataAnalysis 3.3 printed: 10/15/2013 12:08:09 PM Page 1 of 1

Figure A36 HRMS spectrum of *tert*-butyl (2*S*,3*S*)-2-(hydroxymethyl)tetrahydrofuran-3-ylcarbamate (**11**)

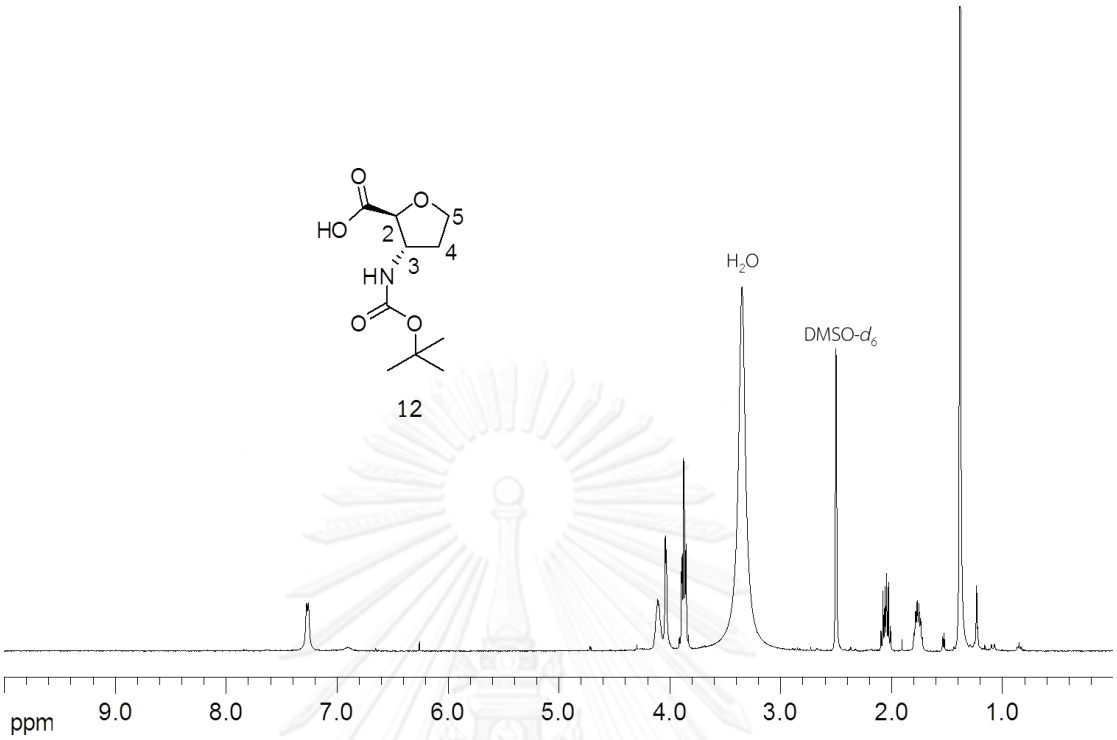

Figure A37 ^{1}H NMR spectrum (400 MHz, DMSO-d_6) of (2*S*,3*S*)-3-(*tert*-butoxycarbonylamino)tetrahydrofuran-2-carboxylic acid (**12**)

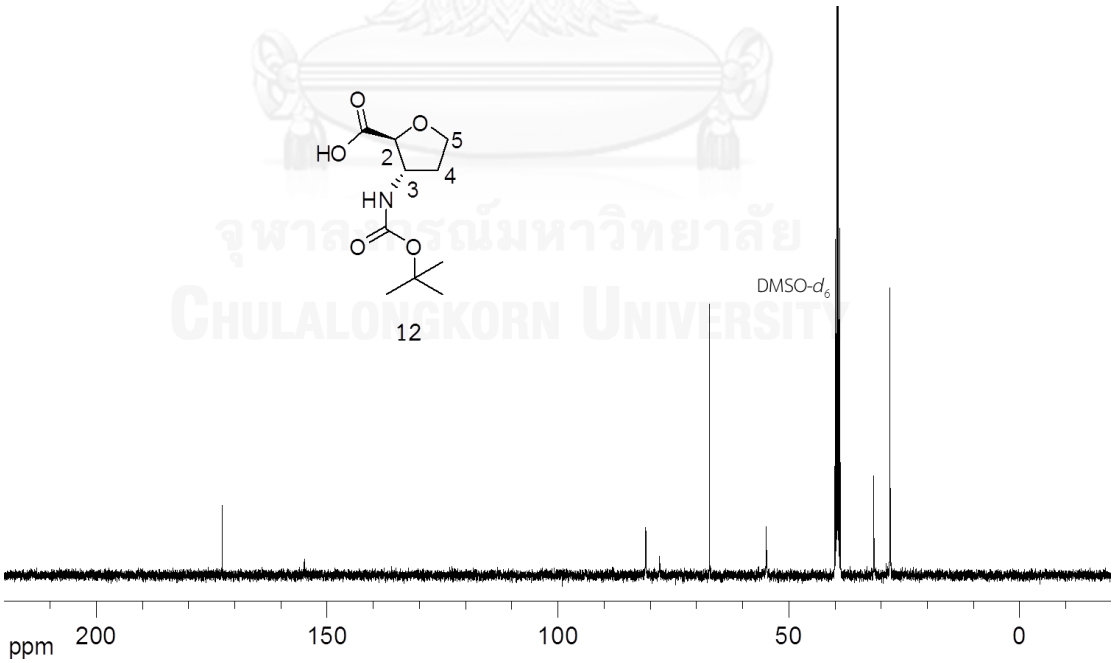

Figure A38 ^{13}C NMR (100 MHz, DMSO-d_6) of (2*S*,3*S*)-3-(*tert*-butoxycarbonylamino)tetrahydrofuran-2-carboxylic acid (**12**)

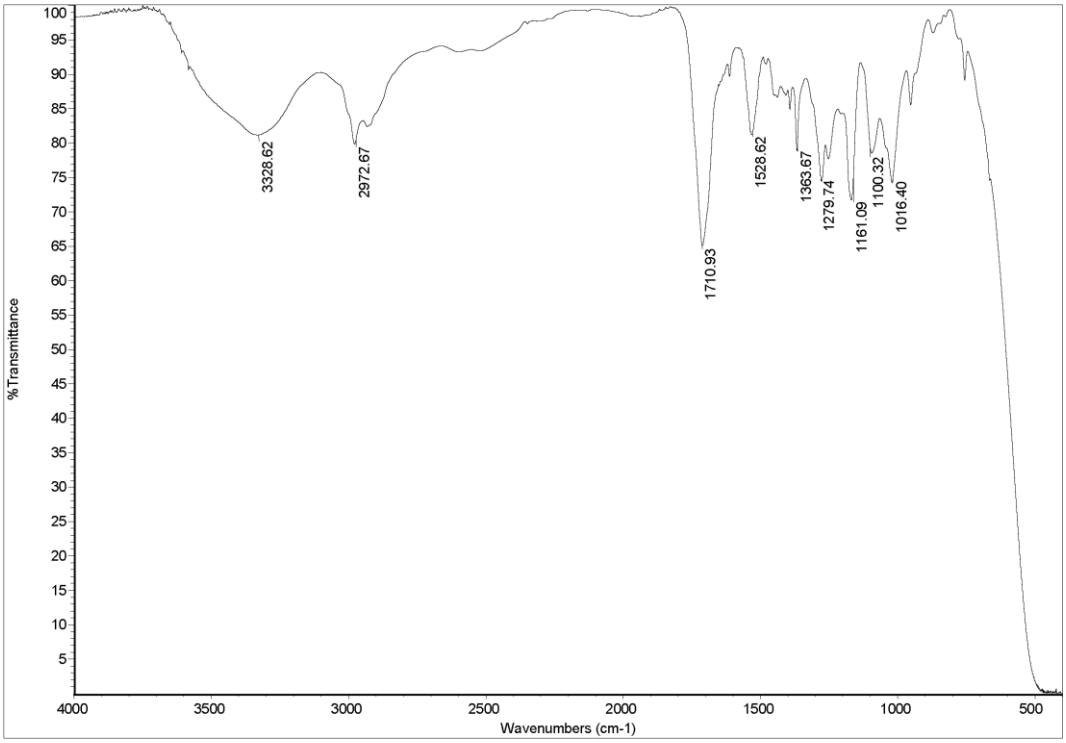

Figure A39 IR spectrum (thin flim) of (2*S*,3*S*)-3-(*tert*-butoxycarbonylamino)tetrahydrofuran-2-carboxylic acid (**12**)

Mass Spectrum List Report

Analysis Info

Analysis Name	OSCUPN561014007.d	Acquisition Date	10/15/2013 11:54:17 AM
Method	MKE_tune_low_positive_20130204.m	Operator	Administrator
Sample Name	Acid-NHBoc Acid-NHBoc	Instrument	micrOTOF 72

Acquisition Parameter

Source Type	ESI	Ion Polarity	Positive	Set Corrector Fill	75 V
Scan Range	n/a	Capillary Exit	150.0 V	Set Pulsar Pull	398 V
Scan Begin	50 m/z	Hexapole RF	90.0 V	Set Pulsar Push	380 V
Scan End	3000 m/z	Skimmer 1	45.5 V	Set Reflector	1300 V
		Hexapole 1	25.0 V	Set Flight Tube	9000 V
				Set Detector TOF	1910 V

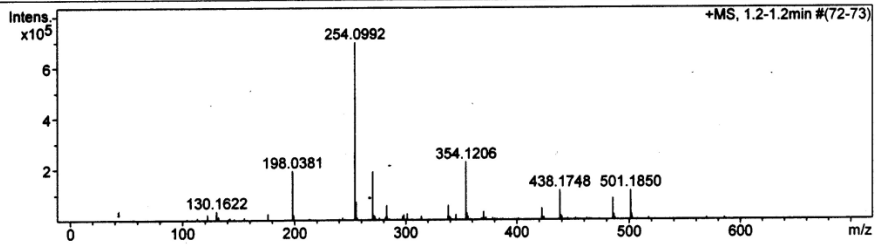

#	m/z	I	I %	S/N	FWHM	Res.
1	122.0443	24046	3.4	58.5	0.0244	4995
2	130.0528	24649	3.5	60.0	0.0276	4710
3	130.1622	36636	5.2	89.3	0.0254	5120
4	132.0690	16421	2.4	39.9	0.0277	4761
5	176.0571	25989	3.7	62.3	0.0339	5200
6	198.0381	192861	27.6	460.2	0.0380	5211
7	199.0326	21953	3.1	52.1	0.0460	4324
8	254.0992	697879	100.0	1627.5	0.0508	4999
9	255.1018	72625	10.4	168.9	0.0500	5103
10	270.0738	190090	27.2	440.0	0.0535	5047
11	271.0765	20596	3.0	47.2	0.0527	5144
12	272.0713	16407	2.4	37.5	0.0572	4760
13	282.5530	58483	8.4	134.3	0.0490	5763
14	297.0889	16647	2.4	37.6	0.0558	5324
15	298.0571	20921	3.0	47.4	0.0612	4869
16	301.0726	25609	3.7	58.1	0.0596	5051
17	338.1424	58366	8.4	131.0	0.0669	5051
18	339.1442	15698	2.2	34.8	0.0664	5105
19	345.0635	22884	3.3	51.2	0.0661	5217
20	354.1206	226884	32.5	519.8	0.0687	5155
21	355.1241	29274	4.2	66.6	0.0680	5223
22	356.1200	16348	2.3	37.0	0.0719	4951
23	370.0941	32970	4.7	76.7	0.0674	5489
24	422.1981	45996	6.6	115.8	0.0782	5402
25	438.1748	116003	16.6	300.4	0.0795	5511
26	439.1777	19394	2.8	49.7	0.0782	5615
27	485.2135	85048	12.2	237.6	0.0901	5383
28	486.2145	22706	3.3	63.0	0.0938	5182
29	501.1850	115333	16.5	331.5	0.0938	5345
30	502.1880	23450	3.4	66.9	0.0929	5403

Bruker Daltonics DataAnalysis 3.3 printed: 10/15/2013 12:08:47 PM Page 1 of 1

Figure A40 HRMS spectrum of (2*S*,3*S*)-3-(*tert*-butoxycarbonylamino)tetrahydrofuran-2-carboxylic acid (**12**)

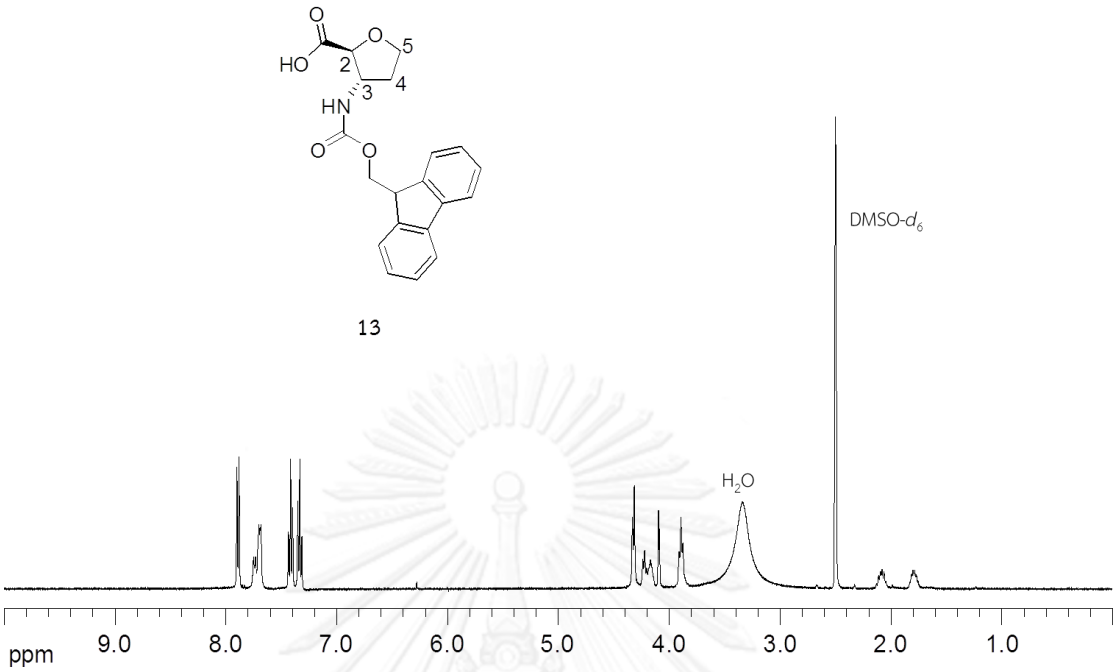

Figure A41 ^{1}H NMR spectrum (400 MHz, DMSO-d_6) of (2*S*,3*S*)-3-(((9H-fluoren-9-yl)methoxy)carbonylamino)tetrahydrofuran-2-carboxylic acid (**13**)

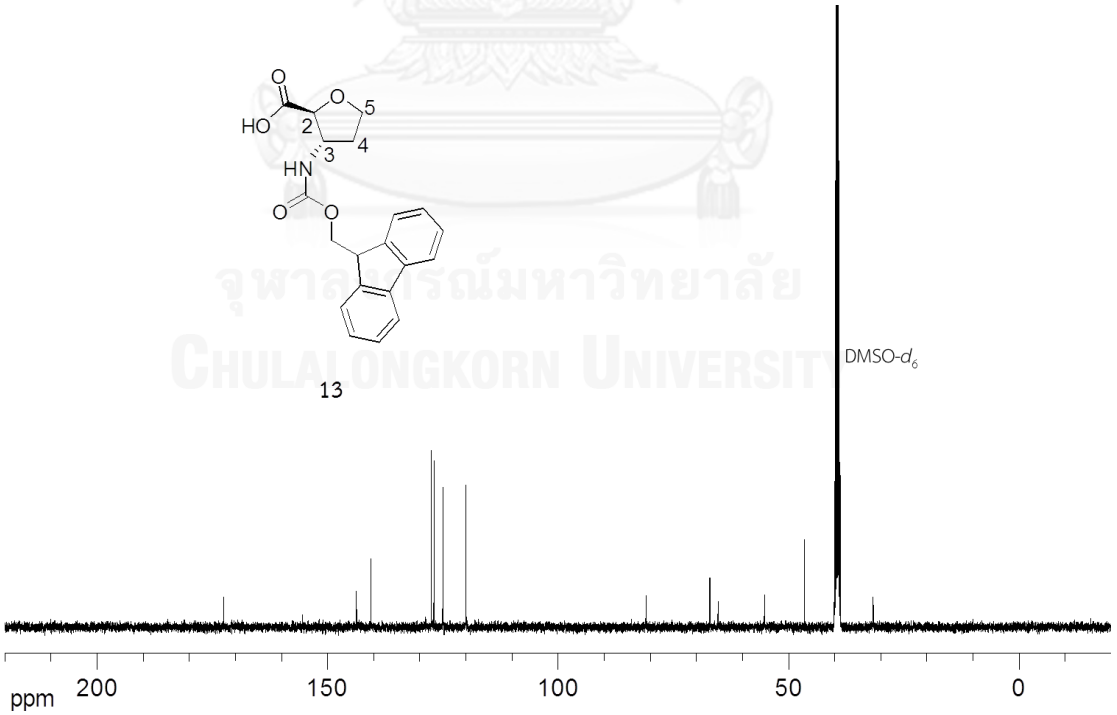

Figure A42 ^{13}C NMR spectrum (100 MHz, DMSO-d_6) of (2*S*,3*S*)-3-(((9H-fluoren-9-yl)methoxy)carbonylamino)tetrahydrofuran-2-carboxylic acid (**13**)

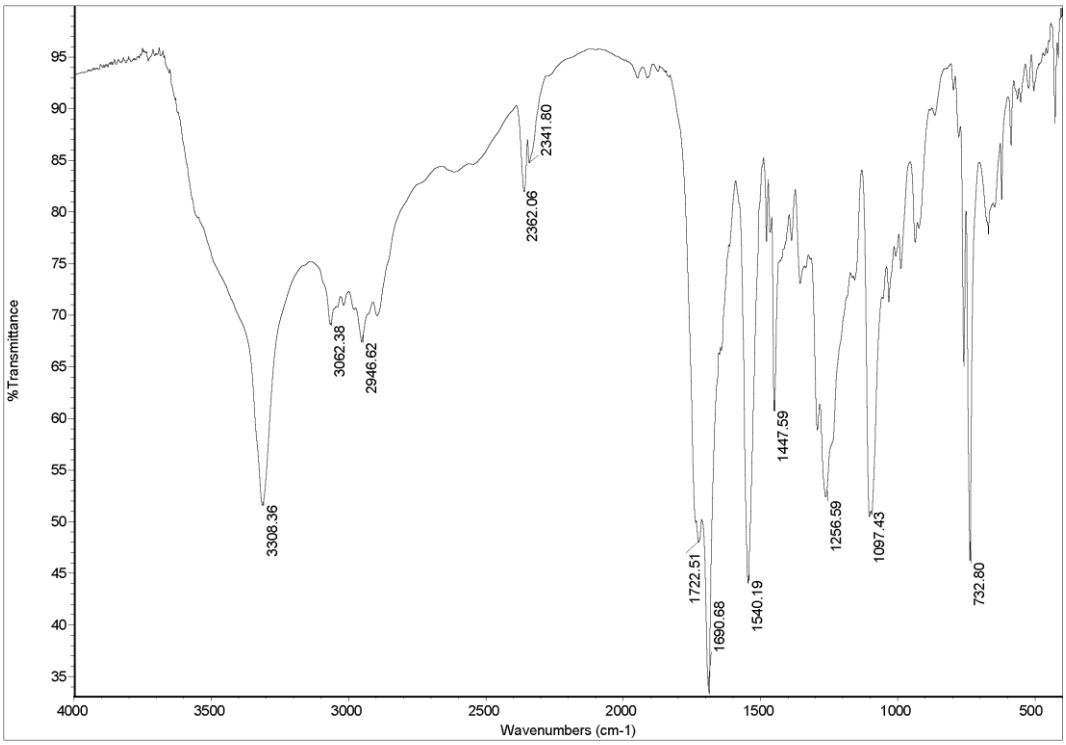

Figure A43 IR spectrum (KBr) of (2*S*,3*S*)-3-(((9H-fluoren-9-yl)methoxy)carbonylamino)tetrahydrofuran-2-carboxylic acid (**13**)

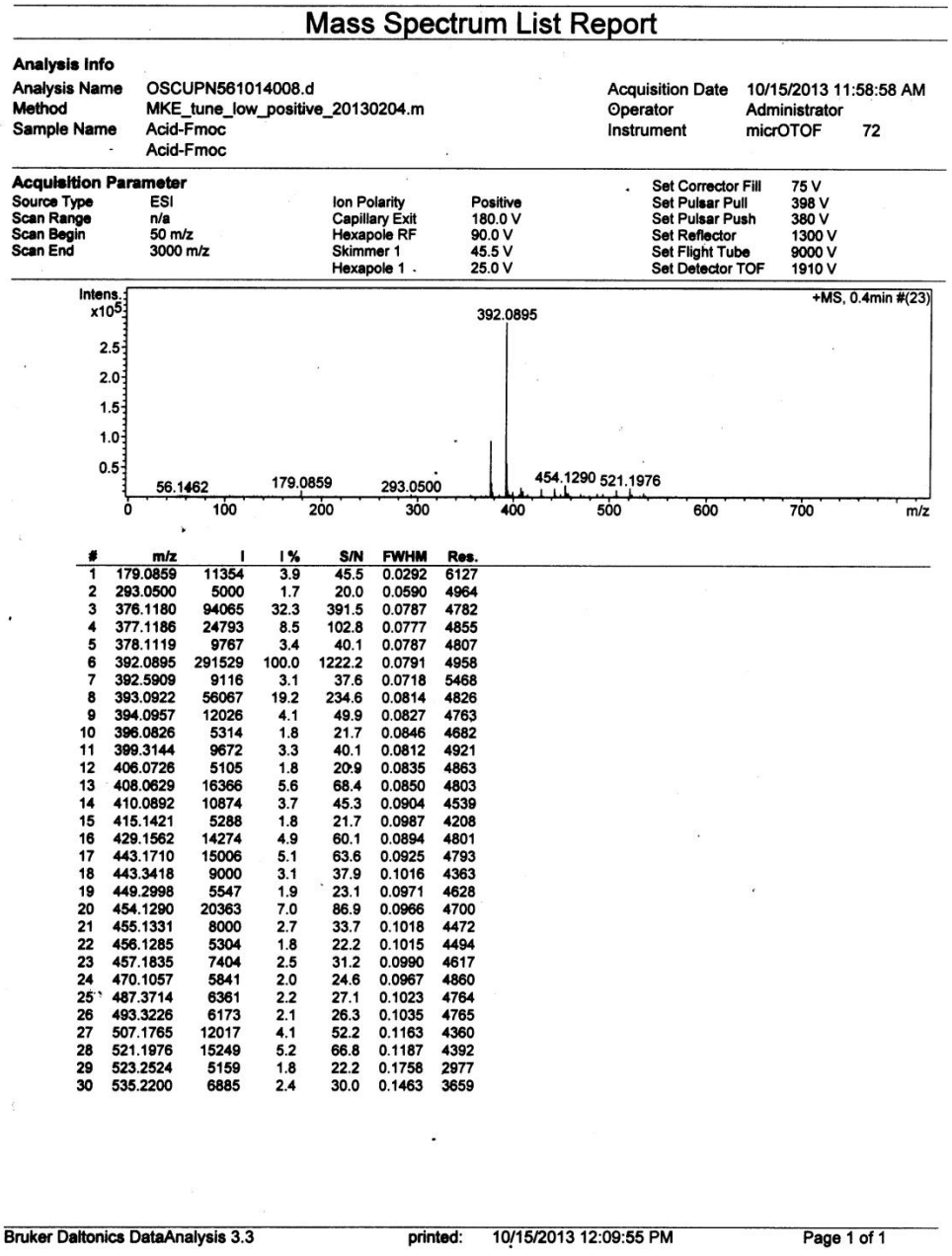

Mass Spectrum List Report

Analysis Info

Analysis Name	OSCUPN561014008.d	Acquisition Date	10/15/2013 11:58:58 AM
Method	MKE_tune_low_positive_20130204.m	Operator	Administrator
Sample Name	Acid-Fmoc	Instrument	micrOTOF 72
	Acid-Fmoc		

Acquisition Parameter

Source Type	ESI	Ion Polarity	Positive	Set Corrector Fill	75 V
Scan Range	n/a	Capillary Exit	180.0 V	Set Pulsar Pull	398 V
Scan Begin	50 m/z	Hexapole RF	90.0 V	Set Pulsar Push	380 V
Scan End	3000 m/z	Skimmer 1	45.5 V	Set Reflector	1300 V
		Hexapole 1	25.0 V	Set Flight Tube	9000 V
				Set Detector TOF	1910 V

#	m/z	I	I %	S/N	FWHM	Res.
1	179.0859	11354	3.9	45.5	0.0292	6127
2	293.0500	5000	1.7	20.0	0.0590	4964
3	376.1180	94065	32.3	391.5	0.0787	4782
4	377.1186	24793	8.5	102.8	0.0777	4855
5	378.1119	9767	3.4	40.1	0.0787	4807
6	392.0895	291529	100.0	1222.2	0.0791	4958
7	392.5909	9116	3.1	37.6	0.0718	5468
8	393.0922	56067	19.2	234.6	0.0814	4826
9	394.0957	12026	4.1	49.9	0.0827	4763
10	396.0826	5314	1.8	21.7	0.0846	4682
11	399.3144	9672	3.3	40.1	0.0812	4921
12	406.0726	5105	1.8	20.9	0.0835	4863
13	408.0629	16366	5.6	68.4	0.0850	4803
14	410.0892	10874	3.7	45.3	0.0904	4539
15	415.1421	5288	1.8	21.7	0.0987	4208
16	429.1562	14274	4.9	60.1	0.0894	4801
17	443.1710	15006	5.1	63.6	0.0925	4793
18	443.3418	9000	3.1	37.9	0.1016	4363
19	449.2998	5547	1.9	23.1	0.0971	4628
20	454.1290	20363	7.0	86.9	0.0966	4700
21	455.1331	8000	2.7	33.7	0.1018	4472
22	456.1285	5304	1.8	22.2	0.1015	4494
23	457.1835	7404	2.5	31.2	0.0990	4617
24	470.1057	5841	2.0	24.6	0.0967	4860
25	487.3714	6361	2.2	27.1	0.1023	4764
26	493.3226	6173	2.1	26.3	0.1035	4765
27	507.1765	12017	4.1	52.2	0.1163	4360
28	521.1976	15249	5.2	66.8	0.1187	4392
29	523.2524	5159	1.8	22.2	0.1758	2977
30	535.2200	6885	2.4	30.0	0.1463	3659

Bruker Daltonics DataAnalysis 3.3 printed: 10/15/2013 12:09:55 PM Page 1 of 1

Figure A44 HRMS spectrum of of (2*S*,3*S*)-3-(((9H-fluoren-9-yl)methoxy)carbonylamino)tetrahydrofuran-2-carboxylic acid (**13**)

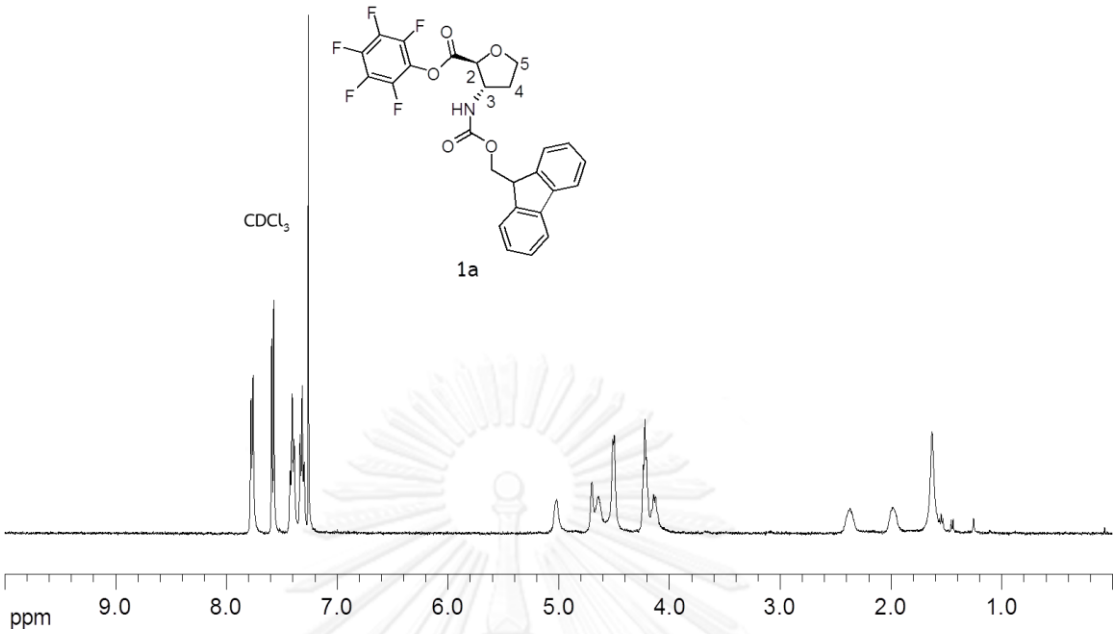

Figure A45 ^{1}H NMR spectrum (400 MHz, $CDCl_3$) of (2*S*,3*S*)-pentafluorophenyl 3-(((9H-fluoren-9-yl)methoxy)carbonylamino)tetrahydrofuran-2-carboxylate (**1a**)

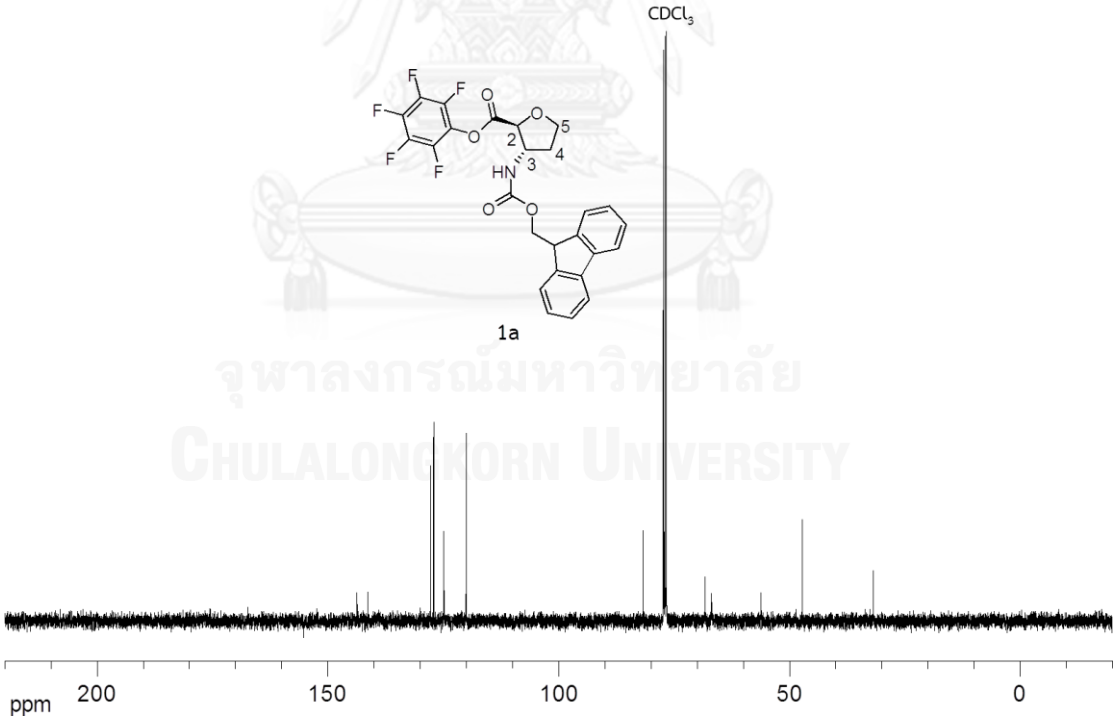

Figure A46 ^{13}C NMR spectrum (100 MHz, $CDCl_3$) of (2*S*,3*S*)-pentafluorophenyl 3-(((9H-fluoren-9-yl)methoxy)carbonylamino)tetrahydrofuran-2-carboxylate (**1a**)

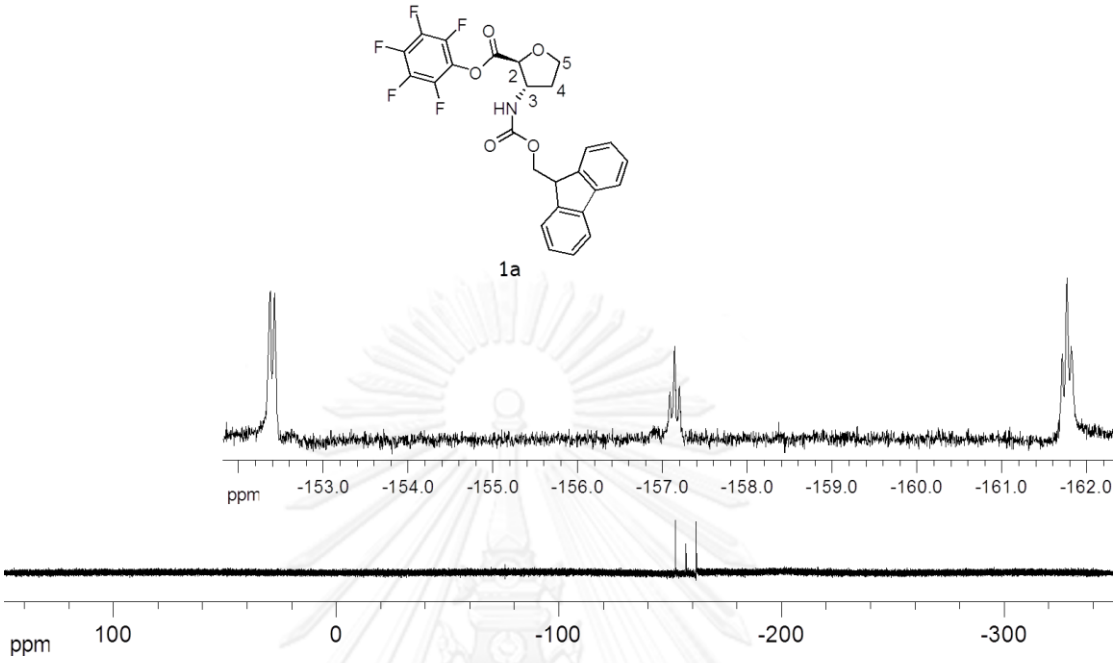

Figure A47 ^{19}F NMR spectrum (376 MHz, $CDCl_3$) of (2*S*,3*S*)-pentafluorophenyl 3-(((9H-fluoren-9-yl)methoxy)carbonylamino)tetrahydrofuran-2-carboxylate (**1a**)

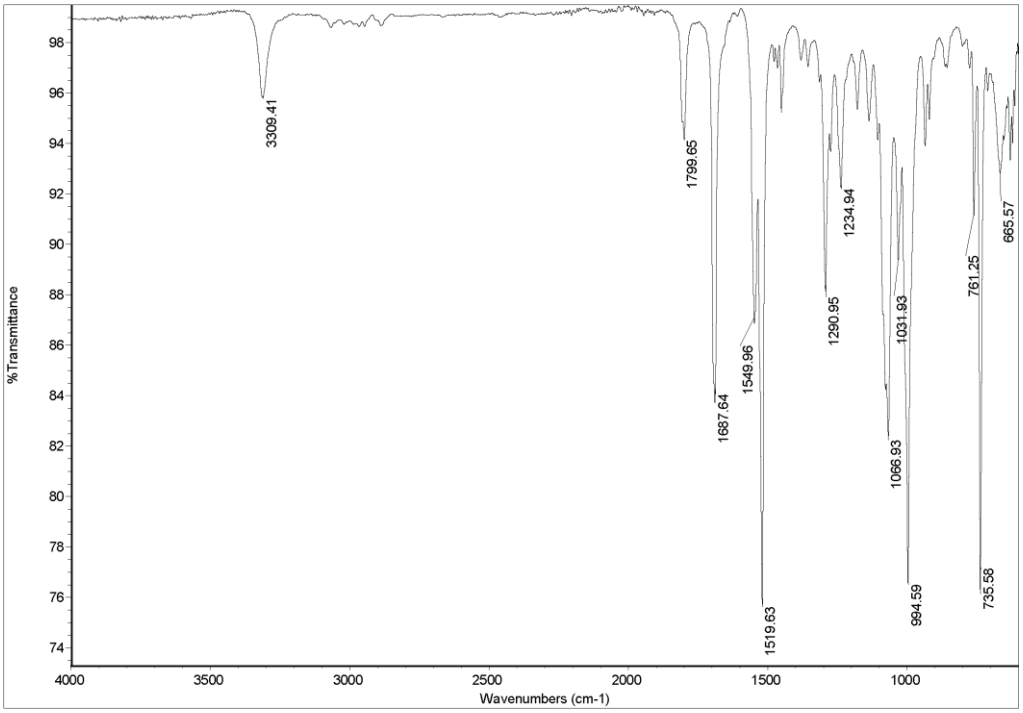

Figure A48 IR spectrum (ATR) of (2*S*,3*S*)-pentafluorophenyl 3-(((9H-fluoren-9-yl)methoxy)carbonylamino)tetrahydrofuran-2-carboxylate (**1a**)

Mass Spectrum List Report

Analysis Info

Analysis Name	OSCUSP5706130013.d	Acquisition Date	6/13/2014 11:36:17 AM
Method	esi_tune.m	Operator	Administrator
Sample Name	1	Instrument	micrOTOF 72
	1		

Acquisition Parameter

Source Type	ESI	Ion Polarity	Positive	Set Corrector Fill	79 V
Scan Range	n/a	Capillary Exit	150.0 V	Set Pulsar Pull	406 V
Scan Begin	50 m/z	Hexapole RF	450.0 V	Set Pulsar Push	388 V
Scan End	3000 m/z	Skimmer 1	50.0 V	Set Reflector	1300 V
		Hexapole 1	23.0 V	Set Flight Tube	9000 V
				Set Detector TOF	1910 V

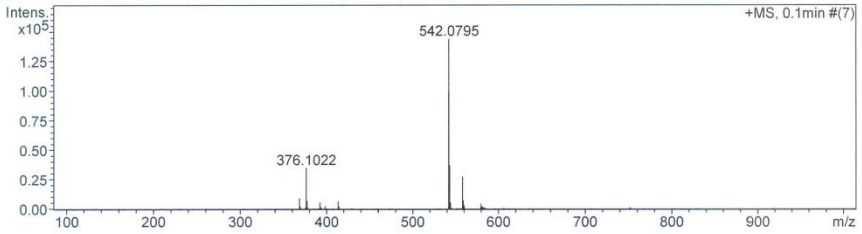

#	m/z	I	I %	S/N	FWHM	Res.
1	368.4123	8973	6.2	615.1	0.0391	9423
2	369.4156	2111	1.5	144.0	0.0414	8933
3	375.1200	1119	0.8	74.8	0.0450	8337
4	376.1022	34862	24.2	2329.7	0.0397	9480
5	377.1055	6820	4.7	454.1	0.0390	9658
6	378.1080	1007	0.7	66.6	0.0407	9287
7	392.0761	5477	3.8	347.5	0.0407	9644
8	393.0803	1447	1.0	91.3	0.0396	9931
9	398.0838	2455	1.7	152.7	0.0421	9462
10	413.2519	6446	4.5	383.5	0.0416	9929
11	414.0570	1367	1.0	80.9	0.0427	9698
12	414.2553	1812	1.3	107.3	0.0402	10305
13	542.0795	143824	100.0	6297.6	0.0562	9649
14	543.0813	36861	25.6	1616.1	0.0494	10988
15	544.0843	5476	3.8	240.1	0.0511	10641
16	545.0867	750	0.5	32.6	0.0469	11617
17	551.4556	709	0.5	31.1	0.0490	11259
18	557.5015	1142	0.8	50.7	0.0510	10930
19	558.0525	27188	18.9	1217.8	0.0545	10241
20	559.0536	7200	5.0	322.7	0.0510	10960
21	560.0528	2992	2.1	134.1	0.0519	10784
22	579.4877	4331	3.0	199.9	0.0522	11107
23	580.4914	1824	1.3	84.1	0.0536	10822
24	581.4999	1640	1.1	75.7	0.0559	10394
25	582.5098	796	0.6	36.6	0.0517	11261
26	583.5201	1148	0.8	53.0	0.0537	10872
27	605.4982	798	0.6	38.0	0.0573	10576
28	751.1929	1229	0.9	75.1	0.0656	11449
29	1061.1633	1932	1.3	148.1	0.0884	12003
30	1062.1693	1168	0.8	89.3	0.0926	11467

Bruker Daltonics DataAnalysis 3.3 printed: 6/13/2014 1:33:28 PM Page 1 of 1

Figure A49 HRMS spectrum of (2*S*,3*S*)-pentafluorophenyl 3-(((9H-fluoren-9-yl)methoxy)carbonylamino)tetrahydrofuran-2-carboxylate (**1a**)

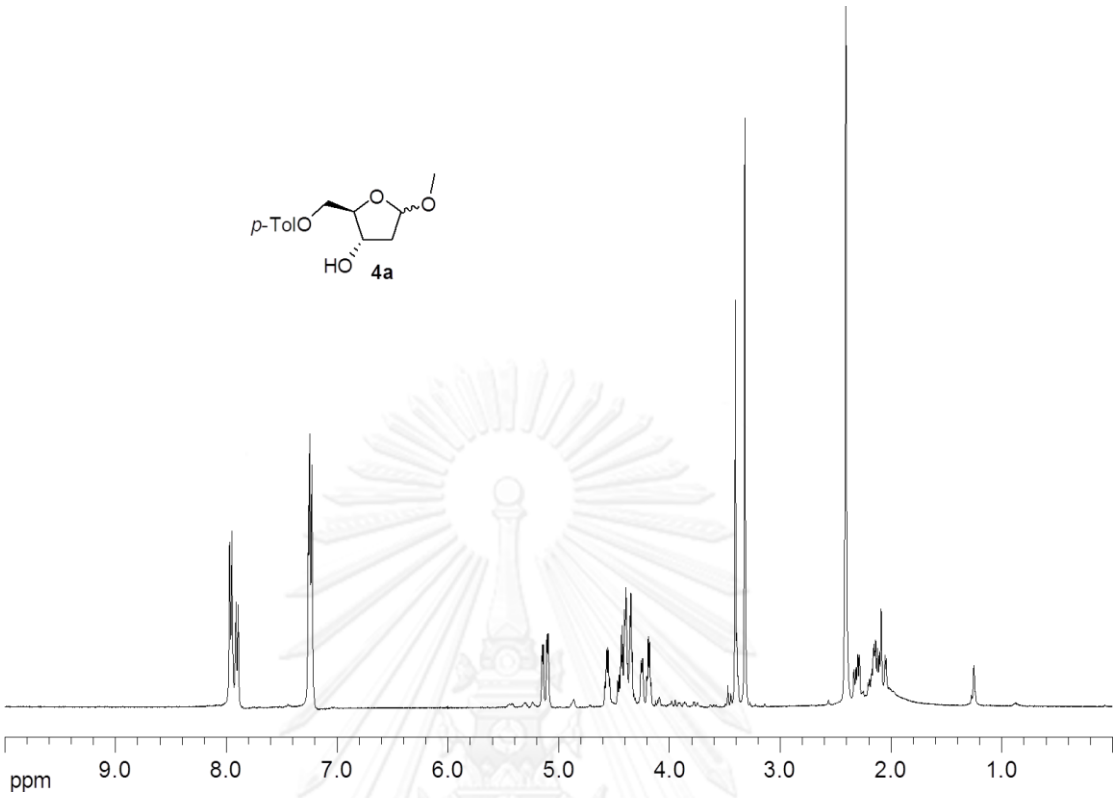

Figure A50 ^{1}H NMR spectrum (400 MHz, $CDCl_3$) of 5-*O*-*p*-toluoyl-2-deoxy-D-ribose methyl glycoside (**4a**) (mixture of α and β anomers)

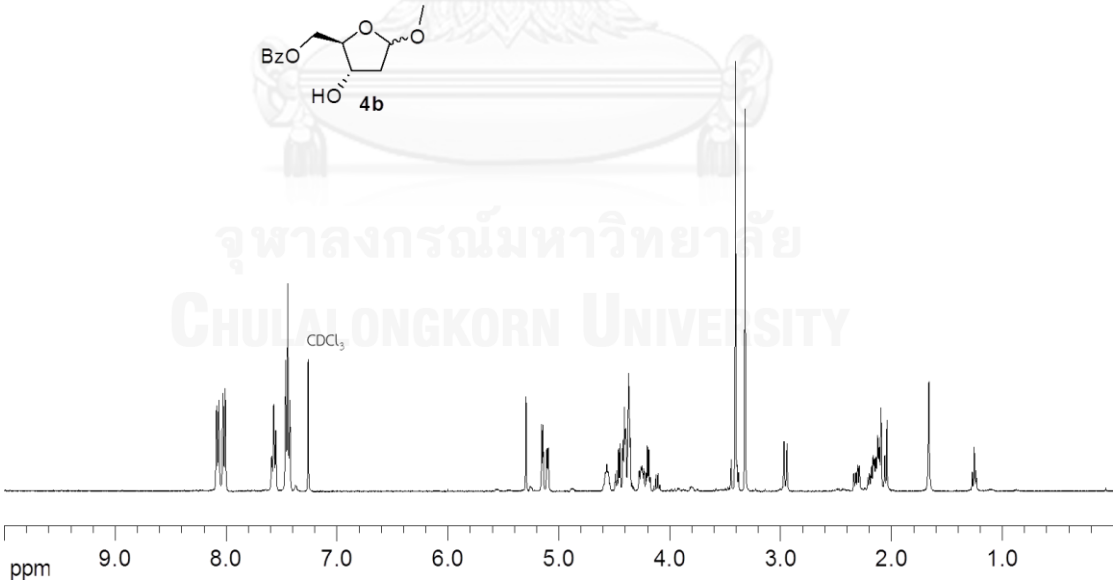

Figure A51 ^{1}H NMR spectrum (400 MHz, $CDCl_3$) of 5-*O*-benzoyl-2-deoxy-D-ribose methyl glycoside (**4b**) (mixture of α and β anomers)

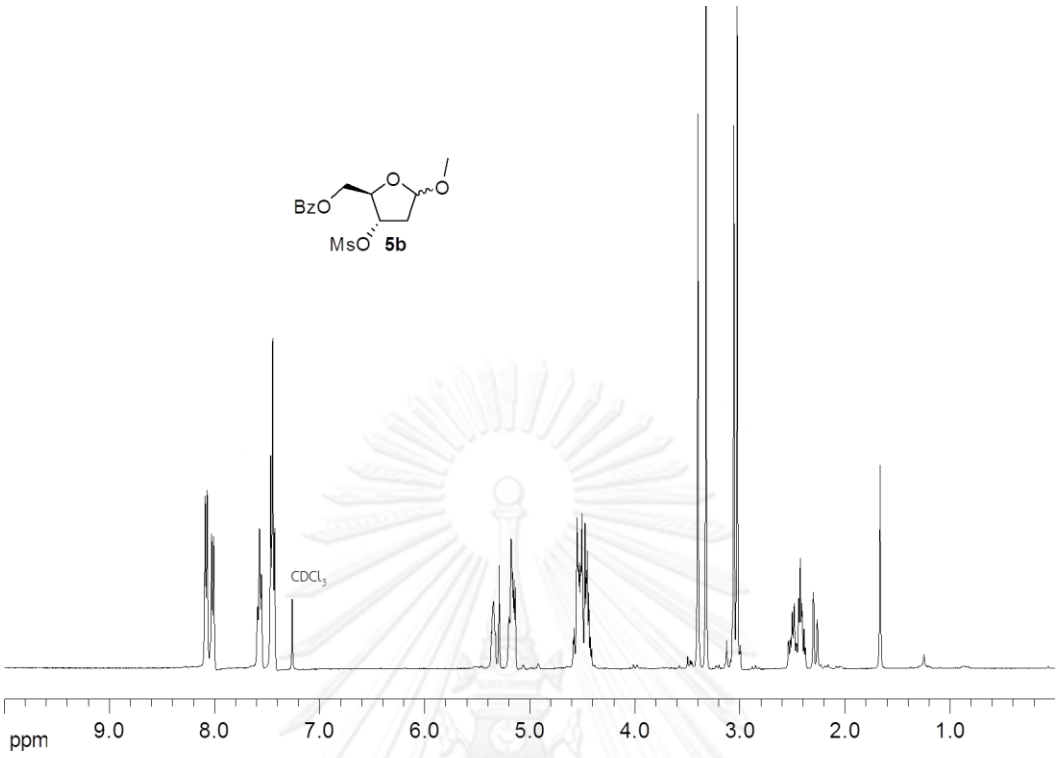

Figure A52 ^{1}H NMR spectrum (400 MHz, $CDCl_3$) of 5-*O*-Benzoyl-3-*O*-methanesulfonyl-2-deoxy-D-ribose methyl glycoside (**5b**) (mixture of α and β anomers)

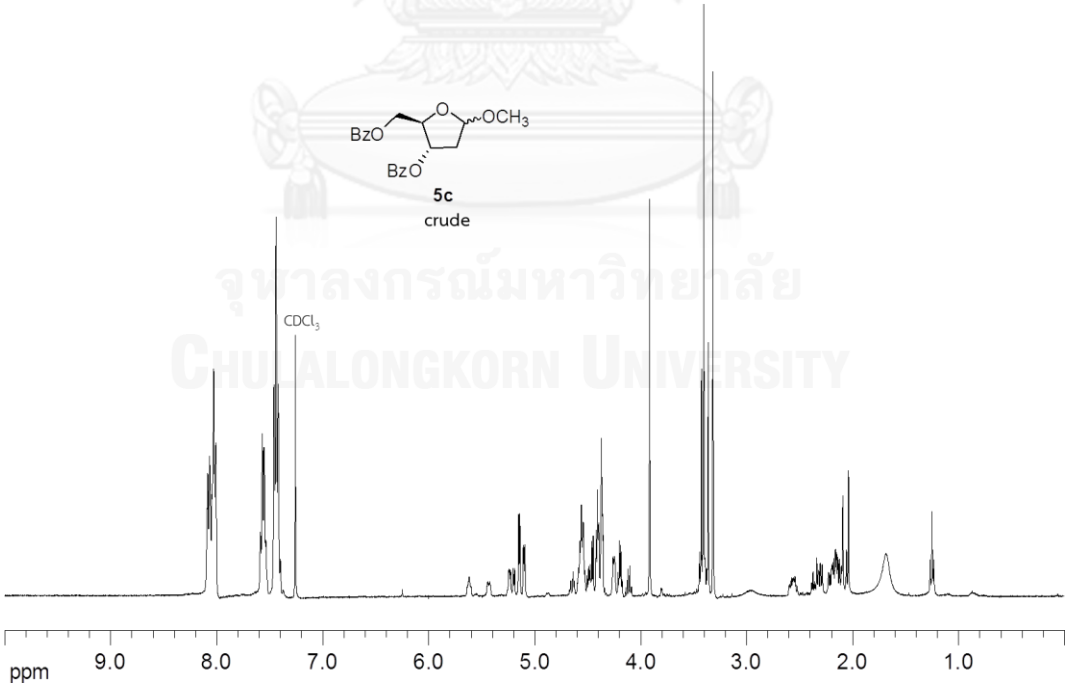

Figure A53 ^{1}H NMR spectrum (400 MHz, $CDCl_3$) of 5-*O*,3-*O*-dibenzoyl-2-deoxy-D-ribose methyl glycoside (**5c**) (mixture of α and β anomers)

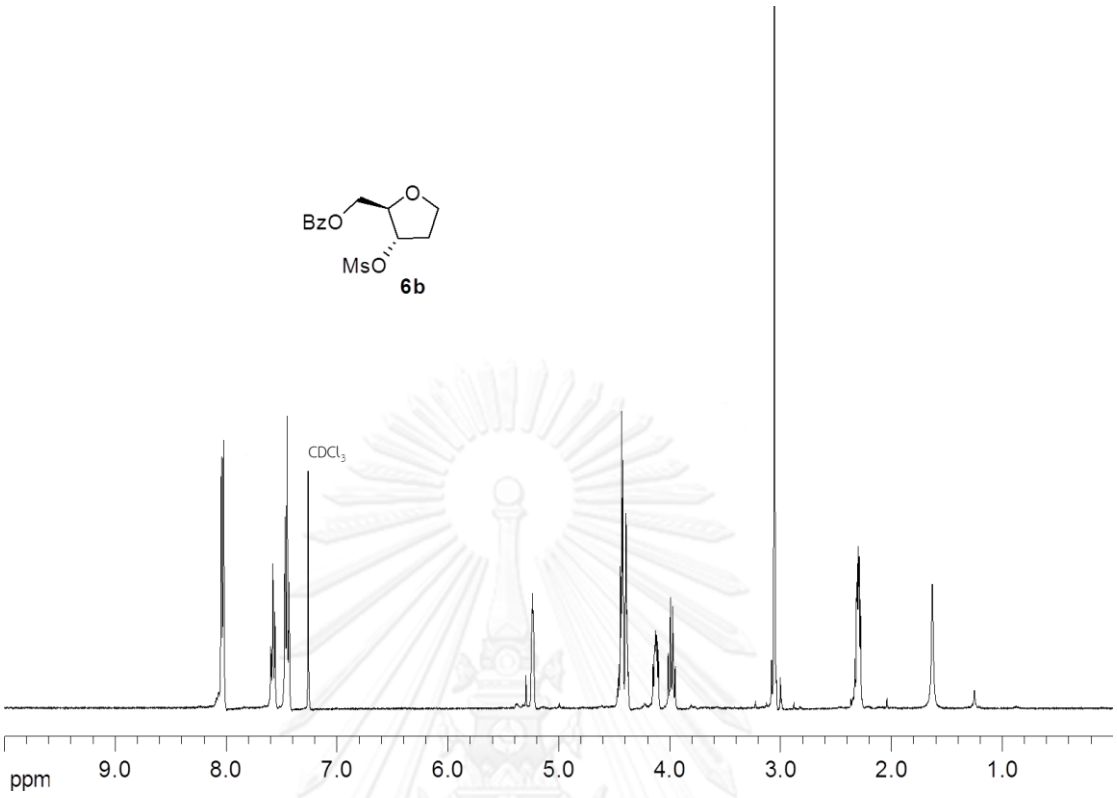

Figure A54 ^{1}H NMR spectrum (400 MHz, $CDCl_3$) of 5-*O*-benzoyl-3-*O*-methanesulfonyl-1,2-dideoxy-D-ribose (**6b**)

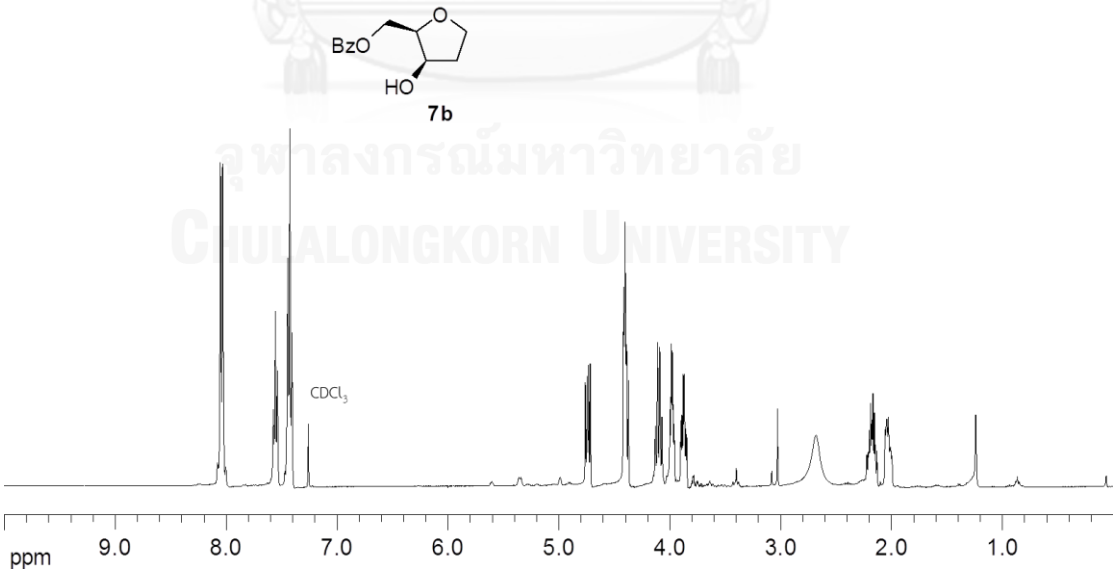

Figure A55 ^{1}H NMR spectrum (400 MHz, $CDCl_3$) of ((2*R*,3*R*)-3-hydroxytetrahydrofuran-2-yl)methyl benzoate (**7b**)

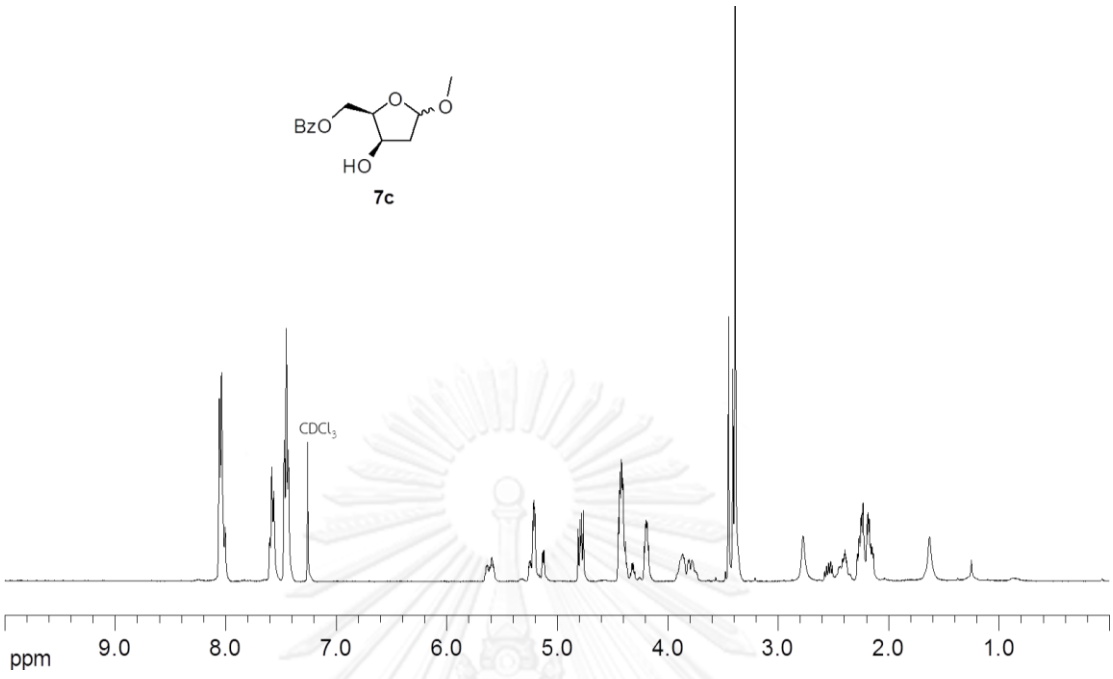

Figure A56 ^{1}H NMR spectrum (400 MHz, $CDCl_3$) of ((2*R*,3*R*)-3-hydroxy-5-methoxytetrahydrofuran-2-yl)methyl benzoate (**7c**) (mixture of α and β anomers)

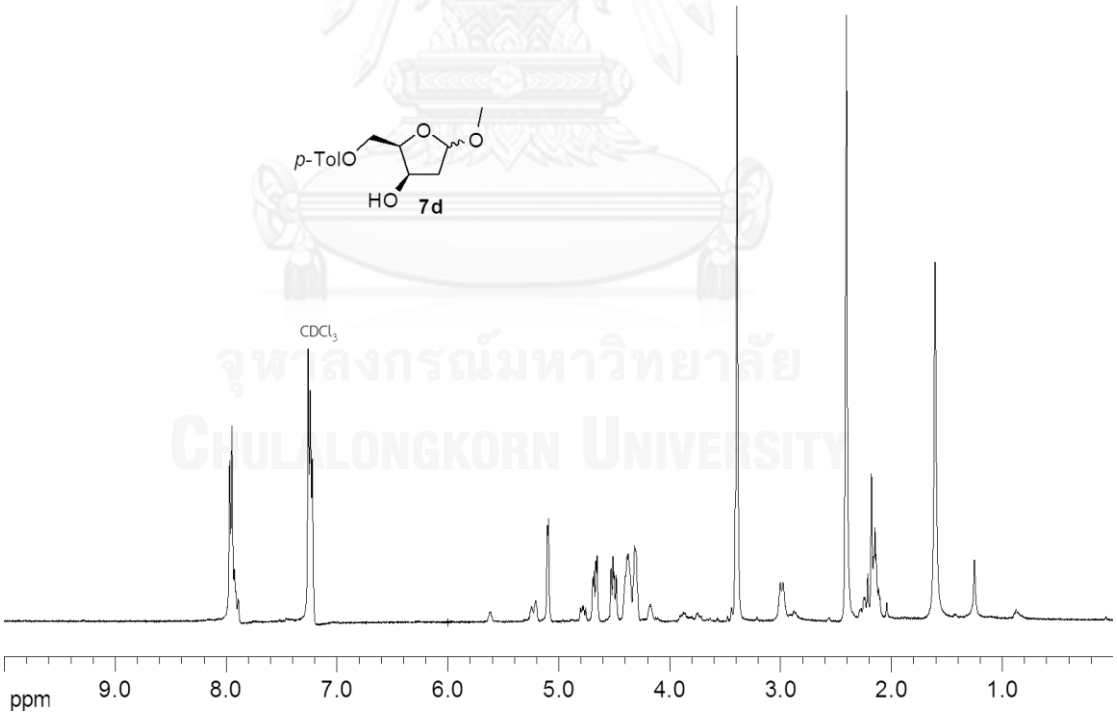

Figure A57 ^{1}H NMR spectrum (400 MHz, $CDCl_3$) of ((2*R*,3*R*)-3-hydroxy-5-methoxytetrahydrofuran-2-yl)methyl 4-methylbenzoate (**7d**) (mixture of α and β anomers)

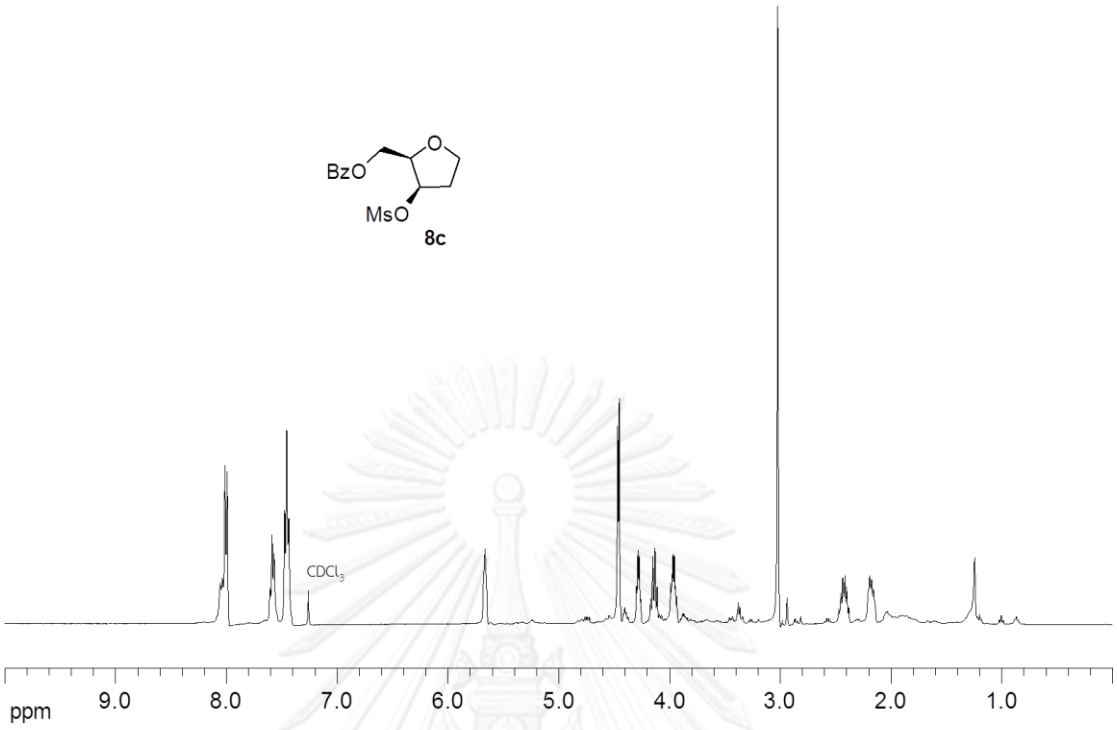

Figure A58 ^{1}H NMR spectrum (400 MHz, $CDCl_3$) of ((2*R*,3*R*)-3-(methylsulfonyloxy)tetrahydrofuran-2-yl)methyl benzoate (**8c**)

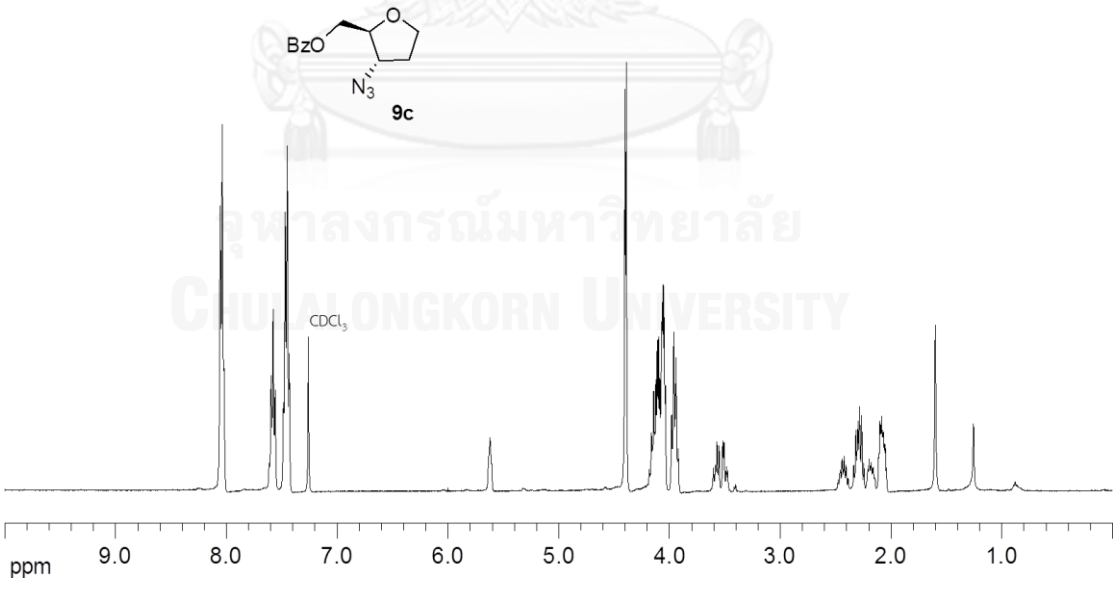

Figure A59 ^{1}H NMR spectrum (400 MHz, $CDCl_3$) of ((2*S*,3*S*)-3-azidotetrahydrofuran-2-yl)methyl benzoate (**9c**)

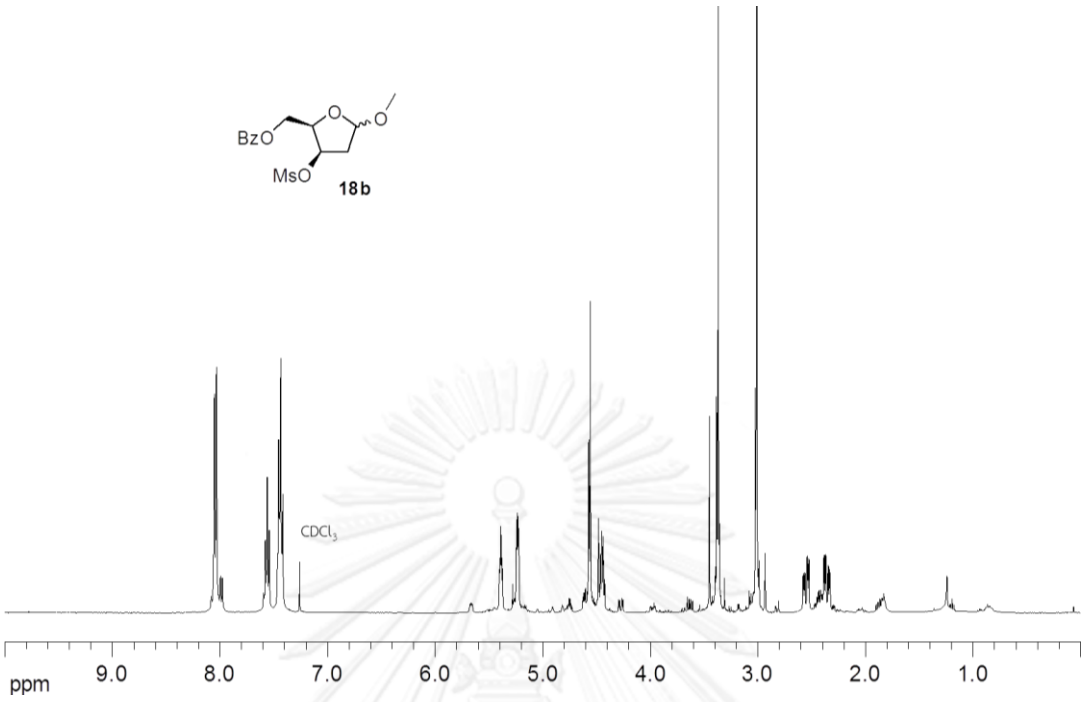

Figure A60 ^{1}H NMR spectrum (400 MHz, $CDCl_3$) of ((2*R*,3*R*)-5-methoxy-3-(methylsulfonyloxy)tetrahydrofuran-2-yl)methyl benzoate (**18b**) (mixture of α and β anomers)

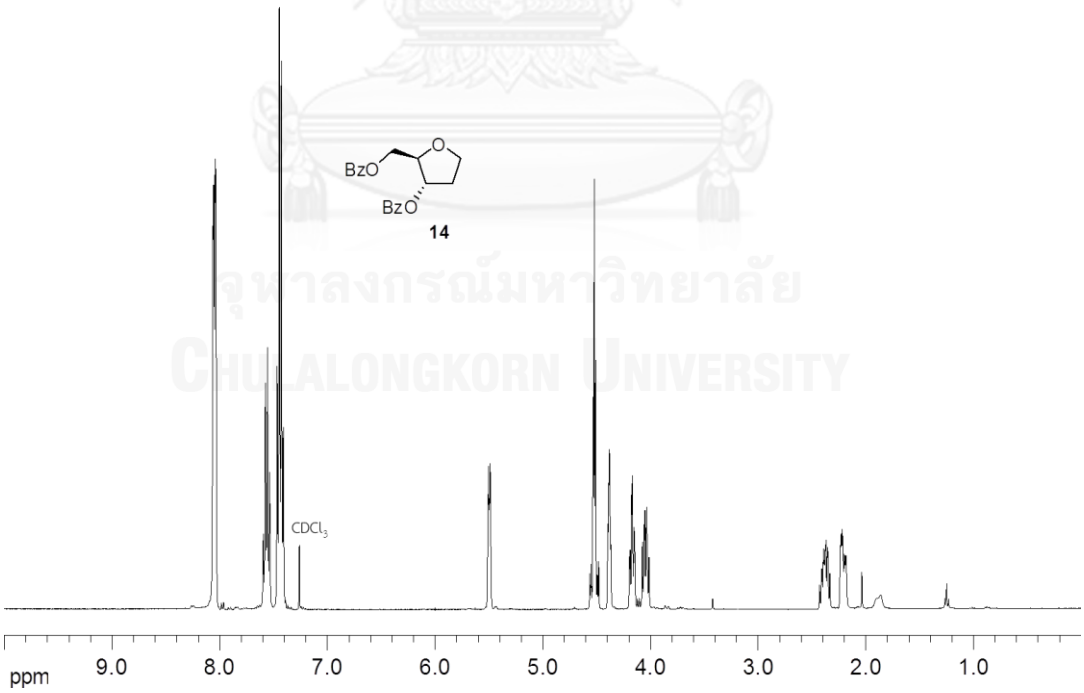

Figure A61 ^{1}H NMR spectrum (400 MHz, $CDCl_3$) of 5-*O*,3-*O*-dibenzoyl-1,2-dideoxy-D-ribose (**14**)

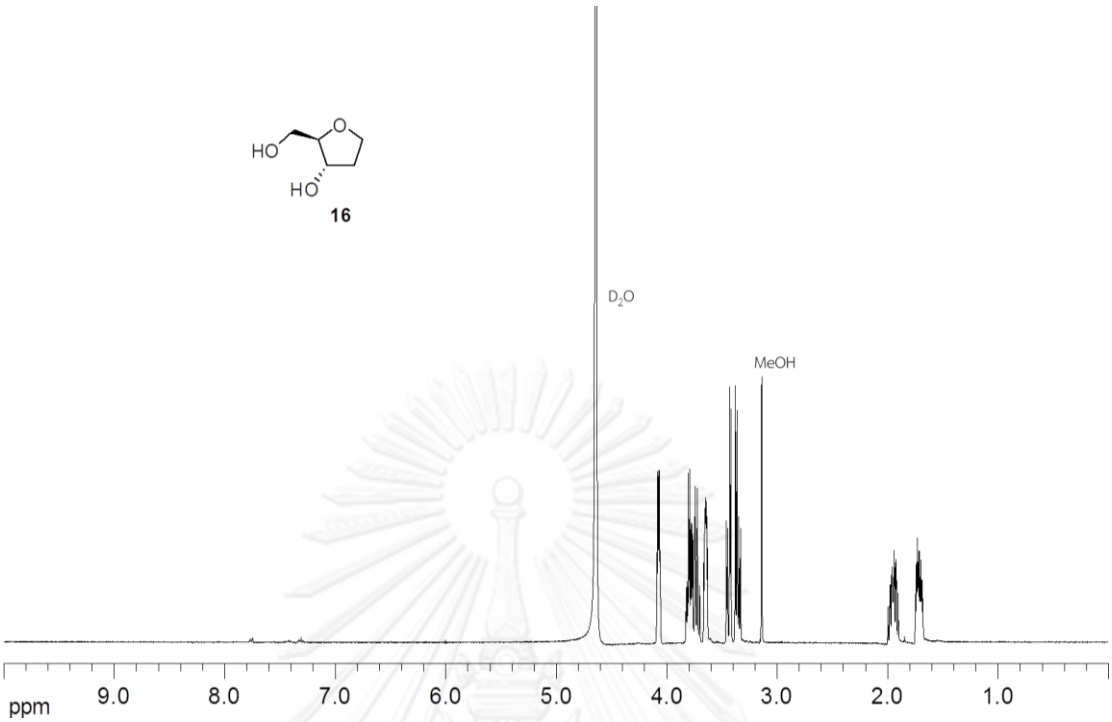

Figure A62 ^{1}H NMR spectrum (400 MHz, D_2O) of 1,2-dideoxy-D-ribose or (2*R*,3*S*)-2-(hydroxymethyl)tetrahydrofuran-3-ol (**16**)

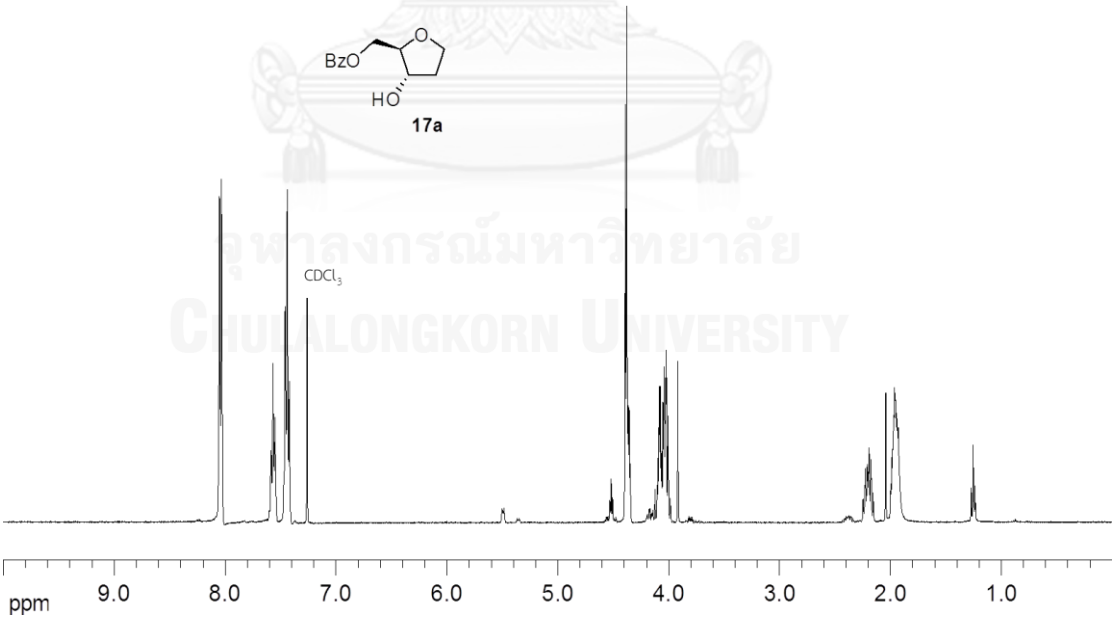

Figure A63 ^{1}H NMR spectrum (400 MHz, $CDCl_3$) of 5-*O*-benzoyl-1,2-dideoxy-D-ribose (**17a**)

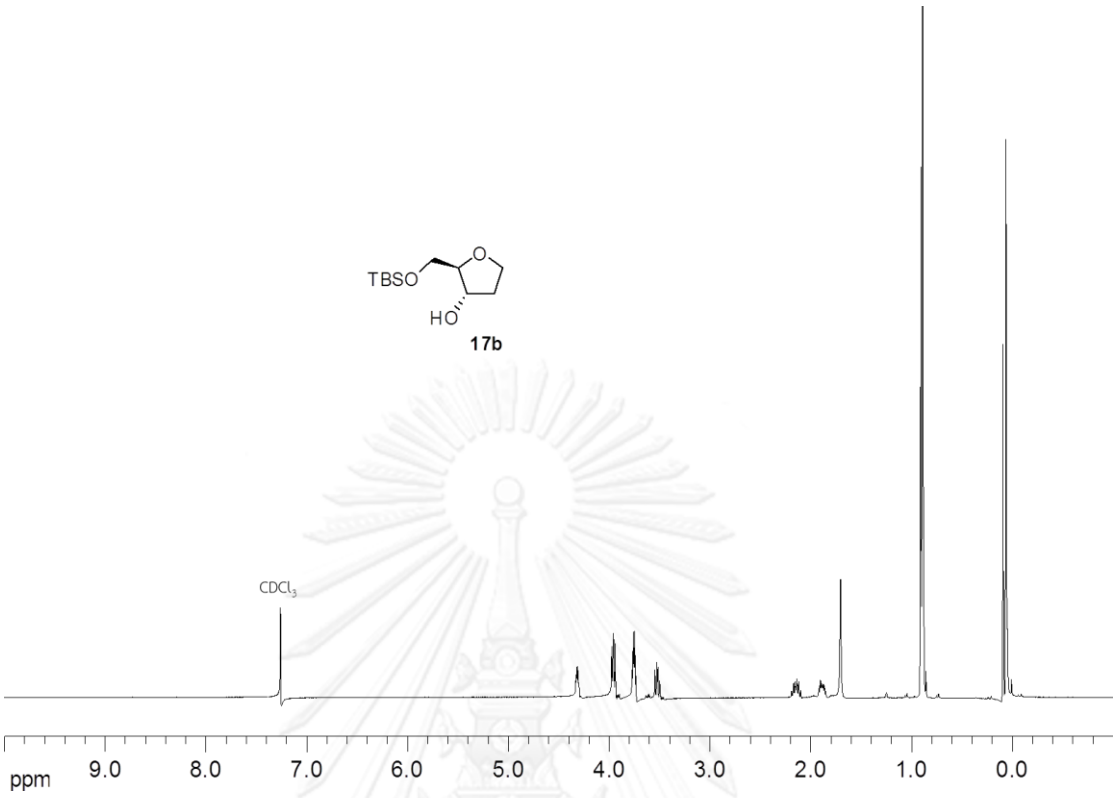

Figure A64 ^{1}H NMR spectrum (400 MHz, $CDCl_3$) of 5-*O*-*tert*-butyldimethylsilyl-1,2-dideoxy-D-ribose (**17b**)

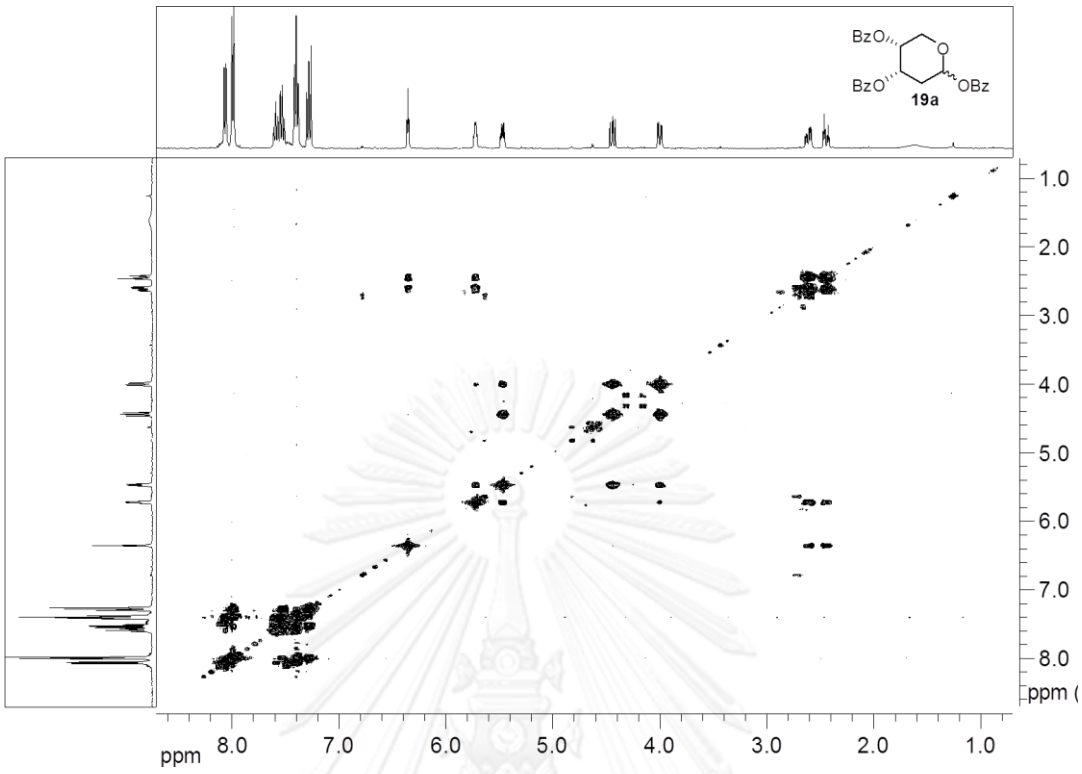

Figure A65 ^{1}H-^{1}H COSY NMR spectrum ($CDCl_3$) of **19a**

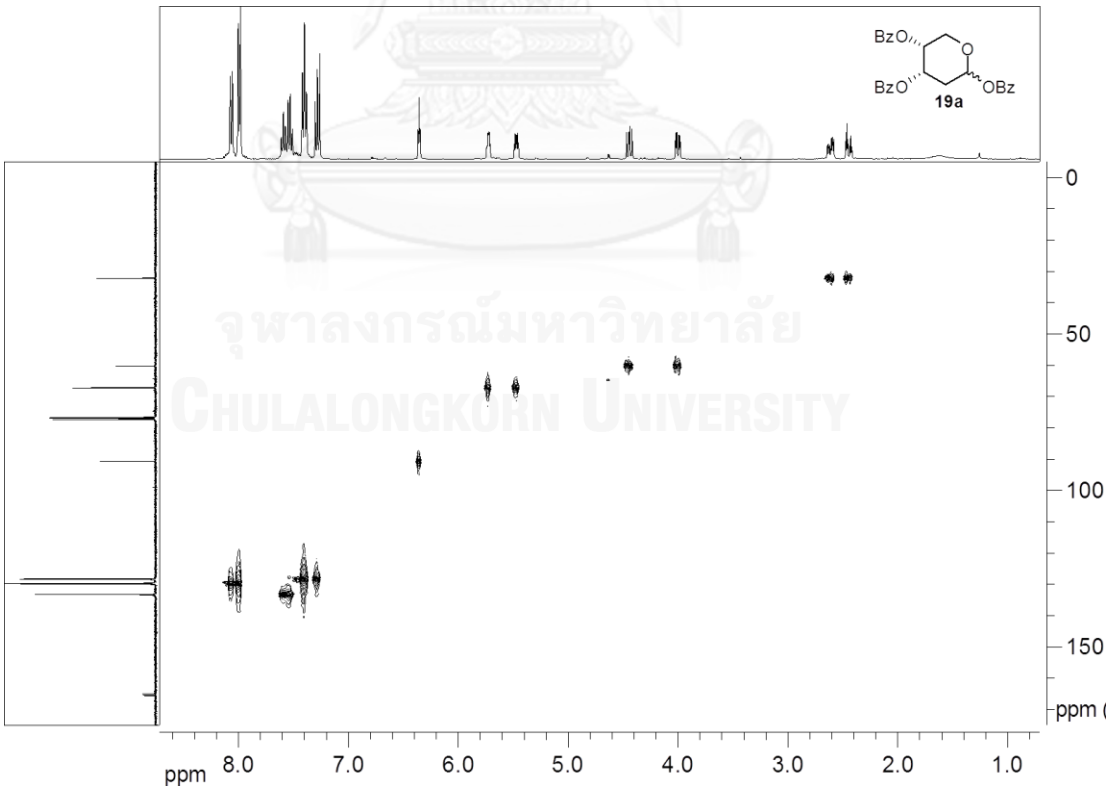

Figure A66 ^{1}H-^{13}C HSQC NMR spectrum ($CDCl_3$) of **19a**

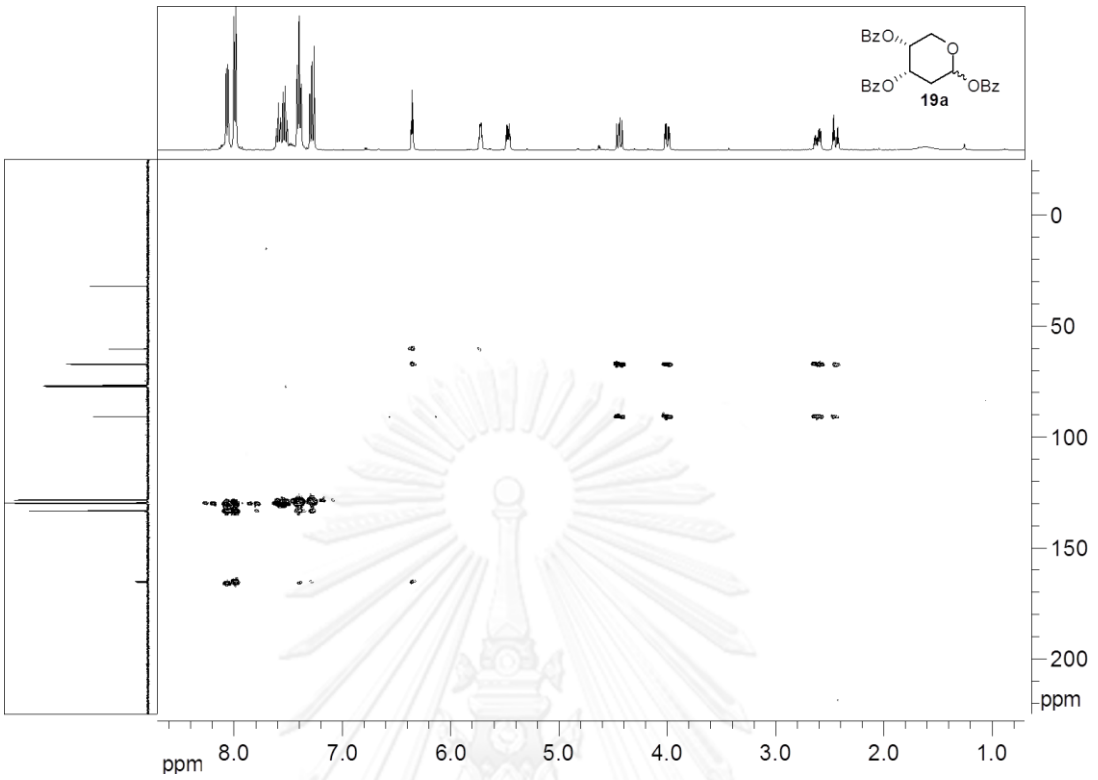

Figure A 67 ^{1}H-^{13}C HMBC NMR spectrum ($CDCl_3$) (**19a**)

Characterization data of PNA oligomers

MALDI-TOF Mass spectra

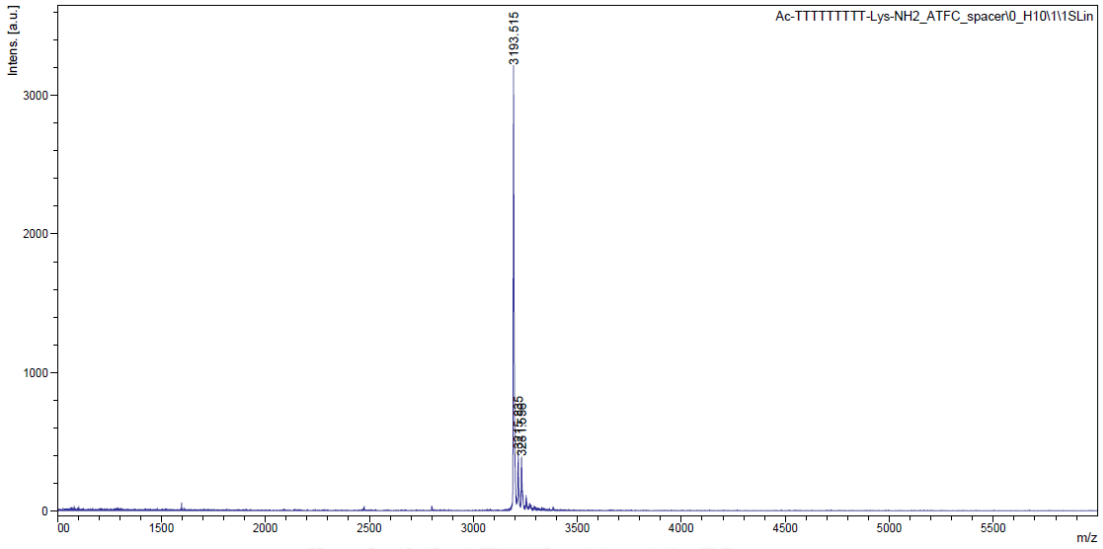

Figure A68 MALDI-TOF mass spectrum of Ac-T_9-LysNH_2; atfcPNA (CCA matrix, linear positive mode)

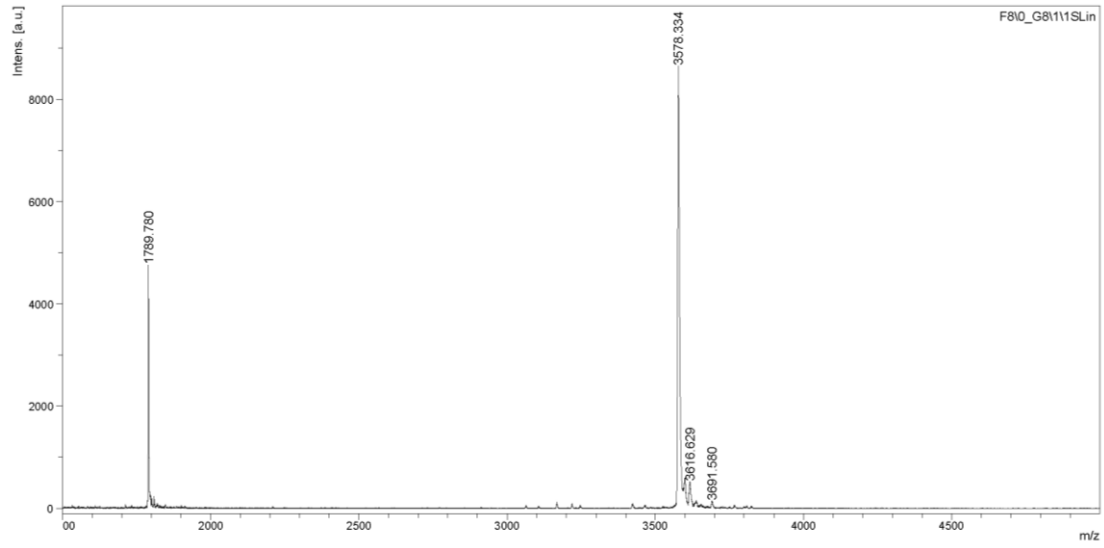

Figure A69 MALDI-TOF mass spectrum of Ac-GTAGATCACT-LysNH_2; atfcPNA (CCA matrix, linear positive mode)

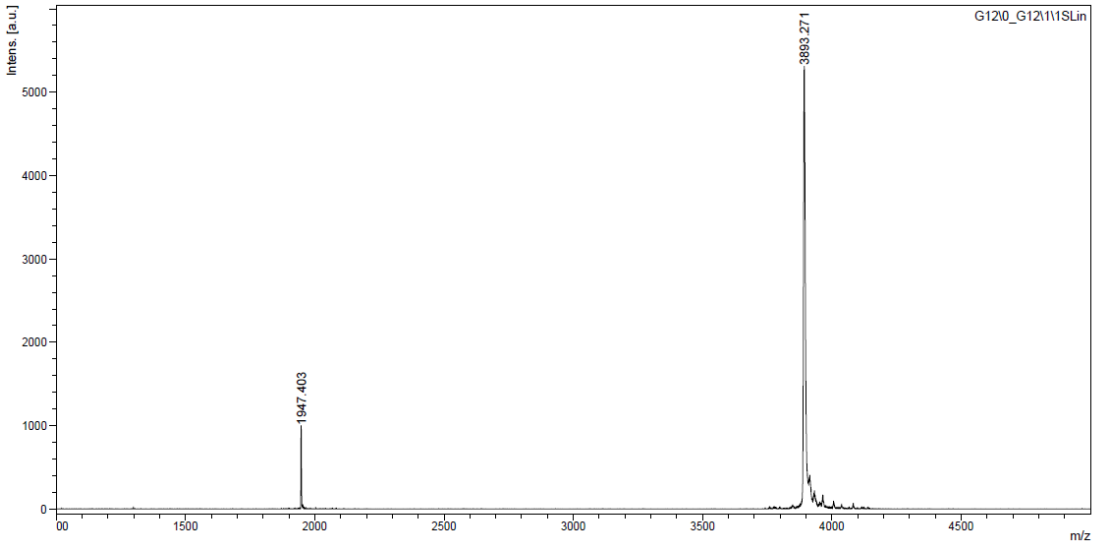

Figure A70 MALDI-TOF mass spectrum of Flu-GTAGATCACT-LysNH_2; atfcPNA (CCA matrix, linear positive mode)

Polarity identification (reverse phase HPLC)

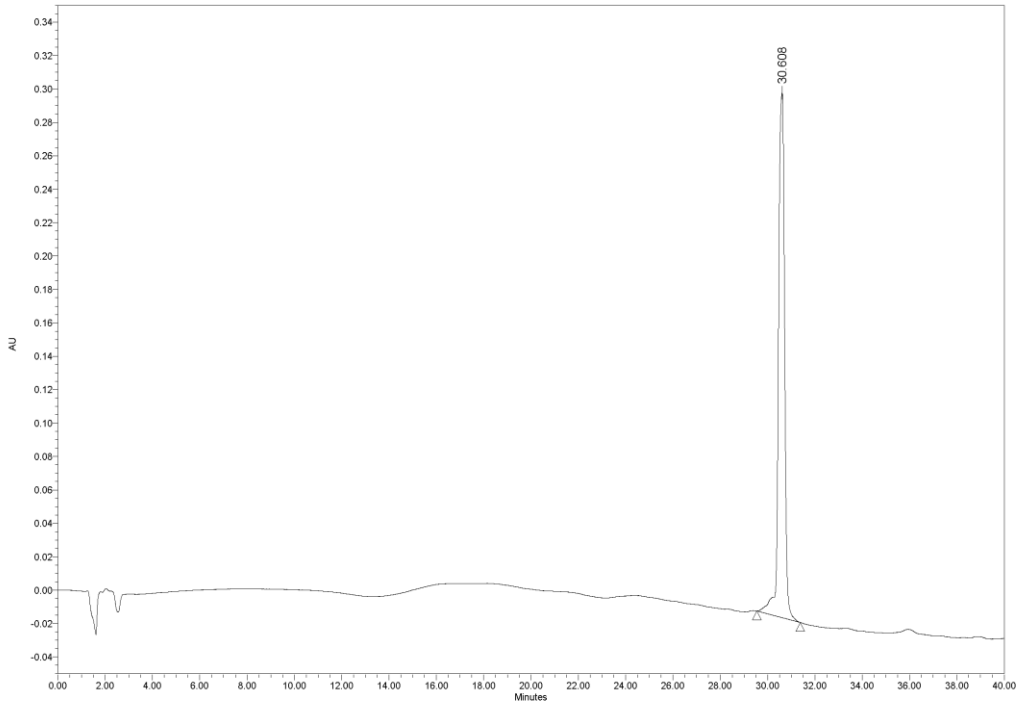

Figure A71 HPLC chromatogram of Ac-T_9-LysNH_2; atfcPNA

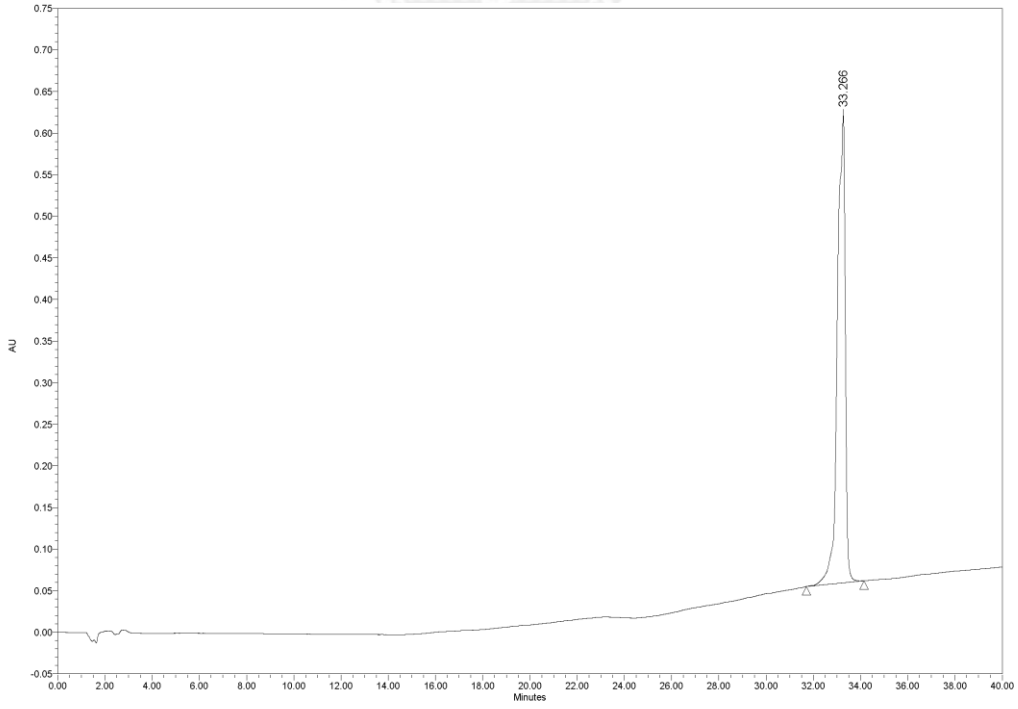

Figure A72 HPLC chromatogram of Ac-T_9-LysNH_2; acpcPNA

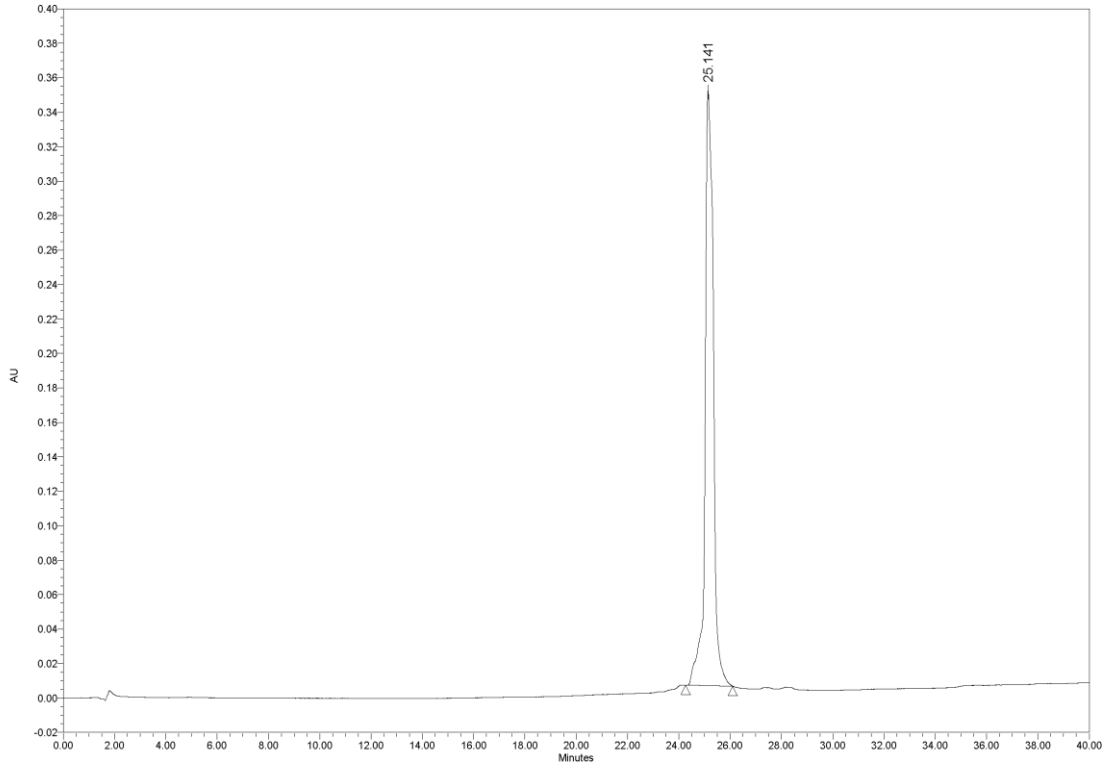

Figure A73 HPLC chromatogram of Ac-GTAGATCACT-LysNH_2; atfcPNA

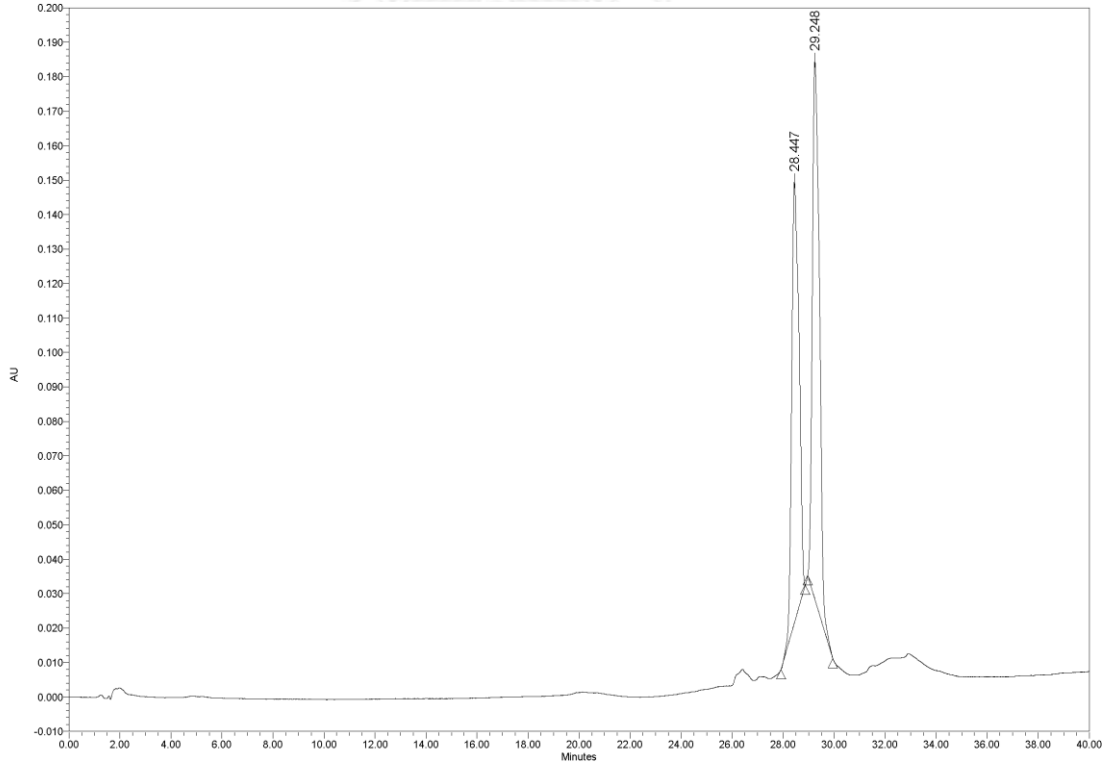

Figure A74 HPLC chromatogram of Flu-GTAGATCACT-LysNH_2; atfcPNA

PNA binding properties with DNA/RNA

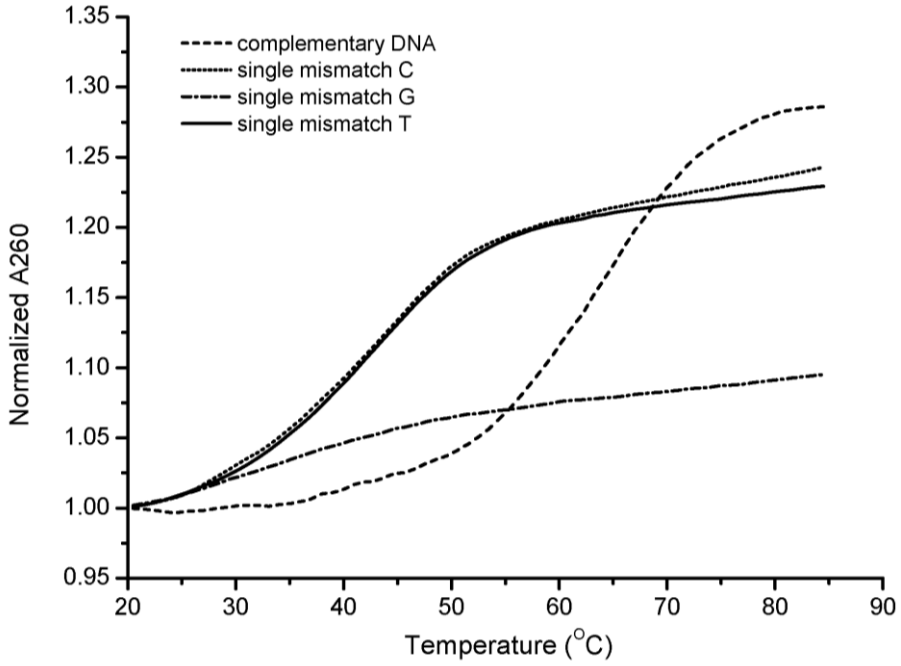

Figure A75 Melting curves of Ac-TTTTTTTTT-LysNH_2 and DNA (full and single mismatch); condition PNA:DNA = 1:1, [PNA] = 1 μM, 0 mM sodium chloride, 10 mM sodium phosphate buffer, pH 7.0, heating rate 1.0 °C/min.

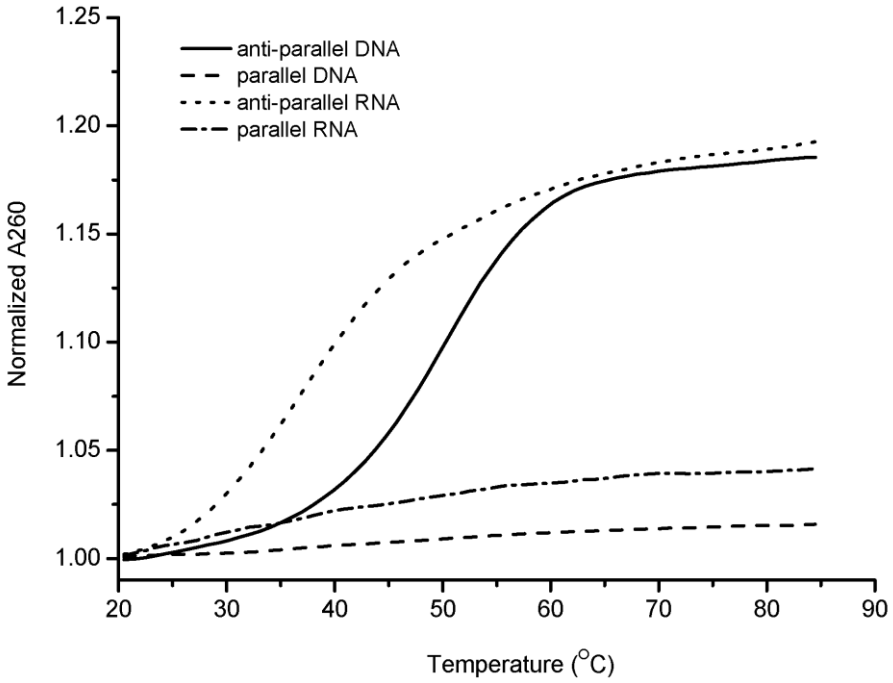

Figure A76 Melting curves of Ac-GTAGATCACT-LysNH_2 and complementary DNA (defined orientation); condition PNA:DNA = 1:1, [PNA] = 1 μM,100 mM sodium chloride, 10 mM sodium phosphate buffer, pH 7.0, heating rate 1.0 °C/min.

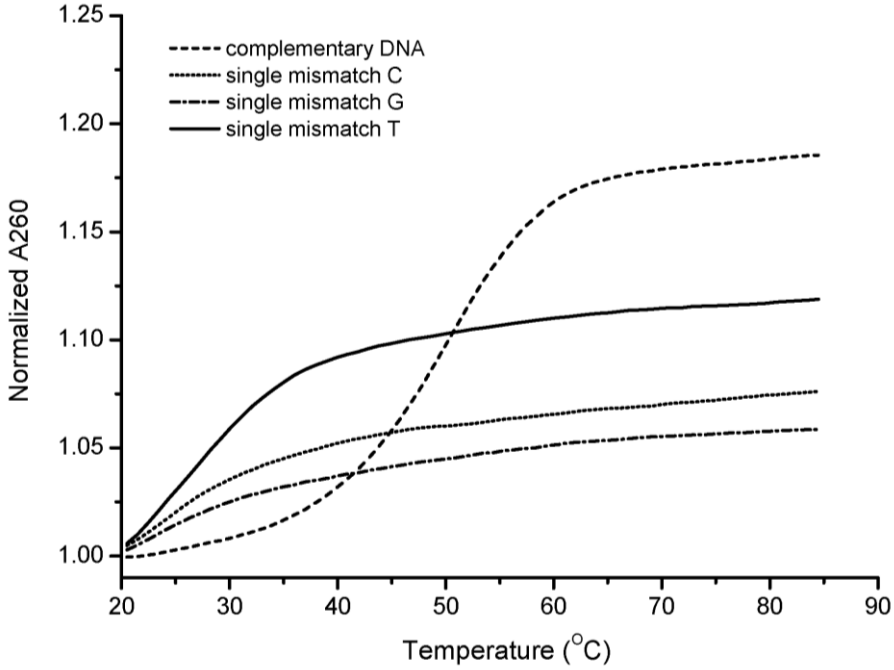

Figure A77 Melting curves of Ac-GTAGATCACT-LysNH2 and DNA (full and single mismatch); condition PNA:DNA = 1:1, [PNA] = 1 μM,100 mM sodium chloride, 10 mM sodium phosphate buffer, pH 7.0, heating rate 1.0 °C/min.

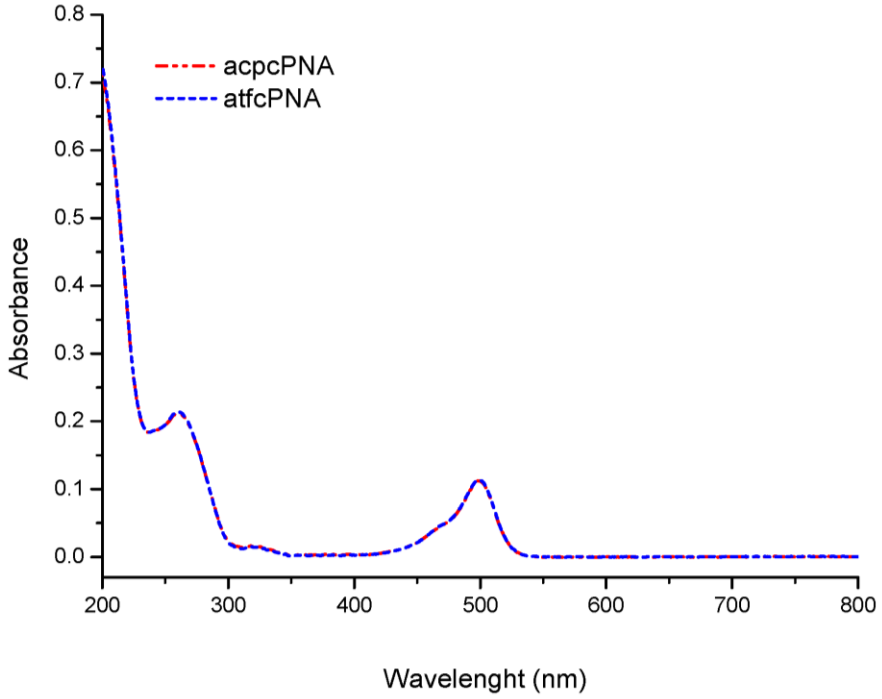

Figure A 78 UV spectra of Flu-GTAGATCACT-LysNH_2 compare between acpcPNA and atfcPNA in 10 mM sodium phosphate buffer, pH 7.0.

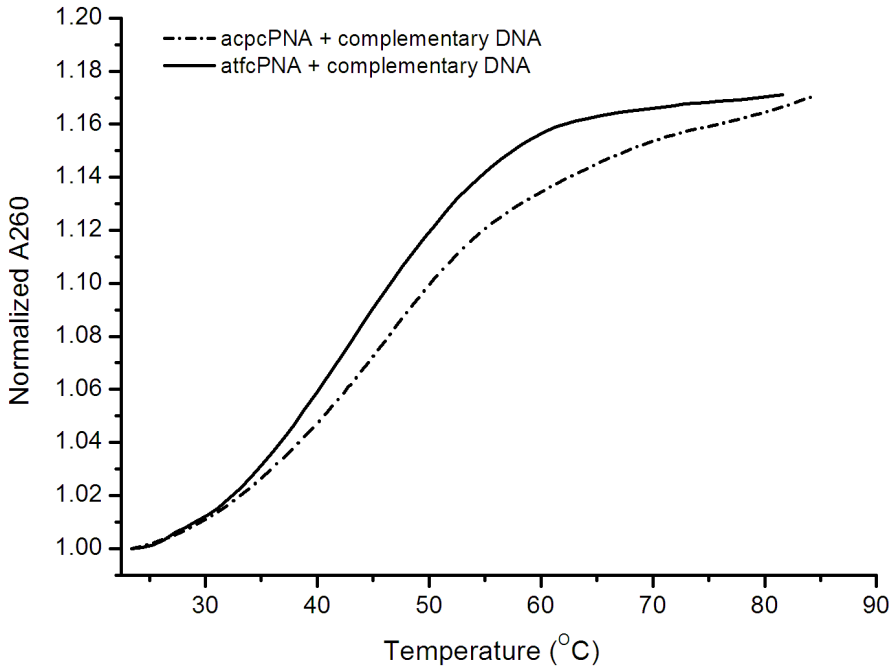

Figure A79 Melting curves of Flu-GTAGATCACT-LysNH_2 compare between acpcPNA and atfcPNA; condition PNA:DNA = 1:1, [PNA] = 1 μM,100 mM sodium chloride, 10 mM sodium phosphate buffer, pH 7.0, heating rate 1.0 °C/min.

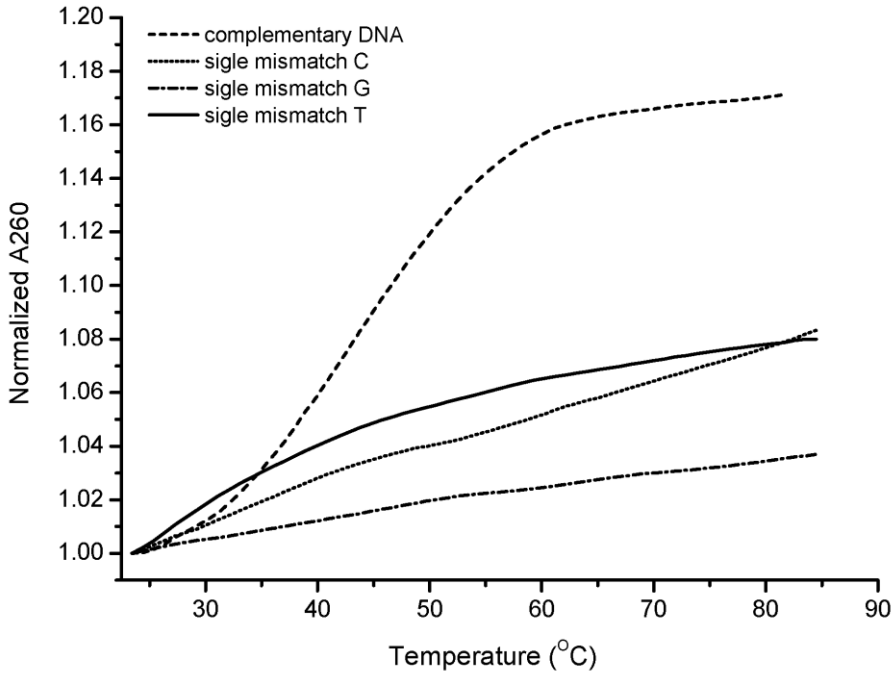

Figure A80 Melting curves of Flu-GTAGATCACT-LysNH_2 and DNA (full and single mismatch); condition PNA:DNA = 1:1, [PNA] = 1 μM,100 mM sodium chloride, 10 mM sodium phosphate buffer, pH 7.0, heating rate 1.0 °C/min.

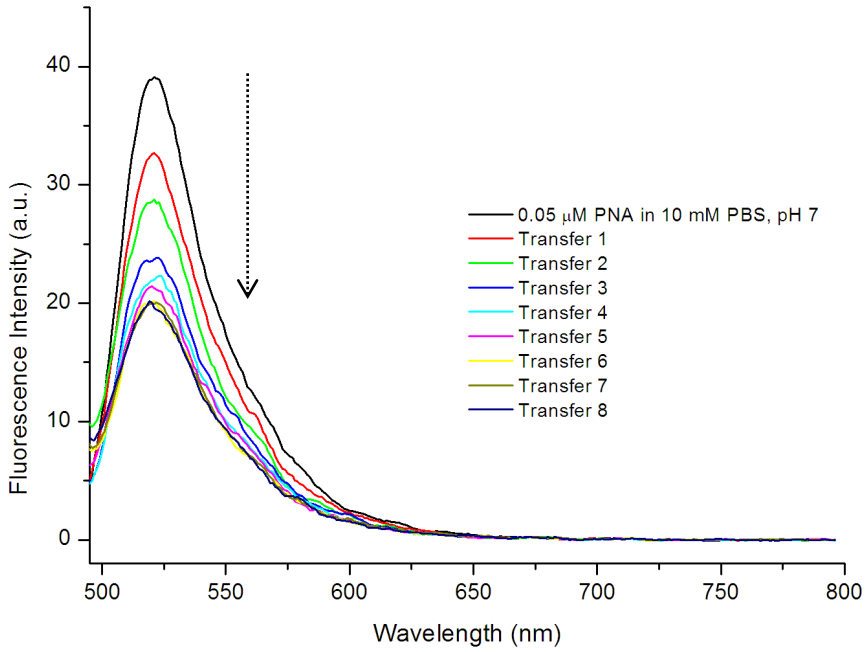

Figure A81 Fluorescence spectra of Flu-GTAGATCACT-LysNH$_2$ (acpcPNA) 0.05 μM of PNA in 10 mM sodium phosphate buffer pH 7, λ_{ex} 480 nm, slit 5 nm, high voltage, without NaCl.

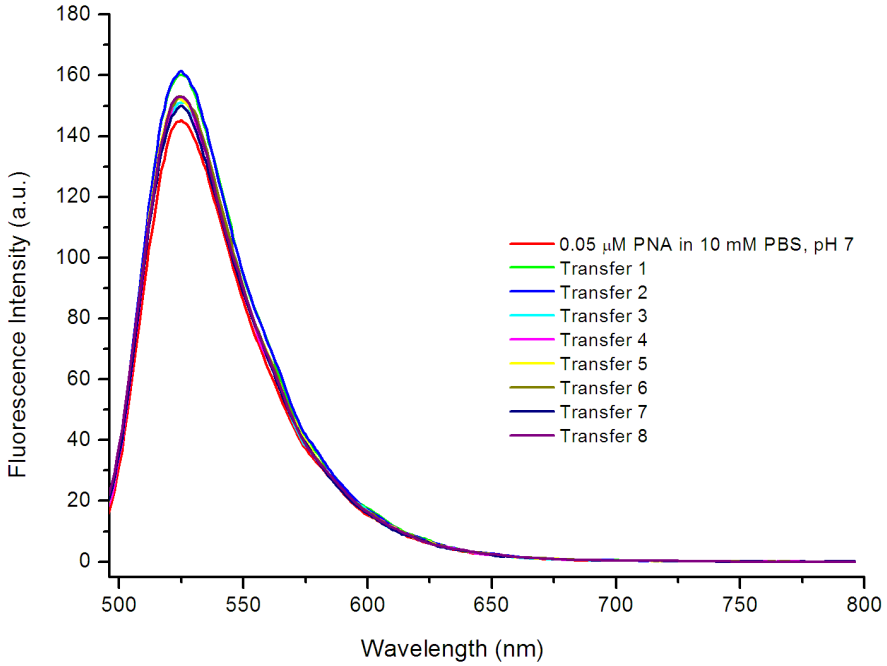

Figure A82 Fluorescence spectra of Flu-GTAGATCACT-LysNH$_2$ (atfcPNA) 0.05 μM of PNA in 10 mM sodium phosphate buffer pH 7, λ_{ex} 480 nm, slit 5, high voltage, without NaCl.

VITA

Pitchanun Sriwarom was born on December 27, 1987 in Ubon Ratchathani, Thailand. She graduated Bachelor's degree of Science (B.Sc) in chemistry from Chulalongkorn university in 2010. She was chemist at RCI labscan Ltd. (Factory) in technique department, Samutsakorn, Thailand during May 2010 to May 2011. Since that she has been a graduated student studying organic chemistry for her Master's degree at Chulalongkorn university.

Contact information: S.PITCHANUN@gmail.com